Characterisation of the Ultramafic and Carbonatite Components of the Schiel Alkaline Complex in the Limpopo Province of South Africa

UZAYR MAHOMED

SUPERVISED BY PROF R.E HARMER

Thesis presented in partial fulfilment of the requirements for the Degree Master of Science in the Department of Geology, Rhodes University

September 2021

Declaration:

I, the undersigned, hereby declare that the work presented in this thesis is my own original work and that I have not previously, in its entirety or in part, submitted it at any other university for a degree.

Signature 

Date: 11 September 2021

Acknowledgements:

I would like to thank the following people for the role they played in assisting me to complete my MSc:

Prof Jock Hamer for his continued support, wisdom and assistance in helping me develop this thesis, as well as improving my academic aptitude;

Dr Sarah Glynn and Dr Michael Widenbeck who assisted with the geochronological analyses and calculations;

The CAF staff at Stellenbosch University who helped with XRF analyses, zircon separation and zircon CL-imaging: Madelaine Frazenburg and Mareli Grobbelaar;

Dr Deon Van Niekerk who assisted with EPMA analyses;

I would also like to thank CIMERA for funding my MSc studies.

Abstract:

Owing to the poor documentation of the phoscorite-carbonatite association present in the Schiel Complex and the associated economic potential of other known phoscorite-bearing complexes, the Schiel Complex is widely thought to have similar economic potential. This complex is often compared to the lucrative Phalaborwa Complex, as it is thought to have crystallised from a common parental melt, with a similar age of emplacement.

This study aims to provide clarity on the physical and chemical characterisation of the various rock types present in the Schiel Complex, with this study being the first petrological investigation based on fresh in-situ samples gathered from 3 borehole cores which were drilled by FOSKOR in the 1960s.

The sampled sections of the ultramafics from the Schiel Complex are comprised of end-member rock compositions of either magmatic phoscorites or pyroxenites or metasomatic glimmerites, where gradational contacts between these various end-members produce rock varieties that contain characteristics of one or more end-member types. Carbonatite rocks are present as medium-grained, coarse-grained and banded calcio-carbonatite varieties where the carbonatite rocks are proposed as being the metasomatic medium for glimmerite production.

Contrary to previous research, the structure of the ultramafic and carbonatite bodies are present as vein and veinlet structures which seem to originate from a single pipe-like body, from which these rock types intruded into the surrounding syenitic country-rock. Metasomatic alteration of the ultramafic sections of the Schiel Complex also show that the carbonatite rocks must have intruded after some ultramafic magmatism.

The presence of the same minerals, with similar chemistries, in both the ultramafic and carbonatite rocks as well as similar REE chondrite-normalised plots show that the various rock types may have originated from a common parental magma, where the accumulation and crystallisation of minerals is the most likely factor in producing the various Schiel Complex rock varieties, causing silicate minerals to be present in the carbonate fraction of the magma, and carbonate minerals in the silicate fraction of the magma.

Apatite is the expected rare earth element (REE) mineralising mineral in phoscorites, but is shown to be depleted in REE content in the Schiel Complex due to metasomatic fluid infiltration causing the scavenging and dissipation of REEs. These rocks have also crystallised containing no significant copper-bearing mineralisation, contrary to that which is seen in the Phalaborwa Complex. A comparison of mica minerals between the Schiel Complex rocks and the Phalaborwa Complex rocks show that the

two complexes have undergone unique emplacement processes and should not be considered as sister complexes.

Efforts to date the glimmerite and carbonatite rocks based on zircon grain U/Pb geochronology proved unsuccessful in constraining the current ages of emplacement provided by previous researchers, but rock relationships show that the current accepted sequence of events cannot be correct, providing scope for further research.

This study provides an update on the chemical and physical characteristics, based on the only available sample suite of the ultramafic and carbonatite components, of the Schiel Complex, increasing the depth of documentation of these rare rock types and aiding in refuting some conclusions on the genesis, emplacement and evolution of the Schiel Complex proposed by previous research.

Table of Contents:

List of Figures:

List of Tables:

Appendices:

Chapter 1: Introduction

The Schiel Complex is commonly linked with the better-known Phalaborwa Complex, as they are contemporaneous intrusive complexes both reported to contain phoscorite-carbonatite components. The economic importance of the Phalaborwa Complex has led people to extrapolate that the Schiel Complex may have petrological components of potential economic value. Phoscorites and carbonatites are host to major economic interest in sulphide mineralisation in the form of copper, together with associated noble-metal deposits in the form of Pt-, Pd-, Rh-, Au- and Ag-bearing minerals (Rudashevsky et al., 2004). The copper mineralisation (bornite, chalcopyrite and chalcosine-group minerals), platinum group elements (PGEs) and Au-Ag-mineralisation of the Loolekop deposit in the Phalaborwa Complex has allowed for economic extraction of these ores (Rudashevsky et al., 2004). The unique mineralisation seen at the Phalaborwa Complex, in turn, offers the prospect that the similar rare rock types reported from the Schiel Complex could also contain comparable mineralisation with the potential for similar copper and platinum group minerals (PGM) mineralisation.

This study provides the first systematic investigation of the geochemistry and petrology of the ultramafic and carbonatite rocks of the Schiel Complex, which enables comparisons to be drawn between phoscorite-carbonatite occurrences from the Phalaborwa Complex and a selection of other complexes.

Most phoscorite bodies are spatially and temporally associated with carbonatite crystallisation, forming multi-phase phoscorite-carbonatite series (Krasnova et al., 2004; Verwoerd, 1986; Eriksson, 1989). These rocks are considered to be mantle-derived (Eriksson. 1989; Zaitsev and Bell. 1995; Verhulst et al., 2000); range texturally from coarse- to fine-grained (Krasnova et al., 2004) and occur in a range of features such as: ring or arcuate zones and veins around carbonatite cores; steeply dipping veins; stockwork pipe-like bodies; oval or lens-like isometric bodies; or as small dykes or as screens of interleaved phoscorite and carbonatite.

Metasomatic zones are common at phoscorite and carbonatite contacts and range in size from millimetres to several metres wide. Being dependant on host rock and phoscorite or carbonatite chemistry, the metasomatic reaction products are difficult to quantify due to the wide variation in chemical compositions of host and intruding rock types (Krasnova et al., 2004). Phoscorite-carbonatite associations are considered as coeval and formed from carbonated parental melts rich in Mg, Fe, Si and P, but do not crystallise homogeneous rock bodies leading to the unknown exact composition of these melts (Lee et al., 2004).

1.1 What is a Phoscorite?

The term phoscorite was first used by Russell et al. (1954) to describe the first recognised occurrence of these rocks in the Phalaborwa Complex: the term initially spelt "foscorite" in honour of South African phosphate and phosphoric acid producer, FOSKOR, exploiting the apatite ores at Phalaborwa. Phoscorites are rare and have been recognised at only 21 localities worldwide, almost all occurring as phoscorite-carbonatite associations (Russell et al., 1954; Krasnova et al., 2004).

According to the International Union of Geological Sciences' (IUGS) classification of igneous rocks (Le Maitre et al., 2002), a phoscorite is a magnetite-, olivine- (often serpentinised) and apatite-bearing rock usually associated with carbonatites. Alternatively, variations observed in phoscorites from complexes reviewed by Krasnova et al. (2004) led these authors to propose an alternative, more inclusive, definition of these extremely variable rock types:

> *"Phoscorites are plutonic, ultramafic rocks, comprising magnetite, apatite and one of the silicates, forsterite, diopside or phlogopite. Common minor minerals are calcite, dolomite, tetraferriphlogopite and richterite. Key accessories are baddeleyite, pyrochlore, pyrrhotite and chalcopyrite. Phoscorites almost always occur in association with carbonatites."*

With reference to the database of around 570 carbonatite complexes of the world (Wolley and Kjarsgaard, 2008), it is evident that phoscorites are extremely rare. However, Krasnova et al. (2004) argued that it is highly possible that phoscoritic bodies are more commonly crystallised in association with carbonatites, but that these have not been defined as such due to their extreme variability in composition and structure, and the ambiguity in the narrow classification of phoscorite provided by the IUGS (Le Maitre et al., 2002).

Appendix A (p111) presents a summary of the variation in mineralogy seen in phoscorites and phoscorite associated rocks from different complexes. Krasnova et al. (2004) reported that mineral assemblages in phoscorites may vary from near monomineralic rocks to two-, three- or polymineralic rock varieties. Krasnova et al. (2004) also highlighted the variable nature of phoscorite textures stating that they may be pegmatitic, coarse- or fine-grained and are commonly breccia-like with angular or round xenoliths of various host rocks, where plastic deformation of xenoliths may generate banded structures on the phoscorites.

1.2 What is a Carbonatite?

The IUGS igneous rock classification scheme (Le Maitre et al., 2002) provides both mineralogical and chemical classification schemes for the naming of carbonatites. The mineralogical classification scheme defines carbonatites as an igneous rock containing greater than 50 modal percent carbonate minerals.

Carbonatites are then named according to the dominant carbonate mineral in the carbonatite: e.g. calcite carbonatite, dolomite carbonatite, etc. Where significant minor phases are present this can be refined by adding these mineral phases to the name in order of increasing abundance: e.g. dolomite calcite carbonatite (where calcite > dolomite); phlogopite magnetite calcite carbonatite (calcite carbonatite containing more magnetite than phlogopite), etc. However, carbonatites composed of iron-rich carbonates: ankerite- or siderite-carbonatites are to be called "ferrocarbonatites" a chemical rather than mineralogical term. An alternative chemical classification scheme is provided for use when the mineralogy of the rock is unknown or if complex carbonate minerals are present. Carbonatites are defined as having less than 20 wt.% SiO_2; rocks with higher silica values are simplistically classified as silico-carbonatite. Carbonatites (*sensu stricto*) are subdivided as either calciocarbonatite, magnesiocarbonatite or ferrocarbonatite based on the weight proportions of CaO, MgO, FeO^+, $Fe_2O_3^+$ and MnO.

Gittins and Harmer (1997) highlighted numerous shortcomings in the 1989 IUGS chemical classification scheme (Le Maitre et al., 1989; these are repeated in the 2002 revision). Gittins and Harmer (1997) described imprecisions in the IUGS carbonatite classification scheme as no distinction is made between ferric and ferrous iron which leads to the improper incorporation of ferric iron, which is only present in oxide minerals and not in the carbonate minerals, in the classification of carbonatites leading to the possible classification of a rock containing Fe-poor carbonate minerals as a ferrocarbonatite. This lead Gittins and Harmer (1997) to propose a modified chemical classification of carbonatites which use molar proportions rather than weight proportions in order to classify carbonatites. They also proposed that the ferrocarbonatite field of the IUGS system be divided into two sections, separating ferruginous calciocarbonatites from much more Fe-rich ferrocarbonatites, where the main carbonate is Fe-rich (Ankerite, siderite).

Mitchell (2005) considered the non-genetic IUGS classification scheme as inadequate for the classification of modally diverse rocks derived from a single magma source, and proposed the preferential use of genetically inclusive classification systems, such as that for kimberlites and related proposed by Mitchell (1995), for carbonatite classification. He defined any rock containing higher than an arbitrary 30 vol% primary igneous carbonate, regardless of the silica content, as a carbonatite. This classification is used to recognise that a carbonate-forming magma will differentiate a suite of genetically similar rocks in which a significant variation in carbonate content may arise, and that the carbonate content is less relevant than the fact that a suite of carbonate-bearing rocks is derived from the same carbonate-rich parental magma (Mitchell, 2005). Mitchell (2005) emphasised the extreme variability in the modal range at small scales seen in carbonatites from the Phalaborwa Phoscorite Complex and considered carbonatite complexes as a package of rocks that are modally diverse but have a common magmatic origin.

The definition of carbonatites proposed by Mitchell (2005) has been be used to classify the carbonatites in this study, due to their close spatial association with phoscorites and their expected variability in mineralogy.

Chapter 2: The Schiel Complex Phoscorite-Carbonatite Association - A Review of the Schiel Complex Geology

2.1 The First Report of a Phoscorite-Carbonatite Complex associated with the Schiel Complex (FOSKOR Unpublished Report)

FOSKOR Corporation provided the only in-situ petrological study of the Schiel Complex ultramafic and carbonate units performed on fresh core samples in an unpublished exploration report compiled by Viljoen (1966) on the results of an exploration programme of 47 boreholes drilled into the core of the eastern Schiel Complex. This report presents petrographic observations on 50 samples and 7885 chemical analyses for different minerals.

Based on this petrographic investigation, Viljoen (1966) argued that phoscorite, carbonatite, pyroxenite and syenite were the principal rock types present in the eastern section of the Schiel Complex, which is hosted in granite and gneiss. He described the pyroxenite, phoscorite and carbonatite components as many thin, discontinuous tongue, lens and tabular structures that are present at the upper area of the intrusion. However, he stated that it was difficult to identify specific rock types in hand samples based on their gradational contacts. He proposed that the pyroxenite-phoscorite components were the oldest intrusion; with the carbonatite being younger than the pyroxenite-phoscorite components and that the syenite may have intruded over different periods. Sections of mica-rich ultramafic material were also present which Viljoen (1966) proposed could be better described as glimmerites upon further investigation.

2.1.1 Glimmerites and Fenitisation associated with Phoscorite-Carbonatite Complexes

Fenites are aureoles of high temperature metasomatically altered country-rock and are composed of predominantly K-Na-feldspars, albite, nepheline, alkaline pyroxene and alkaline amphibole with subordinate biotite-phlogopite mica pairs, magnetite and ilmenite (Zharikov et al., 2007; Elliott et al., 2018). Elliott et al. (2018) argued that the mineral assemblages of fenites are generally variable, as this is dependent on several interacting factors such as protolith mineralogy, permeability and structure, fluid composition, pressure and temperature. The fenitisation process is produced by a metasomatising agent derived from an alkaline-carbonatite system (first described from Fen by Brögger, 1921), where the fenitising fluid is produced and released during cooling and crystallising of an intrusion (Le Bas, 2008), and may be small-scaled or extensive, reaching up to several km in width (Zharikov et al., 2007); the presence of fenitised borders to a carbonate complex is often considered convincing evidence for the occurrence of magmatic carbonate (Kresten, 1988). Fenites are often associated with hydraulic fracturing and brecciation, exhibiting temporal, spatial, mineralogical and chemical variations resulting in both horizontal and vertical zoning (Elliott et al., 2018).

Elliott et al. (2018) argued that fluids derived from cooling alkaline magmas or carbonatite intrusions transport high quantities of alkalis and volatiles, resulting in the loss of these constituents in the carbonatite rock, and stated that intrusion descriptions are incomplete without the characterisation of their associated fenites.

Carbonatites are commonly associated with micaceous metasomatic rocks consisting of almost entirely mica minerals commonly known as glimmerites (Elliot et al., 2018). Phlogopite is the main mica mineral present in glimmerites seen in the Bull Hill Complex in the United States, Aley and Upper Fir in Canada, the Sokli Complex in Finland and Mount Weld in Australia (Elliot et al., 2018). The rocks from these complexes were initially thought to be of igneous origin, but with recent observations regarding these complexes, it is evident that the mica minerals present in these rocks are not of primary igneous origin, but resulted from metasomatic alteration of Mg-rich country-rock due to carbonate intrusions (Elliot et al., 2018). Although the term 'glimmerites' has been traditionally used to describe ultramafic intrusive units, this document will adopt the same terminology used for the complexes mentioned above, where mica-rich rocks associated with carbonatites formed due to metasomatic alteration of Mg-rich country rocks will be termed glimmerites.

2.1.2 Summary

Viljoen (1966) argued that due to the vertical tongue and finger structures seen in the carbonatite and phoscorite bodies cut at depth by borehole SC22, a carbonatite-phoscorite pipe had to be present close to this borehole which he proposed to be deeper than the borehole depth of 426m. He added that the phosphate mineralisation is disappointing, as the complex contains a lower grade than that of the Phalaborwa Complex, and that the structure and distribution of the phosphate zone would only allow for less-favourable selective mining operations.

Viljoen (1966) cited insufficient laboratory work undertaken as a hindrance in generating a full petrological report. Table 1 provides a summary of the investigation on the petrography of fresh core pyroxenite, phoscorite and carbonatite rocks performed by Viljoen (1966).

Table 1: A summary of the investigation performed by Viljoen (1966) on the pyroxenite-phoscorite-carbonatite components from the Schiel Complex.

Rock Type	Hand-sample Description	Mineralogy	Accessory Minerals	Alteration Minerals	Structure	Notes:
Pyroxenite	Medium-grained, dark-green and compact with variable mineralogy that changes on a small-scale	Diopside, augite and enstatite pyroxene and phlogopitic and biotitic mica	Calcite, apatite, magnetite and feldspar	Chlorite and amphibole	Tongue and lens structures originating roughly in the centre of the main syenite body cross-cut by later syenite veins; sharp or gradational contacts with the other Schiel Complex components	Serpentine- and magnetite-rich pyroxenites are present; some areas of the pyroxenite were extremely mica-rich and could better be described as glimmerite; pyroxenite is also present as lens and tongue satellite bodies in syenite; pyroxenites in contact with carbonatite are light grey and calcite-rich
Phoscorite	Grey to very dark-grey containing coarse grains, which are in some cases pegmatite-like	Magnetite, phlogopite, calcite, apatite, diopside, enstatite and augite pyroxene and forsterite	Biotite	Amphibole and serpentine (antigorite and iddingsite)	Tongue and lens structures originating roughly in the centre of the main syenite body	The phoscorite component is described as containing similar chemical and petrographic characteristics as the pyroxenite; phoscorite was distinguished from pyroxenite based on the increased serpentine and magnetite content; a lesser amount of phoscorite is present than pyroxenite
Carbonatite	Coarse-grained, light- to dark-grey rocks which sometimes contain thin bands or foliations of mafic minerals	Magnesium-rich calcite	Apatite, phlogopite and biotite, diopside, enstatite and augite pyroxene and magnetite	Serpentine, tremolite, actinolite, hornblende and chlorite	Veins that penetrate the other igneous rocks; thin vertical veins at depth; veins vary in size from a few centimetres to 10 m; gradational contacts are seen between the carbonatite and other components of the Schiel Complex	No significant copper mineralisation

2.2 Schiel Complex Literature Review

2.2.1 Schiel Complex Geological Setting

The Schiel Complex is located in the Southern Marginal Zone of the Limpopo Belt and crops out over an area of approximately 130 km^2 (Stettler et al., 1993; Graupner et al., 2018). A geological map of the Schiel Complex is provided in Figure 1. The Schiel Complex consists of three large pluton-sized intrusions - Schiel, Mashua and Rivola - along with several other smaller ones (Barton et al., 1996). The Schiel pluton is the largest, has a funnel shape, and was emplaced between the southeast-verging Hout River and Ntabalala shear zones. The more sheet-like Mashua and Rivola intrusions both lie to the north of the Ntabalala shear zone (Barton et al., 1996). The Mashua and Rivola intrusions consist predominantly of syenite and quartz syenites. The Schiel pluton is more lithologically complex having syenite, quartz syenite, hypersthene syenite and hornblende granite (Barton et al., 1996), consisting of predominantly feldspathic phases along with a substantially smaller volume of phoscorite-carbonatite-like rocks in the eastern section. The Schiel Complex intruded into the Baviaanskloof Gneiss and the Bandelierskloof Formation, which are the predominant components of the Archean crustal basement in this region (Walraven et al., 1992; Lubala et al., 1994).

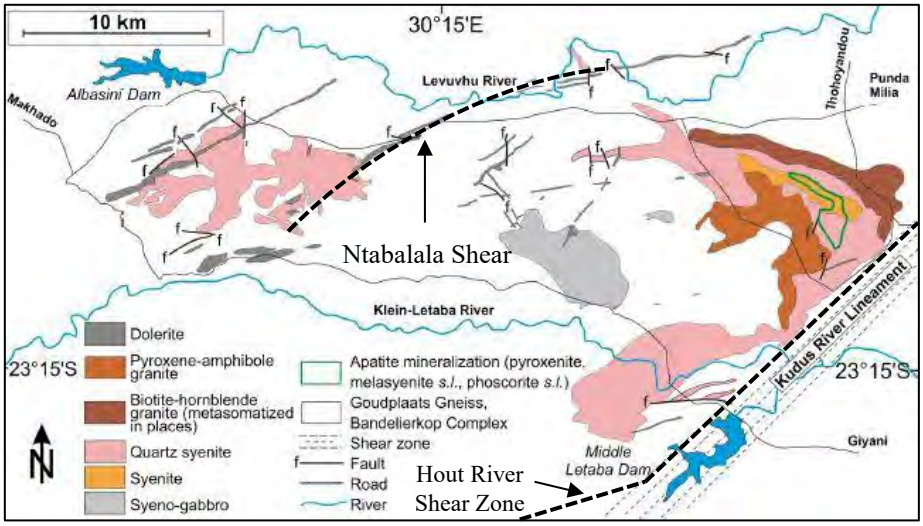

Figure 1: Geological Map of the Schiel Complex (Modified after Graupner et al. (2019))

2.2.1.1 Western Limb

The Mashua and Rivola plutons are situated in the western limb of the Schiel Complex. These intrusions are believed to be contemporaneous with the quartz syenite of the eastern section based on macroscopic similarities (Stettler et al., 1993). The quartz syenites were extensively intruded by dolerite dyke swarms which show gradational contacts between the two units, suggesting that these dykes were emplaced before the complete crystallisation of the quartz syenite (Stettler et al., 1993; Lubala et al., 1994). This section of the Schiel Complex does not incorporate the geological units of interest for this study.

2.2.1.2 Eastern Limb

The Schiel pluton is situated in the eastern limb of the Schiel Complex and is the larger sub-complex. Figure 2 shows a more detailed geological map of the eastern limb of the Schiel Complex that shows the structure of the phoscorite, pyroxenite and carbonatite bodies: present as veins hosted in a high volumetric abundance of syenite. Geophysical modelling and field observations performed by Stettler et al. (1993) suggests that the eastern limb of the complex resembles an annular structure consisting of funnel- or plug-shaped bodies emplaced at shallow depth. The syeno-gabbro, situated in the centre of the Schiel Complex, is also considered to be part of the eastern limb and contains intrusions of dolerite dykes that display sharp contact zones between the two units (Stettler et al., 1993). Geophysical modelling performed by Stettler et al. (1993) provided a gravity model that shows the pyroxenite-phoscorite-carbonatite body and the syenogabbro extending to a maximum depth of approximately 500 m and 800 m, respectively. In contrast, magnetic modelling undertaken by the same authors showed that both bodies extend to approximately 800 m in depth.

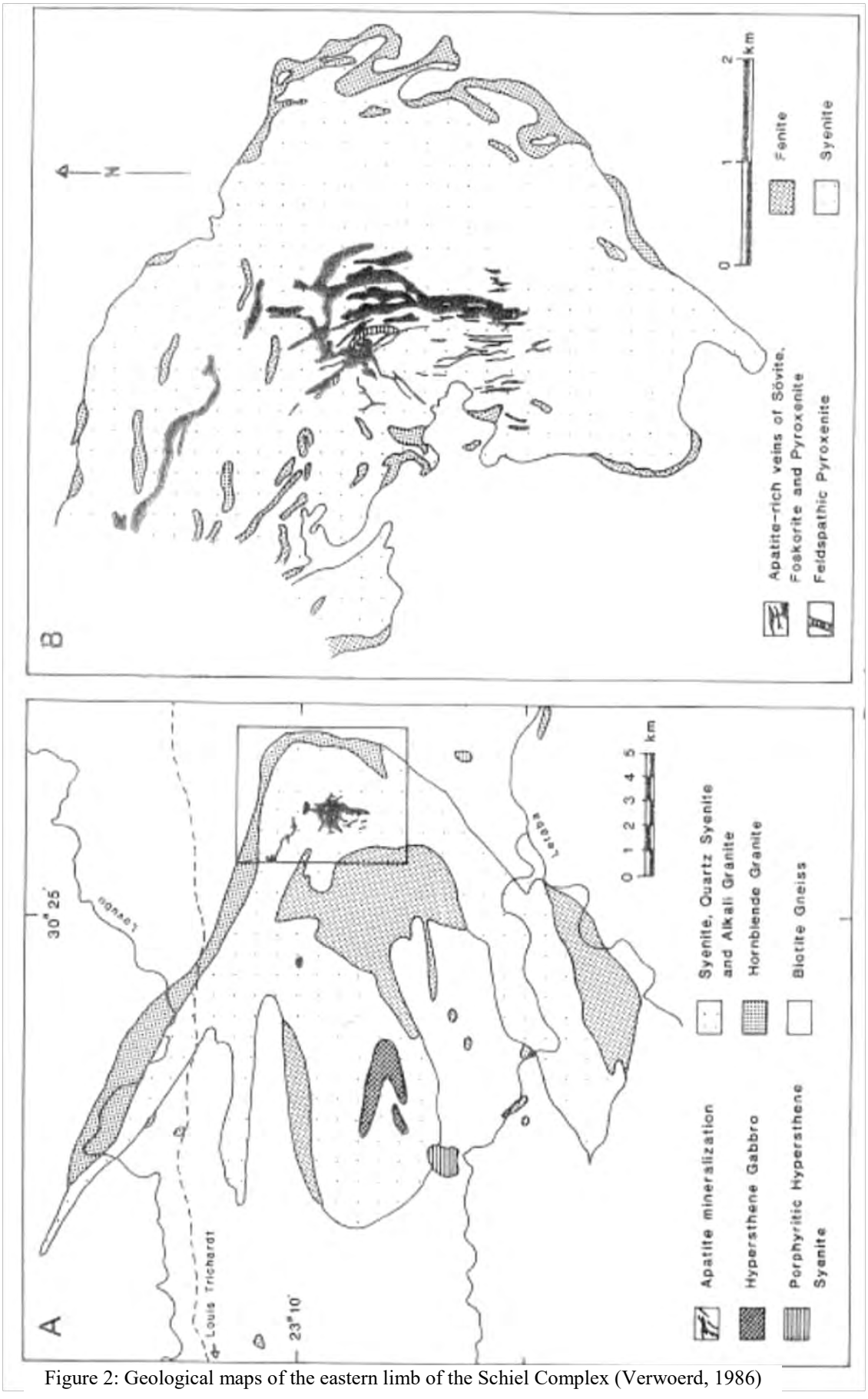

Figure 2: Geological maps of the eastern limb of the Schiel Complex (Verwoerd, 1986)

2.2.2 Petrology and Geochemistry of the Schiel Complex Geological Units

Petrological descriptions of the Schiel Complex felsic units are provided by Graupner et al. (2018), Barton et al. (1996), Lubala et al. (1994) and Verwoerd (1986); Lubala et al. (1994) presenting major and trace element analyses of these units. In addition, Graupner et al. (2018) and Verwoerd (1986) reported petrological studies on pyroxenite and phoscorite samples, with Graupner et al. (2018) also analysing the whole-rock geochemistry, with a focus on REE mineralisation, of syenite, phoscorite and pyroxenite samples from the Schiel Complex. Verwoerd (1986, 1993) is the only author to provide descriptions of the Schiel carbonatites.

2.2.2.1 Felsic Rocks

Lubala et al. (1994) described amphibole biotite-bearing syenite, pyroxene amphibole biotite-bearing syenite and pyroxene biotite-bearing granite as the main felsic components of the Schiel Complex. Barton et al. (1996) described the petrology of a series of syenite, quartz syenite and granite samples, stating that the major minerals present are microcline, orthoclase, quartz and aegirine-augite accompanied by albite, biotite, calcite, diopside and hornblende with accessory apatite, zircon, sphene, magnetite and pyrite. They also state that all the samples had experienced variable degrees of deuteric and vein-controlled hydrothermal alteration.

Lubala et al. (1994) showed that the average composition of syenites are alkaline to slightly peralkaline in nature with the syenites and granites forming two distinct populations with relation to K and Na affinities when plotted on a K-Na-Ca ternary diagram; with the evolution from syenite to granite characterised by an inverse variation of TiO_2, Al_2O_3, FeO, MgO, CaO, K_2O and P_2O_5. Chondrite normalised rare earth element (REE) patterns in syenites and granites show a steep, but progressively smooth decrease from light rare earth element (LREE) to heavy rare earth element (HREE) with no significant depletion in Eu (Lubala et al., 1994). Extreme LREE enrichment of the syenites and granites is also reported by Barton et al. (1996). They showed the quartz syenite to contain a lower total REE content than the granite, which contradicts a chondrite normalised REE diagram plotted by Lubala et al. (1994) which showed all syenite samples to have a higher total REE content than the granites. Correlation trends of major element oxides in total alkali silica (TAS) and Harker diagrams demonstrated by Graupner et al. (2018) show that the silicate rocks are primarily a product of fractional crystallisation.

Graupner et al. (2018) described syenites and melasyenites as having a wide variation of mafic mineral modal abundances between 30 and 75 vol% of diopside, hedenbergite and aegirine-augite, along with quartz, alkali feldspar and potassic feldspar, with accessory zircon, magnetite and pyrite. They also describe minor secondary amphibole as replacement features after clinopyroxene.

Verwoerd (1986) is the only author to describe fenitisation of the syenitic rocks: fenitisation retaining the texture of the syenite, the fenitised syenite being more leucocratic with significantly less quartz. The presence of fenites provides evidence that metasomatic alteration of the syenites has occurred, most likely due to later carbonate magmatism, which is in contrast to the sequence of magmatic events described by various authors in Section 2.1.2.

2.2.2.2 Mafic Rocks

Verwoerd (1986) described the pyroxenite and phoscorite as intimately associated and challenging to distinguish, stating that the phoscorite is less plentiful and forms thinner bands. He described the pyroxenite as consisting of predominantly clinopyroxene, together with phlogopite, apatite, calcite, magnetite, K-feldspar and serpentine and usually weathered to a depth of 45m, the weathered sections consisting of limonite, goethite, montmorillonite and vermiculite. Phoscorite is described as an assemblage consisting of magnetite, phlogopite and apatite, together with lesser amounts of calcite, clinopyroxene and serpentine, containing remnants of forsterite, with biotite as an accessory mineral. Verwoerd (1986) alleged that the Schiel Complex phoscorites have higher apatite contents than the Phalaborwa phoscorites, based primarily on the Foskor exploration report compiled in November 1966 (Viljoen, 1966).

Graupner et al. (2018) described two mafic rocks which would represent alterations of primary assemblages:
(1) a pyroxenite consisting of 70-80 vol% diopsidic clinopyroxene, magnetite, phlogopite as well as secondary chlorite, serpentine and quartz, together with the occasional replacement of diopside by tremolite; allanite, ilmenite and secondary monazite are described as accessory minerals;
(2) a representation of an altered former phoscorite which contains 60-80 vol% vermiculite, 5-30 vol% apatite, 5 vol% sulphides and magnetite, as well as accessory phases of thorite, Th-dominated REE phosphate and zircon and secondary monazite and rhabdophane.

Graupner et al. (2018) reported whole-rock chemical data for three altered pyroxenite samples and two altered phoscorite samples. They showed the phoscorite samples to contain the highest P_2O_5 contents of between 2.3 and 2.7 wt.%, whereas the pyroxenite samples contained P_2O_5 contents of between 0 and 2 wt.%. They also showed that syenite samples contained the highest total REE content even though low P_2O_5 contents (<1.6 wt.%) were recorded, with two syenite samples containing higher total REE contents than the mafic rocks but containing less than 0.2 wt.% P_2O_5. These analyses show that apatite may not be the primary REE carrier in the Schiel Complex.

2.2.2.3 Carbonatites

Verwoerd (1986, 1993) described a 10m thick borehole intersection of sövite from the Schiel Complex as comprising magnesian calcite with significant apatite, phlogopite, magnetite, clinopyroxene with rutile, feldspar, disseminated copper and iron sulphides (chalcopyrite, cubanite, pyrite and pyrrhotite) as accessory phases. Horstmann and Verwoerd (1997) analysed carbon and oxygen isotope composition of Schiel Complex carbonatite samples which were calcite-dominated, consisting of only minor dolomite. They detected $\delta^{13}C$ (-4.8 to -5.2) and $\delta^{18}O$ (8.5 to 9.8) values with little variation, both within the range representing primary igneous carbonatites and appear to have retained their primary igneous C and O isotope composition (Horstmann and Verwoerd, 1997).

2.2.2.4 Summary

Published petrological and geochemical data available regarding the phoscorite-pyroxenite-carbonatite units of the Schiel Complex, the focus of this study, is lacking and has not been documented sufficiently. In addition, the weathered nature of these rocks to depth, as described by Verwoerd (1986), provides doubt about the integrity of all the analyses performed by Graupner et al. (2018) on trench and surface samples of the Schiel Complex phoscorite and pyroxenite units.

2.2.3 Schiel Complex Emplacement

Lubala et al. (1994) argued, on the basis of field observations and geochemical features, that partial melting of lower or intermediate levels of thick continental crust induced by injection of volatile-rich basic magma of mantle origin, is the favourable mechanism in generating the felsic rocks of the Schiel Complex. The Schiel Complex syenites have high Pb contents (15-76 ppm) as well as extremely high initial $^{87}Sr/^{86}Sr$ ratios (0.7292-0.7582) (Barton et al., 1983). These Sr ratios are significantly higher than those expected for mantle-derived magmas and would require an ancient high Rb/Sr protolith, which is unlikely to be present in the lower crust. Lubala et al. (1994) argued further that the high alkali content and LREE enrichment of the Schiel Complex felsic rocks, considering a dominantly crustal source, could be explained by intrusions of hydrous mafic magmas into a granulite facies basement, generating extensive granitic and syenitic magmas by the transmission of heat and volatiles, with the addition of alkalis and incompatible elements needed in order to generate the syenitic magma in the developing crustal melt. The emplacement of the Schiel Complex granites and syenites could have been controlled by the pre-existing faults of the Kudus River Lineament shear zone (Stettler et al., 1993; Lubala et al., 1994; Walraven et al., 1992) and Lubala et al. (1994) argued that substantial lateral movement of this fault, after the compressional stage of the Limpopo orogeny, allowed the upward channelling of mantle-derived primary ultrabasic and carbonatite magma and H_2O-CO_2 fluids into the crust.

Stettler et al. (1993) also provided a second mechanism for the development of the alkaline magmatism: they argued that the magmatism could be related to the transition, occurring along a major thrust fault

and ductile shear zone system, between rocks of the Southern Marginal Zone (SMZ) of the Limpopo belt and low-grade granite-gneiss to the south. They argued that the transportation of rocks from the Central Zone of the Limpopo belt to the west, along major wrench faults in post Bushveld times (±2050 Ma), together with the simultaneous transportation of rocks from the SMZ to the south, allowed movement along thrust faults and shear zones in Bushveld and post-Bushveld times, resulting in relaxation in the lithosphere and associated alkaline magmatism. The undeformed nature of the Schiel Complex rocks, their magmatic mineral associations and the lack of metamorphism indicate that the emplacement of these rocks occurred after the cessation of the main tectono-metamorphic event in the SMZ of the Limpopo Belt (Stettler et al., 1993).

Stettler et al. (1993) reported differences in magnetic signatures between the western and north-western zones of the eastern limb of the complex. They identified differences in magnetic rock type of two arcuate, sub-parallel bodies in the eastern limb through radiometric data, concluding that the eastern limb of the Schiel Complex must have been emplaced as a multi-intrusional event.

Barton et al. (1996) argued a younger age of emplacement of the Schiel pluton (1853 ± 6 Ma) than the proposed age of ±2060 Ma (Walraven et al., 1992, Stettler et al., 1993 and Lubala et al., 1994), and that the magma was generated in old continental lithospheric conditions, which assimilated a small amount of Archean crust material as well as an unidentified 2.0 Ga rock. Barton et al., (1996) based this observation on concordant U-Pb ages for zircon grains, as well as taking into account the unmetamorphosed nature of the Schiel pluton. They argued that the Schiel Complex postdates the Bushveld and Phalaborwa intrusions and could be linked to rifting accompanying the deposition of the Soutpansberg trough.

Stettler et al. (1993); Walraven et al. (1992) and Lubala et al. (1994) all propose two episodes of magmatism for the emplacement of the eastern section of the Schiel Complex: (1) the first episode was the intrusion of a WNW-ESE trending, 7km long, elongated body of glimmerite, phoscorite and carbonatite, proposed to have originally been a continuous plug, that was broken up and altered by later intrusions of quartz syenite and a pyroxene-amphibole granite; (2) the second magmatic episode was the intrusion of a significant body of shonkinitic gabbro, of which a small satellite body containing xenoliths of pyroxene-amphibole granite intruded into the quartz syenite.

By contrast, Verwoerd and Du Toit (2006) argued that the poorly exposed shonkinitic gabbro was intruded after the pyroxenite-phoscorite-carbonatite body, but before the quartz syenite body/bodies, and further stated that intrusions of pyroxene-amphibole granite and possibly biotite-hornblende granite were the last intrusive phases.

2.2.3.1 Phoscorite-Carbonatite Complex Genetic Models

Although little information regarding the genesis of the Schiel Complex phoscorite/pyroxenite and carbonatite units exist, it has been argued that similar mineralogical and geochemical characteristics, coupled with close spatial association, suggest that phoscorite-carbonatite rock pairs are derived from a common parental magma (Krasnova et al., 2004). Phoscorite formation is proposed to be a result of the segregation of high-temperature phases, together with the separation of a carbonate-rich magma (Vartiainen, 1980). Alternatively, a second school of thought suggests that the carbonatite fractions of phoscorite-carbonatite associations represent carbonate cumulates formed by crystal fractionation (Gittins, 1989).

Based on a geochemical study of pyrochlore from the Sokli carbonatite-phoscorite complex, Lee et al. (2006) argued that, from a magmatic perspective, the chemical contrast seen between phoscorite and carbonatites may be a result of both fractional crystallisation and liquid immiscibility processes acting upon a common parental melt. They disregarded the process of liquid immiscibility as the sole process for phoscorite-carbonatite formation based on the occurrence of similar mineral assemblages that contain similar chemical compositions between both rock pairs in the same evolutionary stage. Lee et al. (2004) disregarded fractional crystallisation as being the sole process for the genesis of these rock pairs due to the sizeable compositional gap between the two rock types, leading to the unlikely nature that both rocks are cumulates. It is therefore concluded that a combination of both fractional crystallisation and liquid immiscibility processes would be the most likely processes in producing these rare rock types.

Lee et al. (2004) proposed that liquid immiscibility is the most probable process in the genesis of phoscorite and carbonatite pairs, and considered phoscorites as Fe-rich rocks rather than Si-rich rocks, which is an essential assumption as it explains the relevant immiscibility between Fe-Ti-rich and carbonate-rich melts. This hypothesis explains the presence of P in both phoscorite and carbonatite components, as phosphorous partitions towards carbonate melts in carbonate-silicate pairs, but is a crucial component of Fe-Ti-rich melts that are immiscible with silicate pairs. Experimental studies on the immiscibility between Fe-Ti-rich and carbonate-rich melts are yet to be explored (Lee et al., 2004). Lee et al. (2004) proposed that some fractional crystallisation must have occurred before melt segregation due to similar chemical compositions of minerals in both associated rock pairs. The presence of carbonatite-bearing minerals in the silicate rocks and silicate-bearing minerals in the carbonatite rocks provide further evidence that some fractional crystallisation must have occurred before melt segregation. The different densities, interfacial energies and viscosities of the two liquids may also capture variable phenocryst populations, so that immiscibility may drive some accumulation (Lee et al., 2004).

Similarly, Giebel et al. (2019) argued in favour of multi-episodic crystallisation processes, based on the phoscorite-carbonatite components of the Phalaborwa Complex, due to the similar trends seen in chemistry from micas of carbonatite and phoscorite bodies. They also supported liquid immiscibility for generating phoscorite-carbonatite rock pairs from a carbonate-phosphate/iron-oxide-rich (CPIO) parental magma developed in the upper lithospheric mantle, which addresses the exclusivity of phoscoritic rocks occurring in the presence of carbonatites. However, they differ from Lee et al. (2004) in adding that the CPIO melt is developed from a carbonatitic melt, due to Fe and P partitioning into the carbonatitic melt during silicate-carbonate melt separation. Giebel et al. (2019) predicted that the CPIO magma remains below the crust where it becomes denser through the enrichment in P and Fe until equilibrium with the silicate melt is reached, allowing for a state of levitation of the CPIO melt within the more voluminous silicate melt. These melts could then exploit weak zones in the crust allowing for the channelised magma ascent of both magmas, where decreasing temperature and/or pressure may drive liquid immiscibility of carbonatitic and phoscoritic magmas from the CPIO melt (Giebel et al., 2019).

It is, however, essential to note that these theories cannot be properly assessed until experimental melting and crystallisation studies are undertaken that explore the role of iron and phosphorous in Fe-rich, silicate and carbonate liquids (Krasnova et al., 2004).

2.2.4 Geochronology

Walraven et al. (1992) performed the first geochronological study of the Schiel Complex units: their whole-rock Pb-isotopic data interpreted as indicating an emplacement age of 2059 +35/-36 Ma for the complex. This emplacement age was, however, obtained from a composite of the eastern limb quartz syenite, western limb quartz syenite and gabbro data. Stettler et al. (1993) supported the age determination provided by Walraven et al. (1992) based on the undeformed nature, magmatic mineral associations and the dissapearance of dyke traces in the eastern limb of the Schiel Complex, as their emplacement is thought to be attributed to the exploitation of a tectonic grain formed during tectonometamorphic events in the SMZ. Therefore, Stettler et al. (1993) argued that these factors provide evidence that the complex must have been emplaced after the cessation of the main tectonometamorphic event in the SMZ of the Limpopo Belt. Walraven et al. (1992) attempted to date the alkali granite from the eastern limb of the Schiel Complex, which surrounds the phoscorite-carbonatite rocks. However, implausibly old results were obtained that were inconsistent with petrographic observations, leading to their suggestion that the alkali granite originated by alkali metasomitsm of the acidic country-rocks during the Schiel Complex emplacement, and is not part of the Schiel Complex. This argument is supported by a radiometric survey performed by Stettler et al. (1993), who distinguished between the granite and syenite based on the enrichment of K in the granite

relative to the syenite, stating that at least a significant proportion of the granite is not part of the intrusive complex.

These age ranges are all inconsistent with those of Barton et al. (1996), who analysed U-Pb in 22 zircons from quartz syenites and granites. The weighted mean date from 6 zircon grain yielded the significantly younger date of 1853 ± 6 Ma which Barton et al. (1996) interpreted as the emplacement age of the Schiel Complex, on the assumption that no Pb-loss could have occurred in these zircons due to the unmetamorphosed nature of the rocks. Barton et al. (1996) also generated a date of 2005 ±7 Ma from the weighted mean of 6 other grains, which they interpret as the age of the older hornblende granite unit into which the Schiel quartz syenite intruded.

Laurent and Zeh (2015) reported U-Pb zircon ages of 2051 ± 6 Ma from 2 syenite samples; and 2054 ± 4 Ma from samples of phlogopite- and apatite-rich websterite, associated with the Schiel Complex alkali gabbros. These results are consistent with the age ranges obtained by Walraven et al. (1992) but are significantly older than those of Barton et al. (1996).

Most recently, Graupner et al. (2018) published zircons dates derived from altered phoscoritic and syenitic rocks sampled in weathered surface exposures and in trenches. Their Laser Ablation Inductively Coupled Mass Spectrometry (LA-ICPMS) U/Pb zircon measurements yield concordant dates of 2060.5 ± 5 Ma and 2059.8 ± 4 Ma for the phoscorites; and 2050.1 ± 9.9 Ma for the syenite. Despite these dates being statistically indistinguishable, Graupner et al. (2108) concluded that the formation of phoscorite rocks slightly predates the emplacement of the syenitic rocks.

2.2.4.1 Summary

Although the felsic rocks of the Schiel Complex have been the target for several geochronological studies, only Laurent and Zeh (2005; a websterite associated with the Schiel gabbros), and Graupner et al. (2018; altered phoscorite samples) provide geochronological data for the ultramafic components of the Schiel Complex.

The similarity in isotopic dates for these two units, however, conflicts with the Stettler et al. (1993) argument based on geophysical data that the difference in magnetic anomaly patterns between the syenogabbro and pyroxenite-phoscorite-carbonatite rocks was a result of non-contemporaneous intrusions of the two units.

It is clear, therefore, that some uncertainty remains regarding the absolute emplacement age of the Schiel Complex phoscorite-pyroxenite-carbonatite units.

2.2.5 Concluding Remarks

Stettler et al. (1993) described dolerite dykes in the western limb of the Schiel Complex cutting through the quartz syenite, where gradational contacts between the two units are observed, as evidence that these units were emplaced contemporaneously. However, the same dykes are found in the eastern limb cutting through the supposedly youngest intrusion of syenogabbro (Lubala et al., 1994 and Stettler et al., 1993) containing sharp contacts (Stettler et al., 1993). Laurent and Zeh (2005) dated a websterite associated with the Schiel gabbros and showed that the websterite is older than the syenite. Although Stettler et al. (1993) argued that the emplacement of the dykes in the western limb is evidence of the thin nature of the syenitic body, the presence of the dykes in the 800m thick (Stettler et al. 1993) syenogabbro (containing sharp contact zones) flaw the proposition that this unit was part of the last magmatic episode, emplaced after the Limpopo tectono-metamorphic event and having no preferred grain for the dykes to exploit. Therefore, Verwoerd and Du Toit (2006) provided a more suitable sequence of magmatic episodes. Fenitisation seen in the syenitic rocks of the Schiel Complex described by Verwoerd (1986) also suggests that magmatism containing a fenitising fluid, possibly carbonatitic, must have intruded after the emplacement of the syenites.

The date obtained for the phoscorite by Graupner et al. (2018) may not be completely reliable based on the nature of their sampling scheme and the samples that they analysed. It is clear that no reliable ages for the phoscorite or carbonatite components from the Schiel Complex exist.

The phoscorite-carbonatite components from the Schiel Complex have been poorly documented due to the mostly unexposed nature of the rocks, with expensive borehole coring the only means of gathering fresh rock samples. The only published studies regarding geochemistry or petrology were performed by Graupner et al. (2018), who analysed the phoscorite and pyroxenite components of the Schiel Complex using altered surface and trench sample material, and by Horstmann and Verwoerd (1997) who analysed the carbon and oxygen isotopes in the carbonatite rock. The only other study regarding the phoscorite-carbonatite components was a geophysical investigation by Stettler et al. (1993) where the morphology of the pyroxenite-phoscorite-carbonatite unit was interpreted.

2.3 Aims and Objectives

The main goal of this study is to characterise the available sample suite of the phoscorite, pyroxenite and carbonatite components from the Schiel Complex in the Limpopo Province of South Africa. This will be the first petrological study carried out on in-situ, fresh core samples since FOSKOR's exploration report which was developed in 1966, which was primarily focused on the economic aspects of the complex and contained insufficient analytical work to characterise the associated rock components accurately. The main aims of the study are;

1. To comprehensively characterise the mineralogical and geochemical makeup of the sampled suite of the ultramafic and carbonatite components of the Schiel Complex, with the aid of electron probe micro-analyser (EPMA), whole-rock X-ray fluorescence (XRF), trace element inductively coupled plasma mass spectrometry (ICP-MS) and secondary ion mass spectrometer (SIMS) geochronology data.
2. To evaluate whether the Schiel Complex ultramafic rocks are consistent with other known phoscorite-carbonatite complexes and does the Schiel Complex contain rocks that resemble true phoscorites?
3. To determine possible clues regarding the ultramafic-carbonatite magma genesis, evolution and crystallisation conditions:
    a. Do the Schiel Complex rocks represent magmatic components differentiated from a single parental magma and which processes may have occurred which are responsible for generating these distinct rock varieties?
    b. Did metasomatism affect the magmatic components of the Schiel Complex?
    c. Do the mineral compositions provide any chemical trends representing clues about magma evolution?
    d. Can these rocks be precisely dated in order to generate an exact emplacement age of the Schiel Complex ultramafic and carbonatite components? Are there faults in the proposed sequence of magmatic events presented in Chapter 2.2.3?
    e. To discuss the implications of these rocks being grouped as one of the extremely rare phoscorite-carbonatite complexes around the world, and whether they contain any common characteristics to similar units from the Phalaborwa Complex; does the Schiel Complex have similar economic potential to the Phalaborwa Complex?

Chapter 3: Schiel Complex 1966 Diamond-core Samples

Five available Schiel Complex diamond drilled cores were interrogated at the National Core Library located at Donkerhoek in Pretoria, South Africa which is managed by the Council for Geosciences. These cores were drilled in the eastern limb of the Schiel Complex by Foskor in 1965-66 and form part of the exploration program described in the unpublished report of Viljoen (1966). The exact locations of the curated borehole cores are shown in Figure 3 along with the positions of the other exploration holes drilled by Foskor.

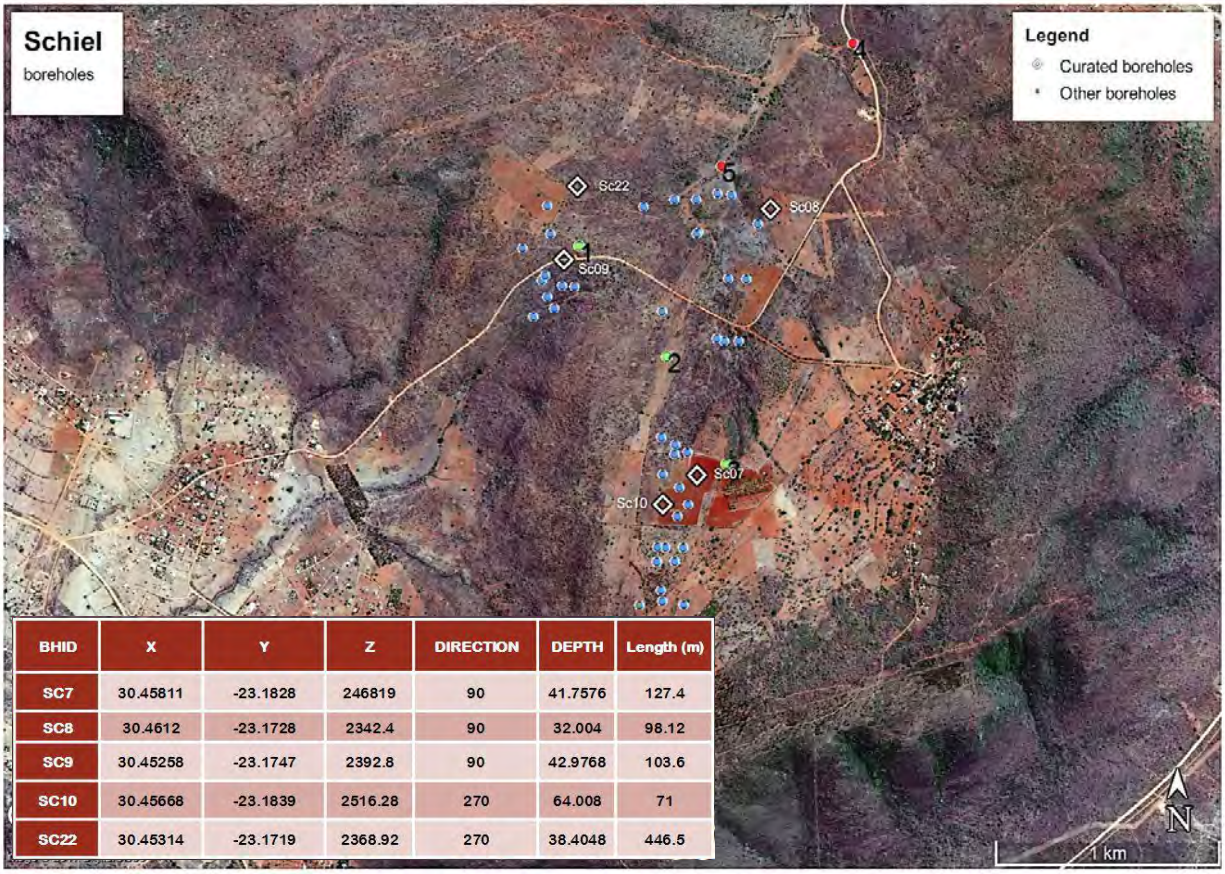

BHID	X	Y	Z	DIRECTION	DEPTH	Length (m)
SC7	30.45811	-23.1828	246819	90	41.7576	127.4
SC8	30.4612	-23.1728	2342.4	90	32.004	98.12
SC9	30.45258	-23.1747	2392.8	90	42.9768	103.6
SC10	30.45668	-23.1839	2516.28	270	64.008	71
SC22	30.45314	-23.1719	2368.92	270	38.4048	446.5

Figure 3: Map containing the borehole locations and location details for the curated boreholes sampled.

3.1 Ultramafic Rocks

The ultramafic rock types present in core SC10 are heterogeneous and consist of varying modal abundances of mica, magnetite, apatite and pyroxene; different rock compositions always grading from one into the other. High silica minerals such as quartz and feldspar are absent. Three different rock types were identifiable in hand specimens: these are proposed as being end-member ultramafic rock compositions; and are:

(1) a medium-grained, dark-grey to black rock consisting of predominantly black vitreous micaceous minerals interspersed with nodules of dull white calcite together with green mafic minerals;

(2) a much heavier rock that contains large magnetite crystals, < 5 cm in size, hosted in medium-grained, green mafic material that incorporates minor amounts of mica. Areas of the rock that contain carbonate material contain fine-grained magnetite grains and a higher abundance of mica;

(3) a predominantly medium- to fine-grained rock that is a darker-green colour than rock (2) and contains the highest modal abundance of pyroxene together with fine-grained magnetite and micaceous material and fine, white veinlets and nodules of calcitic material.

These end-member compositions show clear macroscopic differences to each other, as seen in Figure 4, and are named in accordance with their dominant assemblages, as well as taking into account the rock names provided by previous studies on fresh core samples from the Schiel Complex rocks.

Rock type (1) is classified based on the high mica content. Viljoen (1966) described mica-rich pyroxenites containing with extremely mica-rich sections which he suggested was the result of metasomatic alteration. This rock type will be named a glimmerite.

Rock type (2) is regarded as a phoscorite as its mineral assemblage conforms to range of phoscorite assemblages described by Krasnova et al. (2004) as well as the criteria used for phoscorite identification used by Viljoen (1966). These rocks will be named magnetite-rich phoscorites.

Rock type (3) is named a clinopyroxenite based on the high pyroxene content present in the rock which is consistent with the descriptions of high diopside content in the Schiel Complex pyroxenites provided by Viljoen (1966).

The ultramafic samples from core SC09 do not contain the same mafic mineral concentrations as compared to those from core SC10. These samples are light to dark-grey in hand specimen and are mica-rich rocks containing grains of olivine (or serpentine) present in close association to syenitic wall-rock. The sampled sections SC09-06 and SC09-08 are located at depths of 152 and 154 m, respectively, which is approximately 20 m deeper than the deepest sample from core SC10 (133 m). These samples will be described in a separate section and will be named olivine-bearing glimmerite due to high mica content, similar to that of the glimmerites from core SC10.

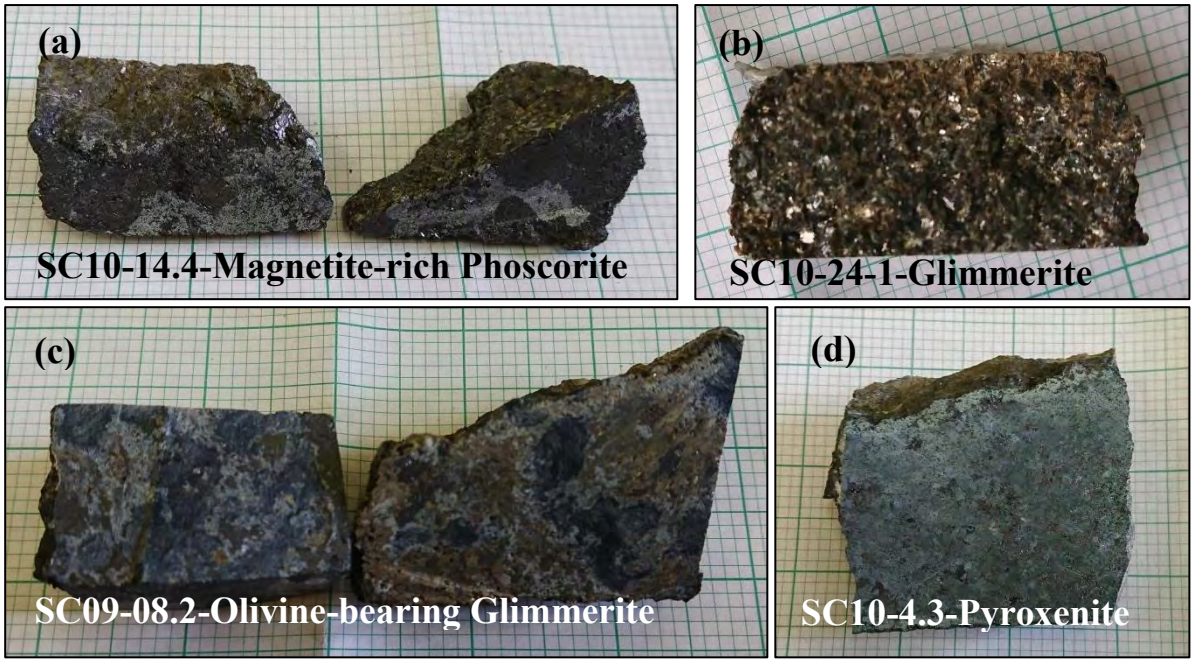

Figure 4: Hand specimen examples of the various Schiel Complex ultramafic rocks.

3.2 Carbonatite Rocks

Carbonatite rock hand specimens from core SC08 show varying modal abundances of mafic minerals distributed through a calcite carbonate-rich matrix: these range from individual phlogopite, apatite or magnetite grains interspersed with carbonate; to large areas/zones of mica-dominated ultramafic assemblages that appear to represent carbonatite-ultramafic or carbonatite-syenite rock reactions. Carbonate mineral grains vary in size with a generalised trend of larger calcite grains at depth (139 – 152 m) than in shallower (117-129 m) sections of the core. Although this observation is generally consistent, some samples do deviate from the trend sporadically throughout the core. Carbonatites displaying sporadic banded or schlieren textures are also interspersed throughout the core. Sections containing concentrations of preferentially aligned mafic minerals are limited in width, due to the mineral alignment being near perpendicular to the BQ size core trajectory. An exception is sample SC08-18 where the mineral alignment is parallel to the core length and is present throughout the entire sample (±46 cm).

Samples from core SC08 have been classified as three different carbonatite types: medium-grained carbonatite; coarse-grained carbonatite; and banded carbonatite. These categories were identified based on the distinct differences seen in textures of mafic minerals, as well as the calcitic matrix grain sizes. Examples of the different carbonatite types are depicted in Figure 5.

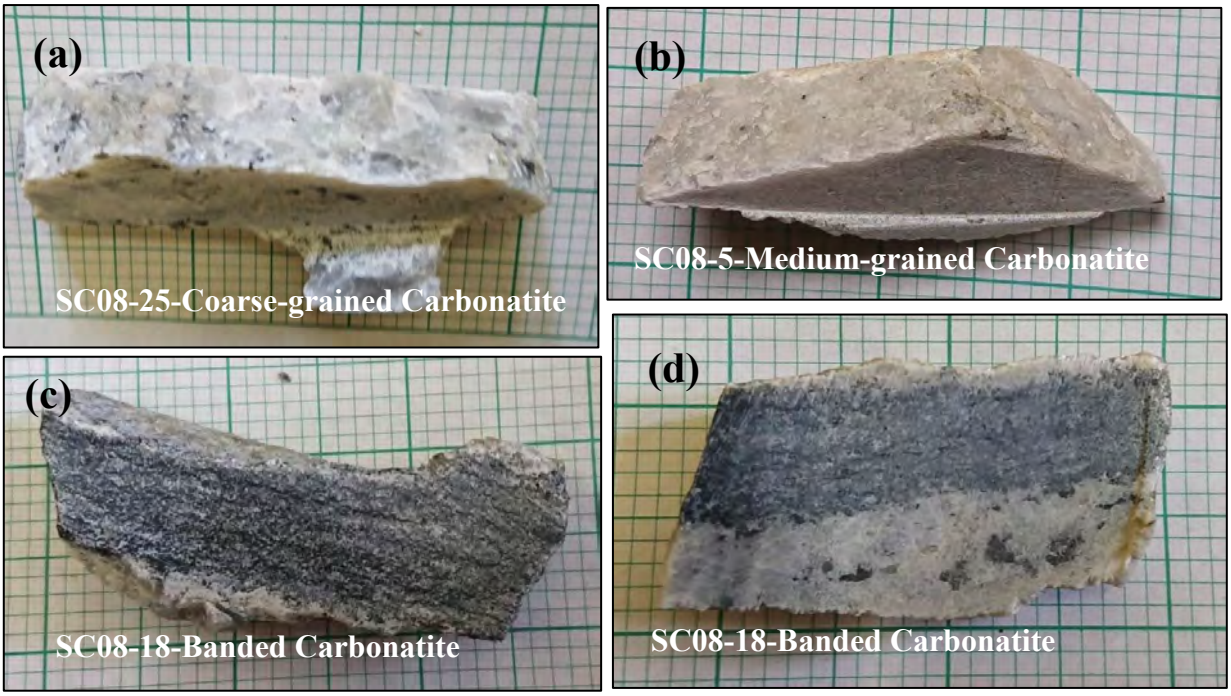

Figure 5: Hand specimen examples of the various Schiel Complex carbonatite rocks.

3.3 Rock Relationships

The cores show that the three major rock types, i.e. ultramafic, carbonatite and syenite rocks, described by the various authors in Chapter 2, are all intimately associated rocks where gradational contacts are always present between carbonatitic and ultramafic/syenitic rocks and mica-rich ultramafic and carbonatitic/syenitic rocks, together with rare sharp contacts present between mica-poor ultramafic and syenitic rocks. The ultramafic and carbonatite rocks are much less abundant than the syenites and are present as dyke and dykelet structures which are always bound by the extremely voluminous syenitic rock.

Core SC08 (59.7-157.8 m) was drilled using a BQ tube size (producing a ~36mm diameter core sample), and the only available sampling size of quarter cores makes the material sampled extremely limited. This core contains a high proportion (±50 %) of carbonatite material. Alternating zones of carbonatite and ultramafic rocks of a glimmeritic nature are present at approximately 30 cm to 1.5 m thick intervals, where these alternating zones are at smaller scales at deeper sections of the core. Abundant carbonatite veinlets having intruded into the felsic country-rocks show micaceous material produced as reaction products between the two units. Similarly, ultramafic rocks that are in contact to carbonate rocks are characterised by abundant mica content, which could indicate that these mica-rich rocks have been produced through reaction processes between the carbonatite and syenitic/phoscorite/pyroxenite wall-rock, creating glimmeritic zones that vary from mm up to 10's of cm in scale. Mica-poor ultramafic rocks are also present, but are restricted to being intrusive sheets in felsic rocks where no carbonatite is present, and vary from extremely fine-grained rocks to rocks that contain coarse (±3 cm) grains of

magnetite. At depth in the core, the presence of carbonatite is lost, and only alternating bands of glimmerite and syenite are present at scales of ±30 cm.

Core SC10 (64-135 m) is approximately 71 m in length and contains syenite (±80%) predominantly, together with ultramafic rocks, made up of alternating bands of glimmerite, pyroxenite and phoscorite. At a depth of 64-96 m, the core is mainly syenite with a thick band, ±3.6 m, of possible phoscorite between 82.3 and 85.9 m down core. Inter-banded syenite and mica-poor ultramafic rocks, at approximately 1.5m thick intervals, are present between 96 and 110 m down the core. Pyroxenite veins are present within syenite rocks, as seen in Figure 6(A), with no syenite veins seen in any ultramafic rock type. The carbonatite rocks are scarce in this core, but where present, they are bound by glimmerites, where mica seems to be formed as a reaction product between the carbonatite and the surrounding wall-rock, similarly as seen in core SC08. Carbonate material is present as both veins in glimmeritic rocks, as well as small carbonate blebs scattered throughout some glimmerites.

Core SC22 (52.7-505.3 m) is the longest core and contains similar characteristics to core SC09. Core SC22 was, however, drilled using a BQ tube size which hindered the sampling of this core, since limited amounts of material would have had to be sampled. These cores are composed of (with increasing depth): ultramafic rock bound by carbonatite, ultramafic rock hosted in syenite, ultramafic rock and carbonatite hosted in syenite, ultramafic rock hosted in syenite, and lastly, ultramafic rock and carbonatite hosted in syenite. This structure clearly shows vertical alternation of the ultramafic and carbonatite rock types. The presence of syenite throughout these cores, as a host to the other two rock types, at the highest volumetric concentration, shows that the syenites must have been the earlier magmatic event into which the carbonatite and ultramafic rock types intruded into. Core SC09 contains abundant coarse-grained olivine/serpentine in the ultramafic rocks, which was not observed in core SC10.

Core SC07 (54.8-182.2 m) contains a thick section of approximately 13 m of glimmerite (102.7-115.5 m) bound by syenitic country-rock, as well as containing a thick section, ±10 m, phoscorite/pyroxenite (64-73.8 m). Carbonatite rocks are always present as veinlets and are commonly seen to penetrate the ultramafic rocks, as well as both carbonatite and ultramafic veins penetrating surrounding syenitic country-rock, as seen in Figure 6(b). This figure may provide critical timing information regarding the three different rock types, as it is seen that the carbonatite vein cross-cuts an ultramafic vein within the syenite country-rock.

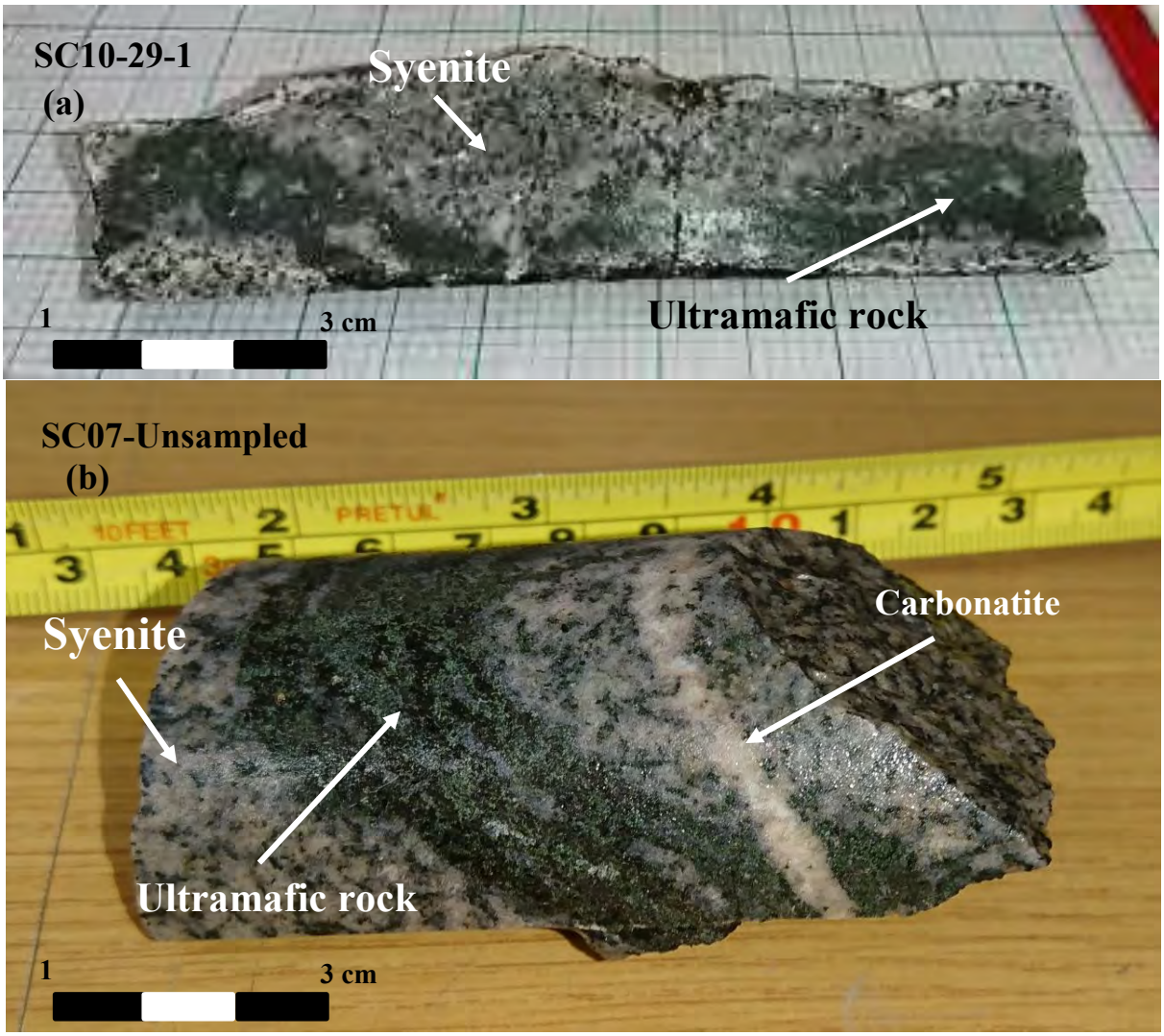

Figure 6: Hand specimen examples illustrating vein intrusions in syenitic wall-rock: (a) ultramafic rock vein intruding into syenite; (b) ultramafic and carbonatite veins intruding into syenite where cross-cutting relationships between the various units are observed.

3.3.1 Summary

The common occurrence of ultramafic and carbonatite vein intrusions in the more voluminous syenitic units, which always bound the intersections of ultramafic or carbonatite intrusions above and below, argues that the emplacement of the syenites must have been the first significant event in the Schiel Complex, with the ultramafic and carbonatite rocks being emplaced later.

Carbonatites almost always show reaction products of glimmeritic material when in close association to phoscorite, pyroxenite or syenitic rocks, as seen in Figures 7 and 8. These micaceous reaction product zones vary in width, ranging from mm scaled mica-rich bands, seen in Figure 7, to large mica-rich zones that are 10s of centimetres wide, as seen in Figure 8. The extent of the glimmeritic zones seem to be directly correlated to the thickness of the carbonatite intrusions, where larger carbonatite intrusions

produce larger glimmerite zones that contain gradational contacts between the carbonatite and the surrounding wall-rock, and thinner veins of carbonatite produce distinct, sharp and thinner reaction zones that form sheaths around the carbonatite, as seen in Figure 7. These veining features are a common occurrence, and would suggest that the carbonate phase would have intruded after syenite and phoscorite/pyroxenite intrusions, contrary to the current published data reported in Chapter 2.

The ultramafic units vary considerably from extremely mica-rich rocks to almost monomineralic pegmatitic magnetite-rich rocks, where gradational contacts are always observed between the various ultramafic rocks. Calcite is absent where mica-poor pyroxenite assemblages are observed, but seem to occur as small rounded blebs in phoscoritic assemblages, that contain a higher degree of mica crystallisation than pyroxenite assemblages.

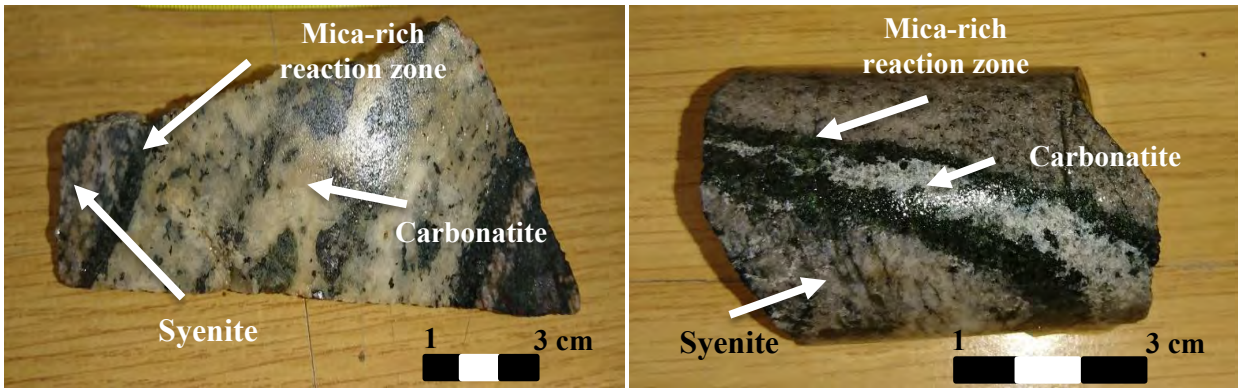

Figure 7: Hand specimen examples of carbonatite veins intruded into syenites which show sheaths of mica-rich reaction assemblages.

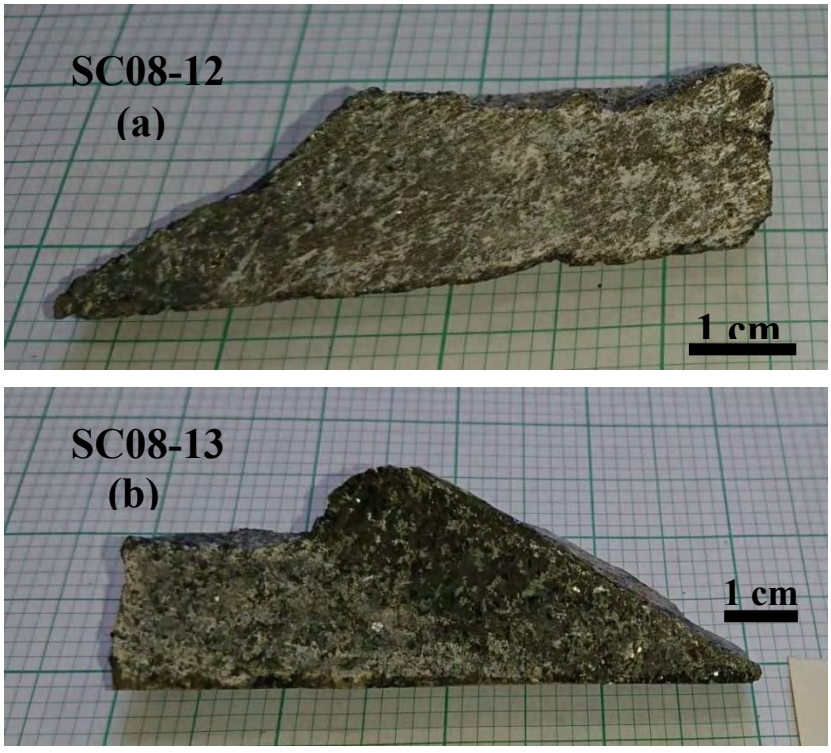

Figure 8: Mica-rich gradational contact zones present between carbonatite and phoscorite/pyroxenite rock units.

3.4 Sampling Scheme

Sampling of borehole cores by Foskor for the Viljoen (1966) investigation used half-core sections spilt mechanically and not sawed. As a consequence, the remaining half-core sections are of limited (typically <15-20cm) length and the volume of remaining material varies significantly. Only quarter core samples could be taken: this meant that an extremely limited amount of material available for analyses, especially from borehole SC8 where narrow diameter BQ sized core was recovered.

Three of the five available cores were sampled: cores SC10 and SC9 (both NQ cores) provided representative sections and comprehensive coverage of ultramafic material. A representative set of carbonatite material was sampled from BQ core SC08; care was taken not to select carbonatite only sections and to include contact zones and inclusions of mafic minerals. Appendix B provides a list of the samples, together with the depths of each sample. Thirty-two samples were collected from borehole SC10, ten samples from borehole SC9 and 25 samples from borehole SC8. Although the most extensively sampled cores SC10 and SC8 were drilled approximately 1.32 km apart, they were selected as containing the most representative sections of each respective geological unit amongst the 5 curated cores. They also provided sections showing the mutual relationships between the ultramafic, felsic and carbonatite components.

Owing to the short lengths of the mechanically split core sections, zones of some cores showed evidence of disturbance: “snaking” (inversion of core section – “up” switched with “down”) of core; or possible displacement of samples within core boxes (sections moved from one row of the core box to another). These uncertainties render the cores unsuitable for a code compliant resource or reserve estimates; however, this does not significantly detract from their usefulness in petrological studies and care was taken to limit sampling from potentially problematic sections.

Chapter 4: Petrography

4.1 Introduction

As established in Chapter 3, distinct macroscopic variations in mineral assemblage and texture are seen in both the ultramafic and carbonatite rock types from the Schiel Complex. These necessitate the mineralogical characterisation of each rock variety based on microscopic differences in order to provide clues as to how each rock type formed and the relationship between the various rock types.

Polished thin sections were prepared as a representation of all borehole cores sampled and studied using transmitted and reflective light optical microscopy, as well as scanning electron microscopy (SEM). SEM studies on carbon-coated sections were performed using a TESCAN Vega TS 5136LM instrument fitted with an Oxford Instruments EDS (Energy Dispersive X-ray Spectroscopy). SEM-EDS data were analysed using INCA software.

4.1.1 Ultramafic Rocks

All ultramafic rocks present in the Schiel Complex contain clinopyroxene, magnetite, apatite and mica as the major rock-forming minerals, where rock naming is based on the modal abundances of these minerals.

4.1.1.1 Magnetite-rich Phoscorite

Magnetite-rich phoscorites contain the highest modal abundance of magnetite and apatite, with lesser amounts of clinopyroxene and mica. Accessory minerals include amphibole, zircon, forsterite/serpentine, calcite, ferriallanite and uranothorianite.

The magnetite grains present in this rock type are medium- to coarse-grained, ranging from 2 mm to > 4 cm, and range from extremely anhedral grains with highly embayed edges, which is resorbed by clinopyroxene, to subhedral grains, all containing exsolution lamellae of ilmenite. Some magnetite grains are present with mica rims around them, as seen in Figure 9.

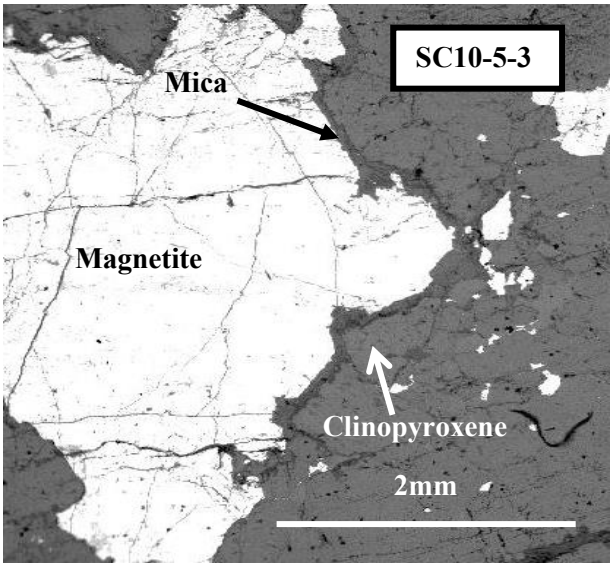

Figure 9: BSE image of magnetite grain containing a mica rim hosted in clinopyroxene.

Coarse-grained magnetite grains (±4 cm) are present, as seen in Figure 10, in sections that contain subhedral clinopyroxene, euhedral apatite and coarse-grained laths of mica (< 2 cm) containing inclusions of clinopyroxene, amphibole and apatite. Magnetite grains in these sections are highly resorbed by clinopyroxene, where some clinopyroxene grains contain inclusions of smaller magnetite grains.

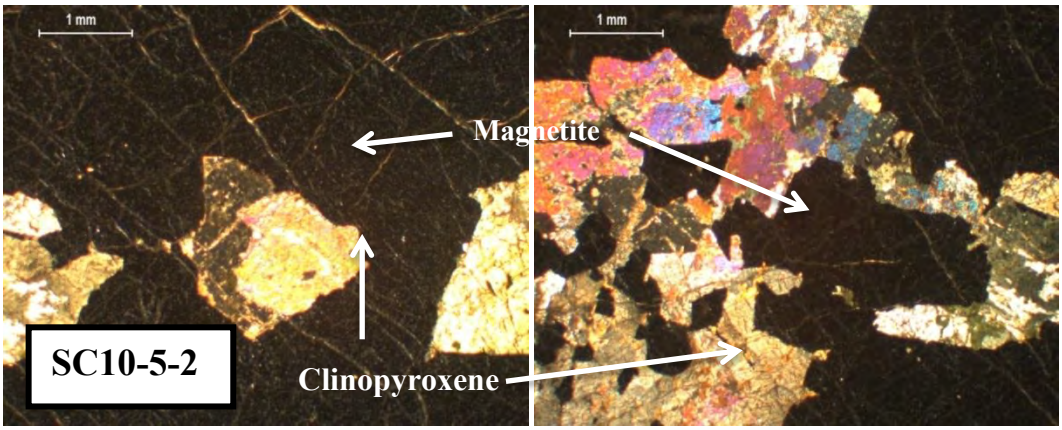

Figure 10: Clinopyroxene grains growing inside magnetite grains showing inclusions of small magnetite grains. (XPL microphotograph)

Apatite is common in all magnetite-rich phoscorites where occasional apatite-rich varieties are present, as seen in Figure 11, with rare globules of calcite present sporadically throughout the apatite-rich rock assemblages. These apatite-rich assemblages contain both anhedral and euhedral grains of clinopyroxene, with larger grains displaying anhedral textures and smaller grains present as euhedral grains.

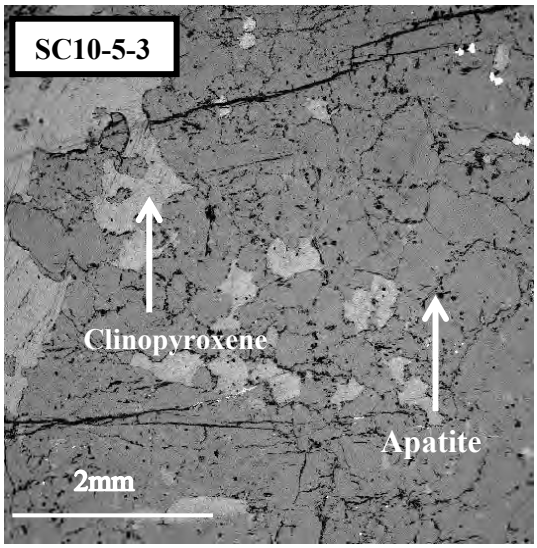

Figure 11: BSE image of an aggregated mass of apatite.

Mica grains are scarce, but present as light-brown to dark-brown pleochroic grains that show extreme resorption of magnetite as well as being inclusions in medium-grained magnetite where they are best preserved. Mica grains are more common in assemblages that are more clinopyroxene-rich where they are present as aggregated laths that contain minor compositional zoning as well as being present as inclusions within large clinopyroxene grains, which in some cases show pyroxene exsolution textures.

Amphibole is present as replacement structures on clinopyroxene, as seen in Figure 12, throughout the magnetite-rich phoscorites. Rare grains of coarse-grained (±1 cm) olivine, entirely pseudomorphed by serpentine, are also present containing abundant magnetite inclusions as well as containing secondary magnetite as fracture fillings and inclusions, as seen in Figure 13. Two separate magnetite varieties are therefore identified: the coarser-grained magmatic magnetite; and a secondary finer-grained magnetite variety formed as a secondary product during the serpentinisation of olivine possibly via the reaction: $(Fe,Mg)_2SiO_4 + H_2O + CO_2 \rightarrow Mg_3Si_2O_5(OH)_4 + Fe_3O_4 + CH_4$.

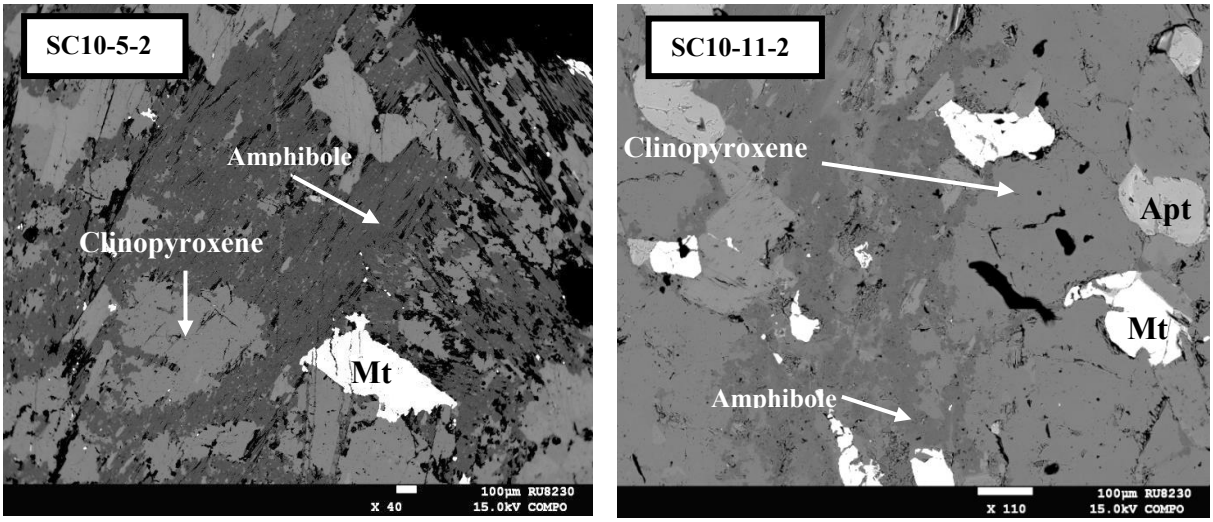

Figure 12: BSE images of amphibole present as an alteration product of clinopyroxene. (Mt-magnetite, Apt-

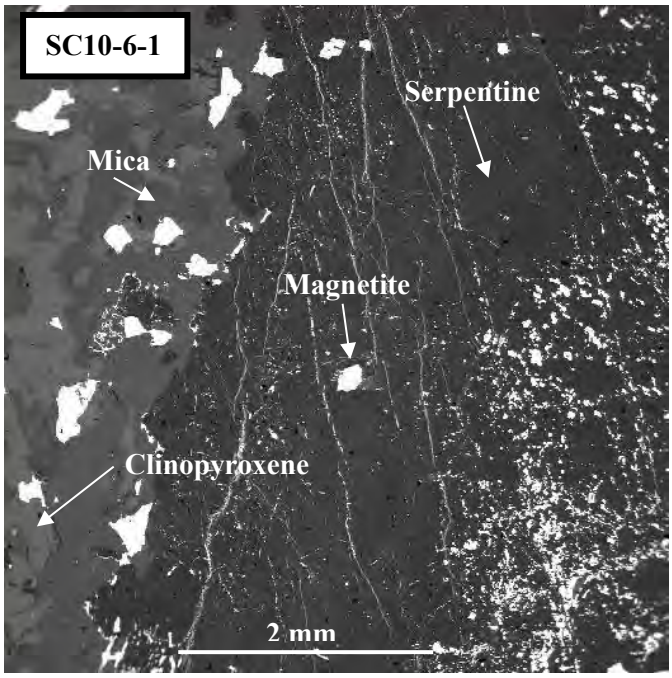

Figure 13: BSE image of serpentine grain containing secondary magnetite as fracture fillings and fine grained inclusions.

4.1.1.2 Olivine-bearing Phoscorite

The two thin sections from core SC09, sampled from greater depths than the samples from core SC10, are the only phoscoritic samples that are abundant in olivine. These rocks are medium-grained with a high abundance of clinopyroxene, as well as containing significant amounts of olivine, magnetite and apatite. Serpentine and amphibole are present as secondary minerals after olivine and clinopyroxene, respectively.

Light- to dark-green pleochroic clinopyroxene, approximately 2 mm in grain-size, is present where alteration to light- to dark-blue pleochroic amphibole is rarely seen. Light- to dark-brown pleochroic mica and subhedral apatite are dispersed throughout the rock. Grains of anhedral magnetite (±1 cm) are present that are encased by mica grains which also seem to resorb the magnetite. Large grains of olivine (±2 cm) are abundant and are partially serpentinised containing secondary magnetite as olivine fracture fillings, seen in image 14(a), similarly to the serpentine seen in core SC10.

Section SC09-08 contains a contact zone between the phoscoritic rock and a syenite which shows no mica production as reaction between these two rock types. Instead, the contact zone between the two rock types is sharp and resembles a chilled margin, where a thin band (±1 mm) of fine-grained green, clinopyroxene material exists, as seen in Figure 14(b). No evidence of significant elemental exchange from the syenite to the phoscorite exists, as no resorption textures are seen in minerals from the phoscorite in contact with syenites, and no syenitic minerals are present in the phoscorite. This shows that the phoscoritic magma must have intruded into the cold syenitic country-rock in order to produce

a chilled margin, which was preserved as the intruding phoscoritic magma did not contain sufficient heat for melting and assimilation of the syenitic country-rock (Huppert and Sparks, 1989).

Figure 14(a) shows the olivine-bearing phoscorite containing increased mica content as well as serpentinisation of the olivine grains, where figure 14(b) shows that syenite-phoscorite reactions did not result in producing a mica-bearing alteration assemblage. Anhedral olivine grains which have been resorbed by mica show that these two minerals are not in equilibrium, with the production of the mica and serpentinisation of the olivine grains attributed as being a product of later metasomatism caused by the intrusion of later carbonatitic magma.

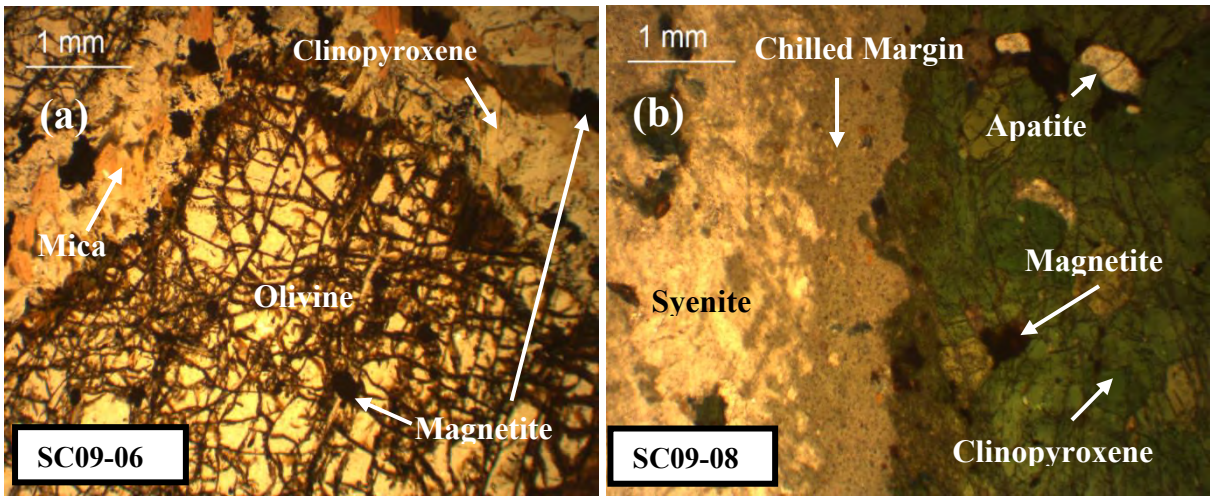

Figure 14: Microphotographs of: (a) partially serpentinised olivine grain seen in the olivine-bearing clinopyroxene-rich phoscorite; (b) reaction zone seen between the syenite and the clinopyroxene-rich phoscorite showing a chilled margin.

The abundance of partially serpentinised olivine, magnetite and apatite in these rocks may suggest that these rocks originally contained mineral assemblages attributed to classic phoscorites, which were susceptible to later metasomatism caused by carbonatitic magmatism, altering the ideal phoscorite mineral assemblage to a more serpentine- and mica-rich variety.

4.1.1.3 Clinopyroxenite

The clinopyroxenites contain predominantly diopsidic clinopyroxene, present as both euhedral and anhedral grains, with lower concentrations of magnetite, apatite and mica. Fine- to coarse-grained magnetite is present that appears to have been resorbed by clinopyroxene. Rare apatite is subhedral and ranges from fine- to medium-grained.

Near contacts with phoscorite *sensu stricto*, rare sections of the clinopyroxenite contain calcite-bearing assemblages are characterised by extremely anhedral magnetite grains (< 6 mm) containing inclusions of apatite, fine-grained clinopyroxene and apatite. Euhedral and anhedral light-brown to dark-greenish-brown pleochroic mica which displays compositional zoning are also present, containing more Mg-rich

cores, seen in Figure 15. These mica-rich clinopyroxenite varieties represent gradational contacts zones between the clinopyroxenite and phoscorite rock types.

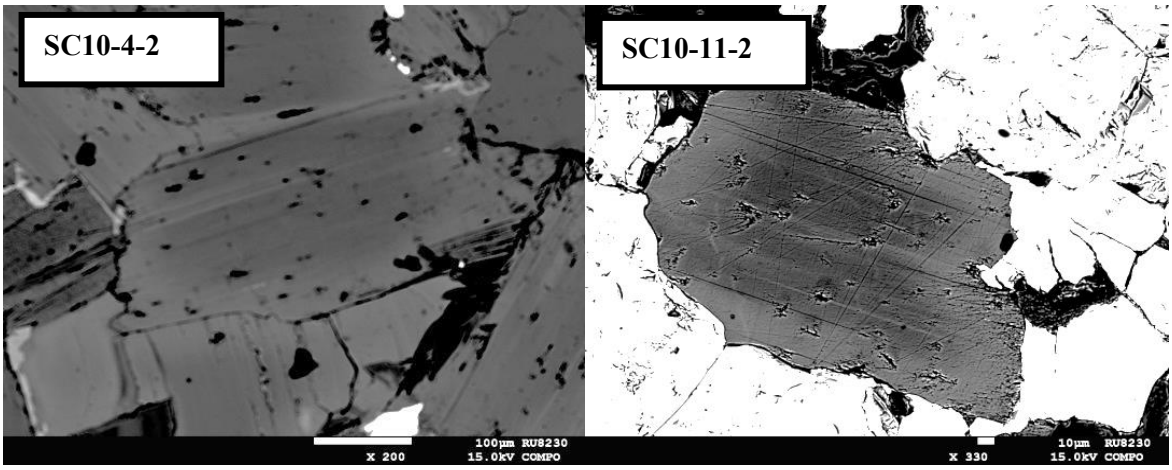

Figure 15: BSE image showing composition zoning seen in mica grains where cores are more Mg-rich.

Figure 16 shows the only sample to contain deep-green to light green pleochroic and zoned aegirine as the principal clinopyroxene, intruding into a syenite, together with anhedral apatite grains <1 mm in size that contain thorianite inclusions. Aegirine is also present in the surrounding syenite as anhedral grains as well as growing around syenite feldspar grains, as seen in Figure 14. The higher Na content of the clinopyroxenes present in this section may indicate that this vein was a result of clinopyroxenite magma intruding into the syenite where reaction processes between the syenite and the infiltrating fluid caused the pyroxenes to crystallise as a more Na-rich end-member than observed where clinopyroxenite magma intruded into phoscoritic rocks.

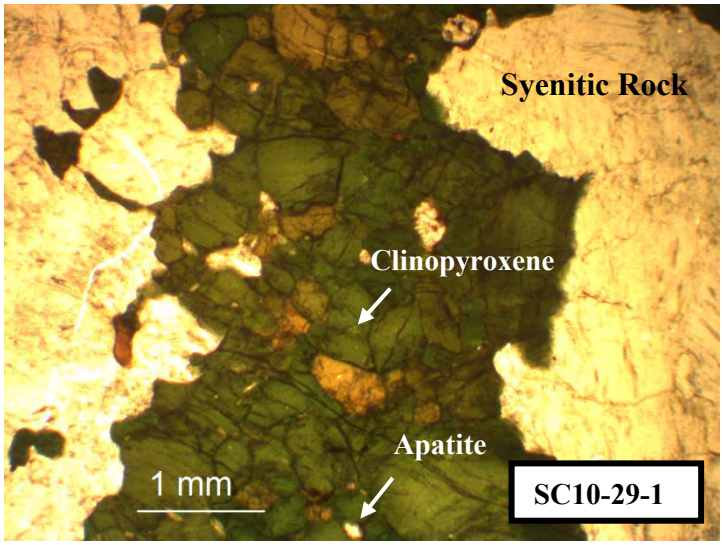

Figure 16: Microphotograph of clinopyroxenite as a vein intruding into the syenite

Figure 17 shows thin-section SC08-09 which contains a ±4 cm band of pyroxene and amphibole together with minor calcite that has intruded into a phoscoritic rock consisting of clinopyroxene, magnetite and apatite, creating deep green to light brown pleochroic mica heavily concentrated at the contact and continuing with a lesser concentration throughout the phoscoritic rock, and not present within the clinopyroxenite band. This shows that the band of mica may have formed through contact metasomatism, whereas the rest of the phoscoritic rock may have experienced infiltration metasomatism. This less common mica type is a more annite-rich mica variety, although EDS data show that significant amounts of Mg are still incorporated in the mica, present in more calcite depleted sections. The annite grains contain inclusions of subhedral apatite, clinopyroxene and magnetite with some grains showing distortion features through the presence of wavy and bended foliation structures within the grains. This mica type is associated with mica-rich rocks in close spatial association to clinopyroxenites. It is also seen that two different diopsidic clinopyroxene minerals are present: one colourless in thin section under PPL and the other light- to dark-green pleochroic under PPL.

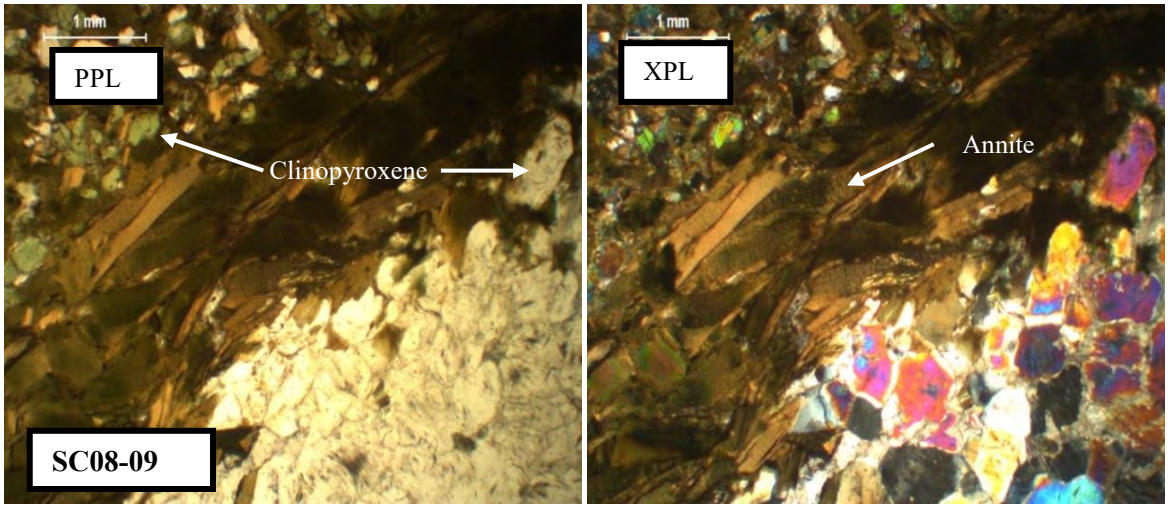

Figure 17: Microphotographs of clinopyroxene-rich vein containing minor calcite intruding into a phoscoritic rock and producing abundant mica at the contact zone as a reaction product.

4.1.1.4 Glimmerite

Glimmerite assemblages contain predominantly micas of a phlogopite composition together with minor amounts of magnetite, clinopyroxene, apatite and serpentine, and include calcite, ilmenite, zircon, ferriallanite and uranothorianite as accessory minerals.

This rock type contains a mica variety that is euhedral to subhedral, pleochroic dark reddish-orange to light brown phlogopitic mica, based on high Mg detected through EDS analyses, where calcite is present as sporadic rounded grains within the rock matrix or as inclusions within the mica grains. Mica grains in this sub-type are characteristically free of other inclusions. These rocks consist of anhedral apatite, magnetite, clinopyroxene and amphibole which all seem to be resorbed by unaligned laths of mica. These mica-rich rock types contain up to 90% mica and are closely associated with the magnetite-rich

phoscorites. This rock type may represent mica-rich reaction zones between calcite-bearing assemblages and the syenitic country rock, as seen in Figure 7, but at a larger scale producing micaceous zones 10's of cm wide rather than thin mm sized zones.

Allanite, seen in Figure 18, is rarely present in the glimmerite samples but abundant within the syenite country-rock (Graupner et al., 2018), and may represent sections of the syenitic country rock that have been altered due to metasomatism of the syenite due to infiltrating calcite-bearing magmatism. The presence of this mineral in the mica-rich rock type suggests that this rock type has been produced through metasomatism of the syenites.

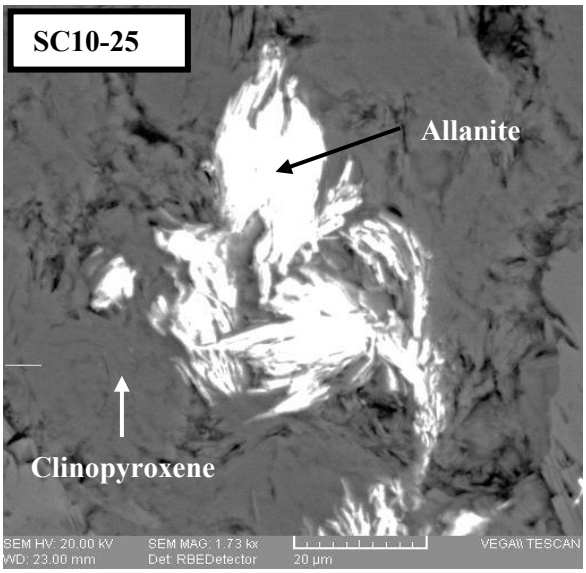

Figure 18: BSE image of allanite incorporated in glimmerite which is proposed to be inherited from the syenitic country-

4.1.1.5 Summary

The various ultramafic phases from the Schiel Complex are present as cumulate rocks where the mineralogy appears to vary at small scales, where varying mineral enrichments of magnetite, apatite, clinopyroxene or olivine are observed and gradational contacts are always present between the various ultramafic rock types. Olivine, a high temperature phase, observed in abundance only in the deepest samples suggests that these minerals aggregated due to early crystallisation and settling at the base of the upwelling magma.

According to the definition of phoscorites proposed by Krasnova et al. (2004), the mineral assemblages seen in the phoscoritic phases of the Schiel Complex meet the criteria for their characterisation as true phoscorites. Although some of the Schiel Complex phoscorites appear to have been subjected to later metasomatic processes, producing mica-rich mineral assemblages of a glimmeritic nature to different degrees at different spatial locations, a suite of rocks containing varying mineral proportions of phoscoritic compositions has been produced. It is also seen from sample SC09-06 that classic olivine-

bearing phoscorites do exist. It is, however, essential to note that the presence of abundant olivine was only seen in one sample (SC09-06), from both cores SC10 and SC09, and should not be considered as an indicator mineral for the Schiel Complex phoscorites.

The occurrence of chilled margins at phoscorite-syenite contacts suggests that the phoscoritic magmatism did not contain sufficient heat in order to alter or melt the surrounding syenitic country-rock. Instead, the presence of abundant mica associate with carbonate-bearing assemblages indicates that metasomatism was due to carbonatite intrusions, with all mica-rich rocks in close spatial association to carbonate-bearing assemblages. Glimmerites that contain allanite, only present as a primary mineral in the syenitic wall-rock, provides evidence that carbonatite intrusions contained sufficient heat and fluid in order to metasomatise the syenitic country-rock.

Annite-dominated micas occur interspersed within large ultramafic sections of the core, where annite production may be attributed to orthomagmatic mica production or clinopyroxenite-phoscorite rock reactions. Some mica-rich rocks contain sections where apatite, magnetite or clinopyroxene are abundant, which may represent the primary mafic minerals present in these ultramafic rocks before metasomatic alteration occurred. The presence of primary magnetite which shows resorption textures when in contact with clinopyroxene and mica, suggests that these phases are not in equilibrium and that clinopyroxene-dominated assemblages must have been introduced into the system after initial Fe-rich magmatism. Amphibole and mica replacing clinopyroxene then suggests that further alteration of the clinopyroxenites occurred, possibly due to metasomatism caused by later carbonatite intrusions.

The ultramafic rocks of the Schiel Complex should, therefore, be considered as a continuum of rocks between the end-member compositions described that may contain characteristics of one or a variation in mineral assemblages of the various rock types. The gradational contacts between these rock types and their intricate associations have to be kept in mind during mineral composition and whole-rock geochemical analyses.

4.1.2 Carbonatites

Carbonatites from the Schiel Complex are calcitic carbonatites comprised of: calcite, magnetite, phlogopite, apatite, olivine and diopside as the principal rock-forming minerals, with the accessory phases being: ilmenite, baddeleyite and zircon with minor pyrite, chalcopyrite, thorianite and sphalerite. Serpentine is present as an alteration product of olivine, and rare amphibole replaces diopside. Calcite carbonatites are present as both medium- and coarse-grained varieties, where the medium-grained carbonatite contains a matrix of calcite grains that are less than 3 mm in size and the coarse-grained variety contains calcite grains up to approximately 2 cm in size. All carbonatite samples contain > 30 vol% calcite, in accordance with the definition of carbonatites proposed by Mitchell (2005).

4.1.2.1 Calcite Carbonatite

The calcite carbonatite contains apatite as subhedral to anhedral grains up to 2 mm in size, containing inclusions of calcite and more rarely thorianite and zircon. The edges of apatite grains are embayed and rarely contain rims of what seems to be needle-like outgrowths of calcic-amphibole. Rare cumulates of apatite are present that are < 0.5 mm in size and are present in a carbonate matrix, as seen in Figure 19, that vary in shape with some grains being sub-rounded and others containing needle-like shapes.

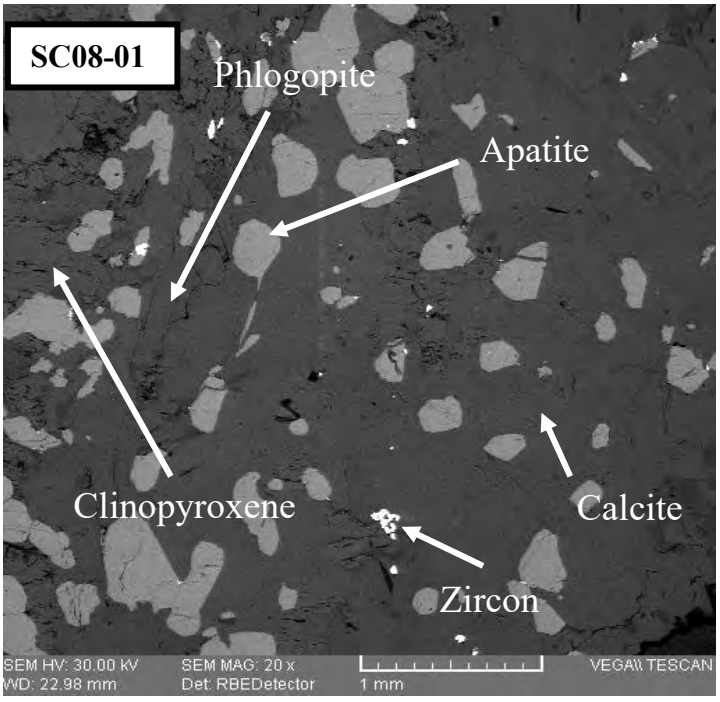

Figure 19: BSE image showing cumulate subhedral apatite seen in a carbonate matrix together with anhedral apatite surrounded by mafic minerals.

Apatites show a more rounded habit when they are situated within a pure carbonate matrix, whereas more anhedral apatites are present in portions of the rock containing silicate minerals such as phlogopite, olivine, clinopyroxene and amphibole. Apatite grains are present containing complex forms of sector zoning, as seen in Figure 20, as well as concentric zoning, identified through SEM imaging. These phases differ in brightness, where grains generally contain brighter zones in the interior sections, where the brighter zones are more REE-enriched and contain higher Cl concentrations detected through EDS analyses. The apatite grains that contain the complex sector zoning contain monazite inclusions which are present randomly throughout the entire grain, as seen in Figure 20.

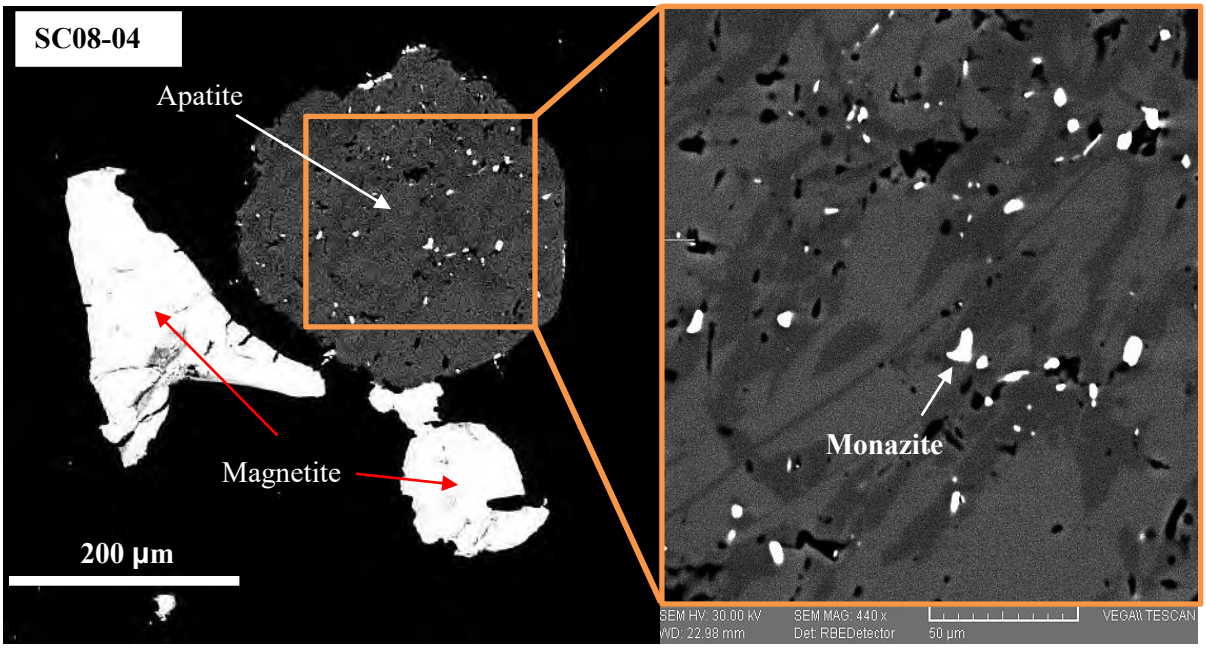

Figure 20: BSE images showing apatite grain containing two different phase compositions as well as inclusions of monazite

Coarse grains of magnetite (< 6 cm), with exsolution lamellae of ilmenite, display highly resorbed edges when in contact with calcite, and contain inclusions of calcite and apatite.

Olivine grains, ±3 mm in size, range from being partially serpentinised to grains fully pseudomorphed by serpentine, and contain apatite inclusions and secondary magnetite as fracture filings and inclusions, similarly to what was seen in the phoscoritic rocks, seen in Figure 21. Figure 22 provides an illustration of an olivine grain entirely pseudomorphed by serpentine, which contains secondary magnetite as fracture fillings.

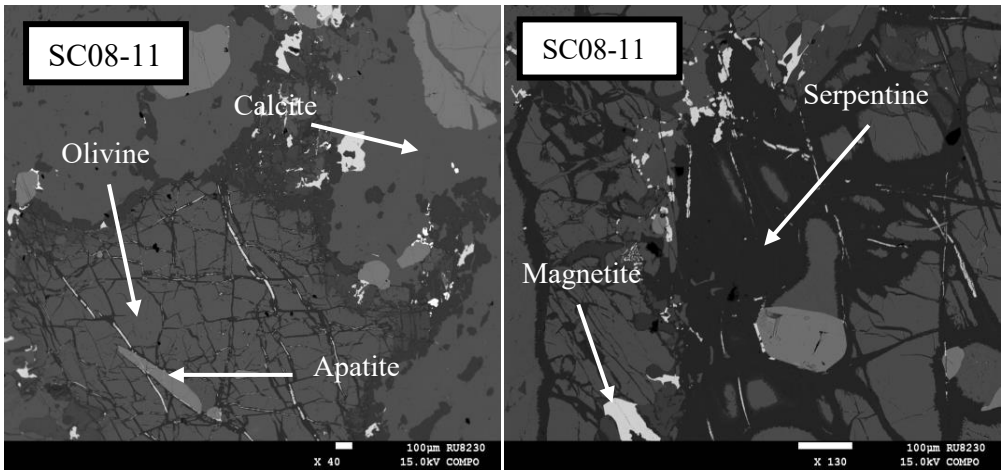

Figure 21: BSE image showing partially serpentinised olivine containing magnetite-rich fracture fillings and apatite inclusions.

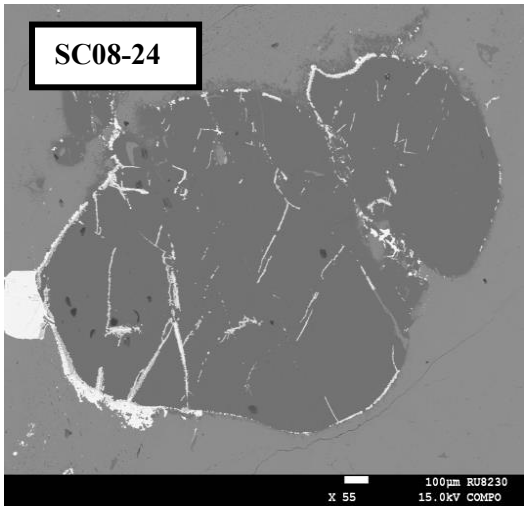

Figure 22: BSE image showing fully serpentinised olivine grain with an iron-rich fracture filling.

Medium-grained pure calcite veins, < 8 mm thick, containing no mafic minerals are present that penetrate ultramafic rocks, causing abundant mica formation along its borders as seen in Figure 23. This hydrothermal fluid seems to penetrate the rock as well, causing more mica production within the phoscoritic rock that shows a preferential alignment of the mica laths with the vein orientation.

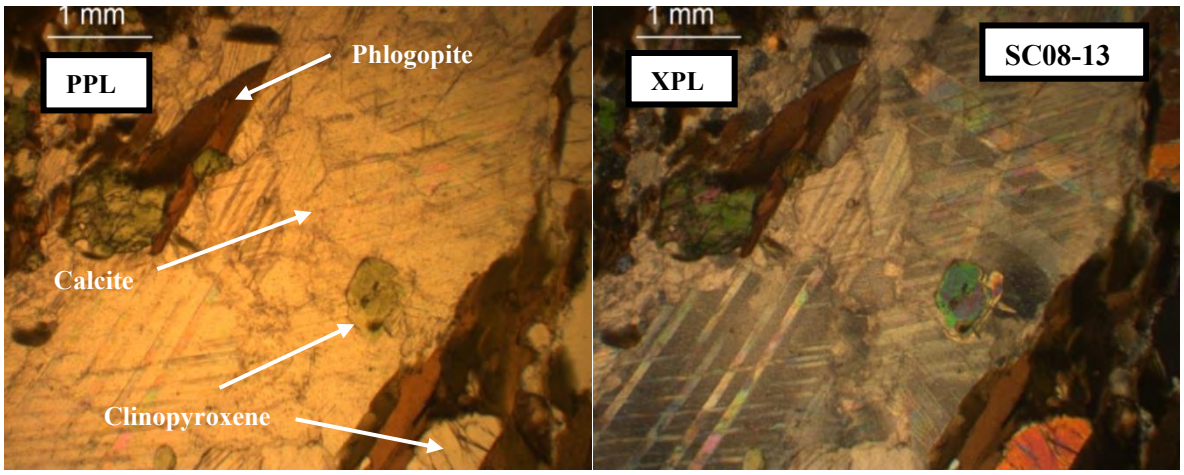

Figure 23: Microphotographs showing a pure calcite vein intruding into a phoscorite rock.

Figure 23 and Figure 24 show that a distinct light brown to a deep reddish-orange phlogopitic mica, detected through EDS analyses, that varies in size up to grains that are ±5 cm in size, occurs throughout the carbonatite rocks. Carbonatite veining structures and the preferential alignment of mica grains with these veining structures, as well as abundant mica at carbonatite-ultramafic rock contact zones indicate that the formation of mica may be a product of reactions between carbonatite-ultramafic rocks.

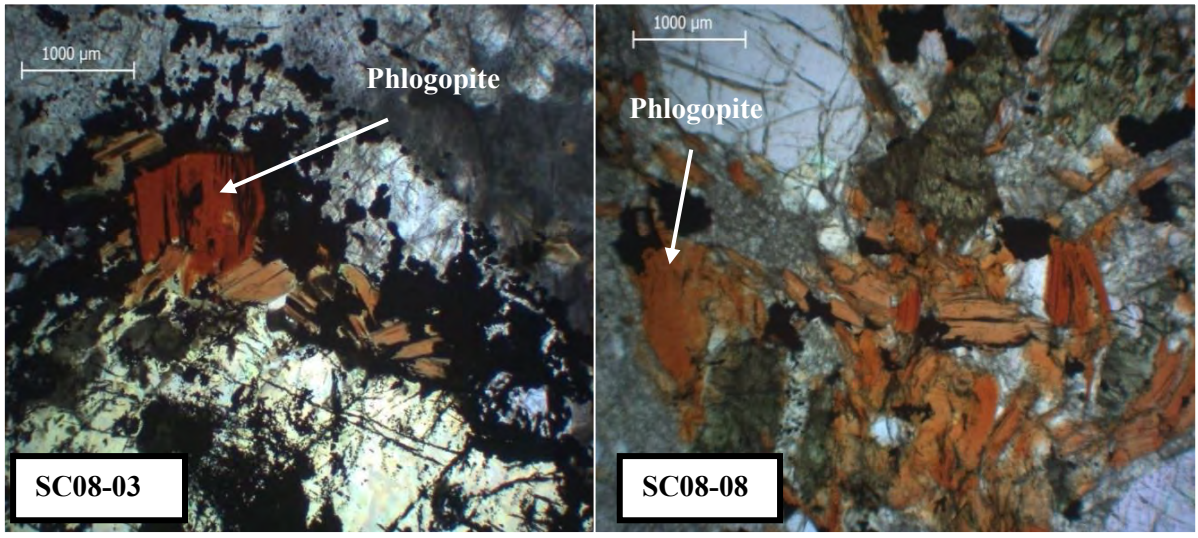

Figure 24: Microphotographs showing light-brown to dark-orange pleochroic mica seen throughout the carbonatites.

Baddeleyite is present as grains that are ±2 mm in size and are rimmed by aggregates of zircon grains displaying botryoidal textures, which contain outgrowths of serpentine at grain boundaries, as seen in Figure 25. These zircon rims may be the product of an increase in silica into the system and will be discussed further in Chapter 7.

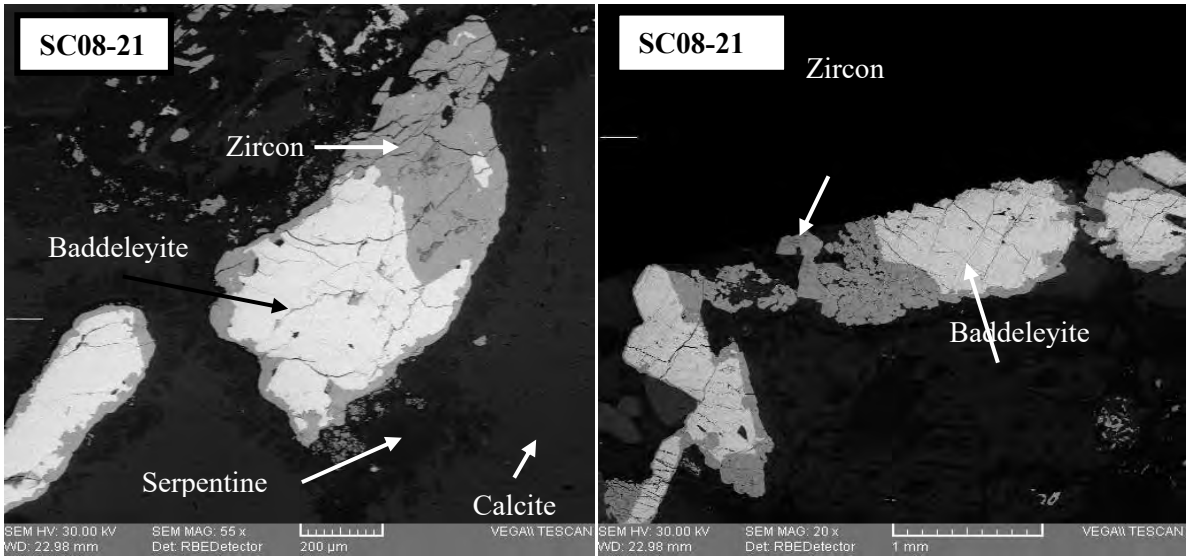

Figure 25: BSE images showing baddeleyite grains that have been altered to zircon along its rims situated in a carbonate matrix. These grains also contain a serpentine reaction zone along its borders.

Sulphides were rarely observed in the carbonatitic samples. Figure 26 shows sulphide photomicrographs imaged under reflected light. Sample SC08-21 contains euhedral to subhedral pyrite grains that have chalcopyrite inclusions, and sample SC08-18 contains only euhedral pyrite without any inclusions.

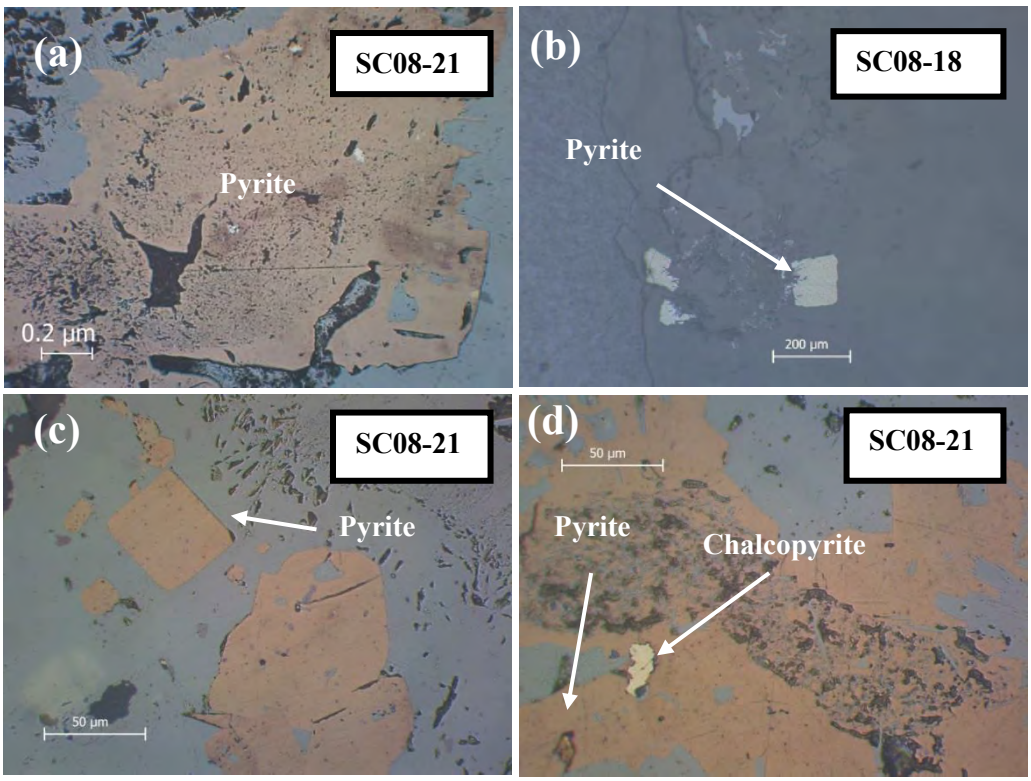

Figure 26: Sulphide minerals imaged using microphotographs within the carbonatite samples: (a) subhedral pyrite; (b) euhedral pyrite; (c) subhedral and euhedral pyrite; (d) anhedral pyrite with an inclusion of chalcopyrite.

4.1.2.2 Carbonatite Containing Schlieren Enriched in Mica and Magnetite

This carbonatite type is host to mica, magnetite, apatite and clinopyroxene present at grain boundaries of subhedral calcite up to ±2 mm in size, displaying distinct preferential alignment of mafic minerals and occur throughout the core as small-scaled zones. This rock type shows schlieren enriched in mica and magnetite drawn out as streaks in the flow foliation and could be classified as phlogopite magnetite calcite carbonatites.

Two distinct mafic mineral assemblages are observed that preserve this unique texture: one composed of predominantly magnetite that is present at grain boundaries between fine-grained calcite, as seen in Figure 27. This preferred orientation seen by the streaks of magnetite is also mirrored by scarce light-brown to orange pleochroic anhedral mica grains, euhedral to subhedral apatite and fine-grained, subhedral clinopyroxene. Large calcite grains are not preserved in direct contact with the mafic mineral streaks, but are present as bounds on either side of these portions; the second variety contains larger grains of mica, magnetite, apatite, and pyroxene together with secondary amphibole. Light-brown to orange pleochroic mica, containing inclusions of apatite and clinopyroxene, is the most abundant mafic mineral and the common orientations of the laths are the primary indicator of the flow direction that these rocks experienced. The other mafic minerals are less abundant, which consists of sub-rounded apatite and clinopyroxene grains together with anhedral magnetite. Clinopyroxene is present showing

exsolution textures in some grains, and also a partial replacement to a light-green to light-blue pleochroic amphibole in other grains.

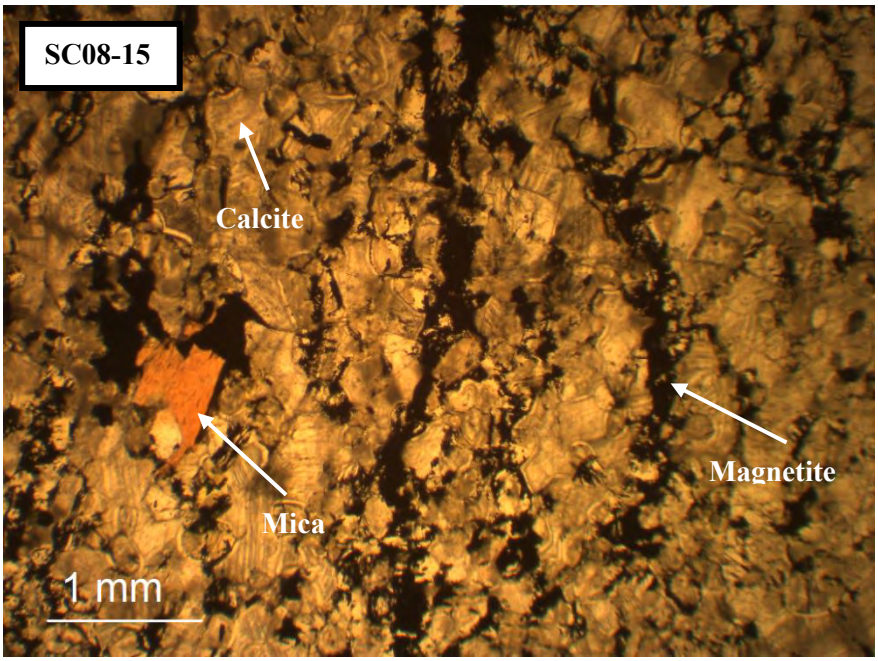

Figure 27: BSE image showing a carbonatite rock showing fine-grained magnetite at calcite grain boundaries present as a schlieren texture.

4.1.2.3 Summary

Much like the ultramafic rocks, the carbonatites contain extremely variable proportions of mafic minerals that vary at small-scales, where in some cases sub-samples of a single sample contain entirely different textures and varying mineral enrichments of olivine, apatite or magnetite. Although some carbonatites contain schlieren enriched in up to 60% mafic minerals, these sections will also be classified as carbonatites based on the definition of carbonatites proposed by Mitchell (2005), which states that any rock containing higher than 30 vol% carbonate minerals should be classified as a carbonatite, as long as a genetic link to carbonate-bearing magmatism is observed.

Carbonatitic magmatism is proposed as being the metasomatic medium for the production of mica-rich reaction assemblages, which are only observed where carbonate-bearing magmatism has intruded into syenitic or phoscoritic/pyroxenitic country-rock. This is supported by mica-rich zones present as sheaths around carbonatite veins, as seen in Figure 7, and the lack of mica-rich assemblages in the absence of carbonate-bearing assemblages. Abundant carbonate vein intrusions present in syenitic, phoscoritic and pyroxenitic rocks suggests that carbonatite magmatism was a discrete event and must have been the last magmatic stage to occur, which contained sufficient heat in order to metasomatise the surrounding syenitic and ultramafic rocks, producing mica-rich rocks as reaction assemblages.

The increase in modal abundance of olivine (serpentine) in the carbonatites is a significant observation, as olivine is widely considered as an important constituent of carbonatites which are associated with phoscorites. If these olivine grains are inherited from a common parental magma shared by the ultramafic magmatism, then it could be evidence of a classic phoscoritic magma, which could have initially crystallised phoscorites with the ideal mineral assemblage seen in other phoscorite-carbonatite complexes, before being altered due to metasomatism caused by later pyroxenitic or carbonatite intrusions. Furthermore, the presence of olivine, apatite and magnetite in both the phoscorites and carbonatites may suggest that these phases may have crystallised and accumulated in a single parental magma, which was then driven into the separation of the carbonatite and Fe-rich melts, both incorporating the same primary mafic mineral compositions.

Electron probe micro-analyser (EPMA) mineral composition data will aid in determining if the common minerals present in the ultramafic and carbonatite rocks do indeed contain identical mineral compositions.

Chapter 5: Mineral Geochemistry

Quantitative mineral chemical compositions of representative grains of apatite, amphibole, pyroxene, olivine, mica, serpentine, and magnetite were obtained on the sections described in Chapter 4 using a JEOL JXA-8230 electron probe micro-analyser. Tables of all the EPMA analyses and a summary of the analytical conditions are presented in Appendix C (p113). Appendix F.2 – F.8 (p195 - 204) provides a comparison of mineral compositions analysed from similar rock types from other phoscorite-carbonatite-bearing complexes.

5.1 Mica

Mica compositions were determined on 13 ultramafic (115 analyses) and 5 carbonatitic (42 analyses) samples. Structural formulae of micas were calculated using the methodology proposed by Brod et al. (2001), based on their study of micas from carbonatites and associated alkaline silicate rocks, and classified based on the classification scheme provided by Foster (1960). The classifications of the mica present in the ultramafic and carbonatite samples are shown in Figure 30(a) and (b) based on apfu (atoms per formula unit) totals of elemental proportions, respectively. The phoscorite and clinopyroxenite samples have micas with compositions that fall along the solid solution series between magnesian biotite and phlogopite, markedly skewed towards the magnesian biotite end member. By contrast, micas in the glimmerite and carbonatite samples are exclusively phlogopite. Tetraferriphlogopite was not detected via chemical analyses in either carbonatite or ultramafic samples.

The mica compositions are dependent on the rock type within the ultramafic rocks, as seen in Figure 30(a), with the glimmerite containing only phlogopite micas (average total Fe = 8.16 wt.%; average Mg = 23.98 wt.%), clinopyroxenites contain the most annite-rich micas (average total Fe = 18.09 wt.%; average Mg = 14.09 wt.%), while micas in the magnetite-rich phoscorites have compositions between those for micas from the glimmerite and clinopyroxenite rock types (average total Fe = 14.04 wt.%; average Mg = 17.29 wt.%).

Most analysed micas displayed little or no compositional zoning: significant zoning was restricted to clinopyroxenite sections SC10-4-2 and SC10-11-2 and magnetite-rich phoscorite section SC10-12-4, illustrated in Figure 28, which displayed an average core Mg:Fe of 2.2:1 apfu and an average rim Mg:Fe of 1.81:1 apfu. Two mica compositions analysed from a single grain in the magnetite-rich phoscorite section SC10-12-4, containing patchy zonation patterns not seen in any other samples, is associated with the clinopyroxenite field as seen in Figures 30, 31 and 32. These analyses contained high annite contents with respect to the other mica grains from the same section. Figure 29 provides an illustration of core-rim compositional analyses variation seen in multiple mica grains, which shows that mica rims contain a more Fe-rich and Mg-poor composition in zoned grains.

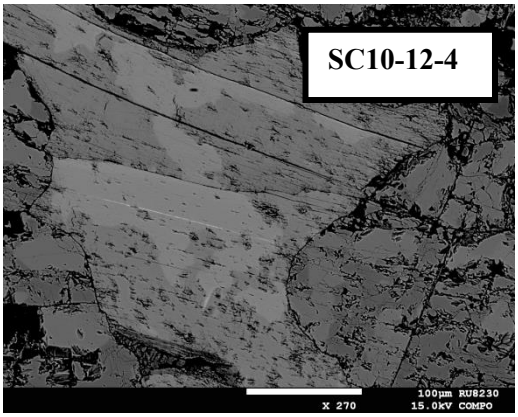

Figure 28: BSE image showing zoned mica grain seen in phoscorite.

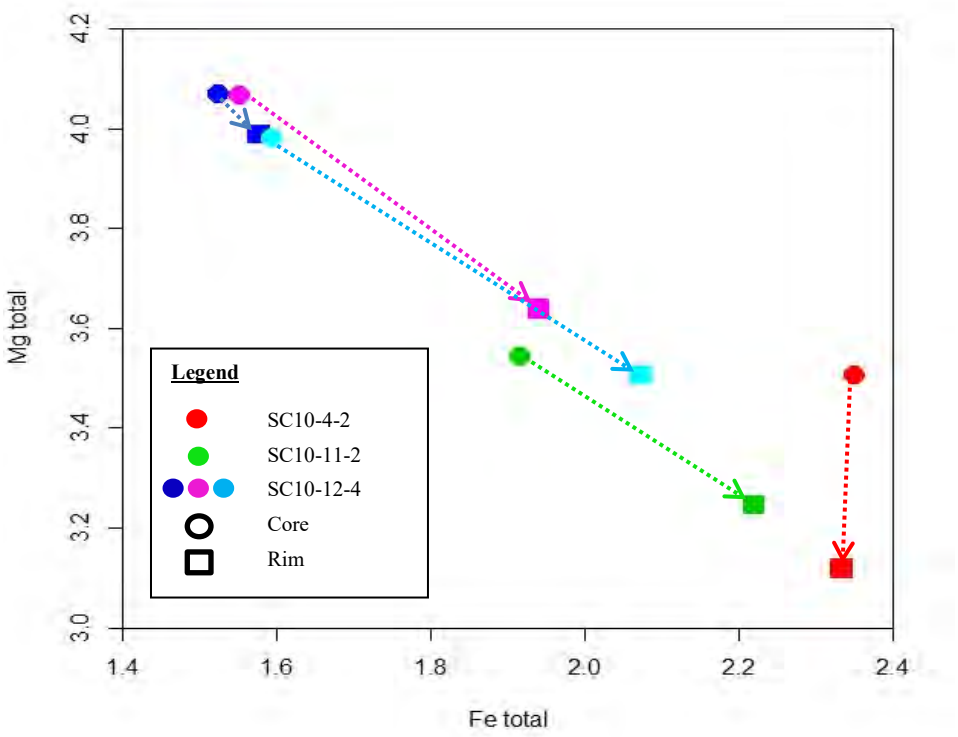

Figure 29: Core-Rim comparison from select mica grains.

Figure 30(b) shows that carbonatite samples contain two compositionally distinct mica populations: one group (the majority of the carbonatite mica analyses) containing phlogopite chemistries that are similar to all the glimmerite phlogopite chemistries; and another higher Fe group (multiple analyses from sample SC08-1-1) containing similar chemistries to that of the phoscoritic phlogopite/magnesian-rich biotite chemistries. This phlogopite magnetite calcite carbonatite is characterised by schlieren enriched in mica with lesser amounts of magnetite and clinopyroxene and contains mica chemistries that are more Fe-enriched than the other carbonatite samples.

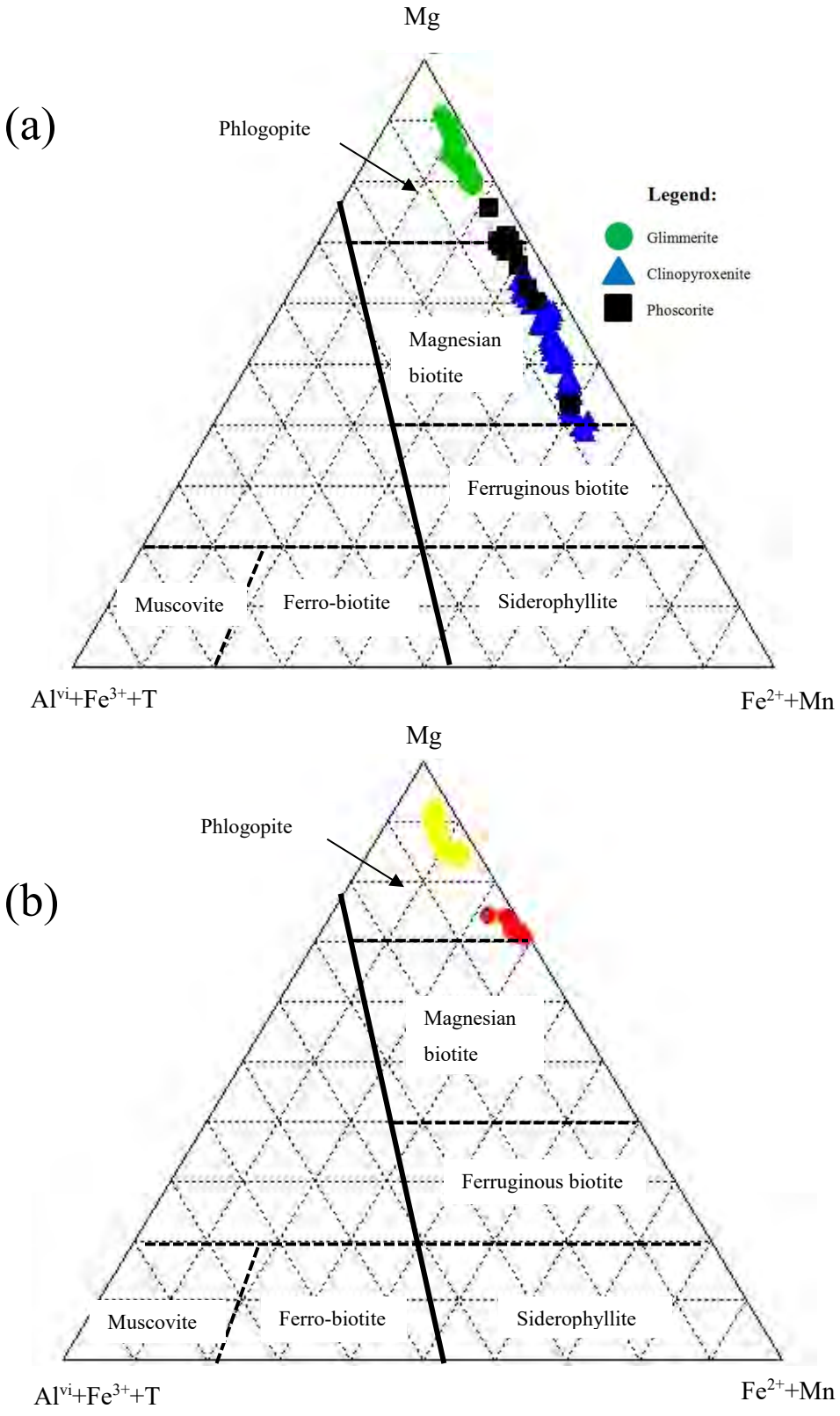

Figure 30: Mica classification diagram based on the classification scheme provided by Foster (1960): (a) ultramafic rocks showing the glimmerites (green), phoscorites (black) and clinopyroxenite (blue) groups; (b) carbonatites showing mica compositions from the calcite carbonatites (yellow) as well as the phlogopite magnetite calcite carbonatite (red).

Figure 31(a) and (b) shows the Mg# versus Al apfu of the micas analysed from the ultramafic and carbonatitic samples, respectively. The Al contents of micas present are all in excess of 1.8 Al apfu, with both ultramafic and carbonatitic samples showing a decrease in Al with increased Mg#. It is seen that the composition of the glimmerite micas overlaps the compositions of the calcite carbonatite micas, and the phlogopite magnetite calcite carbonatite mica compositions overlap those of the phoscorite micas. Distinct mica chemistry variation is seen regarding the various ultramafic and carbonatitic rock types proposed in Chapter 4.

Figure 32(a) and (b) show Mg apfu versus total Fe apfu of micas from the ultramafic and carbonatite samples, respectively. This shows that a negative correlation exists between Mg and total Fe for both ultramafic and carbonatitic rock types. This correlation illustrates the enrichment of phlogopite or biotite with respect to the specific rock type. Similar to Figure 31, a correlation is seen between the compositions of the calcite carbonatite and glimmerite micas and the phlogopite magnetite calcite carbonatite and phoscorite micas.

Figure 32(c) and (d) show the Ti apfu vs Mg apfu binary plot of mica compositions from both ultramafic and carbonatite rocks, respectively. Micas from the ultramafic rock types show a distinct decrease in Mg with increasing Ti, whereas the micas from the carbonatites seem to maintain a constant Ti with fluctuating Mg content. Two distinct lines of evolution are seen between mica compositions from the clinopyroxenite and phoscorite and glimmerite rock types. A clear distinction is also observed between the mica compositions from phlogopite magnetite calcite carbonatite and the phoscorite, where micas from the phoscorites contain higher Ti content.

Figure 32(e) and (f) show Ti apfu vs total Al apfu for micas from the ultramafic and carbonatite rocks, respectively. These figures show a weak correlation where the decrease in Ti leads to a decrease in Al contents of mica grains. Figure 31(e) shows that some mica grains from the clinopyroxenite contain low Ti and high Al contents, which is not seen in the phoscorite. These grains are mainly annite grains that contain unusually high Al contents. It is clear to see that two distinct lines of evolution exist between the glimmerite and phoscorite and the clinopyroxenite rocks.

The chemistry of micas from the calcite carbonatites (Figure 31b) are shown to overlap those of the glimmerites (Figure 31a). This is a critical association due to the possibility that the carbonatite may be the metasomatising medium which reacted with the phoscorite/pyroxenite/syenite to produce the glimmerite. The same mica composition in both of these rocks leads to the assumption that these rocks are closely associated. It is also shown that the phlogopite magnetite calcite carbonatite contains similar mica compositions to those of the phoscorites. The phoscorite and clinopyroxenite rocks are shown to contain distinct mica generations that evolve independently.

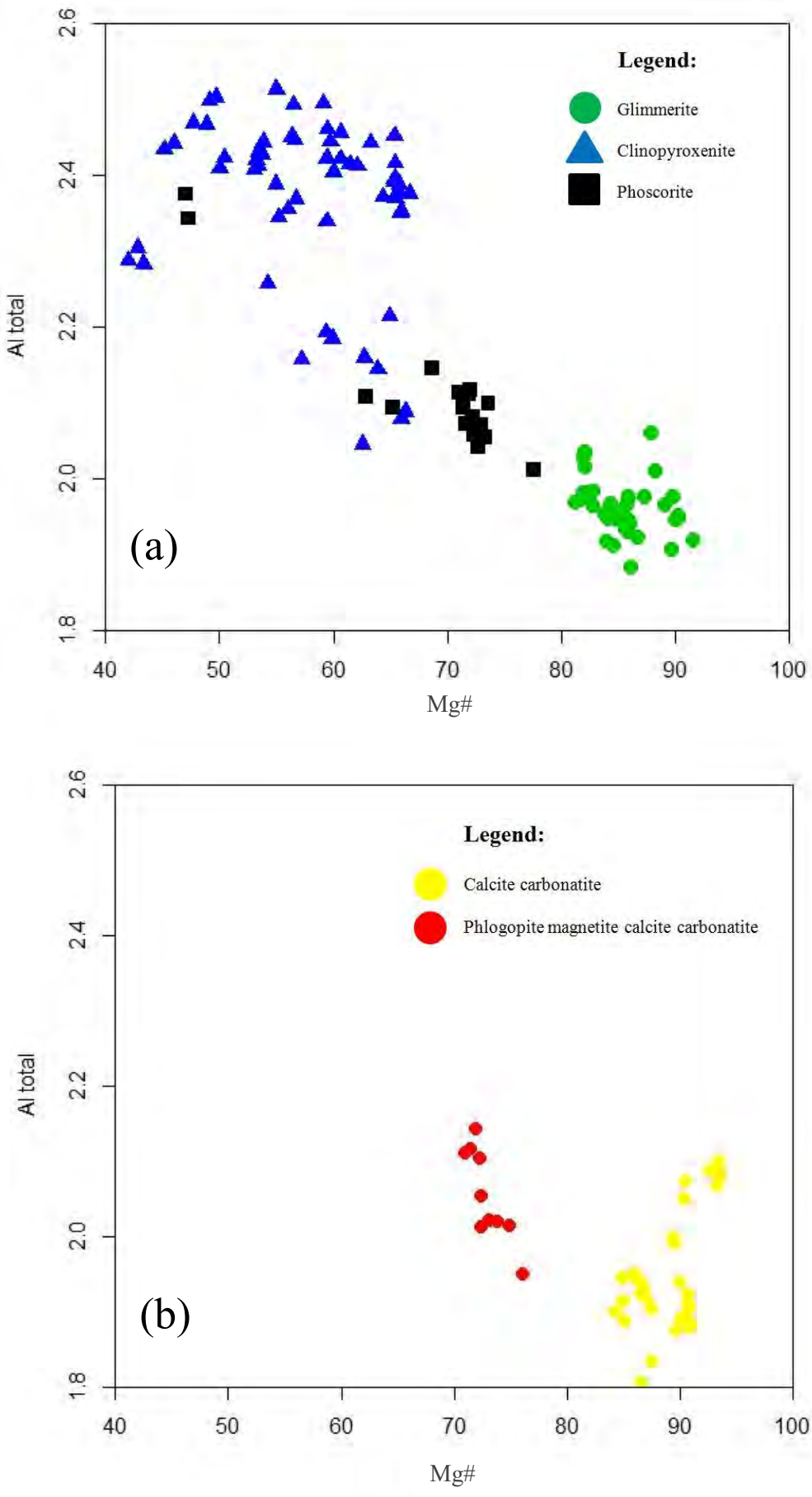

Figure 31: Diagram showing Mg# vs. total Al for the micas from ultramafic rocks (a) and the carbonatites (b).

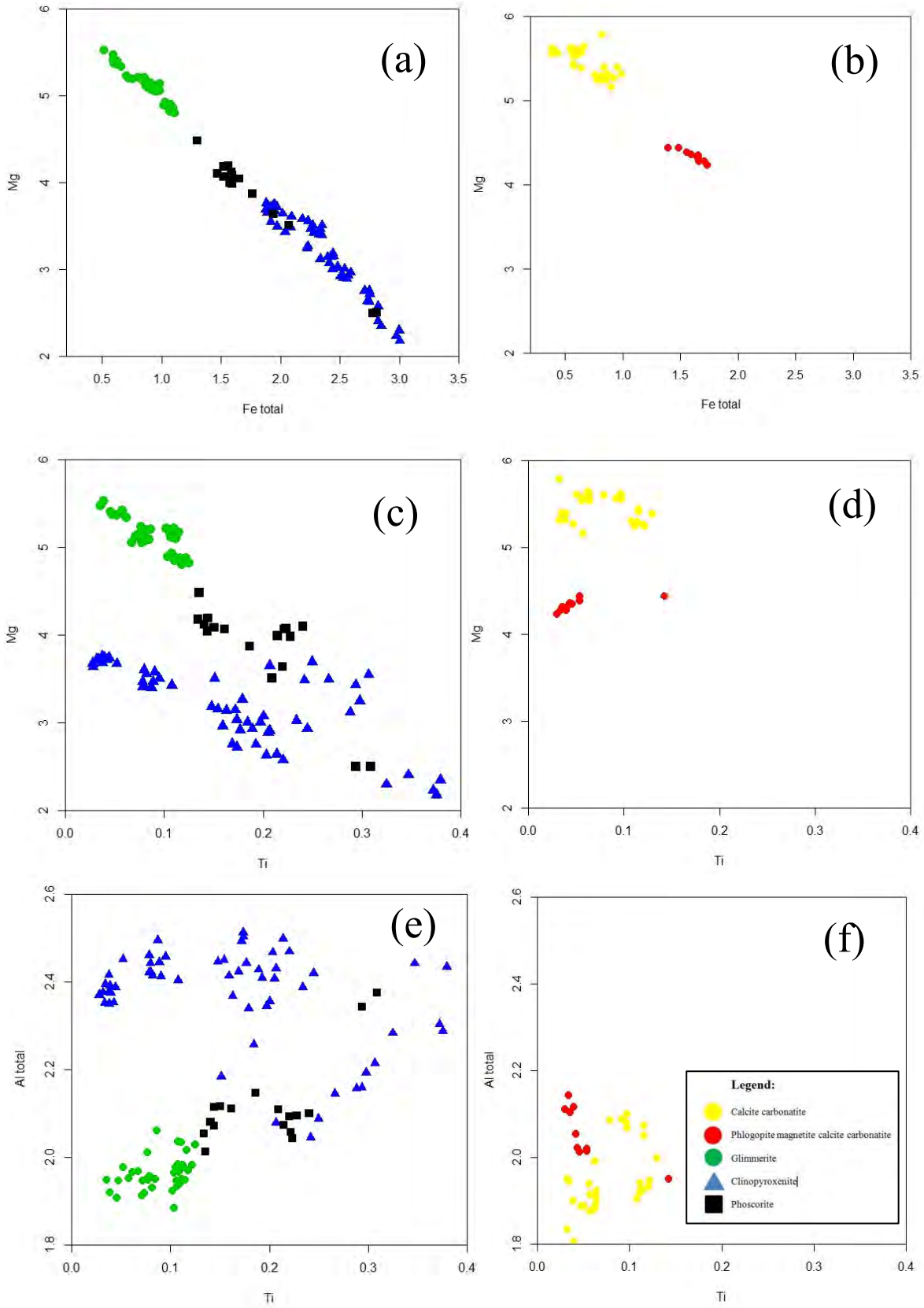

Figure 32: Variation diagrams with respect to mica chemistry: (a-b) plots total Fe vs. Mg for the ultramafic (a) and carbonatite (b) mica analyses; (c-d) plots Ti vs. Mg for the ultramafic (c) and carbonatite (d) mica analyses; (e-f) plots Ti vs. total Al for the ultramafic (e) and carbonatite (f) mica analyses.

5.2 Clinopyroxene

Clinopyroxene was analysed in 13 ultramafic (94 analyses) and 4 carbonatitic samples (24 analyses). The classification ternary diagram plots Na versus Mg versus Fe^{2+} + Mn after Jones (1984), seen in Figure 33, and shows that diopside is the main clinopyroxene mineral present in the glimmerite, with one sample containing salite. In contrast, the clinopyroxenite and magnetite-rich phoscorite types contain clinopyroxene, which is mostly contained in the salite compositional characterisation field.

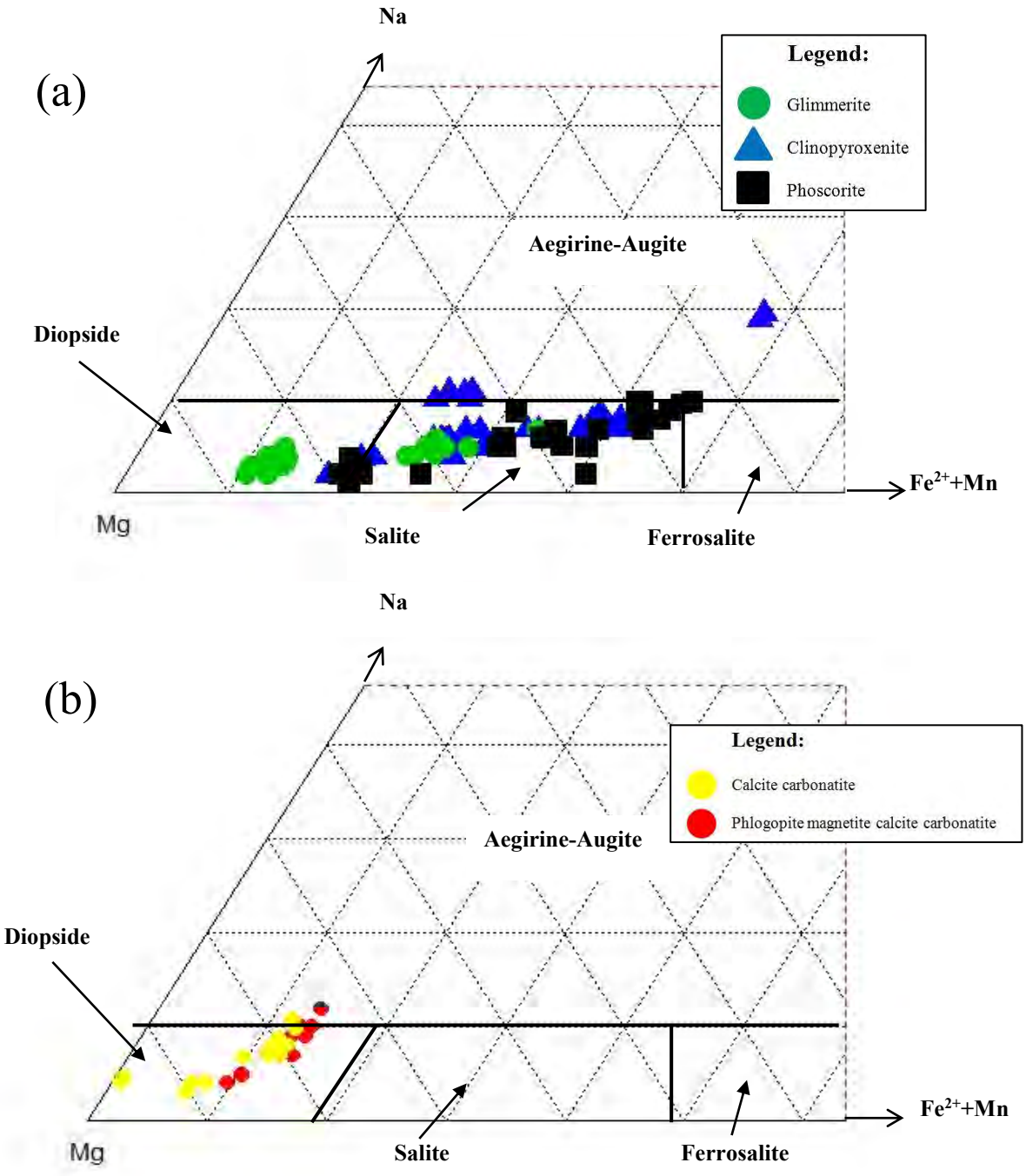

Figure 33: Clinopyroxene classification diagram after Jones (1984) for ultramafic (a) and carbonatite (b) clinopyroxene mineral chemistries.

Only one ultramafic sample (SC10-29-1), which is a clinopyroxenite vein intruding into a syenite as seen in Figure 16, contains 2 separate clinopyroxene mineral compositions distinctly in the aegirine-augite field, which has acmite compositions of 17.61 and 18.19 wt.%Ac. The majority of clinopyroxene in carbonatites are characterised as diopside apart from sample SC08-1-1, which plots some clinopyroxene analyses just inside the aegirine-augite field.

Na_2O contents of all the clinopyroxene grains show an average of 0.80 wt.% in the ultramafic samples and 0.99 wt.% in the carbonatitic samples. These low Na contents reflect the low acmite component averaging 5.47 wt.% and 6.68 wt.%Ac in the ultramafic and carbonatite rocks, respectively. This results in high diopside contents, due to the high Fe, Mg and Ca contents, which was calculated at an average of 80.79 wt.% and 83.95 wt.% for the ultramafic and carbonatite rocks, respectively. Appendix C.2 shows the calculated pyroxene constituents of the clinopyroxene grains.

5.3 Amphibole

Amphibole grains were analysed from 1 clinopyroxenite, 2 magnetite-rich phoscorite, 2 glimmerite (34 total analyses) and 4 carbonatitic (19 analyses) samples. All the amphiboles are present as replacements on clinopyroxene (as seen in Figure 12), some as partial and some as complete replacements. All amphiboles analysed are calcic-amphiboles bedsides sample SC-8-4-1-1, which contains sodic-calcic-amphiboles. All amphiboles have Ca contents of between 1.703 and 1.982 apfu, besides sample SC8-4-1-1, which contains amphiboles with Ca contents of between 1.134 and 1.55 apfu, as well as Na values of between 0.653 and 0.931 apfu, whereas all other amphiboles have Na contents that average 0.113 apfu.

Further classification of amphiboles can be seen in Figures 34 and 35 after Leake et al. (1997) which subdivides the various calcic- and sodic-amphibole types from the various Schiel Complex rock types. The majority of the amphiboles from the ultramafic samples are classified as actinolite, with 2 samples being classified as tremolite. The glimmerite only contains actinolite whereas the phoscorite and clinopyroxenite samples contain either tremolite or actinolite, with no distinct trend seen between the ultramafic rock type and the amphibole type. The glimmerite contains amphibole mineral chemistries depleted in Mg and enriched in total Fe contents with respect to the phoscoritic rocks, which is seen in Figure 34 and Appendix C.3.

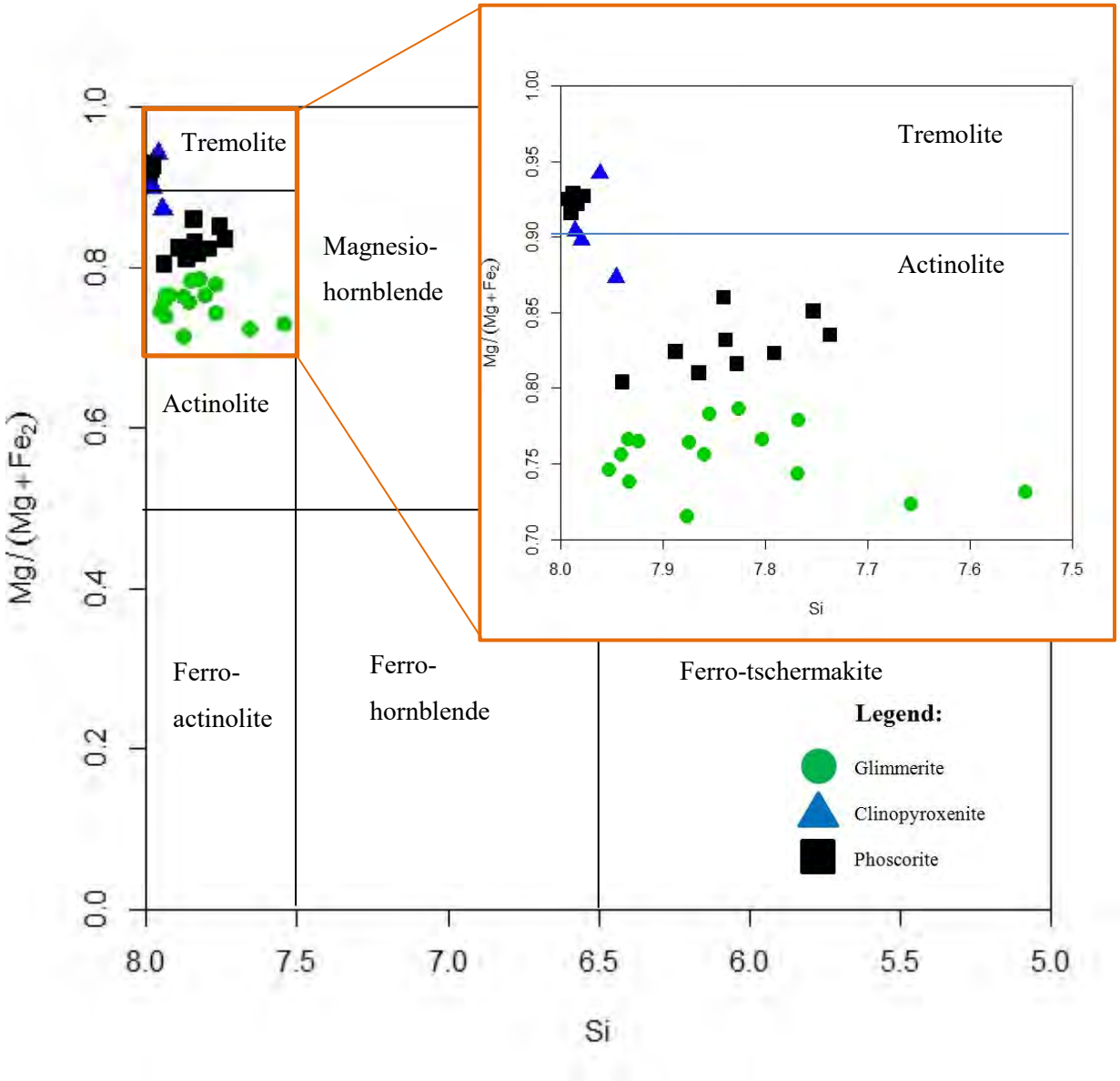

Figure 34: Amphibole classification diagram after Leake et al. (1997) for calcic amphiboles analysed from the ultramafic rocks.

The carbonatite rocks analysed contain both calcic- and sodic-calcic amphiboles, as seen in Figure 35. The majority of the carbonatite samples contain calcic amphiboles classified as tremolite, with 1 grain (1 analysis point) classified as actinolite as seen in Figure 35(a). Figure 35(b) shows all the amphibole analyses from sample SC08-1-1, which is classified as sodic-calcic amphiboles (winchite), together with one analysis of tremolite in the sample.

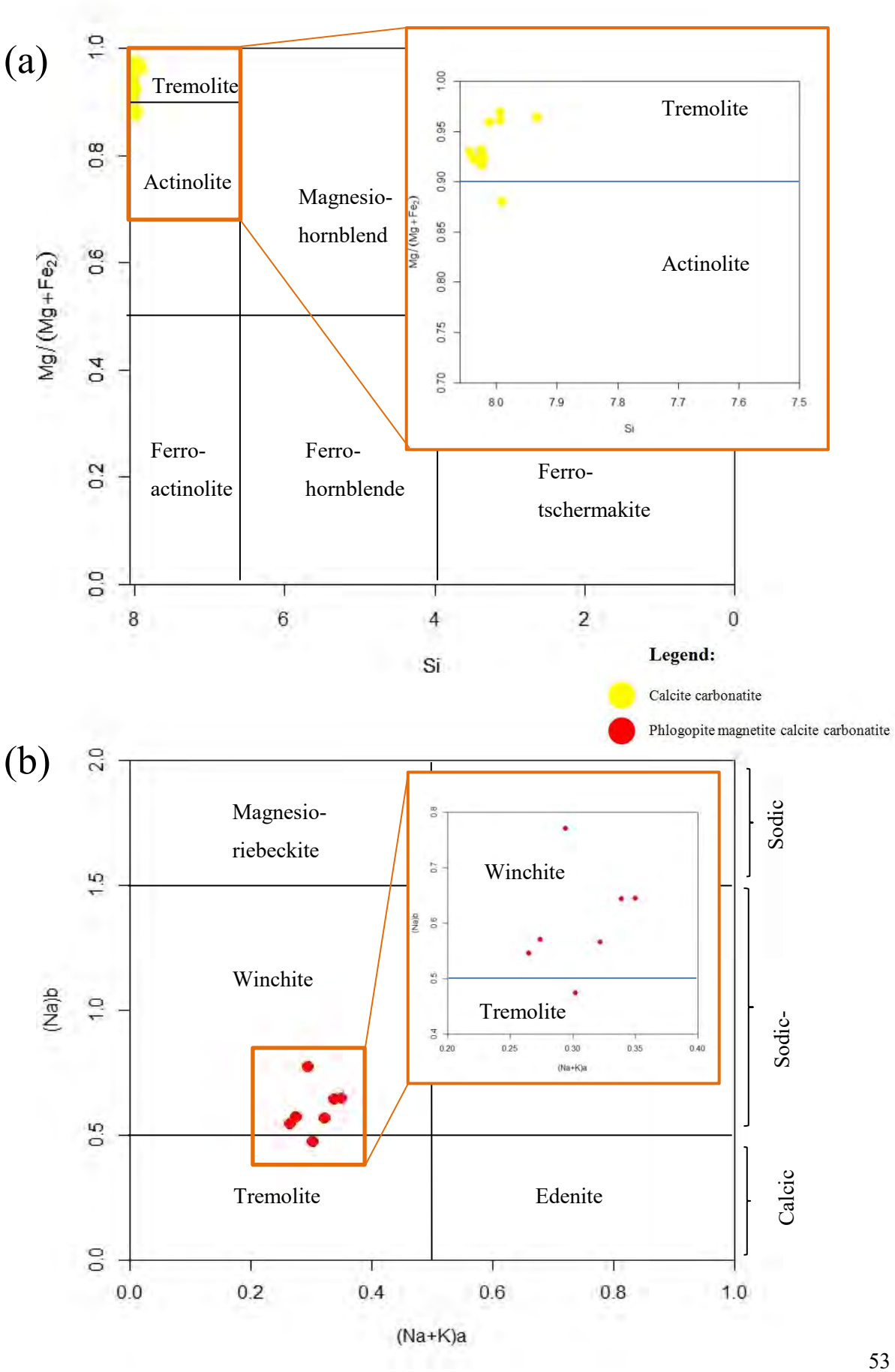

Figure 35: Amphibole classification diagrams after Leake et al. (1997) for carbonatite amphibole mineral chemistries: (a) calcic amphiboles; (b) sodic-calcic amphiboles.

5.4 Olivine/Serpentine

Olivine and serpentine mineral grains were analysed in carbonatite samples only. Chemical analyses of olivine and serpentine grains are provided in Appendices C.4 and C.5. Three samples were analysed for olivine with 20 analyses recorded and 2 samples for serpentine, for which 10 analyses were recorded. Three core-rim analyses of olivine (shown in Table 2) show only minor increases in Si and Mg content and decrease in Fe and Mn from the core to rim. All analysed olivine grains are forsterite-rich: $Fo_{(80.1\text{-}84.3\%)}$, $Fa_{(15.4\text{-}19.4\%)}$ and $Te_{(0.3\text{-}0.4\%)}$.

The serpentine grains were classified based on published mineral chemistry data as no suitable classification scheme is available. The serpentine present in sample SC8-6-3 is antigorite (Sawai et al., 2013), whereas in sample SC8-5-8, the serpentine is ortho-chrysotile (picrolite) (Suzuki & Kirino, 1984). The serpentine grains have higher Mg#'s than olivine grains, with serpentine containing Mg#'s ranging from 88.01-97.89, whereas the olivine grains have Mg#'s ranging from 80.39-84.59.

Table 2: EPMA results from core-rim olivine analyses. ((C)=core; (R)=rim)

Sample	SC8-11_Olv2(C)	SC8-11_Olv2(R)	SC8-11_Olv6(C)	SC8-11_Olv6(R)	SC8-17_Olv6(C)	SC8-17_Olv6(R)
SiO_2	39.52	39.68	39.37	39.48	39.16	39.37
TiO_2	0.00	0.01	0.02	0.00	0.01	0.00
Al_2O_3	0.00	0.02	0.04	0.00	0.00	0.00
Fe_2O_3	-	0.25	-	0.77	0.10	-
FeO	17.45	14.75	17.71	15.35	16.42	16.47
MnO	0.31	0.27	0.35	0.27	0.35	0.31
MgO	42.72	44.86	42.32	44.38	43.15	43.29
CaO	0.01	0.04	0.03	0.02	0.02	0.03
Na_2O	0.02	0.02	0.04	0.04	0.01	0.02
K_2O	0.04	0.02	0.03	0.03	0.03	0.03
Cr_2O_3	0.00	0.00	0.00	0.00	0.00	0.00
NiO	0.00	0.00	0.00	0.03	0.00	0.03
Total	100.07	99.90	99.90	100.37	99.24	99.55
Number of ions calculated on the basis of 4 O						
Si	1.00	1.00	1.00	0.99	1.00	1.00
Fe^{3+}	0.00	0.00	0.00	0.01	0.00	0.00
Fe^{2+}	0.37	0.31	0.38	0.32	0.35	0.35
Mn	0.01	0.01	0.01	0.01	0.01	0.01
Mg	1.62	1.68	1.61	1.66	1.64	1.64
Total	3.00	3.00	3.00	2.99	3.00	3.00
Fo %	81.08	84.05	80.65	83.18	82.04	82.10
Fa %	18.58	15.50	18.94	16.14	17.51	17.52
Te %	0.33	0.28	0.38	0.29	0.38	0.33

5.5 Magnetite

Eighty-nine magnetite grains were analysed from 7 ultramafic samples, where the chemical analyses are provided in Appendix C.6, with little magnetite compositional variation occurring between the phoscorite, clinopyroxenite and glimmerite rock types. Low TiO_2 contents are present in all the magnetite grains with the average Ti content being 0.003 apfu. The analyses show that negligible Cr, Mg, Ni, Ca and V are present in the magnetite, with total Fe making up an average of 99.56% of all cations from all the analyses.

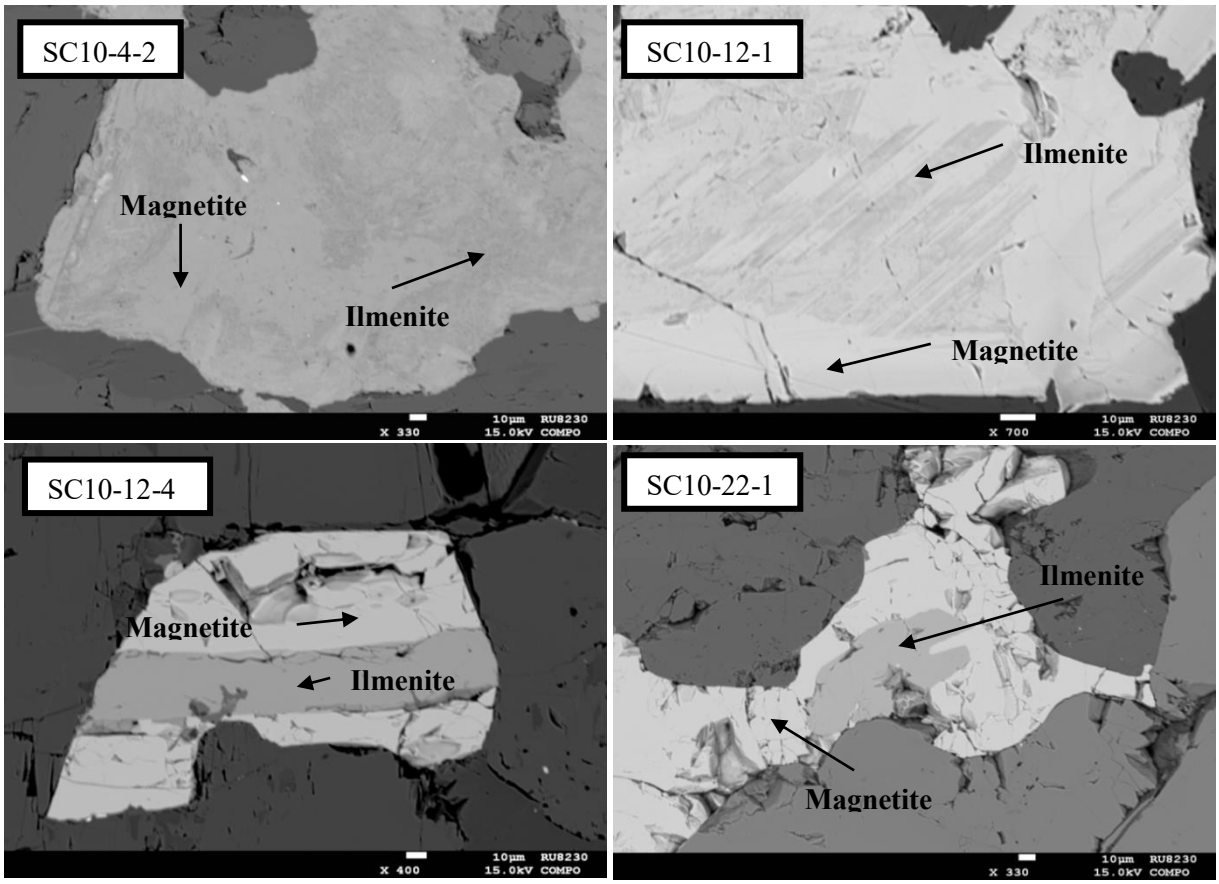

Figure 36: BSE image showing a representation of ilmenite occurring as zones or exsolution lamellae in magnetite grains across all ultramafic samples.

The textures and the chemical composition of magnetite grains provide a comparison to some of the phoscorite types seen at the Kovdor phoscorite-carbonatite Complex in Russia. Ivanyuk et al. (2017) described the apatite-forsterite phoscorite of the marginal zone and the carbonate-rich phoscorite and the carbonatite of the axial zone to contain magnetite with exsolution lamellae of ilmenite-geikielite, similarly to what is seen in the Schiel Complex ultramafic samples, shown in Figure 36. Also described are the kinetics of inclusion nucleation and growth, which are largely dependent on the diffusivity of the cations in magnetite. This shows that the low Ti and Al contents of the magnetite grains and the abundant ilmenite inclusions within these magnetite grains could be a process of Al and Ti having higher diffusivity rates than usual allowing for ilmenite to scavenge and deplete the magnetite of Ti.

This is an indicator of a common process occurring within the phoscorites of the Kovdor phoscorite-carbonatite Complex. Although magnetite in most phoscorites have low TiO_2 contents of between 0.2-1.2 wt.% as well as low Cr and Ni (Krasnova et al., 2004), the magnetite from the Schiel Complex differs in that it extremely depleted in MgO and Al_2O_3 contents compared to that which is usually observed in phoscorite-carbonatite complexes, as seen in Appendix F.4.

Further EPMA analyses need to be carried out on magnetite grains from carbonatite samples, since the late arrival of carbonatite thin sections and a lack of EPMA instrument time meant that these grains could not be analysed.

5.6 Apatite

Apatite compositions were analysed in 4 ultramafic samples (44 analyses) and 4 carbonatitic samples (40 analyses). All apatite chemical analyses are presented in Appendix C.7.

All the apatites are fluorapatites with F contents ranging from 1.7 to 3.49 wt.% in the ultramafic samples and 1.29 to 2.36 wt.% in the carbonatitic samples; none of the apatite analyses contained Cl contents greater than 0.5 wt.%. The SrO content of the ultramafic samples ranges from a low of 0.58 wt.% to highs of 2.91 wt.%, whereas the carbonatitic samples have more consistent concentrations, ranging from 0.61 to 1.14 wt.%. Figure 37 shows compositional zoning within apatite grains for which compositional analyses of the various zones are given in Table 3. Although Sr values seem to remain constant throughout apatite grains, significant core-rim variation in Ce content may provide the variation in contrast detected in the BSE images, seen in Figure 37, due to variations in average Z values detected by the SEM suggesting that the cores of the apatite grains are more enriched in REE content.

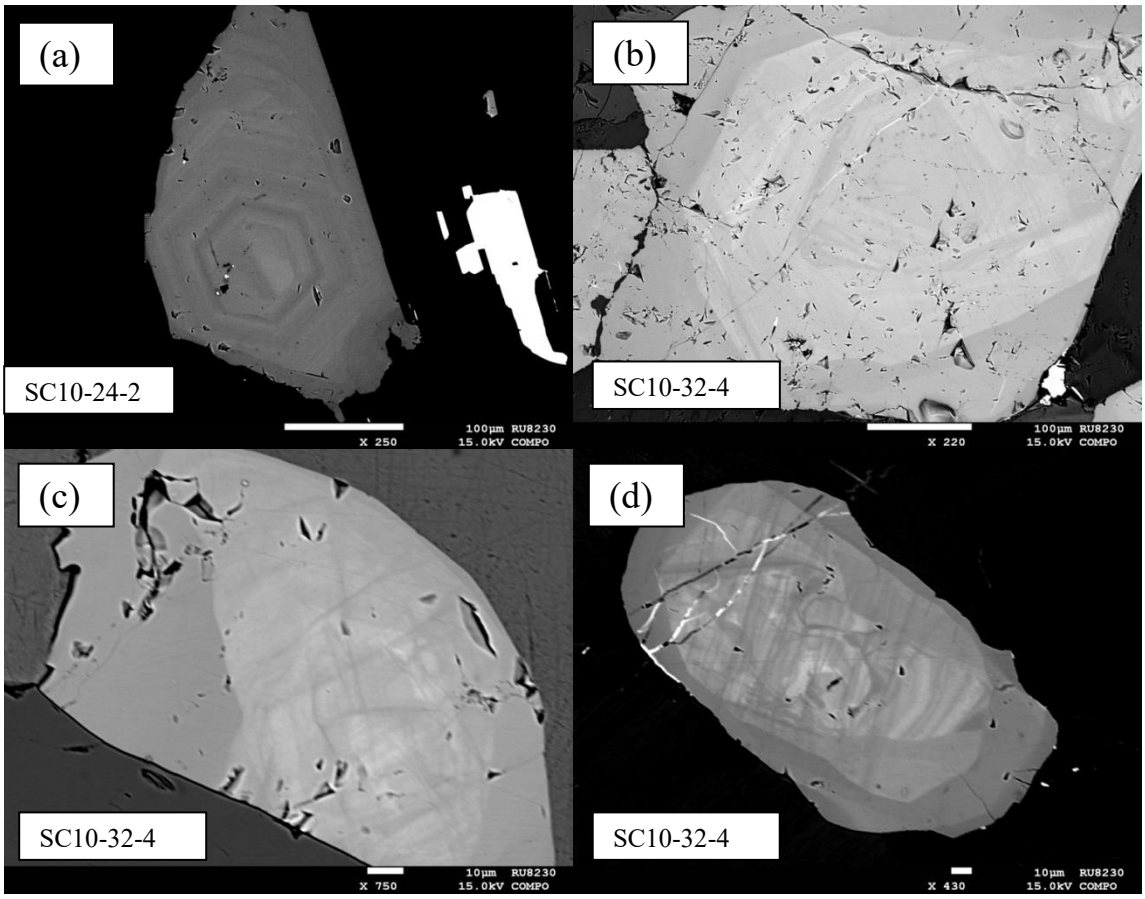

Figure 37: BSE images showing apatite compositional zoning seen in ultramafic samples. Images (a)-(d) correspond with the analyses given in Table 3.

Table 3: EPMA results from zoned apatite grain analyses seen in Figure 37.

Sample #	(a) Dark	(a) Bright	(b) Dark	(b) Bright	(c) Dark	(c) Bright	(d) Dark	(d) Bright
P_2O_5	39.50	39.10	42.13	38.87	41.13	38.94	40.28	38.60
SiO_2	0.35	0.63	0.17	0.86	0.36	1.16	0.17	1.34
MgO	0.02	0.05	0.00	0.00	0.01	0.02	0.00	0.00
CaO	51.58	50.88	52.12	50.77	51.41	49.12	51.69	50.21
Ce_2O_3	0.72	0.99	0.27	1.37	0.28	1.18	0.41	1.30
FeO	0.01	0.04	0.01	0.03	0.20	0.07	0.18	0.12
MnO	0.06	0.15	0.01	0.06	0.04	0.02	0.01	0.05
F	2.05	1.79	1.98	2.07	2.05	2.02	2.21	1.91
Cl	0.44	0.49	0.28	0.43	0.33	0.34	0.20	0.45
SrO	1.47	1.48	1.78	1.73	1.79	1.72	1.77	1.70
O = F, Cl	0.96	0.86	0.90	0.97	0.94	0.93	0.97	0.90
Total	95.24	94.72	97.85	95.21	96.66	93.66	95.95	94.76
Number of ions calculated on the basis of 26 (O,OH,Cl,F)								
P	6.02	6.00	6.19	5.95	6.13	6.01	6.07	5.92
Si	0.06	0.11	0.03	0.16	0.06	0.21	0.03	0.24

Mg	0.00	0.01	0.00	0.00	0.00	0.00	0.00	0.00
Ca	9.94	9.89	9.69	9.83	9.69	9.60	9.86	9.75
Ce	0.05	0.07	0.02	0.09	0.02	0.08	0.03	0.09
Fe	0.00	0.01	0.00	0.00	0.03	0.01	0.03	0.02
Mn	0.01	0.02	0.00	0.01	0.01	0.00	0.00	0.01
F	1.17	1.02	1.09	1.19	1.14	1.17	1.24	1.09
Cl	0.13	0.15	0.08	0.13	0.10	0.10	0.06	0.14
Sr	0.15	0.16	0.18	0.18	0.18	0.18	0.18	0.18
Total Cations	17.69	17.59	17.45	17.72	17.54	17.55	17.68	17.62

5.7 Summary

Distinct mica mineral chemistries present in the various Schiel Complex rock types can be used to discriminate between the various Schiel Complex ultramafic and carbonatitic rock types. Although the calcite carbonatite and glimmerite rocks have mica minerals with similar chemistries, clear variation is seen with respect to the mica compositions from the various ultramafic rock types, as well as differentiating the phlogopite magnetite calcite carbonatite mica compositions from micas from the calcite carbonatites. Calcite carbonatites, phlogopite magnetite calcite carbonatites and glimmerites contain only phlogopite micas, whereas clinopyroxenites contain only magnesian biotite and the phoscorites contain Mg-rich magnesian biotite and phlogopite. The phlogopite magnetite calcite carbonatites contain only a phlogopite variety that is more Mg-poor than the calcite carbonatite mica type. Phlogopite magnetite calcite carbonatites and phoscorite micas seem to contain similar chemistry, but micas from the phlogopite magnetite calcite carbonatites are more depleted in Ti content. It is also seen, from Figure 32, that the phoscorite and clinopyroxenite micas contain different evolutionary paths which suggests that the emplacement of these two units were discrete events.

All clinopyroxene grains are Na-poor and Mg-rich varieties, with all carbonatite rocks containing diopside and all ultramafic rocks containing either diopside or salite, with the majority of the ultramafic rock clinopyroxene grains classified as salite. No distinct pattern is observed between the clinopyroxene type and the various ultramafic rock types. Only one sample, a clinopyroxene vein intruding into a syenite, contained clinopyroxene grains which characterised as aegirine-augite. Calcic-amphiboles, tremolite and actinolite are all present in the Schiel Complex rocks, with the ultramafic rocks containing actinolite as the dominant amphibole and the calcite carbonatites containing tremolite as the dominant amphibole. Only the phlogopite magnetite calcite carbonatite sample contained sodic-calcic-amphiboles, winchite.

Apatite grains from all the rock types show that similar mineral chemistries are recorded in the apatite grains throughout the Schiel Complex ultramafic and carbonatite rocks, where all apatites are present

as the fluorapatite variety. It is also seen that most apatite grains are concentrically zoned, where cores of grains contain a higher Cl and Ce_2O_3 content, resulting in the assumption that the cores of the grains contain a higher REE composition than the rims. This zonation pattern suggests that apatite grains may have originally been REE-rich varieties before scavenging of REE's from the outer sections of the apatite grains occurred, possibly due to reactions with later carbonatitic fluids.

All olivine grains analysed are forsterite-rich, containing minor compositional zoning, which shows a minor increase in Si and Mg content and decrease in Fe and Mn from the core to rim. Serpentine is common and is produced as secondary minerals, together with secondary magnetite as fracture fillings and inclusions in serpentine, through the alteration of olivine.

The analogous chemistries analysed from the mafic minerals: magnetite, clinopyroxene, amphibole and apatite, from the various Schiel Complex rock types, show that these rock types are closely related, and could therefore be a product of a common parental magma where some initial fractional crystallisation must have taken place before magma ascent (Krasnova et al., 2004), producing common minerals with the same compositions hosted in the various ultramafic and carbonatitic rocks.

Chapter 6: Whole-rock Major and Trace Element Geochemistry

Twenty-five pulverised rock samples were submitted to the Central Analytical Facilities (CAF) at Stellenbosch University in the Western Cape of South Africa, for whole-rock major and trace element analyses via X-ray Fluorescence Spectrometry (XRF) and Laser Ablation Inductively Coupled Plasma Mass Spectrometry (LA-ICP-MS), respectively. A total of 10 carbonatite and 15 ultramafic samples, comprising of 1 clinopyroxenite, 5 magnetite-rich phoscorite, 2 olivine-bearing glimmerites and 6 glimmerite samples, were analysed. The whole-rock and trace element analyses results for all samples can be seen in Appendix D, including duplicate samples analysed to ensure quality control. Appendices D 3 – D 5 contain information regarding XRF and ICPMS reference values used, as well as the instrument conditions.

6.1 Major Elements

Figure 38 shows major element oxide variation diagrams comparing all the rocks analysed, using total FeO* (total Fe expressed as FeO) to discriminate between the different rock types.

As expected, the magnetite-rich phoscorites contain the highest total FeO* content due to the high magnetite and magnesian biotite content. Al_2O_3 and K_2O contents reflect the relative mica abundances between the various rock types: glimmerites contain the highest proportion of these oxides, along with higher MgO relative to FeO* content suggesting a more phlogopitic mica end-member composition, with lower magnetite content present indicated by low TiO_2 content. TiO_2 contents are relatively enriched in the magnetite-rich phoscorite, which is expected due to the presence of ilmenite as exsolution lamellae in magnetite grains. Clinopyroxenites are easily distinguishable based on elevated Na_2O content, which is only present in small amounts in clinopyroxene and amphibole minerals, as seen in Chapter 5. P_2O_5 contents are shown to be independent of rock type: where all the Schiel Complex rock types contain a wide range of P_2O_5 content, besides the clinopyroxenites where low concentrations of apatite were detected, supported by the petrographic analyses. The low P_2O_5 and high CaO contents seen in the clinopyroxenite analyses point towards the abundance of calcic-pyroxenes and calcic-amphiboles present in this rock type.

Carbonatite samples show 3 major groupings: a calcite carbonatite which shows minimal mafic mineral major element characteristics relating to minor amounts of magnetite, apatite and mica present in the samples; a magnetite calcite carbonatite which shows a relative enrichment in P_2O_5 and TiO_2 contents indicating a higher degree of magnetite and apatite crystallisation; and the phlogopite magnetite calcite carbonatite which is relatively enriched in magnetite, mica and apatite based on relatively high FeO*, MgO, TiO_2 and P_2O_5 contents. Although this analysis shows the phlogopite magnetite calcite carbonatite to contain low K_2O and Al_2O_3 content, this is contrary to petrographic analyses as only the

sample containing schlieren enriched in magnetite, depicted in Figure 27, contained enough material to allow for whole-rock chemical analyses.

All carbonatite samples have CaO contents between 41.26 and 52.90 wt.% with wide ranges in P_2O_5 contents, besides one magnetite calcite carbonatite sample (SC08-13) which contains 26.83 wt.% CaO. This magnetite calcite carbonatite sample is characterised by a carbonatite vein sheathed by mica-rich material, similarly to what is seen in Figures 7 and 23, containing elevated Al_2O_3, SiO_2 and K_2O contents, as well as containing a relative enrichment in Na_2O.

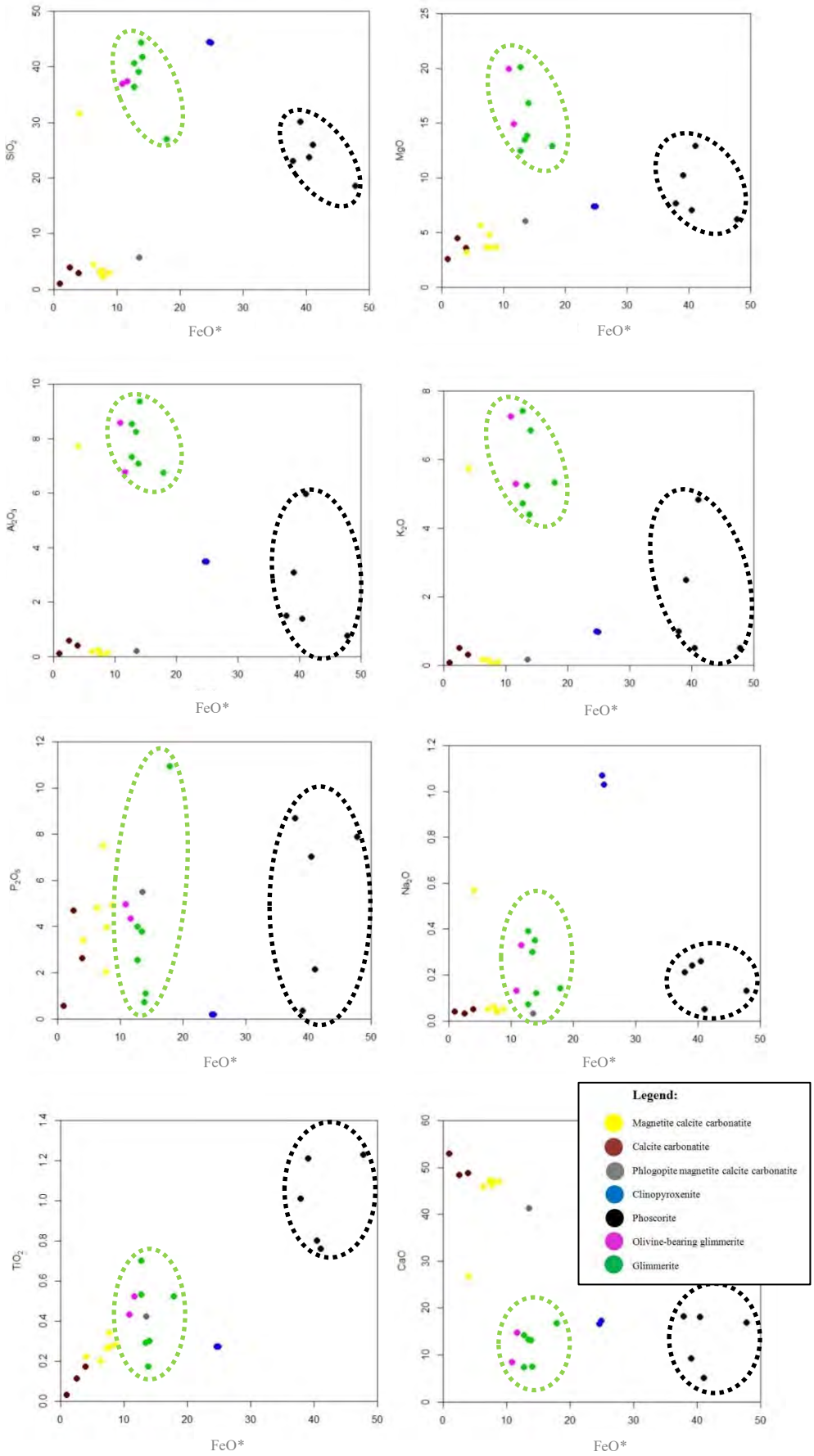

Figure 38: Major element oxide variation diagrams for all the rock types from the Schiel Complex.

6.1.1 Ultramafic Rocks

Magnetite-rich phoscorite samples have high FeO* contents ranging from 37.90 to 47.85 wt.%, reflecting the high modal proportion of magnetite in these samples. K_2O values of 2.47 and 4.82 wt.% and Al_2O_3 contents of 3.07 and 5.97 wt.%, in samples SC10-7.1 and SC10-14.4 respectively, reflect high mica content as either magnesian biotite or phlogopite, together with the lowest P_2O_5 contents (0.33 – 2.13 wt.%). The 3 other samples have low K_2O (< 0.98 wt.%) and Al_2O_3 contents (< 1.48 wt.%), but high P_2O_5 contents ranging from 7.01 to 8.68 wt.%. This reveals a general trend in that the magnetite-rich phoscorites containing low mica contents contain a higher modal proportion of apatite; whereas where mica is abundant, low apatite content is present. This rock type is also deficient in clinopyroxene, which is supported by the low SiO_2 and Na_2O contents as well as the decreasing CaO content with decreasing P_2O_5 content, which indicates that CaO content fluctuation is a function of apatite abundance and not calcic-pyroxene/calcic-amphibole.

Two samples SC10-4.3.1 and SC10-4.3.2 contain FeO* values of 24.65 and 24.94 wt.% , respectively, which show that magnetite crystallisation is prominent, but not as abundant as in the magnetite-rich phoscorite samples. These samples are depleted in P_2O_5 (0.17 wt.%) and enriched in CaO (16.59 and 17.25 wt.%, respectively), reflecting the lack of apatite and abundant diopsidic clinopyroxene content. Low K_2O contents (0.96 and 0.98 wt.%) show minimal mica crystallisation, and MgO contents of 7.35 and 7.38 wt.% show that most of the MgO content can be attributed to clinopyroxene crystallisation. High CaO contents can be attributed to clinopyroxene crystallisation as well as calcic-amphibole present in these samples, which forms as a replacement texture over clinopyroxene. High silica contents (between 44.30 and 44.39 wt.%), as well as the high Na_2O contents (between 1.03 and 1.07 wt.%), support clinopyroxene-dominated assemblages together with amphibole as alteration minerals.

The glimmerite samples have between 4.40 and 7.41 wt.% K_2O and between 6.75 and 9.36 wt.% Al_2O_3 contents, which show the abundance of mica present in the samples. All samples have SiO_2 values between 36.40 and 44.35 wt.%, besides sample SC10-30-4, which has a SiO_2 value of 26.94 wt.%. FeO* values (12.74 – 17.93 wt.%) are depleted relative to the other rock types. In contrast, MgO values (12.46-20.11 wt.%) are enriched with respect to the phoscoritic and clinopyroxenitic rocks from the same core, which point to preferential phlogopite crystallisation in the glimmerites taking into account the uptake of Fe by magnetite and diopsidic clinopyroxene in these rocks. P_2O_5 contents are generally low (0.70 - 3.98 wt.%) with only sample SC10-30-4 having a P_2O_5 content of 10.94 wt.%. This shows that apatite generally occurs in low abundance with the odd apatite enriched zone. CaO content is not a function of apatite in the glimmeritic rocks due to their diopsidic clinopyroxene abundance and close association to carbonate material.

Two olivine-bearing glimmerite samples were analysed from core SC09. These samples are characterised by K_2O (5.29-7.26 wt.%) and Al_2O_3 (6.77-8.58 wt.%) contents which support a high degree of mica crystallisation, with high MgO (14.92-19.92 wt.%) and low FeO* (10.87-11.68 wt.%) pointing towards a higher proportion of phlogopite and olivine/serpentine in the samples. Low FeO* contents are also mirrored by the glimmerites from core SC10. The major element oxide values are consistent with that of the glimmerite rocks analysed from core SC10 with only the P_2O_5 content varying drastically, illustrating the heterogeneous nature of apatite crystallisation.

6.1.2 Carbonatites

The carbonatite samples all have SiO_2 contents of less than 5.62 wt.% besides sample SC08-13, which is an outlier due to its high silicate content of 31.54 wt.% as a consequence of high modal mica content. This is consistent with this sample having the lowest CaO content (26.83 wt.%), associated with highest Al_2O_3 (7.70%) and K_2O (5.73%) contents.

All other samples contain P_2O_5 contents that range between 0.56 and 7.49 wt.% with an average wt.% of 4.06, similarly to the ultramafic samples which have an average P_2O_5 content of 4.43 wt.%. All samples contain low TiO_2 contents of less than 0.42 wt.%, low Na_2O values of less than 0.06 wt.%, MnO contents of less than 0.13 wt.% and K_2O contents of less than 0.5 wt.%. This shows that the carbonatites from the Schiel Complex mostly consist of carbonate-bearing minerals, calcite and apatite, where mafic minerals (mica, magnetite, clinopyroxene) make up a small portion of the rocks constituents.

From what is seen in sample SC10-13, the low SiO_2, Al_2O_3 and K_2O values seen throughout the other carbonatite samples indicate that low degrees of contact between the carbonatite and syenite/ultramafic rock leads to a low yield in mica crystallisation, which could be ascribed to a reaction product between the carbonatite and surrounding wall-rock.

The classification of the carbonatites after Le Maitre (1989), presented in Figure 39, shows that no carbonatites present are magnesio-carbonatites, with 5 samples classified as calcitic carbonatites and 5 samples classified as ferro-carbonatites. Sample SC08-15, the phlogopite magnetite calcite carbonatite as seen in Figure 27, plots as the outlier due to high magnetite content, causing relative total iron-enrichment (FeO* wt.% = 13.53). Another cluster of carbonatite analyses is present close to the calcio-carbonatite and ferro-carbonatite border. These samples are magnetite-bearing carbonatites which contain low K_2O and low Al_2O_3 contents, suggesting little mica crystallisation. Samples that plot distinctly in the calcio-carbonatite field contain high CaO contents with no significant content of other major element oxides attributed to mafic mineral crystallisation. Gittins and Harmer (1997) described imprecisions in the IUGS carbonatite classification, as no distinction is made between ferric and ferrous

iron, which leads to the improper incorporation of ferric iron in the classification, which is only present in oxide minerals and not in the carbonate minerals. These imprecisions can be overcome when plotting the molar ratios of the same oxides on a ternary diagram, as seen in Figure 40. Figure 40 shows that no carbonatite analyses plot in the ferrocarbonatite field, with only sample SC08-15 classified as a ferruginous calciocarbonatite, due to its schlieren enriched in magnetite, with all other samples classified as calciocarbonatites, as would be expected after petrographic analyses.

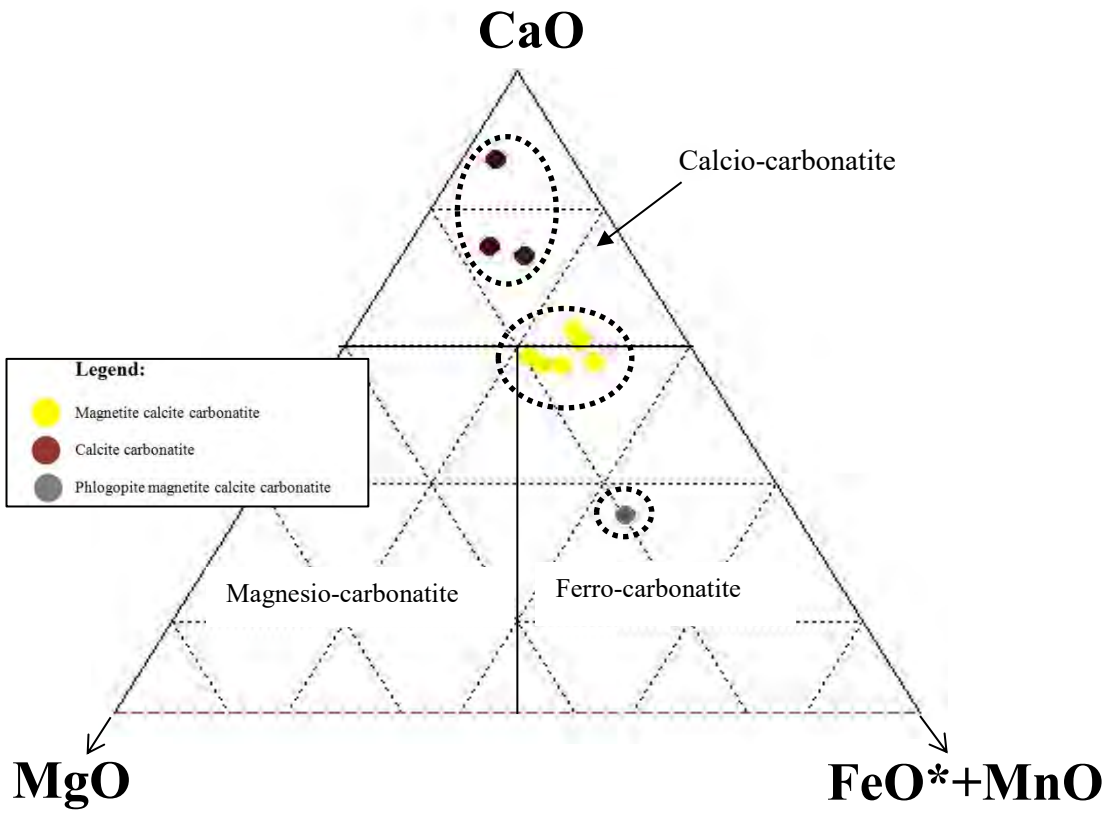

Figure 39: Carbonatite classification diagram using the IUGS chemical classification scheme (Le Maitre, 2002).

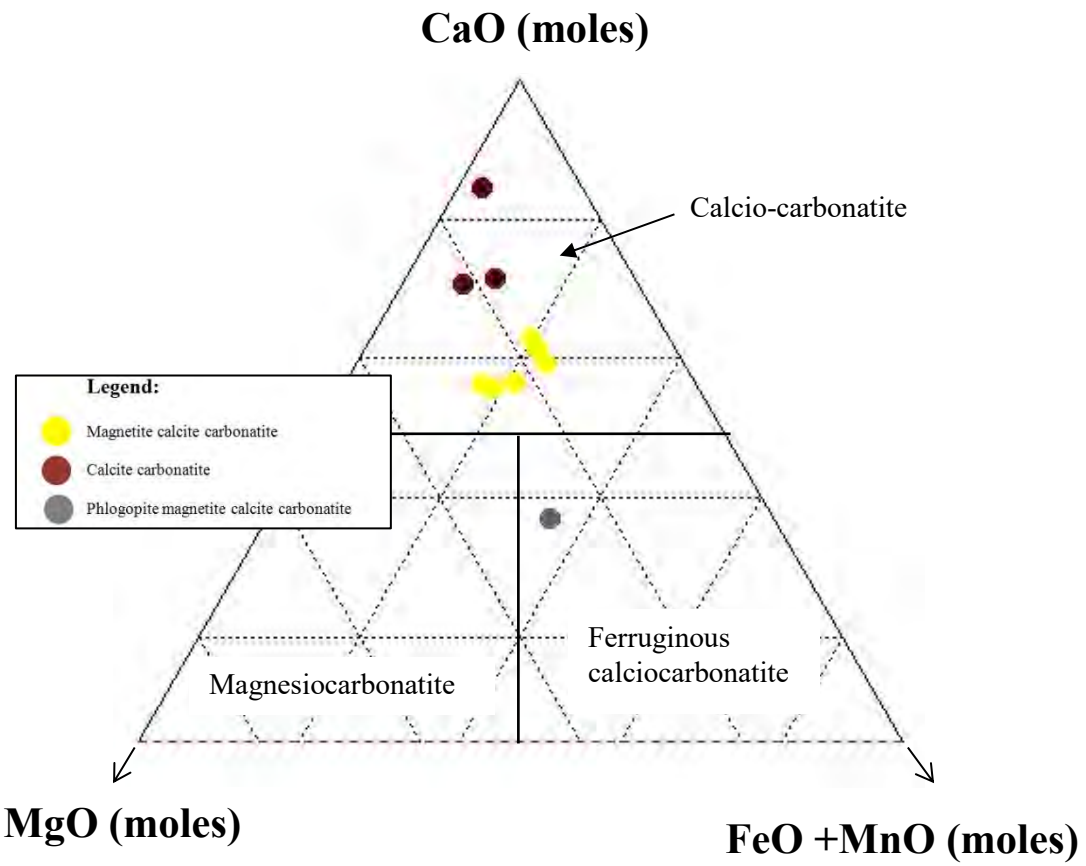

Figure 40: Carbonatite classification diagram using molar proportions after Gittins & Harmer (1997).

6.2 Trace Element Variations

Figure 41 shows the Ba vs K_2O content of the various rock types where a positive correlation is seen between the two variables. It is seen that with an increase in K_2O, suggesting an increase in mica content, the Ba content increases as well. This is seen in the phoscoritic rock type where low mica content yields a low Ba content and glimmerites contain higher Ba contents. This trend is also seen in the carbonatites, which concentrate a higher Ba content than the ultramafic rocks, where carbonatites containing little to no mica minerals still contain higher Ba contents than the phoscoritic rocks, with one carbonatite sample (SC08-13), present as a carbonatite vein sheathed by mica minerals, containing anomalously high Ba content relative to the other samples, possibly due to abundant Ba-rich mica or a due to that sample containing a Ba-rich carbonatite intrusion.

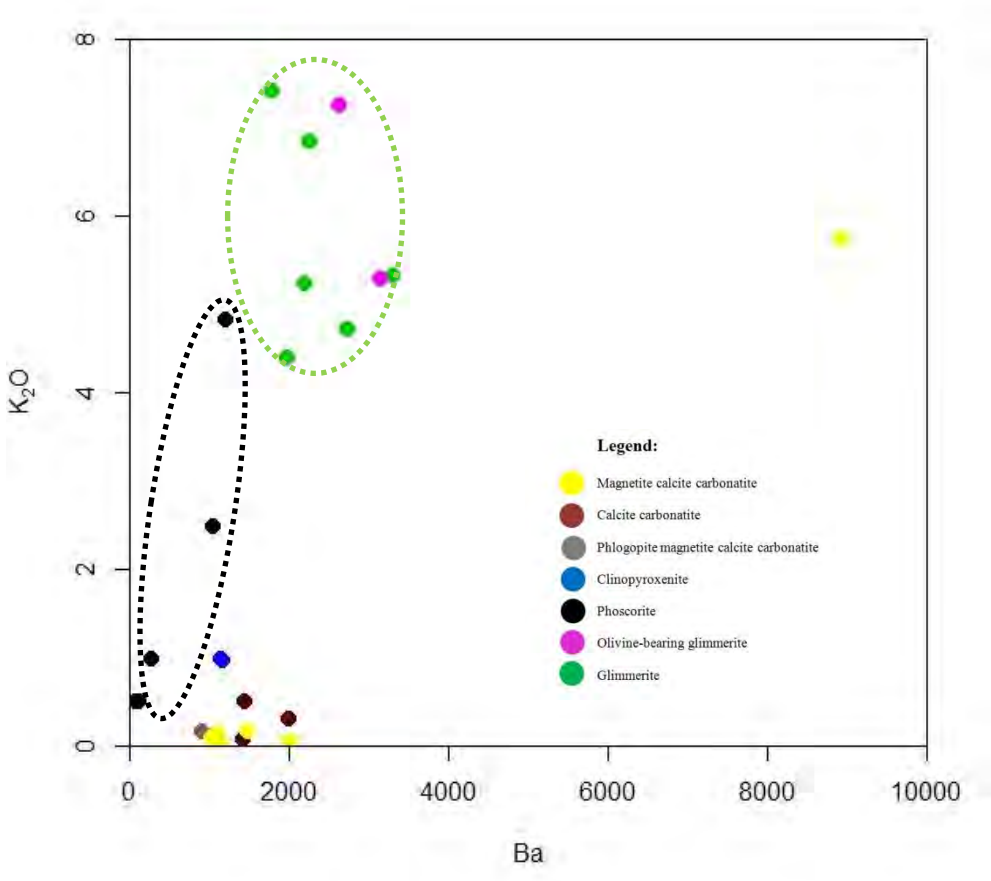

Figure 41: Ba vs K_2O binary plot for all Schiel Complex rocks.

Figure 42 shows the FeO* vs V content amongst the various rock types and clearly shows a highly elevated V content in the phoscoritic rock types relative to all others. This is a reflection of the enrichment in magnetite in phoscoritic rocks relative to the other rock types. Also shown is that the phlogopite magnetite calcite carbonatite contains higher V contents than both the glimmerite and clinopyroxenite; again, a reflection of higher magnetite content.

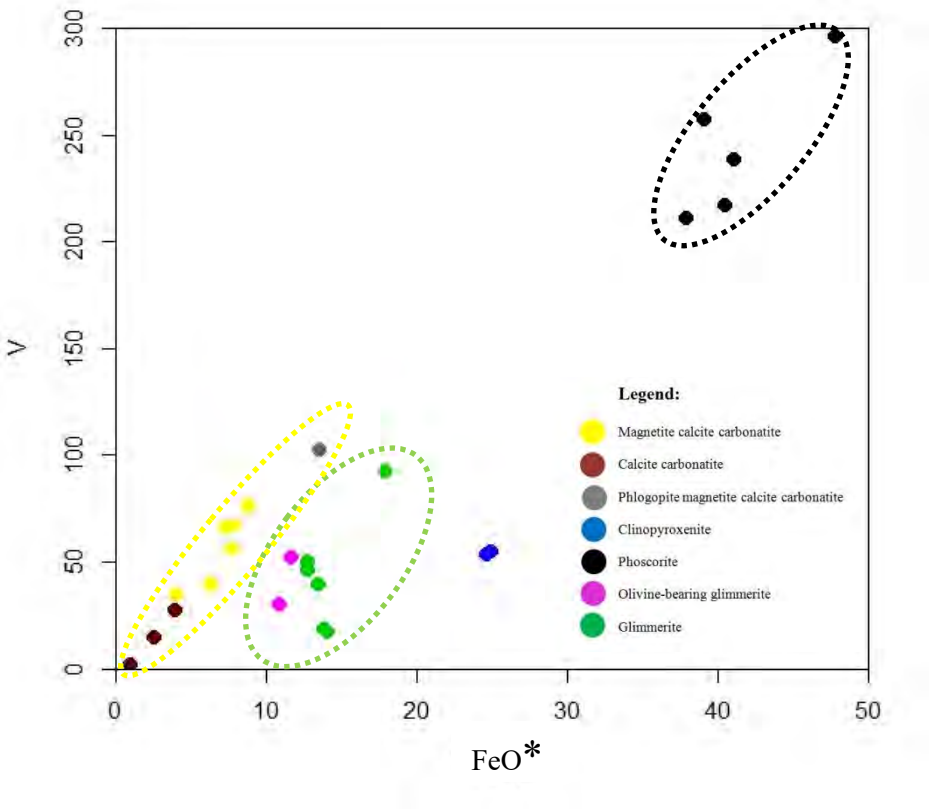

Figure 42: FeO* vs V binary plot for all rock types from the Schiel Complex.

Figure 43 shows the Rb vs Sr content of the analysed rock types, which shows distinct variations between these inversely proportioned variables. The highest Rb values are recorded in the glimmerites, which would be expected due to the probability that Rb could be admitted to the K^+ sites present in mica minerals. High Sr values are expected in calcite-rich assemblages, which are seen in the carbonatite samples, with all other rock types suggesting some degree of Ca-bearing mineral content, possibly due to calcite, diopside or apatite crystallisation.

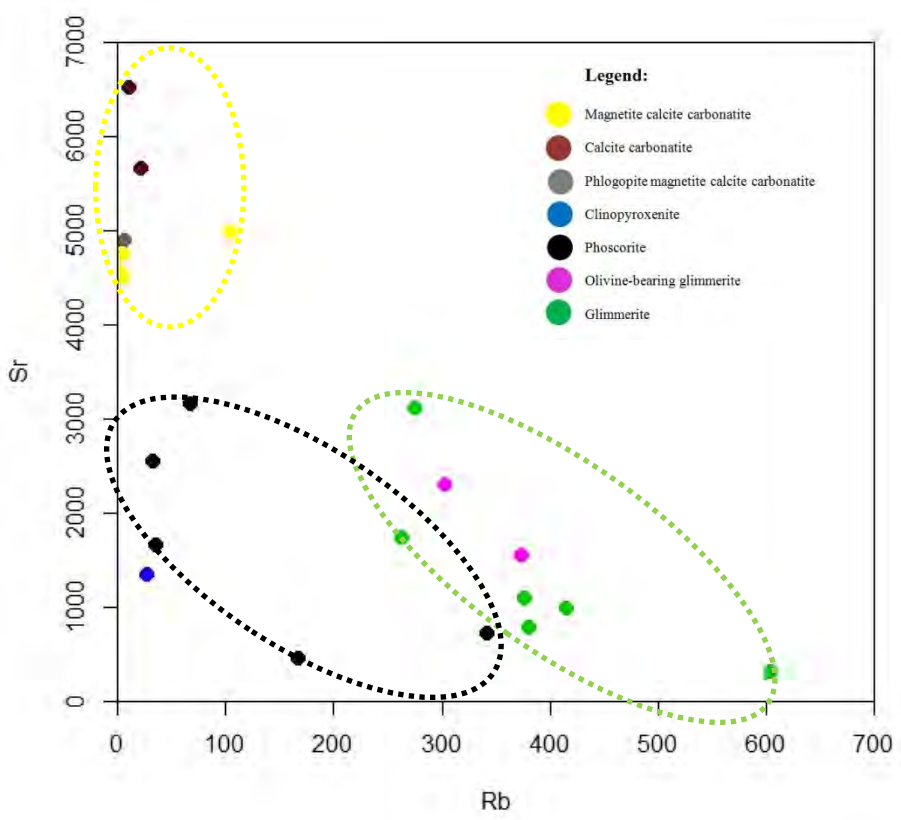

Figure 43: Rb vs Sr binary plot for all rock types from the Schiel Complex

6.2.1 Rare Earth Elements (REE)

Plots of chondrite-normalised REE+Y contents for all the ultramafic types as well as the carbonatites are presented.

Samples have been plotted individually by rock type, as well as together to show the relationships between the different rock types: 15 ultramafic samples subdivided into 2 clinopyroxenite, 5 magnetite-rich phoscorite, 6 glimmerite and 2 olivine-bearing glimmerite samples are plotted in Figure 44. The 10 carbonatite samples are plotted in Figure 45. All chondrite-normalised REE plots are based on the normalisation values provided by McDonough and Sun (1995). Table 4 provides REE ratios calculated for each sample, which helps to illustrate the internal variations within the specific REE profile of each sample. La_N/Yb_N, La_N/Sm_N and Sm_N/Yb_N ratios were calculated to quantify the internal variations of LREE (Light REE) vs HREE (Heavy REE), LREE vs MREE (Middle REE), and MREE vs HREE, respectively.

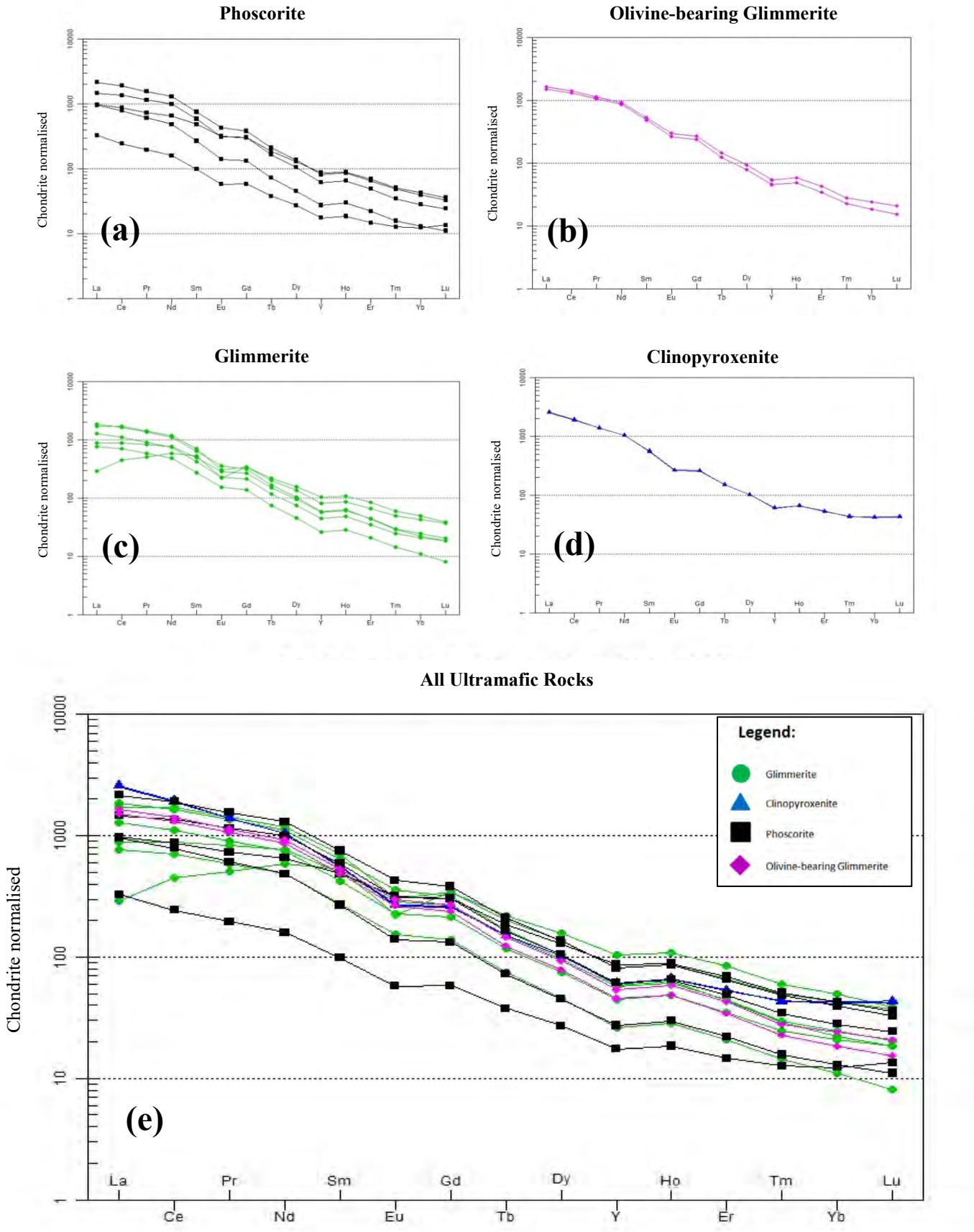

Figure 44: REE chondrite-normalised plots (McDonough and Sun, 1995) of all the ultramafic rocks: (a) glimmerites; (b) clinopyroxenite; (c) Magnetite-rich phoscorite; (d) olivine-bearing glimmerite; (e) All the ultramafic rocks plotted together.

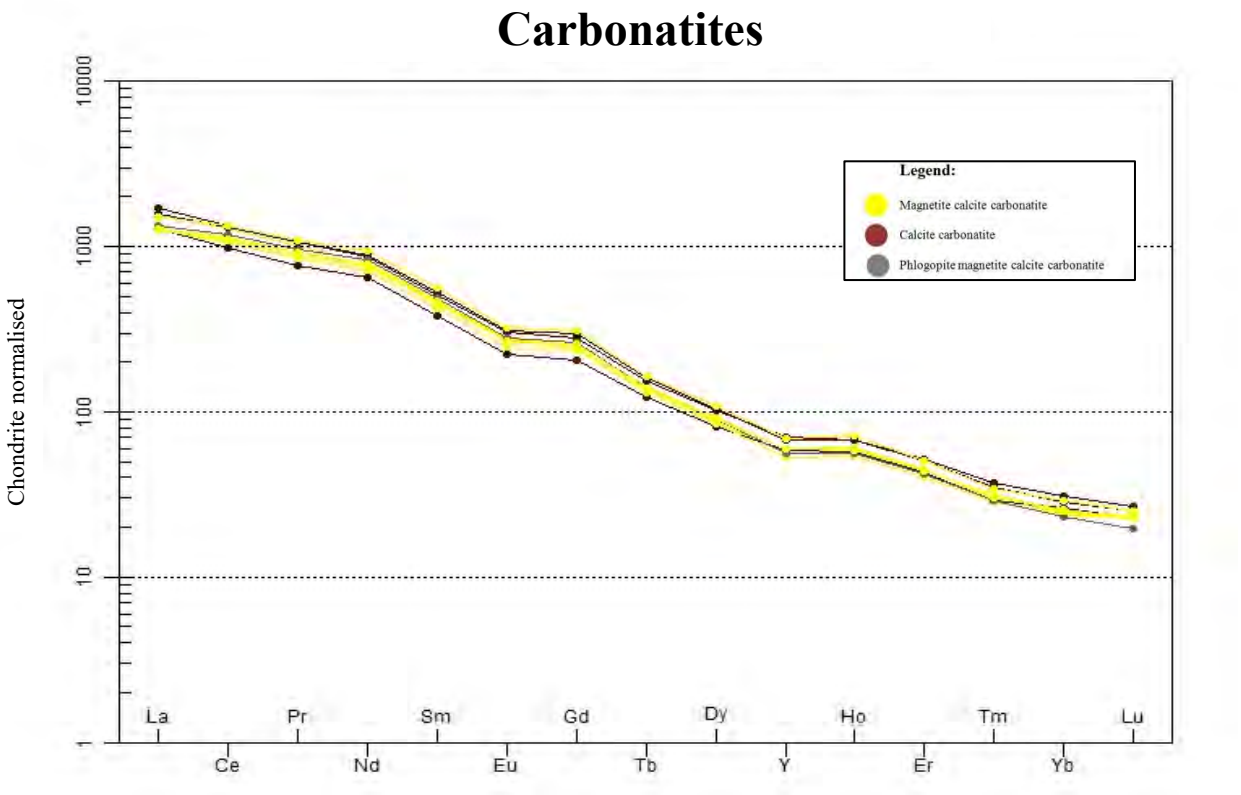

Figure 45: REE chondrite-normalised plot (McDonough and Sun, 1995) of all the carbonatite samples.

Table 4: REE ratios for all Schiel Complex rock types.

Sample name	Rock type	∑LREE (La-Eu)	∑HREE (Gd-Yb) (excl. Y)	LREE/ HREE	La_N/ Yb_N	La_N/ Sm_N	Sm_N/ Yb_N	Eu/Eu_N*
SC10-1.2	Glimmerite	748.60	145.12	5.16	5.85	0.55	10.72	0.50
SC10-2.2	Glimmerite	2246.06	133.04	16.88	40.16	2.43	16.52	0.58
SC10-18.3	Glimmerite	1273.78	97.51	13.06	36.25	1.79	20.30	0.74
SC10-21.2	Glimmerite	1483.36	77.94	19.03	60.64	2.99	20.27	0.71
SC10-24.1	Glimmerite	940.13	48.45	19.40	69.14	2.78	24.88	0.75
SC10-30.4	Glimmerite	2184.38	110.17	19.83	82.69	2.89	28.58	0.74
SC10-4.3.1	Clinopyroxenite	2503.59	102.63	24.39	60.71	4.57	13.28	0.65
SC10-4.3.2	Clinopyroxenite	2464.31	101.89	24.19	61.29	4.61	13.31	0.65
SC10-5.2	Phoscorite	1219.73	123.22	9.90	22.93	2.02	11.33	0.80
SC10-7.1	Phoscorite	1032.31	47.70	21.64	73.89	3.55	20.79	0.70
SC10-12.3	Phoscorite	2552.78	139.53	18.30	54.76	2.88	19.01	0.76
SC10-14.4	Phoscorite	336.21	25.21	13.34	26.73	3.32	8.04	0.74
SC10-15.3	Phoscorite	1842.70	108.46	16.99	51.80	2.48	20.86	0.70
SC09-05	Olv-bearing glimmerite	1877.55	96.43	19.47	68.28	3.08	22.19	0.74
SC09-09	Olv-bearing glimmerite	1742.58	83.00	21.00	82.58	3.13	26.41	0.73
SC08-02	Magnetite calcite carbonatite	1418.13	87.50	16.21	53.34	3.05	17.48	0.75
SC08-08	Magnetite calcite carbonatite	1539.97	93.96	16.39	54.81	2.94	18.62	0.76
SC08-13	Magnetite calcite carbonatite	1697.82	87.20	19.47	65.67	3.35	19.60	0.79
SC08-16	Magnetite calcite carbonatite	1507.81	94.31	15.99	49.47	2.73	18.12	0.74
SC08-19	Magnetite calcite carbonatite	1463.87	90.94	16.10	50.01	2.80	17.88	0.77
SC08-23	Magnetite calcite carbonatite	1799.90	112.14	16.05	51.76	2.69	19.25	0.74
SC08-05	Calcite carbonatite	1340.57	80.25	16.71	49.00	3.33	14.72	0.76
SC08-11	Calcite carbonatite	1812.55	104.44	17.36	55.38	3.38	16.41	0.77
SC08-14	Calcite carbonatite	1777.14	107.24	16.57	56.16	2.97	18.89	0.75
SC08-15	Phlogopite magnetite calcite carbonatite	1590.99	93.08	17.09	58.03	2.77	20.94	0.76

$Eu/Eu_N^* = Eu_N/(0.5x(Sm_N+Gd_N))$

All ultramafic samples analysed have LREE/HREE ratios between 5.16 and 24.39 (average = 17.51), which indicates enrichment of LREE relative to HREE. The clinopyroxenite samples have the highest LREE/HREE ratios, in excess of 24, with all other samples having a wide range in LREE/HREE ratios that do not conform to any pattern. La_N/Sm_N ratios average 2.87, while Sm_N/Yb_N ratios average 18.43, which indicate that the enrichment of MREE to HREE is more pronounced than the enrichment of LREE to MREE in all ultramafic rocks. High Sm_N/Yb_N ratios show significant fractionation between MREE and HREE.

All glimmerite samples contain a slight negative Eu anomaly (Eu/Eu* ranges from 0.712-0.748), apart from samples SC10-1-2 and SC10-2.2, which have more negative Eu anomalies of 0.503 and 0.583, respectively. The phoscoritic and clinopyroxenitic samples contain Eu anomalies ranging from 0.646 to 0.800, with the clinopyroxenite representing the lower values (0.646-0.651) and the magnetite-rich phoscorites representing the higher values (0.696-0.800).

Four samples analysed contain low LREE/HREE ratios of less than 14, namely samples SC10-1-2, SC10-5-2, SC10-18-3 and SC10-14-4. Samples SC10-5-2, SC10-18-3 and SC10-14-4 do preserve the overall profile of the other samples, but are more depleted in LREE compared to all other samples and contain less variation between LREE and HREE. Sample SC10-1-2 contains the same general MREE to HREE profile seen in other samples, but shows a positive gradient from La to Sm, with a low La_N/Sm_N ratio of 0.55, as well as containing a significant Eu anomaly (0.50) compared to the other samples (average = 0.73). This deviation may be due to the abundance of uranothorianite (Bea, 1996) present in section SC10-1-2 of the rock, which is supported by the whole-rock trace element analyses, which show that sample SC10-1-2 has a U content of 514ppm, whereas all other samples have an average U content of 24.7ppm. There are no notable major element variations in samples that contain low LREE/HREE ratios relative to the other samples.

In general, the carbonatite samples show similar chondrite-normalised REE profiles to those of the ultramafic rocks with no relative REE enrichment, as seen in Figure 46, with the carbonatite samples being entirely consistent with each other, displaying little variation. This is illustrated in Table 4, which shows that La_N/Yb_N, La_N/Sm_N and Sm_N/Yb_N ratios do not contain a wide range and have averages of 54.25, 2.99 and 18.21, respectively. All carbonatites show LREE enrichment compared to HREE, where MREE to HREE enrichment is more pronounced than LREE to MREE enrichment. The Eu/*Eu value for all carbonatite samples averages 0.75 and ranges from 0.74 to 0.79.

Table 5 shows that the clinopyroxenites contain the highest average total LREE/HREE and highest average La_N/Sm_N (LREE/MREE) ratios with relatively low average Sm_N/Yb_N (MREE/HREE) values together with average Eu/Eu* values of 0.65; glimmerites contain the moderate average La_N/Yb_N (LREE/HREE) and the highest average Sm_N/Yb_N (MREE/HREE) ratios together with average Eu/Eu* values of 0.69; Phoscorites contain the lowest average La_N/Yb_N (LREE/HREE) and moderate average La_N/Sm_N (LREE/MREE) ratios together with average Eu/Eu* values of 0.74. Although glimmerite and phoscorite rock analyses show that some sample analyses deviate drastically from other samples of the same rock type, the averaged REE ratio values provide a suitable guideline for the variation in REE ratios with respect to rock type.

All carbonatite samples showed little variation with respect to each other, besides one magnetite calcite carbonatite sample (SC08-13). These averaged REE ratios show close REE ratio association between the phoscorites, carbonatite and glimmerites.

Table 5: Average REE ratios calculated for the various Schiel Complex rock types

Rock Type	Total Samples	LREE/HREE	La_n/Yb_n	La_n/Sm_n	Sm_n/Yb_n	Eu/Eu_n^*
Glimmerite	8	16.73	55.70	2.45	21.24	0.69
Clinopyroxenite	2	24.29	61.00	4.59	13.29	0.65
Phoscorite	5	16.03	46.02	2.85	16.00	0.74
Carbonatite	10	16.79	54.36	3.00	18.19	0.76

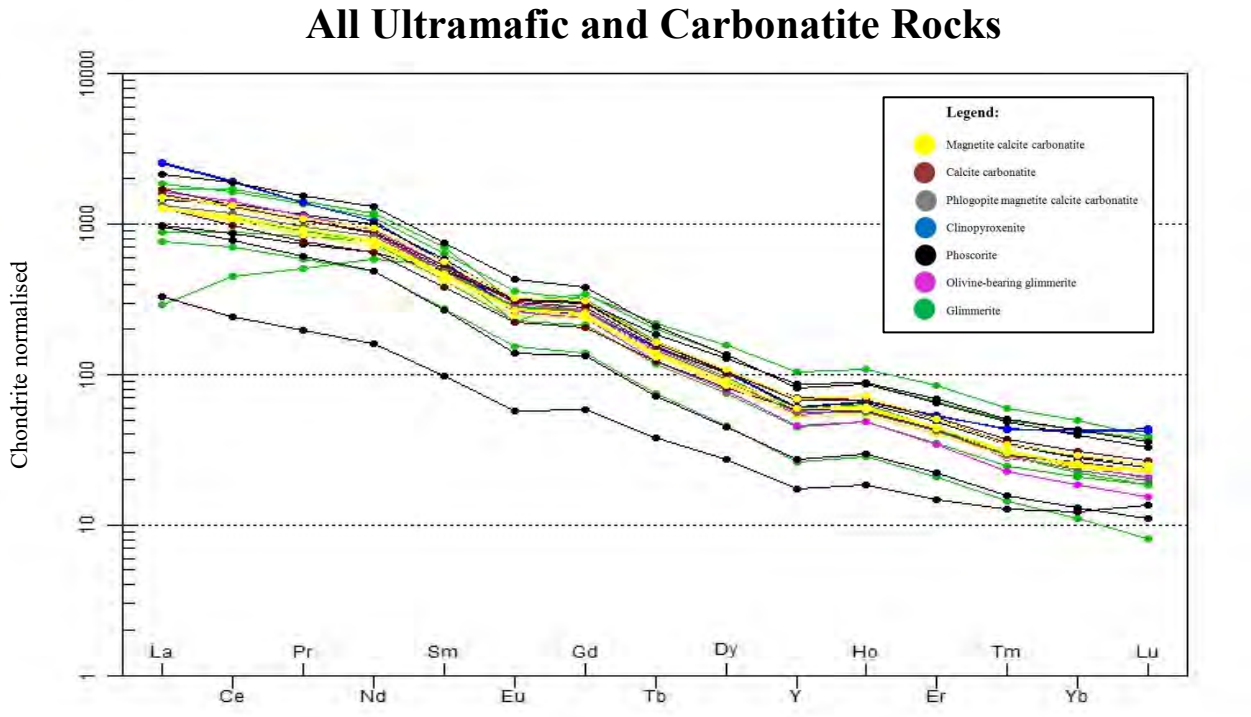

Figure 46: REE chondrite-normalised plot (McDonough and Sun, 1995) of all the ultramafic and carbonatite rocks analysed from the Schiel Complex.

Y/Ho vs Zr/Hf ratios of ultramafic and carbonatitic rock types are plotted in Figure 47 and compared with the field defined by Bau (1996) for high temperature, charge and ionic ratio-controlled ("CHARAC") crystal fractionation processes in common silicate igneous rocks. This plot shows that all the Schiel carbonatites and ultramafic rocks have Y/Ho variations well within the range anticipated for high temperature, CHARAC fractionation.

The glimmerites and carbonatites show variations in Zr/Hf that fall outside of the CHARAC range, suggesting that these rocks show evidence of lower temperature, metasomatic, processes. This is not surprising, due to the extreme variation in glimmerite mineral assemblages and the difficulty in delineating distinct boundaries between the various ultramafic rock types. This plot provides support for the idea that some of the glimmerites could have formed by metasomatic processes and are not truly igneous rocks. A review of the major element oxides shows that there are no distinct chemical differences between the glimmerite samples that plotted inside and the glimmerite samples that plotted outside the field representing crystallisation from a pure silicate melt, besides a slight enrichment in CaO content and a slight depletion in Al_2O_3 content in the samples that plot inside the field.

Carbonatite rocks contain Y/Ho ratios (average = 28.63) that are slightly higher than the ultramafic rocks (average = 26.86), with Zr/Hf ratios plotting in two distinct populations: one between 27.14 and 30.39 and another between 42.26 and 51. The population plotting with low Zr/Hf ratios are extremely depleted in Zr (average = 24.425 ppm) and Hf (average = 0.89 ppm) compared to the other carbonatite samples, which have average Zr and Hf values of 505.65 and 10.29 ppm, respectively. No other significant major or trace element variation is seen between the two distinct populations.

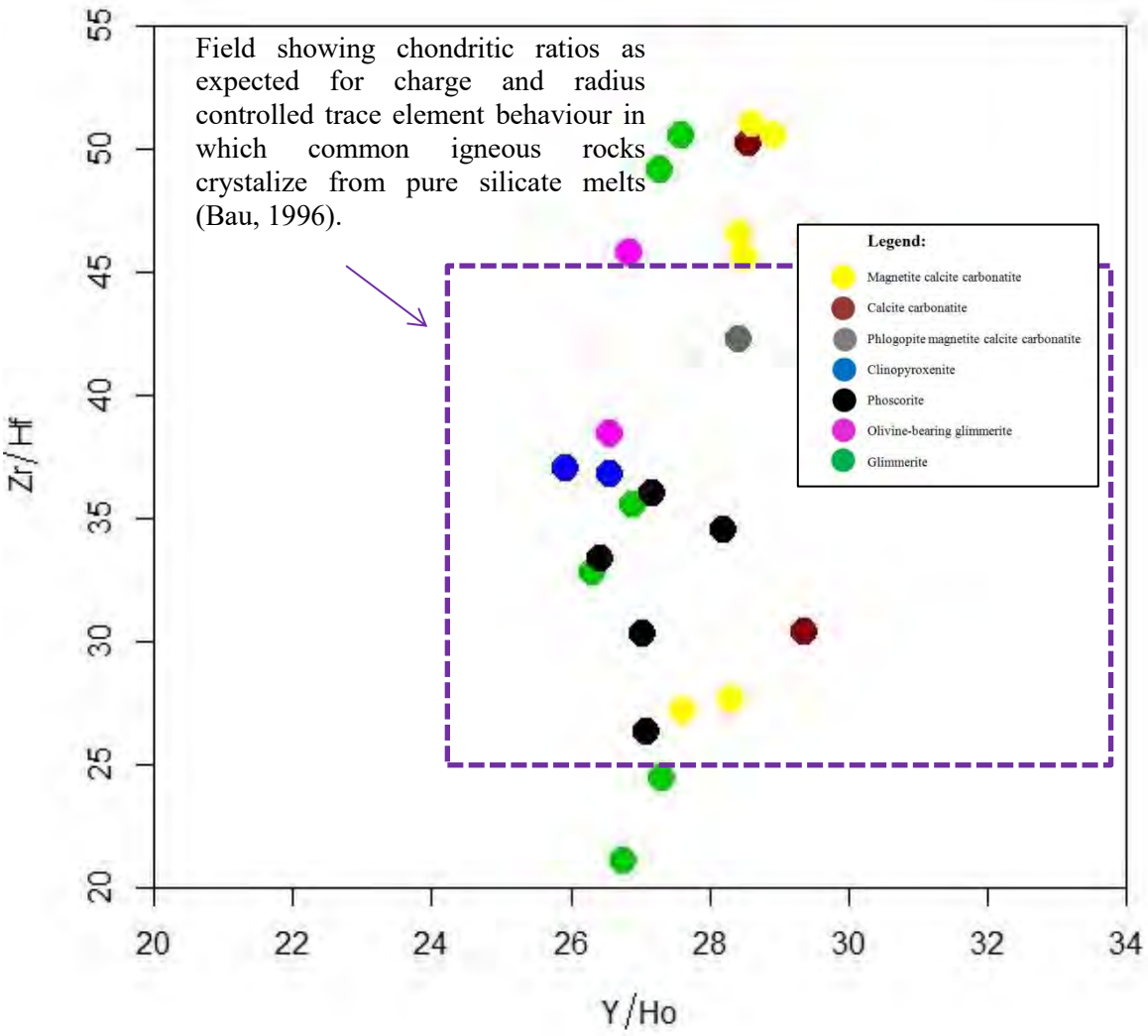

Figure 47: Diagram showing trace element ratios that support magmatic origin (Bau, 1996)

Chapter 7: The Characterisation and Geochronology of Zircon Grains Associated with the Glimmerite and Carbonatite Components of the Schiel Complex

Zircon grains were separated from one carbonatite sample (SC08-15) and one glimmerite sample (SC10-02). The grains were separated at the Central Analytical Facilities (CAF) at Stellenbosch University in the Western Cape. The samples were ground down using a jaw crusher and sieved to capture the 60<350 μm grain-size fraction. The samples were then hand-washed before undergoing gravity separation using the Super Panner to capture the heavy mineral fraction. After drying, the samples were magnetically separated using a hand-magnet to remove the ferro-magnetic fraction. The Franz magnetic separator was not used in this sample preparation due to the small sample size. The non-magnetic fraction then underwent heavy liquid separation using Diiodomethane, which has a density of 3.3. After that, zircon grains were hand-picked, mounted in epoxy and polished using a 3 μm polishing pad followed by a 1 μm polishing pad for 10 minutes each. Grains were then carbon coated for SEM analyses. Zircon grains were cathodoluminescence (CL) imaged at the CAF using the Zeiss MERLIN SEM, backscattered electron (BSE) imaged at Rhodes University using the TESCAN Vega TS 5136LM instrument and final Secondary Ion Mass Spectrometry (SIMS) analyses were performed, using a Cameca 1208-HR instrument housed at the Helmholtz GeoForschungsZentrum Potsdam (GFZ), Germany, through its remote operating centre at the Virtual SIMS Lab at the University if the Witwatersrand in Johannesburg, South Africa.

Zircon grains were more abundant in the glimmerite sample where larger and more euhedral grains were found, whereas the carbonatite sample contained small, anhedral zircon grains. 10 zircons grains from the carbonatitic sample and 35 grains from the glimmerite sample were picked, mounted and imaged in preparation for geochronological analyses.

7.1 SEM Analyses of Zircon Grains

The zircons separated from both samples were found to contain extremely unusual and complex internal structures associated with complex growth conditions.

The glimmerite sample contained two major types of zircon grains on the basis of their internal structures. The majority of the grains showed distinct internal oscillatory zoning indicative of primary zircons grown from a melt together with what seem to be secondary growth zones at rims of the grains, as seen in in Figure 48. Other grains had homogeneous textures with no zoning.

Zoned grains show an apparent magmatic core which is then surrounded by secondary zircon growth which seems to have been abraded down to form an almost rounded and staggered outer shape. Cores of grains show a subhedral abraded nature, but distinct growth zones seen in the zircon cores, as seen in Figure 48, point towards a magmatic origin of these glimmerite sample grains.

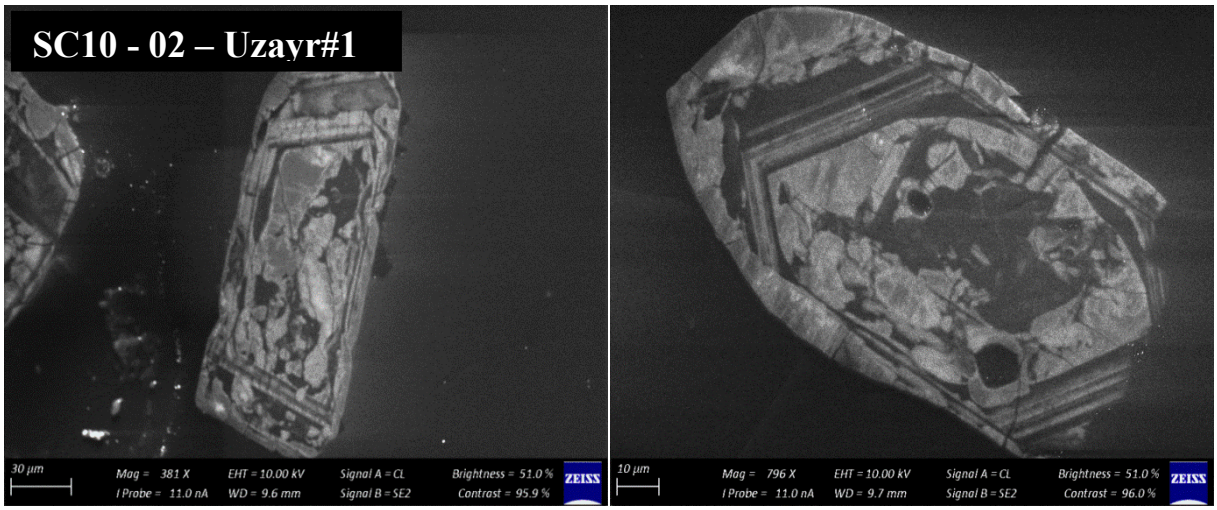

Figure 48: CL images of zircon grains separated from the glimmerite sample that shows subhedral cores followed by a secondary zircon growth event.

Zircons from the carbonatite samples show similar characteristics to that of the glimmerite sample zircons, with most of the grains preserving intricate core growth structures surrounded by more homogenous secondary rim growth. All the zircons seen in the carbonatite fraction appear to be remnants of broken zircon grains, which together with intricate zircon growth zones are a common occurrence in highly fractionated zircon saturated magmas (Markowitz & Kirkland, 2018).

The zircon grain seen in image 49 shows what looks to be an inclusion in the zircon grain highlighted by the darker area of the grain. EDS analyses on the grain shows that this area is also zircon, which contains a slightly lower B and slightly higher Zr content.

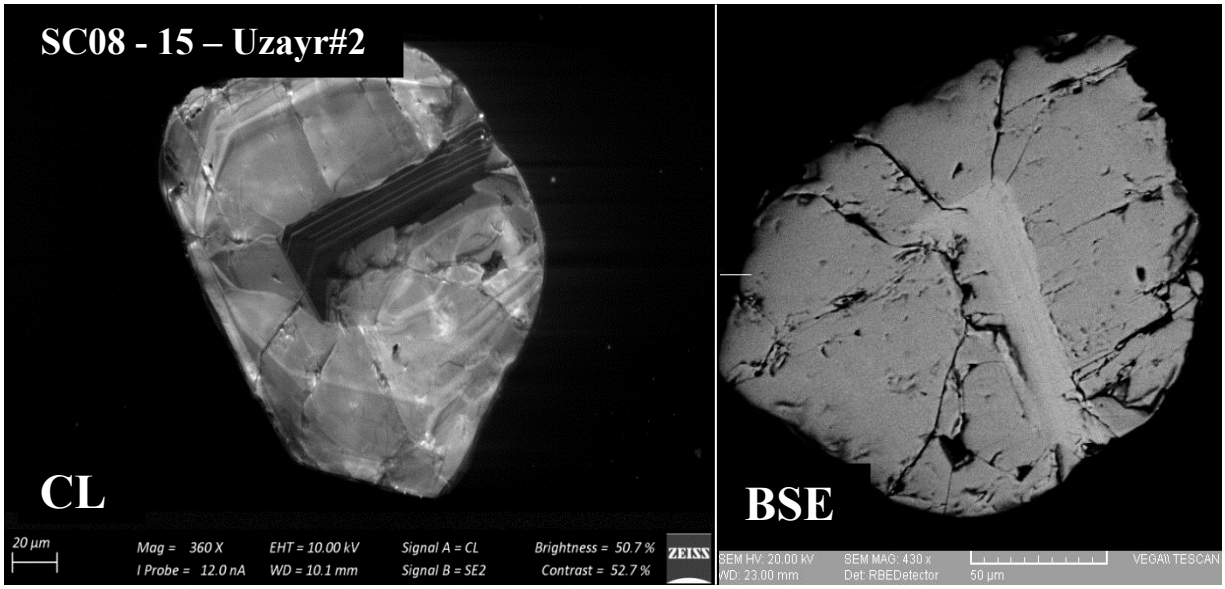

Figure 49: CL and BSE image of a zircon grain separated from the carbonatite sample that shows an inclusion of zircon in the zircon grains, supported by EDS data.

Extremely dark areas are present under CL imaging in both glimmerite and carbonatite zircon grains, but these areas may not be due to metamictisation but due to unusual growth patterns. When analysed using the SEM BSE mode, together with EDS data, the compositional zoning seen under CL-imaging is also seen under BSE imaging, showing clear darker zones due to a variation in zircon composition, and not metamictisation. Cracks are also present in all the grains analysed, as well as small areas of obvious metamictisation, seen by extremely dark, round sections in CL-images and bright spots seen in BSE images. Figure 50 shows the comparison between BSE and CL-images of selected grains. The image shows different degrees of metamictisation seen in various grains, where grain A shows almost no metamictisation and grain C shows a higher degree of metamictisation. EDS data show that the darker zones, under BSE mode, contain slightly lower zirconium and higher silica contents than the slightly brighter zones, whereas the extremely bright areas contain U/Th and sulphur or lead and sulphur, which is in correlation with the extremely dark zones seen in the CL images. EDS analyses show that zircon grains almost always contain calcite and Pb-sulphide inclusions with silicate inclusions (Ca-Mg-Si) detected in only one zircon grain.

The presence of these zircon grains at clear contact zones, in association with alteration assemblages, as well as zircon rims seen around baddeleyite, as seen in Figure 25, provides evidence that some of these zircon grains may have formed due to silica saturation of the magma which may have altered baddeleyite to zircon.

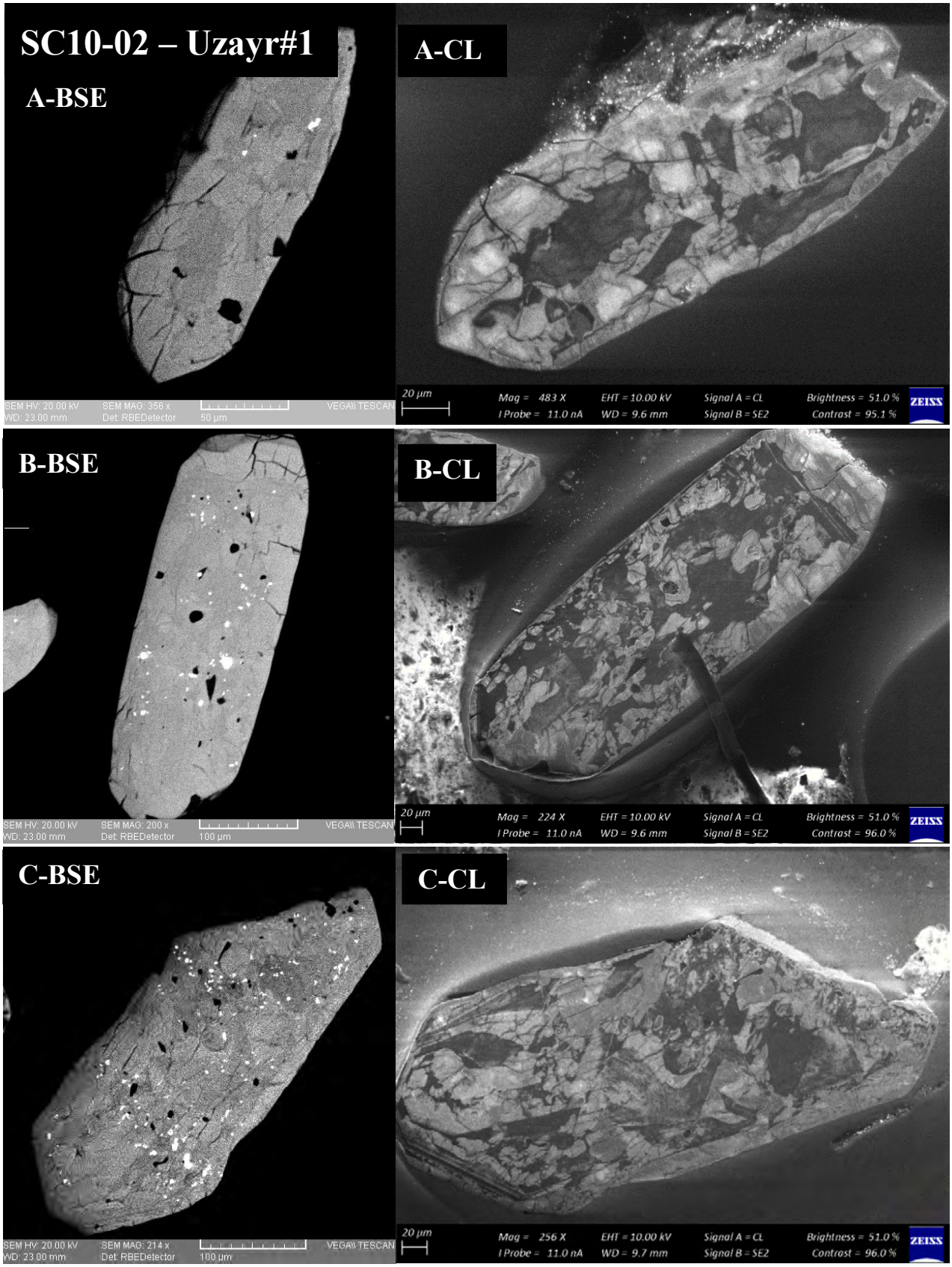

Figure 50: BSE and CL image comparison between zircon grains separated from the glimmerite sample.

7.1.1 Summary

The presence of zircon in the ultramafic rocks without baddeleyite would be expected due to the higher silica activity of the host rock. Zircons in the ultramafic rocks recording the same internal growth structures as seen by the carbonatite zircons may show that these grains were also subject to periods of alternating silica activity in the magma, or that they were only formed at a later stage through hydrothermal infiltration of the carbonatitic fluid which allowed for zirconium to be entrained in the ultramafic rocks, crystallising zircon. The CL-image analyses of zircons studied from the glimmerite sample may not be representative of the magmatic ultramafic rocks, as these grains display similar characteristics to that of the carbonatite zircons and may have formed through the same processes.

Furthermore, some zircon grains that display magmatic internal textures, with distinct core and rim zones. These grains may have experienced a hiatus in growth, after initial compositional alteration from baddeleyite to zircon, together with mineral abrasion followed by another zircon growth event which is why a more magmatic internal structure is observed in the rims creating a more euhedral overall zircon shape.

7.2 Geochronology

7.2.1 Secondary Ion Mass Spectrometry (SIMS) analytical methods

U-Pb determinations were conducted using the virtual SIMS node at the University of the Witwatersrand, connected to the Cameca 1280-HR instrument located at the Helmholtz Zentrum Potsdam (GFZ) via internet link.

Prior to analyses, the two zircon grain mounts were cleaned using ethanol in an ultrasonic bath. The samples were then imaged, uncoated, to assist with navigation and point selection using a motorised Nikon Eclipse LVDIA-N microscope. Point selection from the remote node in Johannesburg was completed manually with the aid of cathodoluminescence (CL) images.

The mounts were subsequently sputter-coated with a film of high-purity gold which was 35nm thick, before being placed and secured in sample holders. The reference materials were kept in the airlock and was exchanged after approximately every 10 analyses on the unknowns.

The SIMS analyses, carried out in Potsdam, made use of a c. 15 nA $^{16}O_2^-$ primary ion beam operating in Köhler mode, resulting in a beam diameter of approximately 20 µm on the sample's surface. Each analysis was preceded by pre-sputtering lasting 120 seconds and employed a 35 µm raster, which locally removed the gold coat, suppressed surface contamination and helped establish equilibrium sputtering

conditions. Oxygen flooding was used to enhance lead sensitivity, with the total pressure in the sample chamber maintained around 8 x 10^{-6} Pa throughout the analytical session.

A single analysis consisted of 12 cycles of the peak stepping sequence: $^{90}Zr_2{}^{16}O$ (1 second integration per cycle), $^{92}Zr_2{}^{16}O$ (1s), 200.5 (4s), $^{94}Zr_2{}^{16}O$ (1s), ^{204}Pb (6s), ^{206}Pb (4s), ^{207}Pb (6s), ^{208}Pb (2s), $^{177}Hf^{16}O_2$ (1s), ^{232}Th (2s), ^{238}U (2s), $^{232}Th^{16}O$ (2s), $^{238}U^{16}O$ (2s) and $^{238}U^{16}O_2$ (2s). Thus, a single such analysis lasted approximately 13 minutes, which included pre-sputtering and the automated centering routines. Data from this peak-stepping sequence were filtered at the 3-standard deviation (sd) level. The typical count rate for $^{90}Zr_2{}^{16}O$ under these conditions was 1.08 x 10^5 counts per second. Data were acquired at a mass resolution of $M/\Delta M \approx 5400$, with the mass spectrometer operating in mono-collection mode.

The U-Pb calibration for this analytical session was based on the primary zircon reference material 91500 ($^{206}Pb/^{238}U$ age: 1062.4 ± 0.4 Ma; $^{207}Pb/^{206}Pb$ age: 1065.4 ± 0.3 Ma; Wiedenbeck et al., 1995) with the Temora 2 reference material ($^{206}Pb/^{238}U$ age: 416.78 ± 0.33 Ma; Black et al., 2004) being used as a quality control material to evaluate the accuracy and stability of the calibration.

The Excel-based program "NordAge" (M. Whitehouse, NORDSIM facility, Stockholm) was used for data reduction, where 31 measurements, made on 91500, were used to establish the U-Pb inter-element fractionation against which the unknowns were calibrated, using a Pb/UO vs UO_2/UO relationship, employing a power-law fit. This resulted in a mean $^{206}Pb/^{238}U$ age of 1062 ± 6 Ma (MSWD = 1). Temora 2 produced a $^{206}Pb/^{238}U$ age of 412 ± 3 Ma (MSWD = 0.7, N = 19). The reference materials are within the reasonable agreement of their published $^{206}Pb/^{238}U$ ages, indicating that no gross bias is present in the U-Pb determinations.

The Excel program Isoplot (Ludwig, 2012), was used to plot the data using the decay constants recommended by the IUGS subcommission on geochronology (Steiger and Jäger, 1977). The observed $^{204}Pb/\ ^{206}Pb$ ratio in conjunction with the recent common lead composition from the model of Stacey and Kramers (1975) was the basis for any corrections for common lead.

Due to large holes surrounding the zircon grains in the original mount, possibly caused by a build-up of charge due to incomplete gold coating, causing errors in the analyses, the samples had to receive a new layer of epoxy and be re-polished. This process meant that some zircon grains were lost and that the initial CL images may not be an entirely accurate representation of the zircon grain surfaces analysed. Updated CL imaging was not possible due to time constraints.

7.2.2 Results

SIMS analyses provided dates on 4 analyses from 4 different zircon grains from a carbonatite sample and 20 analyses from 12 different zircon grains from a glimmerite sample. All data captured during the analyses are displayed in appendix E.2 with the calibration conditions presented in Appendix E.1.

All analyses showed discordance with none plotting on Concordia. Three analyses from the glimmerite sample, were discarded due to high common Pb values or where common Pb correction resulted in unrealistic values. Core and rim analyses were performed to which no real variation in age was observed, with all the analysed points plotting on a single discordant line. Figure 51 shows that the zircons from the carbonatite sample produced an upper intercept age estimate of 2094 ± 150 Ma; Figure 52 shows that the zircons from the glimmerite sample produced an upper intercept age estimate of 2018 ± 56 Ma.

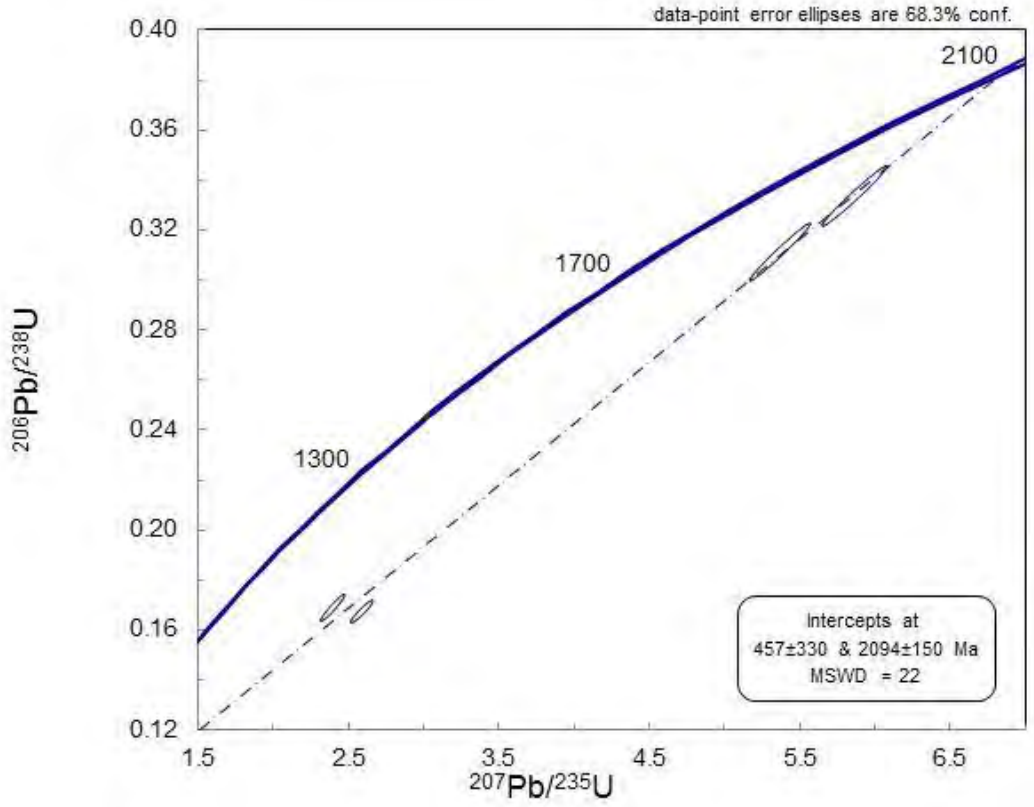

Figure 51: U/Pb Discordia diagram representing the carbonatite sample

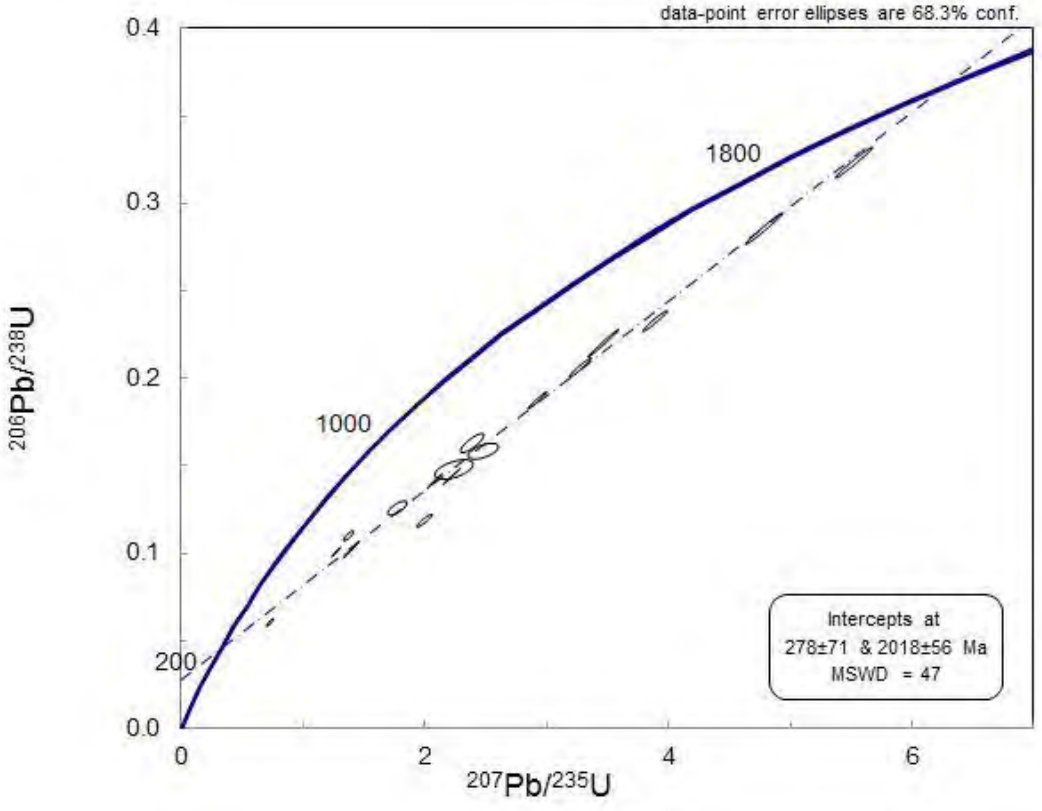

Figure 52: U/Pb Discordia diagram representing the glimmerite sample

Chapter 8: Discussion and Conclusions

8.1 Geological Setting of the Schiel Complex

8.1.1 Introduction

It is important to reiterate that the sample material used in this study were from a limited number (5) of available drill cores and may not provide a representative coverage of the complete range of ultramafic rocks in the Schiel Complex. None of the Foskor holes drilled in centre of the ultramafic/carbonatite intrusion (see Figure 3) are preserved; the available cores are from the periphery of the intrusion and possibly only intersected laterally dispersed veins and sheets of the intrusion. However, the current sample suite is "the best available" and, until further boreholes are drilled, they represent the best material to establish the petrographic and geochemical characteristics of the mostly unexposed ultramafic and carbonatitic rocks. Ideally, additional drill cores should be drilled to prioritise intersecting the main pipe-like structure of the intrusion in order to corroborate the findings in this thesis.

Viljoen (1966) argued that, due to vertical finger and tongue structures, the main pipe-like structure was likely to be in close proximity to borehole SC22, but stated that the pipe had to lie deeper than the drilled depth at this location, 426m below the surface. This information provides a guideline for further exploration of the Schiel Complex ultramafic and carbonatite units.

8.1.2 The Ultramafic Units

The Schiel Complex contains 3 distinct ultramafic rock varieties having mineral assemblages that are a mixture of at least 2 varieties of the 3 distinct ultramafic rock varieties, where the contacts between the various ultramafic rocks are always gradational and never sharp, increasing the difficulty in delineating each specific rock type. Such gradational variation makes it almost impossible to provide specific rock names for each mineral assemblage at thin section scale. Rather, defining end-member mineral-based rock classification would be more suited in classifying these ultramafic rocks, with a continuum of rocks containing mineral assemblages between the major end members: magnetite-rich phoscorite; clinopyroxenite; and glimmerite. Two magmatic rock types are present: the clinopyroxenite which has an assemblage containing predominately diopside with minor amounts of magnetite, fluorapatite, magnesian biotite and amphibole; and phoscorites which contain assemblages of a magnetite-rich nature together with diopside and fluorapatite and minor amounts of phlogopite/magnesian biotite, amphibole and calcite. Feldspar is absent throughout the main ultramafic rock bodies, hence their ultrabasic classification. Rare accumulations of apatite, magnetite or olivine are seen in coarser fractions of the ultramafic rocks: where olivine seems to only be present at the lower sections of the boreholes.

Rare serpentinised olivine grains are present in phoscorites from borehole SC10. All analysed olivine grains (from carbonaatite and glimmerite samples) are forsterite-rich (Fo – 80.11 – 84.29 %) with serpentinisation producing either antigorite or picrolite compositions as either partial or fully pseudomorphed grains. The presence of abundant olivine in core SC09 but not in core SC10 may show that not only vertical, but lateral variation in phoscorite mineralogy is present, as these cores were drilled approximately 1105m apart with the olivine-bearing rocks from core SC09 intercepted at a greater depth than that reached by core SC10. It is therefore clear that the Schiel Complex magmatic ultramafic rocks containing magnetite and apatite with lesser amounts of diopside, phlogopite and olivine resemble true phoscorites.

The similar mineral chemistries, a salite composition, of the clinopyroxene minerals between the phoscorites and clinopyroxenites (Figure 33) and chondrite-normalised REE plots between the phoscorites and clinopyroxenites (Figure 44) show that these phases may have differentiated from a common parental magma. These rocks are only separated by the incorporation of abundant magnetite and apatite in the phoscorite rocks which suggests that these rock varieties are only separated due to the accumulation of specific minerals during crystallisation from different sections of the magma. It is seen that diopside is present in the carbonatites and the glimmerite which may suggest that these mineral chemistries are a product of metasomatic reactions, where salite may have been the initial clinopyroxene mineral to have crystallised.

The compositional evolutionary trend of clinopyroxene is suggested to be from salite to diopside. Salite is a mineral between the diopside ($CaMgSi_2O_6$) and hedenbergite ($CaFeSi_2O_6$) clinopyroxene end members, i.e. Fe-content in diopside < salite < ferrosalite < hedenbergite. This trend suggests depletion in Fe content as the rocks evolve, where the glimmerite clinopyroxene grains would be the most depleted in Fe, which is supported by its clinopyroxene mineral chemistry. Only one sample (SC10-29-1) contained 2 clinopyroxene compositions distinctly in the aegirine-augite field, which is characterised by a pyroxenite vein intruding into a syenite as seen in Figure 16, which may have precipitated aegirine-augite due to element exchange with the syenitic wall rock.

The most abundant ultramafic rock type present in the sampled suite of the Schiel Complex is characterised as mica-rich reaction products, referred to as glimmerites in this study, commonly seen at contact zones between the carbonatite and the ultramafic/syenite rocks. These rocks commonly manifest as distinct reaction bands between carbonatite and ultramafic contacts: producing gradational contacts leading to uncertainty in determining the extent of the reaction zone in hand specimens. Figures 14(b) and 16 show that this mica-rich reaction product is only associated with carbonate-bearing magmatism, as no distinct mica-rich reaction zones are seen between the clinopyroxenite and syenitic rocks, possibly due to the absence of a calcite-rich mineral assemblage. Figures 7, 8, 17 and 23 are in contrast to Figures

14(b) and 16, where distinct mica-rich reaction zones are produced at contact zones between calcite-rich rock assemblages and ultramafic or syenitic rocks. These mica-rich reaction assemblages are characterised by up to 90% phlogopitic mica, where the phlogopite grains are characteristically free of inclusions, suggesting that these mica grains are not of igneous origin and would have formed through metasomatic reactions, producing a glimmeritic metasomatic rock assemblage (Elliott et al., 2018).

Whole-rock Zr/Hf ratios, seen in Figure 46, shows that the majority of glimmerite analyses fall outside the field in which common silicate rocks form from pure silicate melts (Bau, 1996). Although these rocks are not considered as common silicate rocks, the contact relationships and mineral assemblages of these ultramafic zones support the classification of the mica-rich rocks as metasomatic glimmerites. Low variation in Y/Ho ratios seen in the various rock types also suggest that these rocks would have experienced high-temperature processes, possibly due to a carbonatitic fluid causing metasomatism of the ultramafic or surrounding syenitic rocks, producing glimmerites. Glimmerites that plot in the magmatic source field illustrated in Figure 47 may be the result of ultramafic rocks that experienced low degrees of metasomatism, and are sections of the ultramafic rock within gradational contact zones which contain characteristics of both glimmerite and phoscoritic/clinopyroxenite rocks but lean more towards a magmatic mineral assemblage. Phlogopite, the dominant glimmerite mica type, may then be a result of metasomatic alteration produced by the reaction; Dolomite + K feldspar + volatile = Calcite + Phlogopite + CO_2 (Eggert and Kerrick, 1981), (H_2O or F in the case of the Schiel Complex micas as seen in the EPMA analyses in Appendix C1.4) . This is supported by the hand samples seen in Figure 4, as well as the lack of dolomite in the carbonatite rocks. This process would lead the fluid phase to become CO_2-rich, forming tremolite + calcite (Eggert and Kerrick, 1981), which are present in the Schiel Complex carbonatite rocks. An interpretation of the Schiel Complex metasomatism is explored in Chapter 8.2.2.

8.1.3 The Carbonatites

Carbonatites analysed from the sampled suite of the Schiel Complex contain only calcite as the carbonate mineral with lesser amounts of magnetite, apatite, diopside (tremolite/winchite) and olivine, together with accessory ilmenite, baddeleyite and zircon with minor sulphides. These rocks have calcite as the only carbonate mineral; applying the IUGS Chemical classification scheme (Le Maitre et al., 2002), magnetite-poor samples classify as calcio-carbonatite, and magnetite-rich as ferro-carbonatites (Figure 39). The known mineralogy of the Schiel Complex carbonatites determined through petrography, allows for preferred mineralogical classification schemes to be adopted, where The IUGS classifies a ferrocarbonatite as a carbonatite in which the main carbonate mineral is Fe-rich (Le Maitre et al., 2002). The lack of Fe-rich carbonate minerals present in the Schiel Complex carbonatites provide evidence for the occurrence of calcio-carbonatites only. The carbonatite samples classified in the ferro-carbonatite field, seen in Figure 39, can thus be attributed to excess Fe as a result of the presence of

magnetite, supporting the conclusion that all the carbonatites present are calcio-carbonatites. Additionally, all carbonatite analyses were classified in accordance to the criteria provided by Gittins and Harmer (1997) seen in Figure 40, which shows that all carbonatite rocks are classified as calciocarbonatites, besides one sample containing schlieren enriched in magnetite classified as a ferruginous calciocarbonatite. It is therefore concluded that the chemical classification scheme provided by Gittins and Harmer (1997) aligns with the IUGS mineralogical classification scheme and provides a more accurate visual representation of the carbonatite type based on chemical classification. The carbonatite classification after Gittins and Harmer (1997) (Figure 40) shows that the carbonatite samples trend from a starting composition of ±10% MgO and not the CaO apex. This indicates that the calcites are either high-temperature magnesian varieties or that the chemical compositions were influenced by the presence of phlogopite.

Chondritic ratios, shown in Figure 47, indicate charge and radius controlled (CHARAC) behaviour of Y and Ho during genesis and evolution of carbonatitic melts (Bau, 1995). The Y/Ho ratios analysed in the carbonatites (±28-29.8) are slightly higher than the Y/Ho ratios from the ultramafic units (±26-28.5), which could illustrate the mobilisation of REEs from the ultramafic rock due to carbonatite vein intrusions, where increasing migration distance of the fluid is expected to produce decreased Y/Ho ratios (Bau, 1995). However, the similar Y/Ho ratios observed between the carbonatite and ultramafic units suggest little evidence for low-temperature, non CHARAC, related element fractionation. Zr/Hf ratios include spread beyond the CHARAC values, to higher and lower values.

8.1.4 Relative Timing of Emplacement of the Schiel Complex Units

Figure 7 shows a clear carbonatite veinlet, with the production of sheathes of glimmerite around carbonatite veins and veinlets displayed by the bright green zones occurring along its edges, which has intruded into the syenite. Although this image shows small-scale evidence of this process, more extensive carbonatite intrusions will produce more widespread alteration zones (Elliot et al., 2018). Observations show that the metasomatic/fenitising fluid producing glimmerites would most likely be carbonatitic, with the possibility of the fluid being a mixture between a carbonatitic composition and the melting and entrainment of country-rocks upon upwelling of the carbonate magma. Multiple phases of veining, as well as the presence of clear metasomatism caused by these vein intrusions, are strong evidence that the carbonate magmatic fluid was the metasomatic agent, producing reaction assemblages when in contact with the ultramafic and syenitic country-rock (Elliott et al., 2018 & Le Bas, 1981). A small concentration of syenitic veinlets, as well as the entrainment of rare syenitic rock minerals (allanite) within the glimmerite rocks, could show evidence of syenite rheomorphism, which caused dissipation and intrusions of the country-rock due to the heat from the upwelling carbonatitic or ultramafic magmatism. It is, however, more common to find veining of ultramafic and carbonatite material within syenitic country-rocks (Figure 6). Hence, according to contact relationships seen in the

sampled suite of the various Schiel Complex rock types together with the high relative volume of the syenites, it is clearly shown that the carbonatites and ultramafics must have intruded after syenite emplacement, producing glimmerites as the later geological unit.

An updated Schiel Complex emplacement sequence is therefore proposed: syenites → ultramafic rocks and carbonatites → mica-rich metasomatic alteration products; a timing contrary to current published data outlined in Chapter 2.

The upper intercept ages derived from the discordant geochronology diagrams of 2094 Ma (±150 Ma) for the carbonatite (Figure 51) and 2018 Ma (±56) for the glimmerite (Figure 52) cannot be representative of the true age of emplacement of these units. The large error margins obtained in the zircon U/Pb geochronology analyses show that the analyses performed were inconclusive in constraining an absolute age of the various rock units. Although the date provided by the glimmerite unit falls within the age range provided by Graupner et al. (2018) for the ultramafic components of the Schiel Complex, as seen in Chapter 2, it could not be further constrained.

Further geochronology studies should focus on gathering zircon/baddeleyite from carbonatite, glimmerite, phoscorite and clinopyroxenite samples to generate a more appropriate sequence of crystallisation events for the Schiel Complex. Wu et al. (2011) compiled a geochronological assessment from similar units from the Phalaborwa Complex for which similar uncertainties in a precise age estimate of the various units were observed with respect to U/Pb zircon dating. They showed that U/Pb dating of baddeleyite would be the more favourable mineral to analyse as the results from baddeleyite analyses provided a more concise age of emplacement with extremely low error margins (maximum error of ±3 Ma) for all the samples analysed. The presence of abundant baddeleyite at large grain sizes seen in the carbonatite samples of the Schiel Complex could provide an avenue for further geochronological analyses that could constrain a more accurate age of emplacement of the carbonatites. Furthermore, Ar-Ar dating on micas and fission track (FT) dating on apatite would also provide an avenue for further geochronological constraint.

8.1.5 Mica Composition Variation with Rock Type

The classification of biotite and phlogopite is based on the major element proportions characterised by Foster (1960). The biotitic mica is present in the phoscorite and clinopyroxenite bodies and the phlogopitic mica is present in the carbonatite, phoscorite and glimmerite bodies. All biotite grains analysed from the clinopyroxenite rocks contain chemistries indicative of magnesium-rich biotites (Figure 30a). The phlogopitic composition of all the carbonatite micas are of the common phlogopite variety (Average major element oxides of all carbonatite mica analyses in weight %: SiO - 41.13; Al_2O_3

- 11.56; MgO - 24.45; FeO - 7.33; K_2O - 10.04), with slight deficiencies in K or Si content occurring in some analyses.

Figure 32(a) and (b) shows that there is a distinct correlation of Fe and Mg content of the mica grains with respect to their rock type, where Figures 32(c) and (e) show that two mica generations are present containing distinct evolutionary trends. It is seen that the biotitic mica present in the phoscorite contains Fe-rich chemistries which may have evolved to a latter more Mg-rich mica type, indicative of the glimmeritic micas, whereas the clinopyroxenite micas also evolved to an Fe-poorer chemistry, but which does not overlap the mica chemistries from the glimmerites. It is therefore suggested that the initial micas crystallised by both phoscorite and clinopyroxenite rocks evolved to more Fe-poorer chemistries, independently. These distinct trends, seen in Figure 32(c) and (e), show that the biotite from the phoscorite contains a lower initial Ti composition than that of the biotite from the clinopyroxenite, which points to two different generations of mica produced under different initial magma conditions. Magnesian biotite grains in the clinopyroxenite contain an Al-enriched composition with Al_2O_3 values above 13 wt.%, as well as a Ti-enriched composition, not seen in the micas from the phoscorite or glimmerite rocks. This could be due to the close spatial association with an Al-enriched, and possibly Ba-enriched, carbonatitic magma with the accumulation of incompatible elements in the residual liquid caused by magma differentiation (Giebel et al., 2019), resulting in Al incorporation in Ti-rich initial magnesian biotite grains. This Ba enrichment is seen in Figure 40, where one carbonatite sample shows anomalous Ba enrichment. Exsolution lamellae of ilmenite seen in magnetite grains may suggest that the rocks experienced a period where Ti had higher diffusivity rates than usual allowing for ilmenite to scavenge and deplete the magnetite of Ti. This Ti could subsequently be incorporated in the mica grains which could explain the higher Ti content of clinopyroxenite biotitic mica. Mica zoning restricted to clinopyroxenites and phoscorite assemblages, in close contact to each other, suggest they accumulated from a fractionating magma, where the mica grains may be a product of reactions between the two magma types.

The magnetite, pyroxene and apatite inclusions present in biotite may suggest that that these grains either have an orthomagmatic source, or that these inclusions are remnants of the minerals that have not been dissolved during the reaction proposed by Eggert and Kerrick (1981), which may persist as inclusions within metasomatic mica grains. In contrast, the phlogopite grains containing no inclusions are likely to be of a metasomatic origin (Elliott et al., 2018), where metasomatism may have caused the high density of metamorphic mica crystallisation and the production of glimmerites. No biotite grains were analysed in the glimmerites, but this could be due to an element of bias as pristine mica grains were selected for chemical analyses whereas smaller anhedral grains of biotite may have been present in the glimmerite samples but were not analysed.

It is evident that the clinopyroxene associated biotitic mica does not evolve to mica chemistries of the carbonatite/glimmerite phase, seen by the phoscorites, which suggests that the clinopyroxenite micas displayed a separate chemical evolution to that of the phoscorite-carbonatite micas. The more annite-rich chemical composition of the clinopyroxenite and phoscorite associated micas, with respect to the carbonatite and glimmerite micas, may also support the idea that the ultramafic magma would have initially had Fe-rich compositions as described by the hypothesis for phoscorite-carbonatite associations proposed by Lee et al. (2004).

8.2 Petrogenesis/Magma Evolution of the Schiel Complex Units

8.2.1 Were the Schiel Complex Magmatic Rocks Derived from a Common Parental Magma?

Similar minerals with similar mineral compositions from all the Schiel ultramafic rocks, coupled with similar chondrite-normalised REE traces, suggest that all the magmatic rocks analysed could have differentiated from a common parental magma source (Krasnova et al., 2004). Minor calcite globules present in both the phoscoritic and, more rarely, in the clinopyroxenitic rocks, may also be an indication that the parental magma(s) was carbonate-bearing.

All carbonatite rocks contain similar mafic minerals with similar mineral chemistries, to that of the ultramafic rocks, also containing accumulations of mica (but with no annite present), pyroxene, apatite, magnetite or forsterite/serpentine. The mineralogical similarities between the ultramafic and carbonatite phases could be a result of: (1) phoscorite rheomorphism and the entrainment of phoscoritic phases within upwelling of the carbonatite melt as it passes through the phoscoritic fraction (Giebel et al., 2019); (2) fractional crystallisation in the parental magma followed by liquid-liquid separation of the various melt types (Krasnova et al., 2004), allowing for minerals of similar chemistries to be incorporated in both carbonate and ultramafic melts. Jahn et al. (1980) also proposed that the similar REE patterns of both carbonatite and ultramafic rocks illustrate a suite of rocks formed as a result of crystal fractionation differentiated from a common magma source, where similar mineral chemistries prove that immiscibility of the various magmas must have occurred after some initial mineral crystallisation; (3) the emplacement of an accumulation of minerals from a single Fe-rich carbonatite-bearing melt, crystallising different rock types at different spatial locations where no liquid immiscibility of the various magmas occurred.

The presence of different carbonatite textures, i.e. medium-grained, coarse-grained and banded, in contact with each other at small-scaled intervals could be representative of carbonatite magmas that may have intruded as crystal mushes, which indicates that fractional crystallisation did occur allowing for the accumulation of various minerals at different spatial locations in the upwelling magma. This

would explain the banded nature of some carbonatites present, where the mineral alignment of mica is observed, in the absence of regional metamorphism. The presence of the same primary carbonate-bearing minerals in the ultramafic rocks and primary silicate minerals in the carbonatite seen in the Schiel Complex rock varieties, would not occur if the melts were immiscible before any mineral crystallisation.

It is proposed that the ultramafic and carbonatitic rocks may have formed from a common Fe-rich carbonate-bearing magma, where fractional crystallisation and accumulation of minerals was the main factor in producing the various Schiel Complex rock varieties. An evolution to an Fe-poorer magma chemistry is also suggested, based on the two magmatic ultramafic rocks where a more Fe-rich phoscorite were emplaced separately from Fe-poorer clinopyroxenites and carbonatites. This is also supported by mica chemistries which show that a distinct evolutionary trend to a more Fe-poor mica variety is observed. The lack of glimmerite mica chemistries associated with clinopyroxenite mica chemistries suggests that the glimmerite micas were formed by reaction mechanisms associated with carbonate-bearing assemblages in a relatively high pH_2O environment, not available in the clinopyroxenites.

8.2.2 Metasomatism and Fenitisation

The serpentinised olivine grains provide evidence for the presence of a hydrothermal, CO_2-poor, low silica fluid (Moody, 1976). This supports the early crystallisation of olivine-bearing phoscorite rocks which were then been altered due by carbonatitic magma. These forsterite grains may have also reacted to form secondary magnetite via the reaction: Olivine + water + carbon dioxide → serpentine + magnetite + methane, as evidenced by the magnetite occurring as fracture fillings and inclusions in olivine grains.

The presence of H_2O- bearing alteration minerals such as serpentine, biotite and amphibole, as well as fluorine in apatite, is supportive of the idea that a calcite precipitating melt was present, as it is only thought to exist at geologically reasonable temperatures in the presence of water. Harmer and Gittins (1997) argued that parental carbonate melts must have higher concentrations of alkalis, Mg, Fe and Ca than the level preserved in crystalline calcite carbonatites, and that these elements would have been lost to a fluid phase responsible for the extensive alkalic metasomatic alteration, or fenitisation, of the immediate country-rocks. This would explain the production of phlogopite as a reaction product even though low Mg carbonates make up the crystalline carbonatite matrix.

The presence of actinolite and tremolite may be an indication of a high-pressure siliceous dolomite system where the fluid phase becomes rich in CO_2 forming amphibole together with calcite and diopside (Eggert and Kerrick, 1981). However, the lack of tetraferriphlogopite supports the presence of calcitic

carbonatite magmatic fluid as the metasomatic medium (Krasnova et al., 2004). This could indicate that the carbonate phase was initially dolomite-bearing and evolved to a dolomite-free variety at lower pressures allowing for glimmerite formation.

The phase change in the zirconium bearing mineral, from baddeleyite to zircon, seen in carbonatite samples could help to explain the relationship between the ultramafic rock bodies, the carbonatite bodies and the syenite country-rock. Zircon rims around baddeleyite seen in the carbonatite rocks seem to be aggregates of polycrystalline zircon grains that are produced at the expense of baddeleyite, which could ultimately completely alter initial baddeleyite grains. The initial precipitation of baddeleyite in the carbonatite rocks shows that the rock initially crystallised under silica-undersaturated conditions, which would be expected from a carbonate-rich magma (Barker, 2001, Balaganskaya et al., 2007; Krasnova et al., 2004; Lee et al., 2004; R.E Harmer, 2000). However, the presence of zircon rims requires that the silica activity in the carbonatite system had to have increased (Barker, 2001) with time, as zircon is only stable under higher silica activity conditions. Barker (2001) stated that zircon present in carbonatites could be: (1) primary phases precipitated from carbonatite magma with sufficiently high silica activity; (2) entrained from coeval or parental silicate magma; (3) xenocrysts in magmatic carbonatite; (4) products of subsolidus alteration; (5) accidental phase incorporated during subsolidus cooling. The presence of zircon as rims around baddeleyite show that some zircon grains from the Schiel Complex carbonatites could not have been xenocrysts or zircons entrained from coeval or parental magmas. Barker (2001) argued that assimilation of crustal rocks and the dissolution of quartz is more likely than fractional crystallisation to produce a high silica activity.

This silica-saturation/oversaturation needed could have been provided by the reaction between the carbonatites and the surrounding wall-rock, which is supported by metasomatic zones identified. This shows that although the fenitising fluid is proposed to be a carbonatite-derived hydrothermal fluid, rheomorphism and dissolution of the surrounding silica-bearing rocks could have occurred, causing elemental infiltration of the country-rock composition into the carbonatite component as well, increasing the silica content and altering its mineral assemblage. Silica saturation may have occurred through either syenitic- or ultramafic-rock assimilation, or both. The later zircon rims could have also been produced due to fractional crystallisation of nonsilicate phases which would increase the silica activity in the remaining liquid (Barker, 2001). Changes in the nature of the crystallising assemblage, between carbonate-dominated or silicate-dominated, would create fluctuations in the silica activity of the melt, interchangeably favouring either the crystallisation of baddeleyite or zircon. Such a process better explains the complex internal structures of the zircon grains than assimilation of silicate host rocks. The presence of calcite and Pb-sulphide inclusions within zircon grains would link the formation of the zircons grains directly with the carbonate magmatism and would have crystallised together with the carbonatite intrusion. The lack of silicate mineral inclusions within zircon grains also decreases the

likelihood that these zircon grains were inherited from surrounding wall-rock by assimilation (Liu et al., 2018).

Although zircon grains are not a common accessory mineral within carbonatitic rocks, the complex internal growth structures seen in CL-imaging may provide evidence that these zircon grains could have formed through the complete alteration of baddeleyite grains, where the internal structure records the presence of the amalgamating botryoidal zircon structures. Lumpkin (1999) describes the possibility that baddeleyite can alter to zircon due to low-temperature, late-stage aqueous fluid interaction reactions (below 575-625 K) forming botryoidal zircon overgrowths, which is observed in Schiel Complex carbonatites (see Figure 25). Figure 4 clearly shows that a reaction occurred between the carbonatite fraction and the syenite wall rock; although on a small scale in this example, this process could have occurred on a much larger scale (Elliott et al., 2018) allowing for silica saturation of the carbonatite phases. The presence of abundant zircon grains in the vicinity of contacts between the carbonatite and syenitic/ultramafic rocks is consistent with the production of zircon through alteration processes.

Further investigation of the syenitic country-rocks and its possible fenitisation assemblages is required in truly understanding the Schiel Complex metasomatism dynamics, but is, unfortunately, beyond the scope of the current study. Further research could additionally focus on the study of major minerals from a reaction perspective in order to contribute to the understanding of the fluid compositions and physical conditions for genesis and evolution of the Schiel Complex. Ar-Ar analyses of biotites could contribute to further understanding the metasomatic/metamorphic history of the complex, together with amphibole barometry which could be used in order to constrain pressure conditions for the complex.

8.2.3 Does Apatite Chemistry Constrain Metasomatic Alteration? Implications for Apatite REE Content?

Figure 20 shows the presence of monazite inclusions within fluorapatite grains from the carbonatite rocks. Harlov et al. (2002) provide a review on studies regarding monazite inclusions within fluorapatite: they stress the importance of metasomatic fluids as agents which promote the coupled substitution reactions:

$$Na^{+} + (Y+REE)^{3+} = 2Ca^{2+};$$

$$Si^{4+} + (Y+REE)^{3+} = P^{5+} + Ca^{2+}$$

that lead to the removal of REE, Na and Si from the apatite structure: this has been referred to as the "britholite[1] substitution" (Giebel et al., 2017).

[1] Britholite-(Ce): nominally $(Ca,LREE)_5(SiO_4,PO_4)_3(OH,F)$

This results in charge imbalance in the less mobile LREE, inducing nucleation and growth of monazite in apatite via the reaction:

$$\text{apatite}_{(1)} + (Ca^{2+}, P^{5+})_{\text{fluid}} = \text{apatite}_{(2)} + \text{Monazite} + (Si^{4+} \text{ and } Na^{+})_{\text{fluid}}$$

Harlov et al. (2002) argue that this would require a fluid that is capable of transporting P and Ca such that mass balance is maintained, and that a temperature threshold is present below which monazite will not nucleate within apatite (<850 °C).

A study by Graupner et al. (2018) recognised 2 clear generations of apatite growth in Schiel Complex apatite grains on the basis of CL imaging. The first generation of apatites contain high to moderate REE contents, whereas the second generation contains low REE contents. These generations were texturally distinguishable as the first generation of apatite was present as euhedral coarse grains, whereas the second generation was either present as overgrowths on the first generation of apatite, or as fine-grained aggregates. Graupner et al. (2018) also concluded that all apatite grains are magmatic in origin based on textural and Sm-Nd isotope evidence.

Apatite grains almost always show compositional zoning. Figure 37 shows BSE intensity by grey scale, where lower average Z values, represented by darker zones, are characterised by pure apatite that contains Ca and P and low Si, resulting in lower average Z values and a darker BSE response, which can be attributed to REE depletion explained by the britholite substitution (Giebel et al., 2017). This is also supported by the increased Ce contents from lower average Z to higher average Z zones, which shows that apatite zones containing higher average Z values, and a lighter BSE response, contain higher Si and REE contents. This mechanism is also supported by the changing silica content with constantly

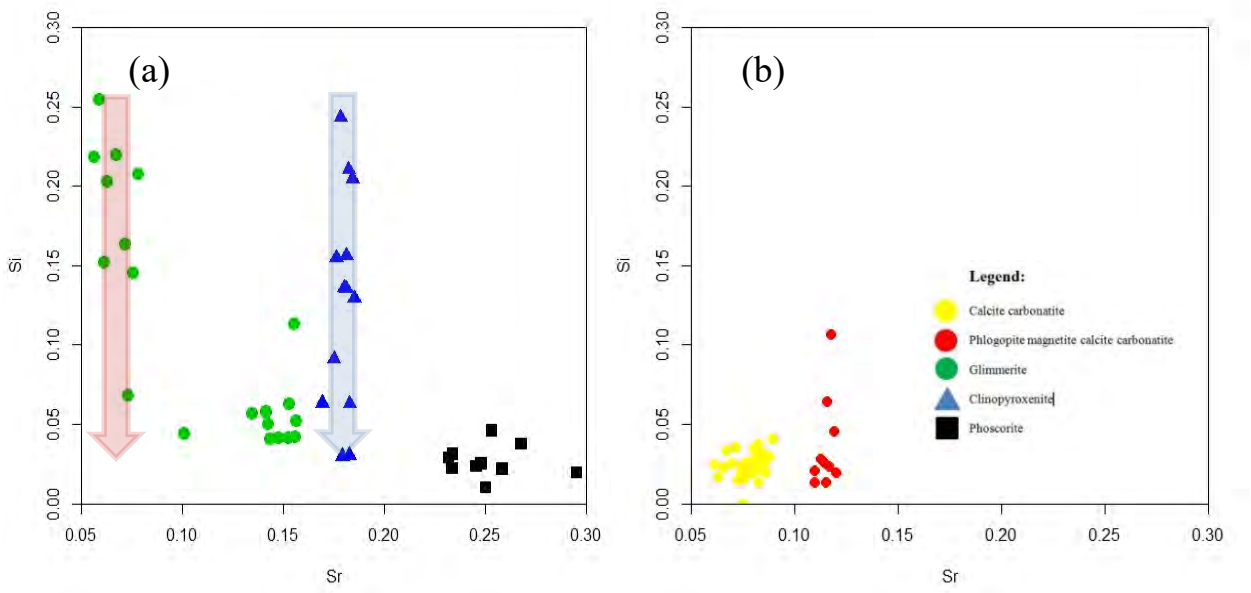

Figure 53: Diagram showing Sr vs. Si for apatite mineral chemistries from the ultramafic rocks (a) and the carbonatites (b).

low strontium content of apatites seen in Figure 53 (Giebel et al., 2017). Changing silica is only seen in the phlogopite magnetite calcite carbonatite, glimmerite and clinopyroxenite, but not in the magnetite-rich phoscorite or calcite carbonatite, that contain magmatic apatite which has not undergone extensive metasomatic alteration and can be considered as more "pure" apatite grains. The low Si contents present in these apatites may, however, indicate that low REE contents are present in apatites from these rocks.

Figure 53 illustrates that the magmatic rocks i.e. phoscorites and carbonatites, have apatites that show little internal variation in Si and Sr content relative to apatite grains from glimmerite, clinopyroxenite and phlogopite magnetite calcite carbonatites. Rocks that have been metasomatised, i.e. glimmerites and phlogopite magnetite calcite carbonatites, contain apatite grains that contain Sr contents with little variation, but varying amounts of Si. It is also shown that the phlogopite magnetite calcite carbonatite apatites have Sr values between the two glimmerite varieties. It is seen that the glimmerites have two clear populations of apatite, one containing Sr and Si contents (Sr (0.15); Si (0.05)) that are clearly grouped and do not vary, and another with a lower Sr content but variable Si content (Sr (<0.1); Si (0.05-0.25)). These two glimmerite groupings are illustrated by the Si and Sr contents of 2 different samples (SC10-2-2 being the lower Sr sample and SC10-24-2 being the higher Sr sample) which shows that the glimmerites may have been produced by varying degrees of metasomatism at different spatial locations, producing a spectrum of rocks, likely exhibiting gradational contact zones, or that multiple processes were involved in the production of the glimmerites producing multiple glimmerite varieties. This figure also illustrates that a glimmerite type occurs that contains apatites with higher relative Si contents than that of the phoscorites and carbonatites and may represent areas of the metasomatic rocks that have apatites with REE contents higher than the phoscorites or carbonatites. Figure 53 therefore illustrates that the low Si content of the apatites from the phoscorites and carbonatites result in apatites that contain low REE contents, due to the scavenging of these elements by a metasomatising fluid.

The clinopyroxenites have varying Si (0.02 – 0.25) at a constant Sr (~0.18), although these extremes were detected in zoned apatite grains, where high Si contents are present at interior zones of apatite grains where a higher average Z value was recorded, opposed to outer apatite zones where lower average Z values were recorded and low REE contents are present (Appendix C.7). This may indicate that apatites from the clinopyroxenites may contain higher REE contents than the phoscorites and that these rocks may have experienced lower degrees of metasomatism and scavenging of REE's, allowing for internal zones of apatite grains to be relatively REE enriched. Although the clinopyroxenite apatite grains could be relatively more REE-enriched than the phoscorites, low modal content of apatite occurs in the clinopyroxenites.

Monomineralic apatite zones seen in the ultramafic rocks show the potential for apatite enrichment, correlating to REE-enrichment that could be present at a large scale within the body of the pluton.

Primary, unaltered and cumulate apatite would be an ideal target for REE exploration but the chances of finding a large enough body to be economically viable would be slim as the ultramafic rocks analysed in this study were represent as discontinuous vein and veinlet structures that do not represent large volumes of rock, together with relatively low P_2O_5 contents seen in the whole-rock XRF analyses (Appendix D). The highly variable rock composition will make it very difficult to pinpoint such an area, especially one that has not been affected by hydrothermal alteration and have had REEs scavenged away. If the main pipe-like structure of the complex can be located, drilled and sampled, it may provide a clearer indication of the amount of unaltered apatite that may be present in the complex, which will produce a more reliable resource and reserve estimation.

This information supports the idea of initial REE-rich apatite crystallisation which experienced different stages of growth/alteration through new magmatic events or metasomatism caused by an infiltrating carbonatite fluid, with Figure 53 showing that REE-enriched apatites may have evolved into a more Ca and P dominated variety at the expense of REE's.

REE chondrite normalised plots, presented in Chapter 6.3, show that although all the Schiel Complex ultramafic rocks display similar trends, distinct differences are seen between the various rock types. Table 5 shows that the enrichment of LREE to MREE is less pronounced than the enrichment of LREE to HREE and MREE to HREE in all the Schiel Complex rock varieties analysed, which indicates a high degree of HREE fractionation. The highest degree of HREE fractionation seen in the ultramafic rocks is present in the glimmerites, which would be expected as these rocks would have experienced the highest degrees of metasomatic alteration, preferentially leaching HREE since they form aqueous complexes more readily than LREE (Reinhardt et al., 2018). Mobile HREE may subsequently be lost in a carbonatitic fluid phase, causing enrichment of LREE relative to HREE as LREE may get absorbed into REE-bearing minerals such as apatite, zircon and thorianite. Figure 54 illustrates that the REE content from the Schiel Complex increases as a function of phosphate content (apatite/monazite crystallisation) with only the clinopyroxenites and one glimmerite sample containing high Ce content at very low P_2O_5 contents; suggesting that these samples contain REE hosted in minerals that are not phosphates. The clinopyroxenes are characterised by relatively high U and Th suggesting the presence of REE enriched urano-thorianite-like minerals.

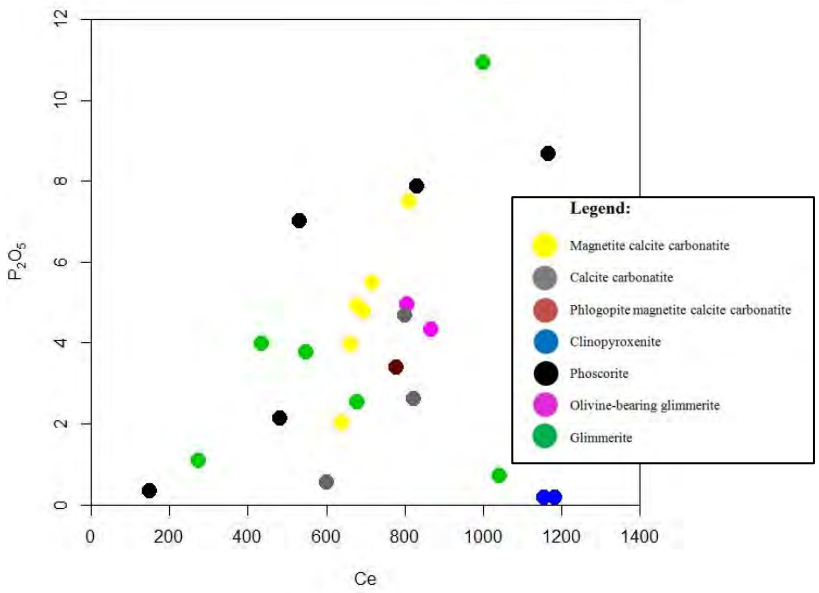

Figure 54: Binary plot indicating the relationship of REE with phosphate minerals.

8.3 Comparison of the Schiel Phoscorites and Carbonatites with Similar Units from other Phoscorite-Carbonatite Complexes

The Schiel Complex has been compared to other phoscorite-bearing complexes, i.e. Kovdor, Kola Peninsula, Phalaborwa Igneous Complex, etc., because of their similar and rare rock types reported. This has been an important association due to the economic interest of these other provinces, leading to the expectation that the Schiel Complex may contain the same or similar mineralisation that could provide economic potential. The Schiel Complex has widely been compared to the Phalaborwa Complex due to their close spatial relationship as well as the Schiel Complexes proposed emplacement age of 2.06 Ga (Graupner et al., 2018) which aligns with the 2.06 Ga Bushveld event and the emplacement age of the phoscorite-carbonatite components of the Phalaborwa Complex (Wu et al., 2011).

This comparative study focuses on the similarities and differences between the Schiel Complex and the Phalaborwa Complex, where XRF whole-rock, whole-rock trace elements and EPMA mineral data between the two complexes, as well as the other known phoscorite-bearing complexes, have been compared, as seen in Appendix F.

8.3.1 Phoscorites

Appendix A shows a mineralogical comparison between the various phoscorite bearing complexes. The Schiel Complex and the Phalaborwa Complex contain similar mineralogy, but the absence of amphibole as well as the presence of Cu-bearing minerals, PGMs, abundant apatite and abundant olivine in the Phalaborwa Complex, lead to apparent differences in initial magma compositions/magma evolution. The Seblyavr Complex phoscorites in Russia is the most closely associated complex to the Schiel Complex based on mineralogy, containing an almost identical mineral assemblage as well as being the only other complex to contain amphibole-bearing assemblages.

Magnetite from the Schiel Complex contains extremely low TiO_2 contents compared to all the other alkaline complexes, as well as containing only trace amounts of MnO and MgO. The magnetite found in the Schiel Complex is almost entirely comprised of Fe-oxides, which is unusual with respect to the other known complexes, which contain appreciable amounts of TiO_2, MnO and MgO. The presence of ilmenite as exsolution lamellae provide evidence that unique processes may have acted on the Schiel Complex to fractionate these elements out of the magnetite grains after initial crystallisation.

Phlogopite/tetraferriphlogopite is the only mica variation found in the other complexes as seen in Appendix F.3, with the Schiel Complex containing phoscoritic rocks with micas of a biotite or phlogopite composition. All other phoscorite-bearing complexes do contain biotite but only associated

with pyroxenites and not phoscorites. The Mg-rich biotite associated with the Schiel Complex clinopyroxenite is also present at the Phalaborwa Complex located in the pyroxenite and fenite rocks (Giebel et al., 2019).

Figure 55 shows a Chondrite-normalised REE comparison diagram between the Schiel Complex phoscorites (black) and four other known phoscorites. This graph shows that the Schiel Complex ultramafic rocks show a similar REE profile to that of classic phoscorite rocks. It shows that the phoscorites found in the Kovdor Complex (red) has a lower total REE content than the other phoscorite complexes. The Phalaborwa Complex phoscorite (light blue) has similar REE pattern to that of the Schiel Complex but drops off considerably with respect to the HREE content. Slight Sm and Eu depletion and Ho enrichment occur across all the rocks plotted. It is also important to note that although the Schiel Complex phoscorites have higher total REE contents, the lack of other mineralisation of economic interest could deem the Schiel Complex as economically unviable.

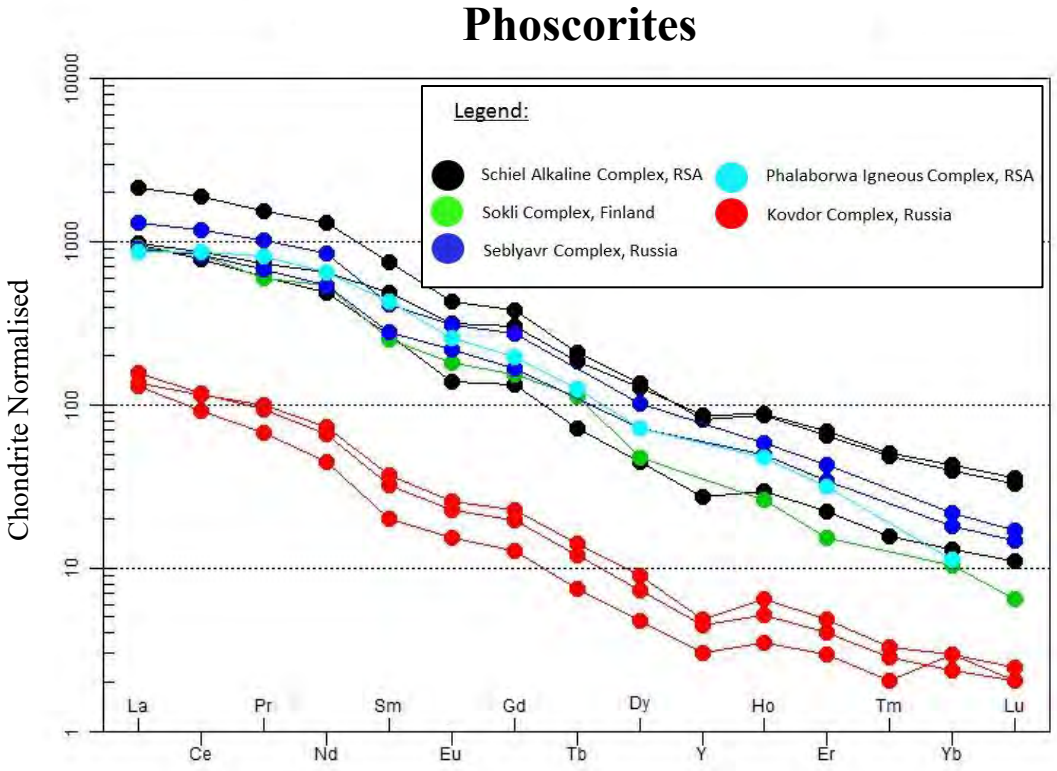

Figure 55: REE-chondrite normalised diagram comparing phoscorite rocks from well-known phoscorite-bearing complexes.

8.3.2 Carbonatites

As shown in Appendix F.2, the carbonatite rocks from the Schiel Complex have whole-rock compositions comparable to carbonatites from other phoscorite-bearing complexes,

Figure 56 shows the REE chondrite-normalised plot of the carbonatites from the Schiel Complex together with four other carbonatites from phoscorite-carbonatite complexes. This plot shows that the carbonatite rocks found at the Schiel Complex conform to what is expected to be seen from carbonatites associated with phoscorite crystallisation. The Phalaborwa Complex banded magnetite sövite and the sövite with Cu-sulphide mineralisation shows similar LREE contents as the Schiel Complex carbonatites, but then drops off considerably and shows depletion in HREE compared to the Schiel Complex carbonatites. The Schiel Complex carbonatites are shown to have the highest total whole-rock REE content of all the carbonatites associated with phoscorites. The main, and probably most important, difference between the Phalaborwa Complex and the Schiel Complex is the lack of Cu-bearing minerals found in the Schiel Complex carbonatites. Although some copper-bearing mineral crystallisation does occur, it is found as insignificant amounts in small sections of the Schiel Complex carbonatites.

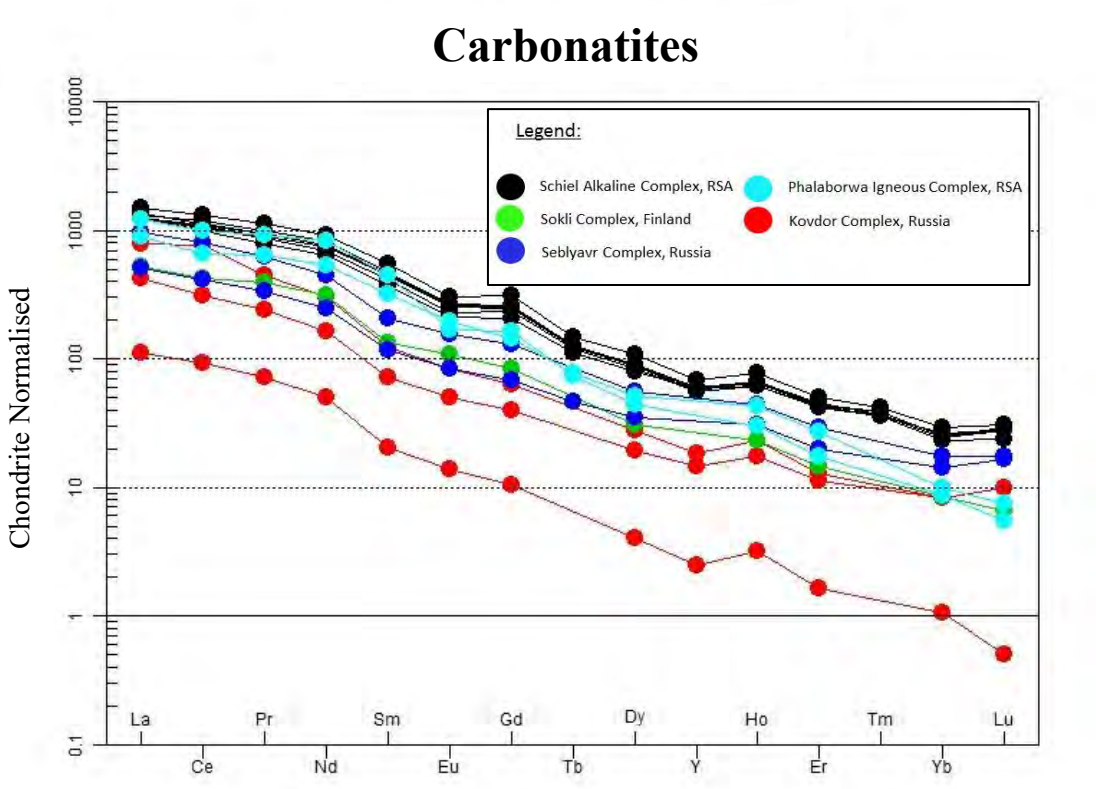

Figure 56: REE-chondrite normalised diagram comparing carbonatites from phoscorite-carbonatite-bearing complexes.

8.3.3 A Mica Chemistry Comparison between the Schiel Complex and Phalaborwa Complex

The Schiel Complex mica EPMA data was recalculated based on the method by Dymek (1983), for comparison purposes, to follow the mica recalculation method used by Giebel et al. (2019). The mica recalculation methods proposed by Dymek (1983) are based on micas that have a metamorphic origin and would not be ideal for micas from magmatic rocks. Although Giebel et al. (2019) does not explain the recalculation method used in detail, analysis of their chemistry tables suggests that they used the normalisation scheme:

Total cations – (K+Na+Ca+Ba) = 7.

This method assumes the total occupancy of octahedral and tetrahedral sites. Dymek (1983) showed that this method would result in overestimated formula proportions if octahedral vacancies were present, and stressed that Ti- and Al-substitution involves vacancies resulting in the 7 cation normalisation procedure being incorrect, stating that it should be abandoned. It is therefore clear that the mica recalculation method used by Giebel et al. (2019) provides doubt regarding the true composition of the micas and that their mica chemistry tables are flawed. This mica chemical comparison was undertaken due to the extensive mica analyses provided by Giebel et al. (2019) and taking into account the theory that the Phalaborwa and Schiel Complexes may be chemically related.

Giebel et al. (2019) analysed micas from the phoscorite-carbonatite complex at Phalaborwa and reported Mg# values of micas from pyroxenite (biotite – 59-62), fenite (biotite – 69-72) and phoscorites (phlogopite and tetraferriphlogopite – 84-97). These Mg# values do not corroborate the Mg# values calculated for the Schiel Complex phoscorite micas (magnesian biotite/phlogopite – 70-74) but do align with the clinopyroxenite micas (biotite – 40-67). The high Mg# values of the phoscorites reported by Giebel et al. (2019), as well as their phoscorite samples being in close association with the Banded Carbonatites and being cut by the Transgressive Carbonatites of the Phalaborwa Complex, may add doubt that these samples are true phoscorites and could be of a more glimmeritic nature, supported by their mineralogy consisting of phlogopite and tetraferriphlogopite. These phoscorite rocks contain similar Mg# values to that of the glimmerites from the Schiel Complex (Phlogopite – 81-93), which could mean that unmetasomatised phoscorites from the Phalaborwa Complex may be scarce or might not be present, and that the phlogopitic micas from the phoscoritic rocks from the Phalaborwa Complex may have formed through metasomatism and were not crystallised as ortho-magmatic products.

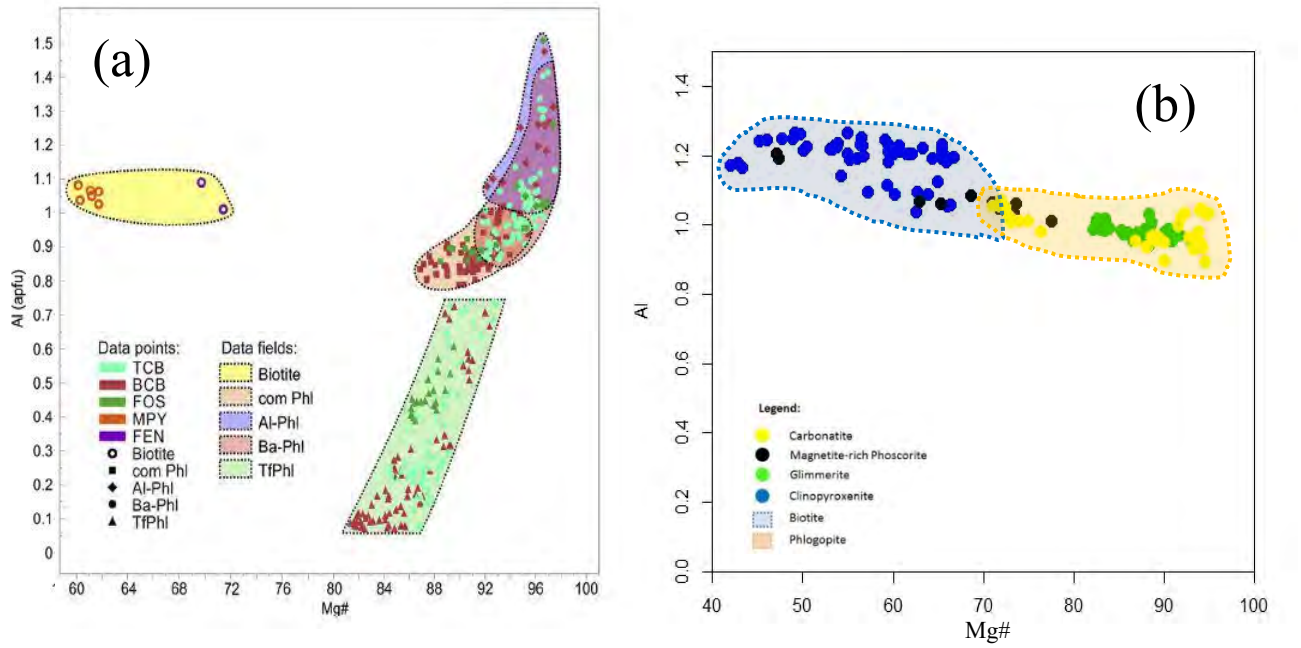

Figure 57: Mg# vs. total Al content of micas from: (a) the Phalaborwa Complex (Giebel et al., 2019); (b) the Schiel Complex. Acronyms used: TCB – transgressive carbonatite; BCB – banded carbonatite; FOS – Foskorite; MPY – micaceous pyroxenite; FEN – fenite; Phl – phlogopite; TfPhl – tetraferriphlogopite.

The Mg# comparison between the Schiel Complex and Phalaborwa Complex can be seen in Figure 57. It is also seen in Figure 58 that the phlogopite mica from the Schiel Complex does not vary significantly in Al content and that no micas from the Schiel Complex are plotted in the tetraferriphlogopite range highlighted by the zone depleted in Al content seen in Figures 57 and 58. This comparison also shows that biotitic micas are indicative of pyroxenite intrusions.

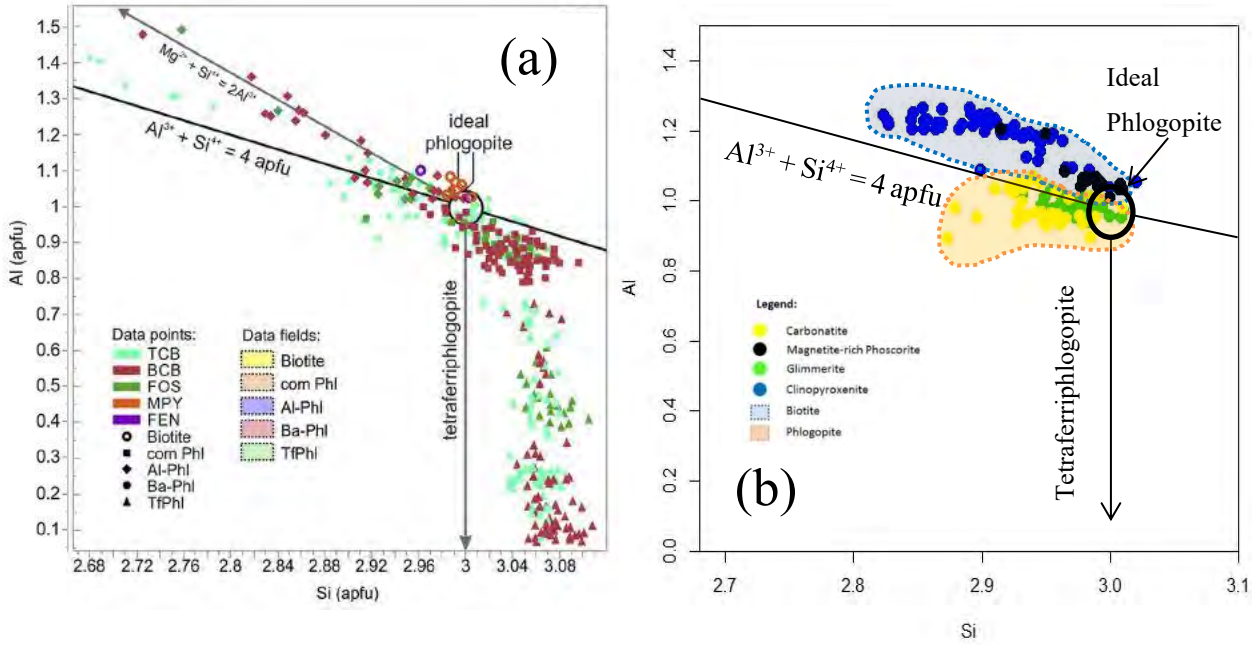

Figure 58: Si content vs. Al content of micas from: (a) the Phalaborwa Complex (Giebel et al., 2019); (b) the Schiel Complex. Acronyms used: TCB – transgressive carbonatite; BCB – banded carbonatite; FOS – Foskorite; MPY – micaceous pyroxenite; FEN – fenite; Phl – phlogopite; TfPhl – tetraferriphlogopite.

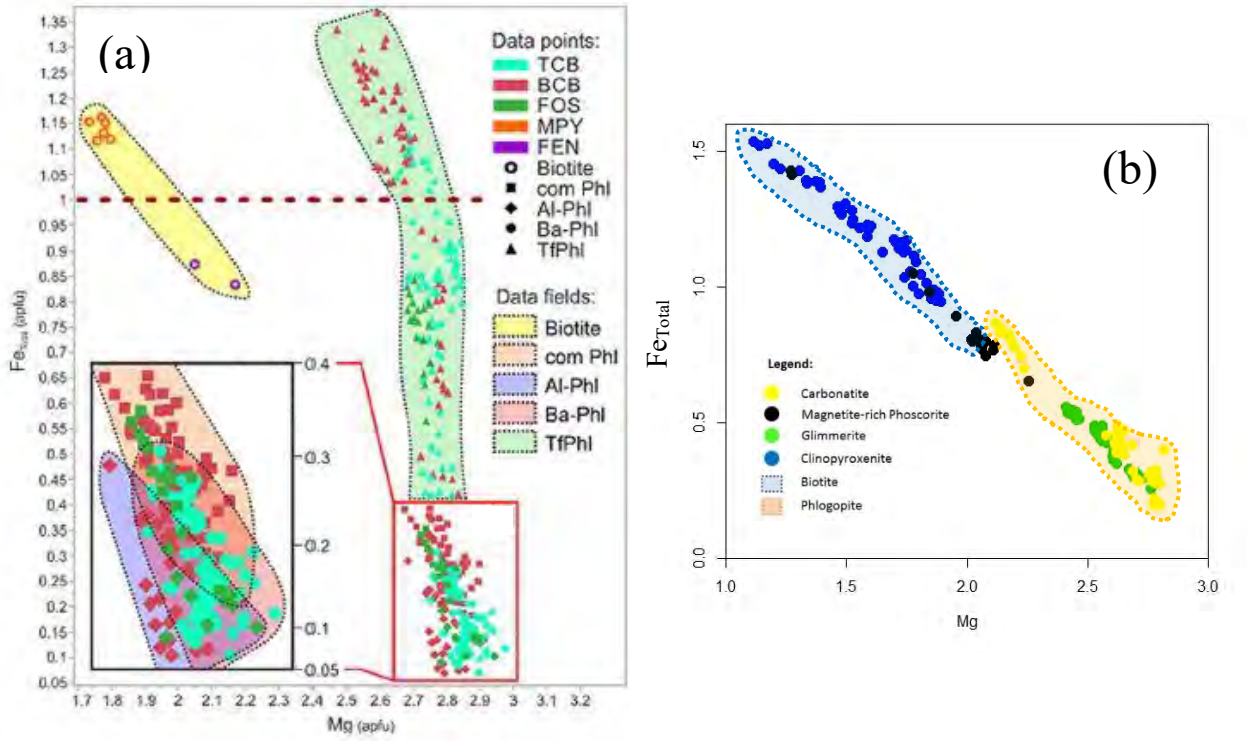

Figure 59: Mg vs. total Fe content of micas from: (a) the Phalaborwa Complex (Giebel et al., 2019); (b) the Schiel Complex. Acronyms used: TCB – transgressive carbonatite; BCB – banded carbonatite; FOS – Foskorite; MPY – micaceous pyroxenite; FEN – fenite; Phl – phlogopite; TfPhl – tetraferriphlogopite.

Figure 60 shows a comparison between the Total Fe and F content from the two different complexes, where no real correlation is observed.

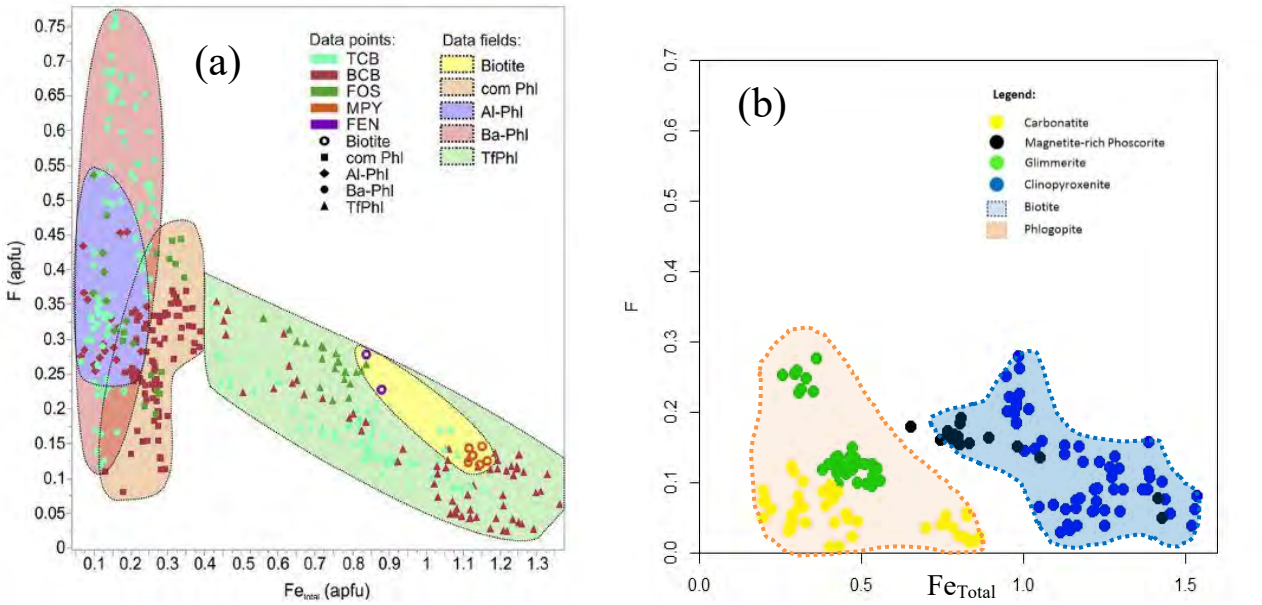

Figure 60: Total Fe vs. F content of micas from: (a) the Phalaborwa Complex (Giebel et al., 2019); (b) the Schiel Complex. Acronyms used: TCB – transgressive carbonatite; BCB – banded carbonatite; FOS – Foskorite; MPY – micaceous pyroxenite; FEN – fenite; Phl – phlogopite; TfPhl – tetraferriphlogopite.

8.4 Concluding Comment

Rudashevsky et al. (2004) described the source of the economic interest of phoscorites and carbonatites in a comparative study between the Kovdor phoscorite-carbonatite Complex and Phalaborwa Complex. The presence of significant Cu-bearing mineralisation, together with Pt, Pd, Au and Ag mineralisation provide economic significance concerning these complexes. No significant mineralisation of this nature was seen in the Schiel Complex, with only negligible amounts of sulphide content detected in small parts of the carbonatite section. The only mineral of economic interest detected in the Schiel Complex phoscorites would be apatite, for which the lack of late-stage REE enrichment seen in apatites from the Schiel Complex, described in Chapter 8.3, also reported by Graupner et al. (2018), is in contrast to late-stage REE enrichment of apatites seen from the Phalaborwa Complex described by Giebel et al. (2019) and Giebel et al. (2017).

It is noted that the REE patterns from both phoscorite and carbonatite components in the various complexes are almost identical. The Kovdor phoscorite-carbonatite Complex is the only exception where the phoscoritic rocks are significantly depleted in REE's as compared to its associated carbonatite rocks. The highest total REE content of the Schiel Complex phoscorites and carbonatites show that these were produced from a melt with the lowest degree of melting in the mantle out of all the other complexes to generate the REE-enriched patterns seen. Although high REE contents are recorded in the Schiel Complex carbonatite and phoscorite rocks, the lack of copper-bearing mineralisation and the complicated structure of the complex would suggest that this alkaline complex would not generate significant economic interest, based on the sample suite present for the Schiel Complex analyses in this thesis.

The variation in mica compositions seen with respect to rock type from the Phalaborwa Complex is not seen in the similar rock units from the Schiel Complex. These complexes should therefore not be compared chemically as it is shown that although these complexes contain similar rock types, the chemical makeup of these rock types differ and do not seem to follow analogous evolutionary processes, which is also supported by the difference in the mineralogy of the two complexes seen in Appendices A and F.

It is therefore suggested that the Schiel Alkaline Complex and the Phalaborwa Complex were emplaced discretely, from separate magmatic sources containing different chemistries.

References

Aldous, R. T. H. (1980). Ore genesis in copper-bearing carbonatites: a mineralogical, fluid inclusion and geochemical study.

Alonso, E., Sherman, A. M., Wallington, T. J., Everson, M. P., Field, F. R., Roth, R., & Kirchain, R. E. (2012). Evaluating rare earth element availability: A case with revolutionary demand from clean technologies. *Environmental science & technology*, *46*(6), 3406-3414.

Amelin, Y., & Zaitsev, A. N. (2002). Precise geochronology of phoscorites and carbonatites:: The critical role of U-series disequilibrium in age interpretations. *Geochimica et Cosmochimica Acta*, *66*(13), 2399-2419.

Anhaeusser, C. R., & Maske, S. (Eds.). (1986). Mineral deposits of southern Africa. Geological Society of South Africa.

Balaganskaya, E., Downes, H., & Demaiffe, D. (2007). REE and Sr-Nd isotope compositions of clinopyroxenites, phoscorites and carbonatites of the Seblyavr massif, Kola peninsula, Russia. *Mineralogia*, *38*(1), 29-45.

Barker, D. S. (2001). Calculated silica activities in carbonatite liquids. *Contributions to Mineralogy and Petrology*, *141*(6), 704-709.

Barton Jr, J. M., Barton, E. S., & Smith, C. B. (1996). Petrography, age and origin of the Schiel alkaline complex, northern Transvaal, South Africa. *Journal of African Earth Sciences*, *22*(2), 133-145.

Bau, M. (1996). Controls on the fractionation of isovalent trace elements in magmatic and aqueous systems: evidence from Y/Ho, Zr/Hf, and lanthanide tetrad effect. *Contributions to Mineralogy and Petrology*, *123*(3), 323-333.

Black, L.P., Kamo, S.L., Allen, C.M., Davis, D.W., Aleinikoff, J.N., Valley, J.W., Mundil, R., Campbell, I.H., Korch, R.J., Williams, I.S., Foudoulis, C., 2004. Improved $^{206}Pb/^{238}U$ microprobe geochronology by monitoring of a trace-element-related matrix effect; SHRIMP, ID-TIMS, ELA-ICP-MS and oxygen isotope documentation for a series of zircon standards. Chemical Geology 205, 115-140.

Brod, J. A., Gaspar, J. C., De Araújo, D. P., Gibson, S. A., Thompson, R. N., & Junqueira-Brod, T. C. (2001). Phlogopite and tetra-ferriphlogopite from Brazilian carbonatite complexes: petrogenetic constraints and implications for mineral-chemistry systematics. *Journal of Asian Earth Sciences*, *19*(3), 265-296.

Brögger, W. C. (1921). *Die Eruptivgesteine des Kristianiagebietes. IV. Das Fengebiet in Telemark, Norwegen*. na.

Buikin, A. I., Verchovsky, A. B., Sorokhtina, N. V., & Kogarko, L. N. (2014). Composition and sources of volatiles and noble gases in fluid inclusions in pyroxenites and carbonatites of the Seblyavr Massif, Kola Peninsula. *Petrology*, *22*(5), 507-520.

Dutta, T., Kim, K. H., Uchimiya, M., Kwon, E. E., Jeon, B. H., Deep, A., & Yun, S. T. (2016). Global demand for rare earth resources and strategies for green mining. *Environmental Research*, *150*, 182-190.

Dymek, R. F. (1983). Titanium, aluminum and interlayer cation substitutions in biotite from high-grade gneisses, West Greenland. *American Mineralogist*, *68*(9-10), 880-899.

Eggert, R. G., & Kerrick, D. M. (1981). Metamorphic equilibria in the siliceous dolomite system: 6 kbar experimental data and geologic implications. *Geochimica et Cosmochimica Acta*, *45*(7), 1039-1049.

Egorov, L. S. (1992). Phoscorites of Maymeicha-Kotui ijolite-carbonatite complex. *Zapiski Vserossiyskogo Mineralogicheskogo Obshchestva*, *121*(3), 13-26.

Elliott, H. A. L., Wall, F., Chakhmouradian, A. R., Siegfried, P. R., Dahlgren, S., Weatherley, S., ... & Deady, E. (2018). Fenites associated with carbonatite complexes: A review. *Ore Geology Reviews*, *93*, 38-59.

Eriksson, S. C. (1989). Phalaborwa: a saga of magmatism, metasomatism and miscibility. In *Carbonatites: Genesis and evolution* (pp. 221-254). Unwin Hyman London.

Foster, M. D. (1960). Interpretation of the composition of trioctahedral micas: US Geol, Survey Prof. *Paper 354B*.

Fourie, P. J., & De Jager, D. H. (1986). Phosphate in the Phalaborwa complex. *Mineral Deposits of Southern Africa*, *2*, 2239-2253.

Gamaletsos, P. N., Godelitsas, A., Filippidis, A., & Pontikes, Y. (2019). The Rare Earth Elements Potential of Greek Bauxite Active Mines in the Light of a Sustainable REE Demand. *Journal of Sustainable Metallurgy*, *5*(1), 20-47.

Giebel, R. J., Gauert, C. D., Marks, M. A., Costin, G., & Markl, G. (2017). Multi-stage formation of REE minerals in the Palabora Carbonatite Complex, South Africa. *American Mineralogist*, *102*(6), 1218-1233.

Giebel, R. J., Marks, M. A., Gauert, C. D., & Markl, G. (2019). A model for the formation of carbonatite-phoscorite assemblages based on the compositional variations of mica and apatite from the Palabora Carbonatite Complex, South Africa. *Lithos*, *324*, 89-104.

Gittins, J. (1989). The origin and evolution of carbonatite magmas. *Carbonatites: genesis and evolution. Unwin Hyman, London*, 580-600.

Gittins, J., & Harmer, R. E. (1997). What is ferrocarbonatite? A revised classification. *Journal of African Earth Sciences*, *25*(1), 159-168.

Goodenough, K. M., Schilling, J., Jonsson, E., Kalvig, P., Charles, N., Tuduri, J., ... & Bertrand, G. (2016). Europe's rare earth element resource potential: An overview of REE metallogenetic provinces and their geodynamic setting. *Ore Geology Reviews*, *72*, 838-856.

Graupner, T., Klemd, R., Henjes-Kunst, F., Goldmann, S., Behnsen, H., Gerdes, A., ... & Opperman, R. (2018). Formation conditions and REY enrichment of the 2060 Ma phosphorus mineralization at Schiel (South Africa): geochemical and geochronological constraints. *Mineralium Deposita*, 1-26.

Harlov, D. E., Andersson, U. B., Förster, H. J., Nyström, J. O., Dulski, P., & Broman, C. (2002). Apatite–monazite relations in the Kiirunavaara magnetite–apatite ore, northern Sweden. *Chemical Geology*, *191*(1-3), 47-72.

Harmer, R. E. (2000). Mineralisation of the Phalaborwa Complex and the carbonatite connection in iron oxide-Cu-Au-U-REE deposits. *Hydrothermal Iron Oxide Copper-Gold and Related Deposits, A Global Perspective, Australian Mineral Foundation*, 331-340.

Harmer, R. E., & Gittins, J. (1997). The origin of dolomitic carbonatites: field and experimental constraints. *Journal of African Earth Sciences*, *25*(1), 5-28.

Hillier, S., Marwa, E. M., & Rice, C. M. (2013). On the mechanism of exfoliation of 'Vermiculite'. *Clay Minerals*, *48*(4), 563-582.

Horstmann, U. E., & Verwoerd, W. J. (1997). Carbon and oxygen isotope variations in southern African carbonatites. *Journal of African Earth Sciences*, *25*(1), 115-136.

Huppert, H.E. and Sparks, R.S.J., 1989. Chilled margins in igneous rocks. *Earth and Planetary Science Letters*, *92*(3-4), pp.397-405.

Ingrid, H. K. (1998). Rare earth elements in sövitic carbonatites and their mineral phases. *Journal of Petrology*, *39*(11-12), 2105-2121.

Ivanyuk, G., Kalashnikov, A., Pakhomovsky, Y., Bazai, A., Goryainov, P., Mikhailova, J., ... & Konopleva, N. (2017). Subsolidus Evolution of the Magnetite-Spinel-UlvöSpinel Solid Solutions in the Kovdor Phoscorite-Carbonatite Complex, NW Russia. *Minerals*, *7*(11), 215.

Jahn, B. M., Bernard-Griffiths, J., Charlot, R., Cornichet, J., & Vidal, F. (1980). Nd and Sr isotopic compositions and REE abundances of Cretaceous MORB (Holes 417D and 418A, Legs 51, 52 and 53). *Earth and Planetary Science Letters*, *48*(1), 171-184.

Jones, A. P. (1984). Mafic silicates from the nepheline syenites of the Motzfeldt centre, South Greenland. *Mineralogical Magazine*, *48*(346), 1-12.

Krasnova, N. I., Balaganskaya, E. G., & Garcia, D. (2004). Kovdor—classic phoscorites and carbonatites. *Phoscorites and Carbonatites from Mantle to Mine: the Key Example of the Kola Alkaline Province. Mineralogical Society, London*, 99-132.

Krasnova, N. I., Petrov, T. G., Balaganskaya, E. G., Garcia, D., Moutte, J., Zaitsev, A. N., & Wall, F. (2004). Introduction to phoscorites: occurrence, composition, nomenclature and petrogenesis. In *Phoscorites and carbonatites from mantle to mine: the Key example of the Kola Alkaline Province* (Vol. 10, pp. 45-74). Mineralogical Society London.

Kresten, P. (1988). The chemistry of fenitization: examples from Fen, Norway. *Chemical Geology*, *68*(3-4), 329-349.

Laurent, O., & Zeh, A. (2015). A linear Hf isotope-age array despite different granitoid sources and complex Archean geodynamics: example from the Pietersburg block (South Africa). *Earth and Planetary Science Letters*, *430*, 326-338.

Le Bas, M. J. (1981). Carbonatite magmas. *Mineralogical Magazine*, *44*(334), 133-140.

Le Maitre, R. W., Streckeisen, A., Zanettin, B., Le Bas, M. J., Bonin, B., Bateman, P., ... & Lamere, J. (2002). Igneous rocks: a classification and glossary of terms: recommendations of the International Union of Geological Sciences. In *Subcommission on the Systematics of Igneous rocks*. Cambridge University Press.

Lee, M. J., Garcia, D., Moutte, J., Williams, C. T., & Wall, F. (2004). Carbonatites and phoscorites from the Sokli Complex, Finland. *Phoscorites and Carbonatites from Mantle to Mine: the Key Example of the Kola Alkaline Province", eds. F. Wall and AN Zaitev, The Mineralogical Society of Great Britain and Ireland, London*, 133-162.

Lee, M. J., Lee, J. I., Garcia, D., Moutte, J., Williams, C. T., Wall, F., & Kim, Y. (2006). Pyrochlore chemistry from the Sokli phoscorite-carbonatite complex, Finland: implications for the genesis of phoscorite and carbonatite association. *Geochemical Journal*, *40*(1), 1-13.

Liu, Y. L., Ling, M. X., Williams, I. S., Yang, X. Y., Wang, C. Y., & Sun, W. (2018). The formation of the giant Bayan Obo REE-Nb-Fe deposit, North China, Mesoproterozoic carbonatite and overprinted Paleozoic dolomitization. *Ore Geology Reviews*, *92*, 73-83.

Lubala, R. T., Frick, C., Rogers, J. H., & Walraven, F. (1994). Petrogenesis of syenites and granites of the Schiel alkaline complex, northern Transvaal, South Africa. *The Journal of Geology*, *102*(3), 307-316.

Ludwig, K.R., 2012. Isoplot/Ex version 3.75: A Geochronological Toolkit for Microsoft Excel. Berkeley Geochronology Center, Special Publication 5, 75 pp.

Lumpkin, G. R. (1999). Physical and chemical characteristics of baddeleyite (monoclinic zirconia) in natural environments: an overview and case study. *Journal of nuclear materials*, *274*(1-2), 206-217.

Mancheri, N. A. (2015). World trade in rare earths, Chinese export restrictions, and implications. *Resources Policy*, *46*, 262-271.

Markwitz, V., & Kirkland, C. L. (2018). Source to sink zircon grain shape: Constraints on selective preservation and significance for Western Australian Proterozoic basin provenance. *Geoscience Frontiers*, *9*(2), 415-430.

Marty, B., Tolstikhin, I., Kamensky, I. L., Nivin, V., Balaganskaya, E., & Zimmermann, J. L. (1998). Plume-derived rare gases in 380 Ma carbonatites from the Kola region (Russia) and the argon isotopic composition in the deep mantle. *Earth and Planetary Science Letters*, *164*(1-2), 179-192.

McDonough, W. F., & Sun, S. S. (1995). The composition of the Earth. *Chemical geology*, *120*(3-4), 223-253.

Mitchell, R. H. (1995). Kimberlites and orangeites. In *Kimberlites, Orangeites, and Related Rocks* (pp. 1-90). Springer, Boston, MA.

Mitchell, R. H. (2005). Carbonatites and carbonatites and carbonatites. *The Canadian Mineralogist*, *43*(6), 2049-2068.

Moody, J. B. (1976). Serpentinization: a review. *Lithos*, *9*(2), 125-138.

Puustinen, K. A. U. K. O. (1973). Tetraferriphlogopite from the Siilinjärvi carbonatite complex, Finland. *Bulletin of the Geological Society of Finland*, *45*, 35-42.

Randive, K., Kumar, J. V., Bhondwe, A., & Lanjewar, S. (2014). Understanding the behaviour of rare earth elements in minerals and rocks. *Gondvana Geol. Mag.*, *29*, 29-37.

Reinhardt, N., Proenza, J. A., Villanova-de-Benavent, C., Aiglsperger, T., Bover-Arnal, T., Torró, L., ... & Dziggel, A. (2018). Geochemistry and Mineralogy of Rare Earth Elements (REE) in Bauxitic Ores of the Catalan Coastal Range, NE Spain. *Minerals*, *8*(12), 562.

Rudashevsky, N. S., Kretser, Y. L., Rudashevsky, V. N., & Sukharzhevskaya, E. S. (2004). A review and comparison of PGE, noble-metal and sulphide mineralization in phoscorites and carbonatites from Kovdor and Phalaborwa. *Phoscorites and Carbonatites from Mantle to Mine: the Key Example of the Kola Alkaline Province", eds. F. Wall and AN Zaitev, The Mineralogical Society of Great Britain and Ireland, London*, 375-405.

Russell, H. D. (1954). The mineralogy and petrology of the carbonatite at Loolekop, Eastern Transvaal. *South African Journal of Geology*, *57*(Transactions 1954), 197-208.

Sawai, M., Katayama, I., Hamada, A., Maeda, M., & Nakashima, S. (2013). Dehydration kinetics of antigorite using in situ high-temperature infrared microspectroscopy. *Physics and Chemistry of Minerals*, *40*(4), 319-330.

Sharygin, V. V., Zhitova, L. M., & Nigmatulina, E. N. (2011). Fairchildite K2Ca (CO3) 2 in phoscorites from Phalaborwa, South Africa: the first occurrence in alkaline carbonatite complexes. *Russian Geology and Geophysics*, *52*(2), 208-219.

Stacey, J.S., Kramers, J.D., 1975. Approximation of terrestrial lead isotope evolution by a two-stage model. Earth and Planetary Science Letters 26, 207-221.

Steiger, R.H., Jäger, E., 1977. Subcommission on geochronology: convention on the use of decay constants in geo- and cosmochronology. Earth and Planetary Science Letters 36, 359-362.

Stettler, E. H., Coetzee, H., Rogers, H. J. J., & Lubala, R. T. (1993). The Schiel Alkaline Complex: geological setting and geophysical investigation. *South African journal of geology*, *96*(3), 96-107.

Stormer, J. C., Pierson, M. L., & Tacker, R. C. (1993). Variation of F and Cl X-ray intensity due to anisotropic diffusion in apatite during electron microprobe analysis. *American Mineralogist*, *78*(5-6), 641-648.

Suzuki, Y., & Kirino, Y. (1984). Reactions between natural serpentinite and quartz under hydrothermal conditions (1). *Mineralogical Journal*, *12*(2), 47-63.

Teiber, H., Marks, M. A., Arzamastsev, A. A., Wenzel, T., & Markl, G. (2015). Compositional variation in apatite from various host rocks: clues with regards to source composition and crystallization conditions. Neues Jahrbuch für Mineralogie-Abhandlungen: Journal of Mineralogy and Geochemistry, 192(2), 151-167.

Tolstikhin, I. N., Kamensky, I. L., Nivin, V. A., Vetrin, V. R., Balaganskaya, E. G., Ikorsky, S. V., ... & Demaiffe, D. (1998). Low mantle plume component in 370 Ma old Kola ultrabasic-alkaline-carbonatite complexes: Evidences from rare gas isotopes and related trace elements. *Russian Journal of Earth Sciences*, *1*(2).

Vartiainen, H. (1980). The petrography, mineralogy and petrochemistry of the Sokli carbonatite massif, northern Finland. *Bulletin of Geological Survey of Finland*.

Verhulst, A., Balaganskaya, E., Kirnarsky, Y., & Demaiffe, D. (2000). Petrological and geochemical (trace elements and Sr–Nd isotopes) characteristics of the Paleozoic Kovdor ultramafic, alkaline and carbonatite intrusion (Kola Peninsula, NW Russia). *Lithos*, *51*(1-2), 1-25.

Verwoerd, W. J. (1986). Mineral deposits associated with carbonatites and alkaline rocks. *Mineral Deposits of Southern Africa*, *2*, 2173-91.

Walraven, F., Frick, C., & Lubala, R. T. (1992). Pb-isotope geochronology of the Schiel complex, northern Transvaal, South Africa. *Journal of African Earth Sciences (and the Middle East)*, *15*(1), 103-110.

Wiedenbeck, M., Allé, P., Corfu, F., Griffin, W.L., Meier, M., Oberli, F., Von Quadt, A., Roddick, J.C., Spiegel, W., 1995. Three Natural Zircon Standards for U-Th-Pb, Lu-Hf, Trace Element and REE Analysis. Geostandards Newsletter 19, 1-23.

Wooley, A. R., & Kempe, D. R. C. (1989). Carbonatites: nomenclature, average chemical compositions and element distributions. *Carbonatites—genesis and evolution/Ed. K. Bell. Unwin Hyman*, 1-14.

Woolley, A. R., Bergman, S. C., Edgar, A. D., Le Bas, M. J., Mitchell, R. H., Rock, N. M., & Scott Smith, B. H. (1996). Classification of lamprophyres, lamproites, kimberlites, and the kalsilitic, melilitic, and leucitic rocks. *The Canadian Mineralogist*, *34*(2), 175-186.

Woolley, A. R. and Kjarsgaard, B.A. (2008). *Carbonatite Occurrences of the World: Map and Database*. Geological Survey of Canada, Open File Report 5796.

Wu, F. Y., Yang, Y. H., Li, Q. L., Mitchell, R. H., Dawson, J. B., Brandl, G., & Yuhara, M. (2011). In situ determination of U–Pb ages and Sr–Nd–Hf isotopic constraints on the petrogenesis of the Phalaborwa carbonatite Complex, South Africa. *Lithos*, *127*(1-2), 309-322.

Zaitsev, A., & Bell, K. (1995). Sr and Nd isotope data of apatite, calcite and dolomite as indicators of source, and the relationships of phoscorites and carbonatites from the Kovdor massif, Kola peninsula, Russia. *Contributions to Mineralogy and Petrology*, *121*(3), 324-335.

ZharikovF, V. A. (2007). 9. Metasomatism and metasomatic rocksF. *A classification of metamorphic rocks and glossary of terms. Recommendations of the International Union of Geological Sciences Subcommission on the Systaematics of Metamorphic Rocks*.

Appendix A: Mineralogical Comparison Between Various Phoscorite-bearing Complexes

Table A 1: Mineralogical comparison between various phoscorite-bearing complexes.

	Location	Rock Types	Rock Forming Minerals	Accessory Minerals	References
Kola Alkaline Province	Kovdor Phoscorite-Carbonatite Complex, Russia	Forsterite- apatite phoscorite	Forsterite (60-80%), apatite (20-30%), richterite, magnetite (<15%)	Baddeleyite, phlogopite, clinohumite, serpentine	(Krasnova et al., 2004)
		Magnetite-apatite-forsterite phoscorite	Magnetite (40-50%), apatite (25-35%), forsterite (15-20%), calcite (<5%)	Baddeleyite, phlogopite, clinohumite, serpentine, pyrrhotite, chalcopyrite	
		Calcite-rich phoscorites	Calcite (<10-30%), magnetite (<55%), apatite (<25%), forsterite (1-18%)	Tetraferriphlogopite, baddeleyite	
		Calcite-rich phoscorites with tetraferriphlogopite	Magnetite, calcite, forsterite, tetraferriphlogopite, apatite	Uranophyrochlore, zirconalite, ilmenite, baddeleyite, pyrrhotite, chalcopyrite	
		Magnetite-dolomite-richterite	Magnetite, ilmenite, forsterite, apatite, dolomite, calcite, tetraferriphlogopite	Richterite, zircon, pyrochlore	
		Magnetite-dolomite-forsterite	Magnetite (50-80%), forsterite (5-10%), calcite, apatite	phlogopite, tetraferriphlogopite, zircon, baddeleyite	
	Sokli Complex, Finland	Phoscorite	Calcite (10-30%), fluorapatite, magnetite, forsterite, phlogopite (± tetraferriphlogopite)	Baddeleyite, pyrochlore, zirconalite	(Lee et al., 2004)
		Carbonatite	Calcite (60-80%), fluorapatite, magnetite, forsterite, phlogopite (± tetraferriphlogopite)	Baddeleyite, pyrochlore, zirconalite	
	Seblyavr Complex, Russia	Phoscorite	Apatite, diopside, phlogopite, magnetite	Amphibole (tremolite), baddeleyite, chlorite	(Marty et al., 1998), (Buikin et al., 2014), (Balaganskaya et al., 2007) (Tolstikhin et al., 1998)
		Clinopyroxenite	Diopside, phlogopite, titamagnetite, perovskite	Amphibole, apatite, calcite	
		Carbonatite	Calcite, apatite, phlogopite, magnetite, dolomite	Forsterite, ancylite, baddeleyite, amphibole (tremolite), pyrochlore, pyrrhotite, chalcopyrite, galena	
South Africa	Phalaborwa Complex, South Africa	Foskorite	Olivine/serpentine, magnetite, apatite, phlogopite, calcite	Baddeleyite, bornite, chalcocite	(R.E Harmer, 2000), (Russell et al., 1954)
		Carbonatite	Magnetite, apatite	Phlogopite, chondrodite, olivine, chalcopyrite, bornite, uranothorianite, cubanite	
	Schiel Alkaline Complex, South Africa	Glimmerite	Phlogopite, diopside, magnetite, actinolite, fluorapatite	Ilmenite, baddeleyite, zircon, calcite, uranothorianite	Present study
		Magnetite-rich phoscorite	Magnetite, diopside, fluorapatite, annite/phlogopite, amphibole	Ilmenite, serpentine/olivine, zircon, calcite, ferriallanite, uranothorianite	
		Clinopyroxenite	Diopside, magnetite, amphibole, annite	Fluorapatite, ilmenite, zircon, thorianite	
		Carbonatite	Calcite, apatite, magnetite, forsterite, serpentine, diopside, tremolite, phlogopite	Ilmenite, baddeleyite, zircon, pyrite, chalcopyrite, thorianite, sphalerite	

Appendix B: Samples Used in Study

Table B 1: Details of samples used for this study: borehole number, sampling depth, length of core sampled, which type of thin section was produced, and if geochemical analysis was undertaken.

Borehole	Sample	Depth (m)	Length (cm)	Chemistry	Section type
SC08	Sc08-01	117.35	30.0		polished
	Sc08-02	120.78	28.0	x	Covered
	Sc08-03	123.42	26.0		Polished
	Sc08-04	125.43	29.0		Polished
	Sc08-05	125.60	16.0	x	Polished
	Sc08-06	125.81	29.0		Polished
	Sc08-07	127.81	19.0		Covered
	Sc08-08	128.02	30.0	x	Polished
	Sc08-09	129.29	37.0		Polished
	Sc08-10	129.67	15.0		-
	Sc08-11	139.70	19.0	x	-
	Sc08-12	139.90	25.0		Covered
	Sc08-13	141.27	42.0	x	Polished
	Sc08-14	142.77	40.0	x	-
	Sc08-15	144.17	46.0	x	Covered
	Sc08-16	145.87	47.0	x	-
	Sc08-17	146.23	48.0		Polished
	Sc08-18	147.27	46.0		Polished
	Sc08-19	149.35	21.0	x	Covered
	Sc08-20	149.58	17.0		Polished
	Sc08-21	149.68	15.0		-
	Sc08-22	150.42	13.0		-
	Sc08-23	150.57	15.0	x	Covered
	Sc08-24	150.72	18.0		Polished
	Sc08-25	152.02	14.0		-
SC10	Sc10-01	82.13	26.0	x	
	Sc10-02	82.85	15.5	x	Polished
	Sc10-03	83.29	19.0		
	Sc10-04	84.35	25.0	x	Polished
	Sc10-05	84.73	14.0	x	Polished
	Sc10-06	85.12	24.0		Polished
	Sc10-07	85.47	21.0	x	Polished
	Sc10-08	86.84	18.0		
	Sc10-09	90.58	32.0		Polished
	Sc10-10	93.27	27.0		
	Sc10-11	96.19	18.0		Polished
	Sc10-12	96.52	24.0	x	Polished
	Sc10-13	96.75	28.0		Polished
	Sc10-14	97.04	31.0	x	
	Sc10-15	97.38	37.0	x	Polished
	Sc10-16	98.09	24.0		
	Sc10-17	101.02	22.0		Polished
	Sc10-18	101.24	15.0	x	
	Sc10-19	101.65	27.0		Polished
	Sc10-20	103.02	22.0		Polished
	Sc10-21	104.39	16.0	x	
	Sc10-22	108.46	22.0		Polished
	Sc10-23	109.58	14.0		Polished
	Sc10-24	109.75	15.0	x	Polished
	Sc10-25	109.91	15.0		Polished
	Sc10-26	111.07	23.0		Polished
	Sc10-27	118.21	18.0		Polished
	Sc10-28	118.87	21.0		Polished
	Sc10-29	124.00	11.0		
	Sc10-30	129.01	12.0	x	
	Sc10-31	131.37	14.0		
	Sc10-32	133.30	29.0	x	Polished
SC09	Sc09-01	127.10	10		
	Sc09-02	127.41	27		
	Sc09-03	142.34	31		
	Sc09-04	147.83	43		
	Sc09-05	151.51	33.0	x	
	Sc09-06	152.25	24.0		Polished
	Sc09-07	153.62	33		
	Sc09-08	154.46	18.0		Polished
	Sc09-09	154.64	15.0	x	
	Sc09-10	164.29	42		

Appendix C: EPMA Methodology

The beam was generated by a Tungsten cathode, and excited with 15 kV accelerating potentials at beam currents of either 2-, 10- or 20 nA depending on the sensitivity of the minerals to beam damage. A beam size of 1-10 µm was used depending on the beam sensitivity of the material. Four wavelength dispersive spectrometers were used. Element concentrations were measured on K-alpha peaks, except for Sr and Ce for which L-alpha peaks were used. Overlap of Ti-Kβ on V-Kα was corrected for. Counting times on peak were 10s (except 15s for serpentine and Ce, Si, and Sr in apatite), and 10s total (except 15s for serpentine Ce, Si, and Sr in apatite) on background. Apatite was analysed in a manner to minimise the effect of migrating halogens documented by Stormer et al. (1993). Fluorine was measured first and with a TAP crystal. Interference of P on F in apatite was minimized through differential signal filtering. Overlap of Ti-Kβ on V-Kα in magnetite was corrected for.

Commercial "SPI" standards were used for intensity calibration. The standards were pyrope/biotite/kaersutite/plagioclase (Al, Si, Mg), pyrope/biotite/hematite (Fe), albite (Na), rhodonite/Mn-metal (Mn), pyrope/apatite/plagioclase (Ca), apatite (P), Mg_2F/apatite (F), Orthoclase (K), Cr_2O_3 (Cr), Ni-metal (Ni), V-metal (V), rutile (Ti), strontium titanate (Sr), cerium pentaphosphate (Ce), and tugtupite (Cl). The data was collected with JEOL software (PC EPMA 1.9.2.0) and its ZAF matrix algorithm (Heinrich/Duncumb-Reed with FFAST-2005 MACs) was applied to correct for differential matrix effects. Oxygen was calculated by stoichiometry and H_2O by difference before the correction. Thirty micron thick polished sections were prepared for all samples and vacuum carbon coated to 25 nm (+/-5) thickness.

Appendix C.1: Mica EPMA Data

Table C 1.1: Mica EPMA analyses

Rock type	Glimmerite										
Sample	SC10-32-4_Mica1	SC10-32-4_Mica10	SC10-32-4_Mica2	SC10-32-4_Mica3	SC10-32-4_Mica4	SC10-32-4_Mica5	SC10-32-4_Mica6	SC10-32-4_Mica7	SC10-32-4_Mica8	SC10-32-4_Mica9	SC10-4 -2-Mica-10
SiO_2	37.22	37.37	37.54	36.79	37.89	36.94	37.40	37.39	36.83	36.98	39.19
Al_2O_3	13.40	13.35	13.47	13.56	13.72	13.56	13.42	13.43	13.79	13.54	11.80
MgO	15.60	15.03	15.78	15.27	16.00	14.85	15.19	14.91	14.85	15.17	16.50
FeO	17.46	17.84	17.17	17.67	16.55	18.06	17.61	18.15	18.31	18.21	14.66
Fe_2O_3											0.52
TiO_2	0.71	0.94	0.79	0.82	0.70	0.68	0.68	0.69	0.75	0.77	2.21
MnO	0.20	0.27	0.20	0.21	0.22	0.26	0.23	0.24	0.25	0.25	0.22
K_2O	10.15	10.32	10.27	10.13	9.88	10.13	10.26	9.94	10.09	9.98	10.28
Na_2O	0.17	0.10	0.05	0.12	0.24	0.12	0.11	0.17	0.10	0.14	0.15
CaO	0.03	0.00	0.00	0.01	0.10	0.03	0.00	0.06	0.01	0.03	0.02
F	0.13	0.14	0.30	0.17	0.28	0.27	0.27	0.33	0.34	0.16	0.87
H_2O*	3.86	3.86	3.80	3.82	3.84	3.77	3.79	3.76	3.75	3.84	3.58
subtotal	98.92	99.21	99.37	98.56	99.41	98.65	98.96	99.07	99.08	99.07	100.01
O=F,Cl	0.05	0.06	0.13	0.07	0.12	0.11	0.11	0.14	0.14	0.07	0.37
Total	98.86	99.15	99.25	98.48	99.29	98.54	98.85	98.93	98.94	99.00	99.64
	Number of ions calculated on the basis of 24 (O,OH,F)										
Si	5.69	5.71	5.71	5.66	5.72	5.69	5.72	5.72	5.65	5.66	5.88
Al^{iv}	2.31	2.29	2.29	2.34	2.28	2.31	2.28	2.28	2.35	2.34	2.09
Fe^{3+}	0.00	0.00	0.00	0.00	0.00	0.00	0.00	0.00	0.00	0.00	0.03
Fe^{2+}	2.23	2.28	2.18	2.27	2.09	2.32	2.25	2.32	2.35	2.33	1.85
Al^{vi}	0.11	0.11	0.12	0.11	0.17	0.15	0.14	0.14	0.15	0.11	0.00
Ti	0.08	0.11	0.09	0.09	0.08	0.08	0.08	0.08	0.09	0.09	0.25
Mn	0.03	0.03	0.03	0.03	0.03	0.03	0.03	0.03	0.03	0.03	0.03
Mg	3.56	3.42	3.58	3.50	3.60	3.41	3.46	3.40	3.40	3.46	3.69
Ca	0.00	0.00	0.00	0.00	0.02	0.00	0.00	0.01	0.00	0.00	0.00
Na	0.05	0.03	0.02	0.03	0.07	0.04	0.03	0.05	0.03	0.04	0.04
K	1.98	2.01	1.99	1.99	1.90	1.99	2.00	1.94	1.97	1.95	1.97
OH*	3.94	3.93	3.86	3.92	3.87	3.87	3.87	3.84	3.84	3.92	3.59
F	0.06	0.07	0.14	0.08	0.13	0.13	0.13	0.16	0.16	0.08	0.41
Sum	20.03	20.00	20.00	20.03	19.96	20.02	20.01	19.98	20.02	20.02	19.83

Table C 1.2: Mica EPMA analyses

Rock type	Glimmerite											
Sample	SC10-4-2-Mica-2 C	SC10-4-2-Mica-2R	SC10-4-2-Mica-3	SC10-4-2-Mica-4	SC10-4-2-Mica-5	SC10-4-2-Mica-6	SC10-4-2-Mica - 7	SC10-4-2-Mica - 8	SC10-4-2-Mica - 9	SC10-11-1-Mica - 1	SC10-11-1-Mica - 2	SC10-11-1-Mica-3
SiO_2	37.70	38.15	36.77	36.86	36.59	38.62	38.73	39.76	39.05	36.23	36.86	36.45
Al_2O_3	12.02	11.94	12.45	12.36	12.28	12.11	12.00	11.78	11.45	13.54	13.16	13.54
MgO	15.26	13.66	9.52	9.28	9.75	15.21	15.45	16.35	15.41	11.63	11.88	11.30
FeO	18.17	18.21	22.65	22.86	22.72	16.12	15.56	15.04	16.09	20.96	21.14	20.86
Fe_2O_3	0.11								0.67			
TiO_2	1.30	2.50	3.15	3.18	2.74	2.58	2.34	1.83	2.12	1.47	1.65	1.82
MnO	0.23	0.26	0.28	0.37	0.39	0.22	0.22	0.21	0.29	0.29	0.25	0.27
K_2O	9.07	10.12	9.96	10.01	10.10	9.91	10.33	10.18	9.97	9.94	10.15	9.84
Na_2O	0.11	0.16	0.12	0.11	0.12	0.21	0.10	0.19	0.25	0.26	0.14	0.16
CaO	0.05	0.00	0.02	0.00	0.00	0.01	0.02	0.00	0.08	0.00	0.01	0.00
F	0.66	0.56	0.17	0.35	0.27	0.64	0.63	0.96	0.69	0.68	0.50	0.39
H_2O*	3.58	3.65	3.74	3.65	3.67	3.66	3.66	3.55	3.63	3.50	3.62	3.65
subtotal	98.26	99.21	98.82	99.03	98.61	99.29	99.02	99.85	99.71	98.50	99.36	98.27
O=F,Cl	0.28	0.24	0.07	0.15	0.11	0.27	0.26	0.40	0.29	0.29	0.21	0.16
Total	97.98	98.98	98.75	98.88	98.50	99.02	98.76	99.44	99.42	98.21	99.15	98.10
	Number of ions calculated on the basis of 24 (O,OH,F)											
Si	5.81	5.85	5.77	5.79	5.77	5.84	5.87	5.95	5.92	5.68	5.72	5.71
Al^{iv}	2.18	2.15	2.23	2.21	2.23	2.16	2.13	2.05	2.04	2.32	2.28	2.29
Fe^{3+}	0.01	0.00	0.00	0.00	0.00	0.00	0.00	0.00	0.04	0.00	0.00	0.00
Fe^{2+}	2.34	2.33	2.97	3.00	3.00	2.04	1.97	1.88	2.05	2.75	2.75	2.73
Al^{vi}	0.00	0.00	0.08	0.08	0.06	0.00	0.02	0.03	0.00	0.18	0.13	0.21
Ti	0.15	0.29	0.37	0.38	0.32	0.29	0.27	0.21	0.24	0.17	0.19	0.21
Mn	0.03	0.03	0.04	0.05	0.05	0.03	0.03	0.03	0.04	0.04	0.03	0.04
Mg	3.51	3.12	2.23	2.17	2.29	3.43	3.49	3.65	3.48	2.72	2.75	2.64
Ca	0.01	0.00	0.00	0.00	0.00	0.00	0.00	0.00	0.01	0.00	0.00	0.00
Na	0.03	0.05	0.04	0.03	0.04	0.06	0.03	0.05	0.07	0.08	0.04	0.05
K	1.78	1.98	1.99	2.01	2.03	1.91	2.00	1.94	1.93	1.99	2.01	1.96
OH*	3.68	3.73	3.92	3.83	3.87	3.69	3.70	3.55	3.67	3.66	3.75	3.81
F	0.32	0.27	0.08	0.17	0.13	0.31	0.30	0.45	0.33	0.34	0.25	0.19
Sum	19.86	19.80	19.72	19.71	19.79	19.77	19.80	19.80	19.82	19.93	19.91	19.84

Table C 1.3: Mica EPMA analyses

Rock type	Glimmerite											
Sample	SC10-11-1-Mica-4	SC10-11-1-Mica-5	SC10-11-1-Mica-6	SC10-11-1-Mica-7	SC10-11-1-Mica-8	SC10-11-2-Mica-1	SC10-11-2-Mica-10	SC10-11-2 Mica-11	SC10-11-2-Mica-2	SC10-11-2-Mica-3	SC10-11-2-Mica-4	SC10-11-2 Mica-5
SiO_2	36.82	36.77	36.26	36.31	36.57	37.56	37.11	37.33	37.48	37.56	37.79	37.21
Al_2O_3	13.16	13.43	13.31	13.22	13.33	12.35	13.20	13.38	12.99	12.90	12.94	13.39
MgO	11.82	11.31	10.96	10.06	10.36	13.00	12.53	12.76	13.40	13.05	14.27	12.65
FeO	20.71	21.07	21.42	21.79	21.68	19.57	19.78	19.57	18.74	18.89	17.38	19.63
Fe_2O_3												
TiO_2	1.44	1.73	1.86	3.23	2.97	1.58	1.76	1.63	1.73	1.70	1.55	1.79
MnO	0.24	0.29	0.25	0.25	0.29	0.24	0.23	0.28	0.30	0.23	0.25	0.26
K_2O	10.17	10.07	9.66	9.97	9.89	10.28	10.16	9.84	10.18	10.29	10.02	10.17
Na_2O	0.10	0.11	0.19	0.17	0.18	0.09	0.14	0.21	0.09	0.09	0.21	0.09
CaO	0.01	0.02	0.08	0.01	0.02	0.00	0.00	0.04	0.01	0.08	0.02	0.00
F	0.39	0.47	0.44	0.24	0.33	0.59	0.52	0.46	0.39	0.56	0.66	0.39
H_2O*	3.65	3.63	3.60	3.72	3.70	3.59	3.63	3.68	3.71	3.62	3.60	3.71
subtotal	98.51	98.90	98.03	98.98	99.32	98.85	99.04	99.16	99.01	98.97	98.69	99.29
O=F,Cl	0.16	0.20	0.18	0.10	0.14	0.25	0.22	0.19	0.16	0.24	0.28	0.16
Total	98.34	98.70	97.85	98.88	99.18	98.60	98.82	98.97	98.85	98.74	98.41	99.13
	Number of ions calculated on the basis of 24 (O,OH,F)											
Si	5.75	5.73	5.71	5.67	5.69	5.82	5.74	5.75	5.77	5.79	5.80	5.73
Al^{iv}	2.25	2.27	2.29	2.33	2.31	2.18	2.26	2.25	2.23	2.21	2.20	2.27
Fe^{3+}	0.00	0.00	0.00	0.00	0.00	0.00	0.00	0.00	0.00	0.00	0.00	0.00
Fe^{2+}	2.71	2.75	2.82	2.85	2.82	2.54	2.56	2.52	2.41	2.44	2.23	2.53
Al^{vi}	0.18	0.20	0.18	0.11	0.13	0.08	0.15	0.17	0.12	0.14	0.14	0.16
Ti	0.17	0.20	0.22	0.38	0.35	0.18	0.20	0.19	0.20	0.20	0.18	0.21
Mn	0.03	0.04	0.03	0.03	0.04	0.03	0.03	0.04	0.04	0.03	0.03	0.03
Mg	2.75	2.63	2.57	2.34	2.40	3.00	2.89	2.93	3.07	3.00	3.26	2.90
Ca	0.00	0.00	0.01	0.00	0.00	0.00	0.00	0.01	0.00	0.01	0.00	0.00
Na	0.03	0.03	0.06	0.05	0.05	0.03	0.04	0.06	0.03	0.03	0.06	0.03
K	2.03	2.00	1.94	1.99	1.96	2.03	2.00	1.93	2.00	2.02	1.96	2.00
OH*	3.81	3.77	3.78	3.88	3.84	3.71	3.75	3.77	3.81	3.73	3.68	3.81
F	0.19	0.23	0.22	0.12	0.16	0.29	0.25	0.23	0.19	0.27	0.32	0.19
Sum	19.90	19.85	19.84	19.75	19.75	19.90	19.87	19.85	19.87	19.86	19.87	19.86

Table C 1.4: Mica EPMA analyses

Rock type	Glimmerite											
Sample	SC10-11-2-Mica-6	SC10-11-2-Mica-7	SC10-11-2-Mica-9C	SC10-11-2-Mica-9R	SC10-26-1_Mica10	SC10-26-1_Mica2	SC10-26-1_Mica3	SC10-26-1_Mica4	SC10-26-1_Mica7	SC10-26-1_Mica8	SC10-26-1_Mica9	SC10-22-1-Mica-1
SiO_2	36.70	36.51	38.22	37.50	36.69	37.18	36.90	36.74	36.74	36.76	36.56	38.36
Al_2O_3	13.24	13.08	12.42	12.05	13.70	13.02	13.09	13.29	13.83	13.43	13.39	13.12
MgO	12.50	12.68	15.73	14.11	13.66	13.65	13.10	12.71	13.19	13.82	13.62	16.54
FeO	19.12	19.80	15.09	17.01	18.77	18.56	19.16	19.90	19.23	18.89	18.82	15.26
Fe_2O_3			0.13	0.34								
TiO_2	1.50	1.35	2.70	2.56	1.48	1.40	2.01	2.11	1.49	1.27	1.32	0.33
MnO	0.29	0.25	0.20	0.17	0.25	0.29	0.29	0.25	0.25	0.24	0.26	0.15
K_2O	10.04	10.35	10.32	10.47	9.90	9.98	9.92	9.96	10.07	10.08	10.04	10.32
Na_2O	0.20	0.06	0.14	0.10	0.12	0.21	0.08	0.09	0.08	0.13	0.15	0.15
CaO	0.01	0.01	0.04	0.06	0.01	0.36	0.01	0.03	0.01	0.02	0.06	0.01
F	0.53	0.39	0.86	0.61	0.26	0.26	0.26	0.26	0.17	0.32	0.40	0.96
H_2O*	3.58	3.65	3.56	3.60	3.76	3.76	3.75	3.76	3.81	3.73	3.67	3.49
subtotal	97.72	98.13	99.39	98.57	98.60	98.66	98.58	99.09	98.88	98.68	98.28	98.68
O=F,Cl	0.22	0.16	0.36	0.25	0.11	0.11	0.11	0.11	0.07	0.13	0.17	0.40
Total	97.49	97.96	99.03	98.31	98.49	98.55	98.47	98.98	98.81	98.55	98.12	98.28
	Number of ions calculated on the basis of 24 (O,OH,F)											
Si	5.74	5.72	5.78	5.79	5.66	5.74	5.71	5.68	5.67	5.68	5.68	5.83
Al^{iv}	2.26	2.28	2.21	2.19	2.34	2.26	2.29	2.32	2.33	2.32	2.32	2.17
Fe^{3+}	0.00	0.00	0.01	0.02	0.00	0.00	0.00	0.00	0.00	0.00	0.00	0.00
Fe^{2+}	2.50	2.59	1.91	2.20	2.42	2.40	2.48	2.57	2.48	2.44	2.44	1.94
Al^{vi}	0.19	0.13	0.00	0.00	0.16	0.11	0.10	0.10	0.18	0.13	0.13	0.18
Ti	0.18	0.16	0.31	0.30	0.17	0.16	0.23	0.24	0.17	0.15	0.15	0.04
Mn	0.04	0.03	0.03	0.02	0.03	0.04	0.04	0.03	0.03	0.03	0.03	0.02
Mg	2.92	2.96	3.54	3.25	3.14	3.14	3.02	2.93	3.03	3.18	3.15	3.75
Ca	0.00	0.00	0.01	0.01	0.00	0.06	0.00	0.00	0.00	0.00	0.01	0.00
Na	0.06	0.02	0.04	0.03	0.03	0.06	0.02	0.03	0.02	0.04	0.05	0.05
K	2.00	2.07	1.99	2.06	1.95	1.96	1.96	1.96	1.98	1.99	1.99	2.00
OH*	3.74	3.81	3.59	3.70	3.87	3.88	3.87	3.87	3.92	3.85	3.80	3.54
F	0.26	0.19	0.41	0.30	0.13	0.12	0.13	0.13	0.08	0.15	0.20	0.46
Sum	19.89	19.96	19.82	19.86	19.91	19.93	19.85	19.86	19.91	19.96	19.96	19.98

Table C 1.5: Mica EPMA analyses

Rock type	Glimmerite											
Sample	SC10-22-1-Mica-10	SC10-22-1-Mica-11	SC10-22-1-Mica-1a	SC10-22-1-Mica-1b	SC10-22-1-Mica-2	SC10-22-1-Mica-3	SC10-22-1-Mica-4	SC10-22-1-Mica-5	SC10-22-1-Mica-6	SC10-22-1-Mica-7	SC10-22-1-Mica-8	SC10-22-1-Mica-9
SiO_2	38.60	38.31	38.19	38.11	38.23	38.25	38.35	38.62	38.11	38.36	38.43	38.17
Al_2O_3	13.22	13.21	13.33	13.22	13.06	13.35	13.08	13.33	13.70	13.28	13.43	13.45
MgO	16.22	16.04	16.51	16.47	16.34	16.39	16.35	16.69	16.21	16.44	16.45	16.21
FeO	15.27	15.85	15.31	15.31	15.11	15.49	15.03	14.87	15.31	15.43	15.54	15.29
Fe_2O_3												
TiO_2	0.24	0.25	0.39	0.34	0.29	0.34	0.37	0.33	0.45	0.28	0.30	0.33
MnO	0.15	0.23	0.15	0.18	0.19	0.17	0.14	0.18	0.20	0.19	0.19	0.14
K_2O	10.04	10.51	10.24	10.17	10.23	10.06	9.91	10.37	10.04	10.20	10.24	10.25
Na_2O	0.23	0.10	0.16	0.16	0.29	0.16	0.34	0.14	0.20	0.18	0.14	0.16
CaO	0.02	0.00	0.01	0.03	0.05	0.02	0.09	0.00	0.01	0.02	0.00	0.00
F	0.92	0.88	0.81	0.80	0.87	1.13	0.87	1.09	0.93	1.21	0.98	0.90
H_2O*	3.51	3.52	3.56	3.55	3.51	3.41	3.52	3.45	3.51	3.38	3.50	3.51
subtotal	98.41	98.89	98.65	98.33	98.16	98.78	98.05	99.06	98.66	98.97	99.20	98.40
O=F,Cl	0.39	0.37	0.34	0.34	0.36	0.48	0.37	0.46	0.39	0.51	0.41	0.38
Total	98.02	98.52	98.31	97.99	97.80	98.30	97.68	98.60	98.27	98.46	98.78	98.02
	Number of ions calculated on the basis of 24 (O,OH,F)											
Si	5.87	5.83	5.80	5.81	5.84	5.81	5.85	5.84	5.79	5.82	5.81	5.82
Al ^{iv}	2.13	2.17	2.20	2.19	2.16	2.19	2.15	2.16	2.21	2.18	2.19	2.18
Fe^{3+}	0.00	0.00	0.00	0.00	0.00	0.00	0.00	0.00	0.00	0.00	0.00	0.00
Fe^{2+}	1.94	2.02	1.95	1.95	1.93	1.97	1.92	1.88	1.94	1.96	1.97	1.95
Al ^{vi}	0.24	0.20	0.19	0.19	0.19	0.21	0.20	0.21	0.24	0.20	0.21	0.23
Ti	0.03	0.03	0.04	0.04	0.03	0.04	0.04	0.04	0.05	0.03	0.03	0.04
Mn	0.02	0.03	0.02	0.02	0.02	0.02	0.02	0.02	0.03	0.02	0.02	0.02
Mg	3.68	3.64	3.74	3.74	3.72	3.71	3.72	3.76	3.67	3.72	3.71	3.68
Ca	0.00	0.00	0.00	0.00	0.01	0.00	0.01	0.00	0.00	0.00	0.00	0.00
Na	0.07	0.03	0.05	0.05	0.09	0.05	0.10	0.04	0.06	0.05	0.04	0.05
K	1.95	2.04	1.98	1.98	1.99	1.95	1.93	2.00	1.95	1.98	1.98	1.99
OH*	3.56	3.57	3.61	3.61	3.58	3.46	3.58	3.48	3.55	3.42	3.53	3.57
F	0.44	0.43	0.39	0.39	0.42	0.54	0.42	0.52	0.45	0.58	0.47	0.43
Sum	19.92	19.99	19.97	19.97	19.99	19.95	19.94	19.96	19.94	19.97	19.96	19.96

Table C 1.6: Mica EPMA analyses

Rock type	Clinopyroxenite										
Sample	SC10-23_Mica1	SC10-23_Mica10	SC10-23_Mica2	SC10-23_Mica3	SC10-23_Mica4	SC10-23_Mica5	SC10-23_Mica6	SC10-23_Mica7	SC10-23_Mica8	SC10-23_Mica9	SC10-24-2_Mica1
SiO_2	41.34	41.10	40.80	40.49	40.88	40.86	41.08	41.11	40.66	40.27	41.62
Al_2O_3	11.54	11.65	11.86	11.76	11.93	11.61	11.67	11.54	11.49	11.86	11.15
MgO	22.73	22.66	22.32	22.50	22.49	22.58	22.92	22.27	22.43	22.59	24.35
FeO	7.83	7.92	8.29	7.87	8.25	7.94	7.68	8.40	8.02	7.95	5.68
Fe_2O_3	1.17	1.53	1.03	1.76	1.03	1.86	1.71	1.53	1.89	1.78	2.69
TiO_2	0.96	1.03	1.15	1.06	1.02	1.12	0.99	1.08	1.01	0.98	0.96
MnO	0.14	0.13	0.10	0.14	0.10	0.15	0.12	0.15	0.10	0.15	0.03
K_2O	10.31	10.56	10.27	10.64	10.35	10.50	10.64	10.55	10.40	10.37	10.46
Na_2O	0.15	0.13	0.12	0.17	0.19	0.13	0.10	0.08	0.18	0.23	0.14
CaO	0.03	0.01	0.04	0.02	0.05	0.00	0.01	0.01	0.05	0.03	0.03
F	0.54	0.43	0.47	0.41	0.54	0.52	0.42	0.45	0.52	0.53	0.58
H_2O*	3.89	3.95	3.91	3.93	3.89	3.89	3.96	3.93	3.87	3.86	3.90
subtotal	100.61	101.09	100.37	100.76	100.73	101.15	101.29	101.09	100.62	100.61	101.59
O=F,Cl	0.23	0.18	0.20	0.17	0.23	0.22	0.18	0.19	0.22	0.22	0.25
Total	100.39	100.91	100.17	100.58	100.50	100.93	101.11	100.91	100.40	100.39	101.34
	Number of ions calculated on the basis of 24 (O,OH,F)										
Si	5.97	5.93	5.92	5.89	5.91	5.92	5.92	5.95	5.92	5.87	5.97
Al^{iv}	1.96	1.98	2.03	2.02	2.03	1.98	1.98	1.97	1.97	2.04	1.88
Fe^{3+}	0.06	0.08	0.06	0.10	0.06	0.10	0.09	0.08	0.10	0.10	0.15
Fe^{2+}	0.95	0.96	1.01	0.97	1.00	0.97	0.93	1.03	0.99	0.98	0.69
Al^{vi}	0.00	0.00	0.00	0.00	0.00	0.00	0.00	0.00	0.00	0.00	0.00
Ti	0.10	0.11	0.13	0.12	0.11	0.12	0.11	0.12	0.11	0.11	0.10
Mn	0.02	0.02	0.01	0.02	0.01	0.02	0.02	0.02	0.01	0.02	0.00
Mg	4.89	4.88	4.82	4.88	4.85	4.87	4.93	4.80	4.87	4.91	5.21
Ca	0.00	0.00	0.01	0.00	0.01	0.00	0.00	0.00	0.01	0.00	0.00
Na	0.04	0.04	0.03	0.05	0.05	0.04	0.03	0.02	0.05	0.06	0.04
K	1.90	1.94	1.90	1.97	1.91	1.94	1.96	1.95	1.93	1.93	1.91
OH*	3.75	3.81	3.78	3.81	3.75	3.76	3.81	3.80	3.76	3.75	3.74
F	0.25	0.19	0.22	0.19	0.25	0.24	0.19	0.20	0.24	0.25	0.26
Sum	19.91	19.95	19.91	20.00	19.94	19.96	19.97	19.94	19.97	20.00	19.96

Table C 1.7: Mica EPMA analyses

Rock type	Clinopyroxenite										
Sample	SC10-24-2_Mica10	SC10-24-2_Mica2	SC10-24-2_Mica3	SC10-24-2_Mica4	SC10-24-2_Mica5	SC10-24-2_Mica6	SC10-24-2_Mica7	SC10-24-2_Mica8	SC10-24-2_Mica9	SC10-25-1_Mica1	SC10-25-1_Mica10
SiO_2	41.18	41.32	41.47	41.86	41.93	41.28	41.90	41.30	41.34	41.17	41.13
Al_2O_3	11.52	11.50	11.55	11.52	11.50	11.74	11.82	11.53	11.68	11.29	11.43
MgO	24.19	24.14	23.89	24.10	24.64	24.27	24.59	24.49	24.26	23.94	23.47
FeO	5.88	5.98	6.30	6.29	5.59	5.97	5.64	5.71	6.03	6.78	6.99
Fe_2O_3	2.71	2.26	2.05	1.94	2.36	2.32	1.51	2.94	2.39	2.73	1.96
TiO_2	1.06	0.99	1.04	1.00	0.96	1.05	0.99	1.03	1.01	0.68	0.72
MnO	0.06	0.10	0.09	0.08	0.13	0.09	0.06	0.11	0.08	0.09	0.12
K_2O	10.71	10.45	10.64	10.40	10.75	10.59	10.49	10.68	10.73	10.39	10.65
Na_2O	0.14	0.15	0.12	0.15	0.09	0.16	0.11	0.11	0.12	0.18	0.13
CaO	0.00	0.01	0.00	0.06	0.00	0.02	0.09	0.01	0.00	0.00	0.00
F	0.55	0.50	0.52	0.58	0.54	0.50	0.51	0.59	0.57	0.43	0.58
H_2O*	3.92	3.94	3.94	3.94	3.97	3.96	3.99	3.92	3.93	3.96	3.87
subtotal	101.92	101.33	101.60	101.93	102.47	101.94	101.69	102.42	102.13	101.63	101.05
O=F,Cl	0.23	0.21	0.22	0.24	0.23	0.21	0.21	0.25	0.24	0.18	0.24
Total	101.69	101.13	101.38	101.69	102.24	101.73	101.47	102.17	101.89	101.45	100.81
	Number of ions calculated on the basis of 24 (O,OH,F)										
Si	5.90	5.93	5.94	5.96	5.95	5.90	5.94	5.90	5.90	5.93	5.95
Al^{iv}	1.95	1.95	1.95	1.93	1.92	1.98	1.98	1.94	1.97	1.92	1.95
Fe^{3+}	0.15	0.12	0.11	0.11	0.13	0.13	0.08	0.16	0.13	0.15	0.11
Fe^{2+}	0.72	0.73	0.76	0.76	0.67	0.72	0.68	0.69	0.73	0.83	0.85
Al^{vi}	0.00	0.00	0.00	0.00	0.00	0.00	0.00	0.00	0.00	0.00	0.00
Ti	0.11	0.11	0.11	0.11	0.10	0.11	0.11	0.11	0.11	0.07	0.08
Mn	0.01	0.01	0.01	0.01	0.02	0.01	0.01	0.01	0.01	0.01	0.01
Mg	5.17	5.17	5.10	5.12	5.21	5.17	5.20	5.21	5.16	5.14	5.06
Ca	0.00	0.00	0.00	0.01	0.00	0.00	0.01	0.00	0.00	0.00	0.00
Na	0.04	0.04	0.03	0.04	0.03	0.04	0.03	0.03	0.03	0.05	0.04
K	1.96	1.91	1.94	1.89	1.95	1.93	1.90	1.95	1.95	1.91	1.96
OH*	3.75	3.78	3.76	3.74	3.76	3.78	3.77	3.73	3.74	3.80	3.74
F	0.25	0.22	0.24	0.26	0.24	0.22	0.23	0.27	0.26	0.20	0.26
Sum	20.01	19.97	19.96	19.93	19.97	19.99	19.93	20.01	20.00	20.02	20.00

Table C 1.8: Mica EPMA analyses

Rock type	Clinopyroxenite										
Sample	SC10-25-1_Mica2	SC10-25-1_Mica3	SC10-25-1_Mica4	SC10-25-1_Mica5	SC10-25-1_Mica6	SC10-25-1_Mica7	SC10-25-1_Mica8	SC10-25-1_Mica9	SC10-6 - 1 - Mica - 1	SC10-6 - 1 - Mica - 10	SC10-6 - 1 - Mica - 3
SiO_2	41.03	41.27	41.71	41.27	41.20	41.52	41.47	41.75	42.92	42.49	41.91
Al_2O_3	11.51	11.37	11.59	11.46	11.50	11.54	11.29	11.69	11.77	11.52	12.01
MgO	23.95	24.22	23.80	23.88	23.56	23.85	23.96	23.73	25.72	26.26	24.71
FeO	6.37	5.95	6.88	6.61	7.14	6.85	6.64	7.24	4.78	3.65	5.55
Fe_2O_3	2.33	2.38	1.47	1.99	2.03	1.89	2.44	1.30	0.69	1.45	0.73
TiO_2	0.73	0.75	0.74	0.67	0.72	0.78	0.66	0.63	0.45	0.37	0.72
MnO	0.07	0.09	0.10	0.06	0.07	0.06	0.12	0.08	0.07	0.04	0.11
K_2O	10.61	10.68	10.48	10.70	10.46	10.62	10.65	10.61	10.54	10.78	10.53
Na_2O	0.26	0.12	0.14	0.11	0.20	0.06	0.14	0.14	0.15	0.12	0.22
CaO	0.01	0.00	0.02	0.00	0.03	0.00	0.00	0.00	0.03	0.00	0.02
F	0.49	0.42	0.54	0.51	0.56	0.60	0.65	0.51	1.12	1.10	1.00
H_2O*	3.93	3.97	3.94	3.92	3.90	3.90	3.87	3.96	3.75	3.72	3.75
subtotal	101.26	101.23	101.40	101.18	101.35	101.66	101.88	101.64	101.99	101.52	101.26
O=F,Cl	0.20	0.18	0.23	0.21	0.23	0.25	0.27	0.22	0.47	0.46	0.42
Total	101.06	101.05	101.17	100.96	101.11	101.41	101.61	101.43	101.52	101.05	100.84
	Number of ions calculated on the basis of 24 (O,OH,F)										
Si	5.92	5.94	5.97	5.94	5.94	5.95	5.95	5.96	6.02	6.00	5.95
Al ^{iv}	1.96	1.93	1.95	1.95	1.95	1.95	1.91	1.97	1.95	1.92	2.01
Fe^{3+}	0.13	0.13	0.08	0.11	0.11	0.10	0.13	0.07	0.04	0.08	0.04
Fe^{2+}	0.78	0.73	0.83	0.80	0.87	0.83	0.81	0.87	0.56	0.44	0.66
Al ^{vi}	0.00	0.00	0.00	0.00	0.00	0.00	0.00	0.00	0.00	0.00	0.00
Ti	0.08	0.08	0.08	0.07	0.08	0.08	0.07	0.07	0.05	0.04	0.08
Mn	0.01	0.01	0.01	0.01	0.01	0.01	0.01	0.01	0.01	0.00	0.01
Mg	5.15	5.20	5.08	5.13	5.06	5.09	5.13	5.05	5.38	5.53	5.23
Ca	0.00	0.00	0.00	0.00	0.00	0.00	0.00	0.00	0.00	0.00	0.00
Na	0.07	0.03	0.04	0.03	0.05	0.02	0.04	0.04	0.04	0.03	0.06
K	1.95	1.96	1.91	1.97	1.92	1.94	1.95	1.93	1.89	1.94	1.91
OH*	3.78	3.81	3.76	3.77	3.75	3.73	3.71	3.77	3.50	3.51	3.55
F	0.22	0.19	0.24	0.23	0.25	0.27	0.29	0.23	0.50	0.49	0.45
Sum	20.04	20.01	19.95	20.01	20.00	19.97	20.01	19.97	19.92	19.99	19.95

Table C 1.9: Mica EPMA analyses

Rock type	Clinopyroxenite						Magnetite-rich phoscorite				
Sample	SC10-6-1-Mica-4	SC10-6 -1-Mica-5	SC10-6-1-Mica-6	SC10-6-1-Mica-7	SC10-6-1-Mica-8	SC10-6-1-Mica-9	SC10-12-2-Mica-1	SC10-12-2-Mica-10	SC10-12-2-Mica-2	SC10-12-2-Mica-3	SC10-12-2-Mica-4L
SiO_2	41.16	42.16	41.99	41.76	42.14	42.25	40.17	40.01	39.88	39.89	40.12
Al_2O_3	12.20	11.68	11.79	11.68	11.65	11.36	11.73	12.14	12.11	12.08	11.93
MgO	24.36	25.67	25.33	25.11	25.89	25.45	18.89	18.37	18.48	18.42	18.68
FeO	5.67	4.30	4.71	4.84	4.31	4.55	12.25	13.38	12.84	12.83	12.82
Fe_2O_3	0.70	1.39	0.96	1.37	1.45	1.43					
TiO_2	0.80	0.54	0.49	0.57	0.34	0.43	1.20	1.29	1.35	1.45	1.26
MnO	0.10	0.07	0.09	0.08	0.06	0.02	0.17	0.20	0.21	0.20	0.15
K_2O	10.75	10.62	10.61	10.61	10.59	10.22	10.32	10.44	10.36	10.41	10.36
Na_2O	0.10	0.20	0.22	0.20	0.20	0.40	0.16	0.10	0.10	0.14	0.13
CaO	0.01	0.01	0.00	0.03	0.01	0.04	0.01	0.04	0.01	0.02	0.04
F	1.20	1.11	0.99	1.08	1.12	1.01	0.75	0.68	0.67	0.80	0.67
H_2O*	3.62	3.71	3.75	3.69	3.70	3.73	3.68	3.74	3.73	3.67	3.74
subtotal	100.65	101.45	100.91	101.03	101.45	100.89	99.34	100.38	99.75	99.89	99.89
O=F,Cl	0.50	0.47	0.42	0.45	0.47	0.42	0.31	0.29	0.28	0.34	0.28
Total	100.14	100.98	100.50	100.57	100.98	100.46	99.02	100.09	99.46	99.56	99.61
Number of ions calculated on the basis of 24 (O,OH,F)											
Si	5.90	5.97	5.97	5.96	5.97	6.02	5.96	5.91	5.91	5.91	5.94
Al ^{iv}	2.06	1.95	1.98	1.96	1.95	1.91	2.04	2.09	2.09	2.09	2.06
Fe^{3+}	0.04	0.07	0.05	0.07	0.08	0.08	0.00	0.00	0.00	0.00	0.00
Fe^{2+}	0.68	0.51	0.56	0.58	0.52	0.55	1.52	1.65	1.59	1.59	1.59
Al ^{vi}	0.00	0.00	0.00	0.00	0.00	0.00	0.02	0.02	0.03	0.02	0.02
Ti	0.09	0.06	0.05	0.06	0.04	0.05	0.13	0.14	0.15	0.16	0.14
Mn	0.01	0.01	0.01	0.01	0.01	0.00	0.02	0.03	0.03	0.02	0.02
Mg	5.21	5.42	5.37	5.34	5.47	5.40	4.18	4.04	4.08	4.07	4.12
Ca	0.00	0.00	0.00	0.00	0.00	0.01	0.00	0.01	0.00	0.00	0.01
Na	0.03	0.06	0.06	0.06	0.06	0.11	0.05	0.03	0.03	0.04	0.04
K	1.97	1.92	1.92	1.93	1.92	1.86	1.95	1.97	1.96	1.97	1.95
OH*	3.46	3.50	3.56	3.51	3.50	3.55	3.65	3.68	3.69	3.63	3.69
F	0.54	0.50	0.44	0.49	0.50	0.45	0.35	0.32	0.31	0.37	0.31
Sum	19.98	19.98	19.98	19.99	20.00	19.97	19.88	19.89	19.87	19.88	19.88

Table C 1.10: Mica EPMA analyses

Rock type	Magnetite-rich phoscorite											
Sample	SC10-12-2-Mica-5	SC10-12-2-Mica-6	SC10-12-2-Mica-8	SC10-12-4-Mica-1C	SC10-12-4-Mica-1R	SC10-12-4-Mica-2C	SC10-12-4-Mica-2R	SC10-12-4-Mica-3C	SC10-12-4-Mica-3R	SC10-12-4-Mica-5	SC10-12-4-Mica-8D	SC10-12-4-Mica-8L
SiO_2	39.78	40.77	39.13	39.62	40.06	39.73	38.80	39.88	39.02	40.08	36.21	37.02
Al_2O_3	11.82	11.68	12.13	11.73	11.68	11.95	11.76	11.77	11.74	12.12	12.73	12.71
MgO	18.92	20.58	17.31	17.85	18.41	17.97	15.47	18.41	16.14	18.71	10.59	10.71
FeO	12.38	10.32	14.08	12.57	12.12	12.81	16.30	12.22	15.28	11.88	21.22	21.24
Fe_2O_3	0.30	0.58			0.34	0.03		0.57	0.12	0.15		
TiO_2	1.29	1.23	1.65	1.90	2.00	2.04	1.83	1.99	1.93	2.17	2.59	2.50
MnO	0.20	0.18	0.18	0.26	0.24	0.16	0.18	0.24	0.22	0.23	0.33	0.30
K_2O	10.36	10.66	10.45	10.06	10.24	10.37	10.40	10.37	10.46	10.22	9.73	10.03
Na_2O	0.15	0.04	0.06	0.12	0.13	0.11	0.07	0.13	0.03	0.21	0.12	0.07
CaO	0.00	0.00	0.00	0.04	0.02	0.00	0.01	0.01	0.01	0.01	0.01	0.00
F	0.69	0.78	0.71	0.72	0.72	0.83	0.59	0.73	0.65	0.69	0.21	0.33
H_2O*	3.71	3.74	3.66	3.66	3.70	3.64	3.67	3.70	3.66	3.75	3.69	3.68
subtotal	99.59	100.54	99.36	98.53	99.65	99.64	99.07	100.00	99.26	100.22	97.43	98.60
O=F,Cl	0.29	0.33	0.30	0.30	0.30	0.35	0.25	0.31	0.27	0.29	0.09	0.14
Total	99.30	100.22	99.06	98.22	99.35	99.29	98.83	99.70	98.99	99.92	97.34	98.46
	Number of ions calculated on the basis of 24 (O,OH,F)											
Si	5.91	5.96	5.87	5.94	5.94	5.90	5.90	5.91	5.90	5.89	5.73	5.79
Al^{iv}	2.07	2.01	2.13	2.06	2.04	2.09	2.10	2.06	2.09	2.10	2.27	2.21
Fe^{3+}	0.02	0.03	0.00	0.00	0.02	0.00	0.00	0.03	0.01	0.01	0.00	0.00
Fe^{2+}	1.54	1.27	1.77	1.58	1.51	1.59	2.07	1.52	1.93	1.46	2.81	2.78
Al^{vi}	0.00	0.00	0.02	0.01	0.00	0.00	0.01	0.00	0.00	0.00	0.11	0.13
Ti	0.14	0.14	0.19	0.21	0.22	0.23	0.21	0.22	0.22	0.24	0.31	0.29
Mn	0.02	0.02	0.02	0.03	0.03	0.02	0.02	0.03	0.03	0.03	0.04	0.04
Mg	4.19	4.48	3.87	3.99	4.07	3.98	3.51	4.07	3.64	4.10	2.50	2.49
Ca	0.00	0.00	0.00	0.01	0.00	0.00	0.00	0.00	0.00	0.00	0.00	0.00
Na	0.04	0.01	0.02	0.04	0.04	0.03	0.02	0.04	0.01	0.06	0.04	0.02
K	1.96	1.99	2.00	1.92	1.94	1.97	2.02	1.96	2.02	1.92	1.97	2.00
OH*	3.68	3.64	3.66	3.66	3.66	3.61	3.72	3.66	3.69	3.68	3.89	3.84
F	0.32	0.36	0.34	0.34	0.34	0.39	0.28	0.34	0.31	0.32	0.11	0.16
Sum	19.91	19.90	19.88	19.79	19.80	19.82	19.86	19.84	19.85	19.81	19.77	19.76

Table C 1.11: Mica EPMA analyses

Rock type	Carbonatite										
Sample	SC8-1_Mica1	SC8-1_Mica10	SC8-1_Mica2	SC8-1_Mica3	SC8-1_Mica4	SC8-1_Mica5	SC8-1_Mica6	SC8-1_Mica7	SC8-1_Mica8	SC8-1_Mica9	SC8-4_Mica1
SiO_2	39.68	40.68	39.78	39.95	39.80	41.03	40.35	40.10	40.24	40.70	40.94
Al_2O_3	12.14	11.71	12.30	12.15	12.06	11.36	11.63	11.81	11.58	11.65	11.29
MgO	19.41	20.07	19.40	19.25	19.56	20.43	19.80	19.71	19.76	20.29	24.45
FeO	13.64	12.47	13.47	14.05	13.30	10.71	12.70	13.05	12.91	11.92	5.32
Fe_2O_3	0.33	0.47			0.12	1.41	0.47	0.59	0.94	0.41	2.91
TiO_2	0.35	0.49	0.31	0.27	0.32	1.30	0.39	0.38	0.42	0.49	1.03
MnO	0.08	0.07	0.06	0.09	0.06	0.04	0.00	0.05	0.04	0.05	0.07
K_2O	10.73	10.70	10.68	10.62	10.60	10.83	10.85	10.73	10.71	10.80	10.16
Na_2O	0.04	0.07	0.05	0.11	0.10	0.04	0.03	0.09	0.05	0.02	0.15
CaO	0.01	0.02	0.02	0.03	0.01	0.01	0.02	0.00	0.01	0.04	0.09
F	0.07	0.16	0.07	0.10	0.25	0.16	0.11	0.09	0.23	0.17	0.42
H_2O*	4.02	4.02	4.03	4.02	3.93	4.04	4.01	4.02	3.96	4.01	3.95
subtotal	100.51	100.91	100.16	100.62	100.11	101.35	100.34	100.62	100.84	100.55	100.75
O=F,Cl	0.03	0.07	0.03	0.04	0.10	0.07	0.05	0.04	0.09	0.07	0.18
Total	100.48	100.84	100.13	100.58	100.01	101.29	100.30	100.58	100.75	100.48	100.58
	Number of ions calculated on the basis of 24 (O,OH,F)										
Si	5.87	5.95	5.88	5.89	5.89	5.97	5.95	5.91	5.93	5.96	5.92
Al^{iv}	2.12	2.02	2.12	2.11	2.10	1.95	2.02	2.05	2.01	2.01	1.92
Fe^{3+}	0.02	0.03	0.00	0.00	0.01	0.08	0.03	0.03	0.05	0.02	0.16
Fe^{2+}	1.69	1.53	1.66	1.73	1.65	1.31	1.57	1.61	1.60	1.46	0.65
Al^{vi}	0.00	0.00	0.02	0.00	0.00	0.00	0.00	0.00	0.00	0.00	0.00
Ti	0.04	0.05	0.03	0.03	0.04	0.14	0.04	0.04	0.05	0.05	0.11
Mn	0.01	0.01	0.01	0.01	0.01	0.00	0.00	0.01	0.01	0.01	0.01
Mg	4.28	4.38	4.27	4.23	4.32	4.43	4.35	4.33	4.34	4.43	5.27
Ca	0.00	0.00	0.00	0.01	0.00	0.00	0.00	0.00	0.00	0.01	0.01
Na	0.01	0.02	0.01	0.03	0.03	0.01	0.01	0.03	0.01	0.01	0.04
K	2.02	2.00	2.01	2.00	2.00	2.01	2.04	2.02	2.01	2.02	1.87
OH*	3.97	3.93	3.97	3.95	3.88	3.93	3.95	3.96	3.90	3.92	3.81
F	0.03	0.07	0.03	0.05	0.12	0.07	0.05	0.04	0.10	0.08	0.19
Sum	20.05	19.99	20.03	20.04	20.04	19.92	20.02	20.04	20.03	19.99	19.97

Table C 1.12: Mica EPMA analyses

Rock type	Carbonatite										
Sample	SC8-4_Mica10	SC8-4_Mica2	SC8-4_Mica3	SC8-4_Mica4	SC8-4_Mica5	SC8-4_Mica6	SC8-4_Mica7	SC8-4_Mica8	SC8-4_Mica9	SC8-17_Mica1	SC8-17_Mica10
SiO_2	41.72	40.70	40.72	41.24	41.08	41.17	41.44	41.21	41.70	41.74	41.76
Al_2O_3	11.34	11.44	11.28	12.25	12.38	11.88	11.48	11.49	11.39	11.19	11.17
MgO	25.01	24.36	24.57	25.57	25.69	25.31	24.70	24.55	24.63	26.46	26.28
FeO	5.01	5.50	5.19	4.06	4.00	4.24	5.34	5.51	5.33	3.22	3.80
Fe_2O_3	2.85	3.24	3.31	1.73	1.68	2.34	2.74	2.84	2.44	2.97	3.37
TiO_2	1.00	1.12	1.05	1.08	1.08	1.21	1.12	1.03	1.04	0.59	0.53
MnO	0.04	0.04	0.01	0.04	0.00	0.02	0.00	0.03	0.01	0.00	0.06
K_2O	10.59	10.29	10.32	10.29	10.21	10.13	10.20	10.72	10.55	10.41	10.21
Na_2O	0.08	0.28	0.11	0.34	0.37	0.30	0.25	0.06	0.09	0.05	0.18
CaO	0.00	0.00	0.06	0.02	0.01	0.02	0.02	0.00	0.05	0.02	0.08
F	0.38	0.38	0.33	0.50	0.53	0.44	0.37	0.35	0.29	0.14	0.28
H_2O*	4.03	3.98	3.99	3.99	3.97	4.00	4.02	4.02	4.07	4.14	4.08
subtotal	102.06	101.32	100.92	101.12	101.00	101.05	101.69	101.80	101.58	100.91	101.80
O=F,Cl	0.16	0.16	0.14	0.21	0.22	0.18	0.16	0.15	0.12	0.06	0.12
Total	101.90	101.16	100.79	100.91	100.77	100.87	101.53	101.65	101.46	100.85	101.68
Number of ions calculated on the basis of 24 (O,OH,F)											
Si	5.94	5.87	5.89	5.86	5.84	5.87	5.92	5.90	5.95	5.96	5.94
Al^{iv}	1.90	1.95	1.92	2.05	2.07	2.00	1.93	1.94	1.92	1.88	1.87
Fe^{3+}	0.16	0.18	0.18	0.09	0.09	0.13	0.15	0.16	0.13	0.16	0.18
Fe^{2+}	0.61	0.68	0.64	0.49	0.48	0.51	0.65	0.67	0.65	0.39	0.46
Al^{vi}	0.00	0.00	0.00	0.00	0.00	0.00	0.00	0.00	0.00	0.00	0.00
Ti	0.11	0.12	0.11	0.12	0.12	0.13	0.12	0.11	0.11	0.06	0.06
Mn	0.00	0.01	0.00	0.01	0.00	0.00	0.00	0.00	0.00	0.00	0.01
Mg	5.31	5.24	5.30	5.41	5.44	5.38	5.26	5.24	5.24	5.63	5.57
Ca	0.00	0.00	0.01	0.00	0.00	0.00	0.00	0.00	0.01	0.00	0.01
Na	0.02	0.08	0.03	0.09	0.10	0.08	0.07	0.02	0.02	0.01	0.05
K	1.92	1.90	1.90	1.86	1.85	1.84	1.86	1.96	1.92	1.89	1.85
OH*	3.83	3.83	3.85	3.78	3.76	3.80	3.83	3.84	3.87	3.94	3.87
F	0.17	0.17	0.15	0.22	0.24	0.20	0.17	0.16	0.13	0.06	0.13
Sum	19.97	20.02	20.00	19.98	19.99	19.96	19.96	20.00	19.95	19.99	20.02

Table C 1.13: Mica EPMA analyses

Rock type	Carbonatite										
Sample	SC8-17_Mica2	SC8-17_Mica3	SC8-17_Mica4	SC8-17_Mica5	SC8-17_Mica6	SC8-17_Mica7	SC8-17_Mica8	SC8-17_Mica9	SC8-21_Mica1	SC8-21Mica2	SC8-21_Mica3D
SiO_2	41.84	40.76	41.24	41.77	41.44	41.83	42.07	41.60	41.78	40.86	41.04
Al_2O_3	11.13	11.78	11.36	11.42	11.29	11.29	11.30	11.55	10.66	10.99	10.82
MgO	26.17	26.41	25.84	26.27	26.30	26.43	26.57	26.09	25.18	24.25	26.99
FeO	3.51	4.07	3.42	3.41	3.23	3.68	3.55	3.96	5.29	6.14	4.47
Fe_2O_3	2.48	2.97	2.76	2.94	3.14	3.11	2.85	2.48	3.49	2.92	4.83
TiO_2	0.56	0.58	0.59	0.59	0.59	0.59	0.47	0.53	0.36	0.43	0.30
MnO	0.02	0.06	0.02	0.05	0.00	0.04	0.00	0.05	0.01	0.03	0.05
K_2O	10.17	9.50	10.49	10.46	10.51	10.34	10.51	10.47	10.56	10.50	8.23
Na_2O	0.06	0.05	0.37	0.46	0.11	0.05	0.04	0.12	0.03	0.05	0.04
CaO	0.06	0.05	0.12	0.02	0.15	0.00	0.04	0.00	0.02	0.00	0.12
F	0.17	0.19	0.24	0.21	0.15	0.28	0.20	0.35	0.19	0.20	0.04
H_2O*	4.11	4.09	4.06	4.12	4.12	4.09	4.14	4.04	4.08	4.02	4.15
subtotal	100.27	100.51	100.50	101.74	101.03	101.72	101.72	101.23	101.64	100.39	101.07
O=F,Cl	0.07	0.08	0.10	0.09	0.06	0.12	0.08	0.15	0.08	0.09	0.02
Total	100.19	100.43	100.40	101.65	100.97	101.61	101.64	101.09	101.57	100.31	101.05
	Number of ions calculated on the basis of 24 (O,OH,F)										
Si	5.99	5.85	5.93	5.93	5.93	5.94	5.96	5.93	6.00	5.95	5.90
Al^{iv}	1.88	1.99	1.92	1.91	1.90	1.89	1.89	1.94	1.80	1.89	1.83
Fe^{3+}	0.14	0.16	0.15	0.16	0.17	0.17	0.15	0.13	0.19	0.16	0.27
Fe^{2+}	0.43	0.50	0.42	0.41	0.39	0.45	0.43	0.48	0.65	0.76	0.55
Al^{vi}	0.00	0.00	0.00	0.00	0.00	0.00	0.00	0.00	0.00	0.00	0.00
Ti	0.06	0.06	0.06	0.06	0.06	0.06	0.05	0.06	0.04	0.05	0.03
Mn	0.00	0.01	0.00	0.01	0.00	0.00	0.00	0.01	0.00	0.00	0.01
Mg	5.58	5.65	5.53	5.56	5.61	5.59	5.61	5.54	5.39	5.27	5.78
Ca	0.01	0.01	0.02	0.00	0.02	0.00	0.01	0.00	0.00	0.00	0.02
Na	0.02	0.02	0.10	0.13	0.03	0.01	0.01	0.03	0.01	0.01	0.01
K	1.86	1.74	1.92	1.89	1.92	1.87	1.90	1.90	1.93	1.95	1.51
OH*	3.92	3.92	3.89	3.90	3.93	3.88	3.91	3.84	3.91	3.91	3.98
F	0.08	0.08	0.11	0.10	0.07	0.12	0.09	0.16	0.09	0.09	0.02
Sum	19.95	19.97	20.06	20.06	20.03	19.99	20.00	20.02	20.03	20.04	19.91

Table C 1.14: Mica EPMA analyses

Rock type	Carbonatite								
Sample	SC8-21_Mica4	SC8-21_Mica5	SC8-21_Mica6L	SC8-21_Mica7L	SC8-24_Mica1	SC8-24_Mica2	SC8-24_Mica3	SC8-24_Mica4	SC8-24_Mica6
SiO_2	41.43	41.04	41.11	40.72	42.02	41.92	41.74	41.79	41.88
Al_2O_3	11.22	11.16	11.46	11.40	12.64	12.52	12.60	12.58	12.69
MgO	23.96	24.67	24.71	25.00	26.85	26.86	26.56	26.86	26.55
FeO	6.66	6.65	6.19	6.44	3.07	2.91	3.35	2.83	3.11
Fe_2O_3	1.70	3.10	2.08	2.97	0.62	1.14	0.86	1.05	0.46
TiO_2	0.53	0.36	0.30	0.32	0.75	0.92	0.87	0.91	0.92
MnO	0.03	0.09	0.19	0.18	0.00	0.05	0.03	0.04	0.00
K_2O	10.15	9.64	9.97	9.27	8.92	8.91	8.99	8.97	8.92
Na_2O	0.08	0.06	0.05	0.05	1.13	1.08	1.00	1.03	1.19
CaO	0.03	0.04	0.02	0.00	0.02	0.01	0.00	0.02	0.00
F	0.24	0.20	0.04	0.10	0.22	0.33	0.27	0.31	0.38
H_2O*	4.03	4.06	4.14	4.10	4.18	4.13	4.14	4.12	4.09
subtotal	100.06	101.06	100.25	100.54	100.42	100.77	100.41	100.52	100.19
O=F,Cl	0.10	0.08	0.01	0.04	0.09	0.14	0.11	0.13	0.16
Total	99.96	100.98	100.23	100.50	100.33	100.63	100.30	100.39	100.03
	Number of ions calculated on the basis of 24 (O,OH,F)								
Si	5.99	5.93	5.94	5.89	5.88	5.87	5.87	5.86	5.88
Al ^{iv}	1.91	1.90	1.95	1.94	2.09	2.07	2.09	2.08	2.10
Fe^{3+}	0.09	0.17	0.11	0.16	0.03	0.06	0.05	0.06	0.02
Fe^{2+}	0.81	0.82	0.76	0.79	0.36	0.34	0.40	0.33	0.37
Al ^{vi}	0.00	0.00	0.00	0.00	0.00	0.00	0.00	0.00	0.00
Ti	0.06	0.04	0.03	0.03	0.08	0.10	0.09	0.10	0.10
Mn	0.00	0.01	0.02	0.02	0.00	0.01	0.00	0.00	0.00
Mg	5.17	5.31	5.32	5.39	5.60	5.61	5.57	5.62	5.55
Ca	0.00	0.01	0.00	0.00	0.00	0.00	0.00	0.00	0.00
Na	0.02	0.02	0.01	0.01	0.31	0.29	0.27	0.28	0.32
K	1.87	1.78	1.84	1.71	1.59	1.59	1.61	1.61	1.60
OH*	3.89	3.91	3.98	3.95	3.90	3.86	3.88	3.86	3.83
F	0.11	0.09	0.02	0.05	0.10	0.14	0.12	0.14	0.17
Sum	19.94	19.98	19.98	19.96	19.95	19.94	19.94	19.94	19.94

Appendix C.2: Clinopyroxene EPMA Data

Table C 2. 1: Clinopyroxene EPMA data

Rock type	Glimmerite						
Sample	SC10-11-1 Pyx 1 C	SC10-11-1 Pyx 10 C	SC10-11-1 Pyx 2 C	SC10-11-1 Pyx 3 C	SC10-11-1 Pyx 4 C	SC10-11-1 Pyx 5 C	SC10-11-1 Pyx 6 C
SiO_2	49.77	50.58	51.25	50.05	50.71	51.48	51.64
TiO_2	0.10	0.14	0.10	0.22	0.08	0.08	0.08
Al_2O_3	1.39	1.50	1.01	1.68	1.29	1.08	1.06
FeO	12.51	12.21	10.64	12.36	11.27	10.66	10.56
Fe_2O_3	2.32	2.69	1.96	2.82	2.41	2.09	2.20
MnO	0.56	0.44	0.42	0.46	0.48	0.45	0.47
MgO	8.87	8.88	10.25	8.57	9.62	10.29	10.17
CaO	21.41	20.86	21.70	20.81	21.21	21.54	21.65
Na_2O	0.92	1.08	0.78	1.16	0.95	0.83	0.86
K_2O	0.03	0.02	0.03	0.03	0.03	0.02	0.04
Cr_2O_3	0.00	0.03	0.00	0.03	0.03	0.00	0.00
NiO	0.00	0.01	0.02	0.00	0.01	0.01	0.00
Total	97.89	98.43	98.17	98.20	98.08	98.54	98.73
	Number of ions calculated on the basis of 6 O						
Al	0.06	0.07	0.05	0.08	0.06	0.05	0.05
Si	1.97	1.98	1.99	1.97	1.98	1.99	1.99
Ti	0.00	0.00	0.00	0.01	0.00	0.00	0.00
Na	0.07	0.08	0.06	0.09	0.07	0.06	0.06
Mg	0.52	0.52	0.59	0.50	0.56	0.59	0.59
Fe^{2+}	0.41	0.40	0.35	0.41	0.37	0.34	0.34
Fe^{3+}	0.07	0.08	0.06	0.08	0.07	0.06	0.06
Mn	0.02	0.01	0.01	0.02	0.02	0.01	0.02
Ni	0.00	0.00	0.00	0.00	0.00	0.00	0.00
Ca	0.91	0.87	0.90	0.88	0.89	0.89	0.90
K	0.00	0.00	0.00	0.00	0.00	0.00	0.00
Cr	0.00	0.00	0.00	0.00	0.00	0.00	0.00
Sum Cations	4.03	4.02	4.01	4.03	4.02	4.01	4.01
$KFeSi_2$ %	0.13	0.11	0.14	0.16	0.13	0.12	0.19
NaTiSiAl %	0.26	0.38	0.27	0.61	0.22	0.21	0.23
$NaFeSi_2$ % (acmite)	6.22	7.21	5.28	7.53	6.48	5.61	5.87
$CaAl_2Si$ % (kushiroite)	5.69	6.02	4.12	6.57	5.32	4.43	4.36
$CaMnSi_2$ % (johannsenite)	1.71	1.35	1.32	1.42	1.47	1.40	1.47
$Ca(FM)Si_2$ % (diopside)	75.86	73.60	79.99	72.76	75.83	78.14	79.14
$(FM)_2Si_2$ %	10.13	11.34	8.88	10.95	10.56	10.09	8.73

Table C 2. 2: Clinopyroxene EPMA data

Rock type	Glimmerite						
Sample	SC10-11-1 Pyx 7 C	SC10-11-1 Pyx 8 C	SC10-11-1 Pyx 9 C	SC10-11-2 pyx 1	SC10-11-2 pyx 10	SC10-11-2 pyx 2	SC10-11-2 pyx 3
SiO_2	50.59	50.66	50.92	51.56	51.51	53.08	52.75
TiO_2	0.18	0.13	0.07	0.01	0.07	0.03	0.04
Al_2O_3	1.54	1.41	1.05	0.60	0.99	0.42	0.46
FeO	11.59	11.63	12.13	8.46	10.01	8.50	8.57
Fe_2O_3	2.55	2.39	2.45	1.82	2.44	1.43	1.58
MnO	0.47	0.44	0.53	0.39	0.44	0.43	0.49
MgO	9.43	9.44	9.19	12.10	10.69	12.31	12.47
CaO	21.21	21.08	21.29	21.82	21.33	22.23	22.07
Na_2O	1.04	0.95	0.97	0.70	0.95	0.56	0.61
K_2O	0.02	0.04	0.01	0.02	0.03	0.01	0.03
Cr_2O_3	0.05	0.00	0.00	0.00	0.00	0.03	0.03
NiO	0.00	0.00	0.00	0.00	0.02	0.00	0.05
Total	98.67	98.17	98.60	97.48	98.47	99.03	99.14
	Number of ions calculated on the basis of 6 O						
Al	0.07	0.06	0.05	0.03	0.04	0.02	0.02
Si	1.97	1.98	1.99	1.99	1.99	2.01	2.00
Ti	0.01	0.00	0.00	0.00	0.00	0.00	0.00
Na	0.08	0.07	0.07	0.05	0.07	0.04	0.04
Mg	0.55	0.55	0.53	0.70	0.62	0.70	0.71
Fe^{2+}	0.38	0.38	0.40	0.27	0.32	0.27	0.27
Fe^{3+}	0.07	0.07	0.07	0.05	0.07	0.04	0.05
Mn	0.02	0.01	0.02	0.01	0.01	0.01	0.02
Ni	0.00	0.00	0.00	0.00	0.00	0.00	0.00
Ca	0.88	0.88	0.89	0.90	0.88	0.90	0.90
K	0.00	0.00	0.00	0.00	0.00	0.00	0.00
Cr	0.00	0.00	0.00	0.00	0.00	0.00	0.00
Sum Cations	4.03	4.02	4.02	4.02	4.02	4.00	4.01
$KFeSi_2$ %	0.11	0.18	0.04	0.07	0.14	0.06	0.13
NaTiSiAl %	0.49	0.37	0.20	0.04	0.18	0.09	0.12
$NaFeSi_2$ % (acmite)	6.77	6.33	6.69	4.90	6.49	3.86	4.13
$CaAl_2Si$ % (kushiroite)	6.03	5.65	4.33	2.52	4.02	1.71	1.83
$CaMnSi_2$ % (johannsenite)	1.43	1.34	1.63	1.19	1.34	1.34	1.50
$Ca(FM)Si_2$ % (diopside)	74.05	74.76	77.39	81.24	77.25	83.92	81.43
$(FM)_2Si_2$ %	11.12	11.37	9.73	10.04	10.58	9.03	10.87

Table C 2. 3: Clinopyroxene EPMA data

Rock type	Glimmerite						
Sample	SC10-11-2 pyx 4	SC10-11-2 pyx 5	SC10-11-2 pyx 6	SC10-11-2 pyx 7	SC10-11-2 pyx 8	SC10-11-2 pyx 9	SC10-4-2 pyx 1
SiO_2	52.64	52.03	53.36	53.46	51.98	51.14	52.68
TiO_2	0.05	0.04	0.03	0.00	0.01	0.05	0.02
Al_2O_3	0.53	0.77	0.17	0.13	0.29	1.06	0.34
FeO	9.24	9.31	6.12	5.50	6.33	10.26	8.74
Fe_2O_3	1.88	1.89	1.28	0.80	1.28	2.49	1.40
MnO	0.48	0.44	0.45	0.43	0.38	0.47	0.36
MgO	11.79	11.27	14.37	15.25	13.81	10.53	12.50
CaO	21.46	21.65	22.47	22.92	22.50	21.09	22.43
Na_2O	0.74	0.73	0.48	0.30	0.48	0.97	0.54
K_2O	0.02	0.02	0.03	0.02	0.02	0.02	0.02
Cr_2O_3	0.00	0.00	0.01	0.00	0.00	0.02	0.04
NiO	0.00	0.05	0.00	0.01	0.05	0.00	0.03
Total	98.83	98.21	98.77	98.82	97.12	98.10	99.12
	Number of ions calculated on the basis of 6 O						
Al	0.02	0.03	0.01	0.01	0.01	0.05	0.02
Si	2.01	2.00	2.01	2.00	2.00	1.99	2.00
Ti	0.00	0.00	0.00	0.00	0.00	0.00	0.00
Na	0.05	0.05	0.04	0.02	0.04	0.07	0.04
Mg	0.67	0.65	0.81	0.85	0.79	0.61	0.71
Fe^{2+}	0.30	0.30	0.19	0.17	0.20	0.33	0.28
Fe^{3+}	0.05	0.05	0.04	0.02	0.04	0.07	0.04
Mn	0.02	0.01	0.01	0.01	0.01	0.02	0.01
Ni	0.00	0.00	0.00	0.00	0.00	0.00	0.00
Ca	0.88	0.89	0.91	0.92	0.93	0.88	0.91
K	0.00	0.00	0.00	0.00	0.00	0.00	0.00
Cr	0.00	0.00	0.00	0.00	0.00	0.00	0.00
Sum Cations	4.00	4.01	4.01	4.01	4.02	4.02	4.01
$KFeSi_2$ %	0.08	0.11	0.15	0.09	0.11	0.10	0.11
NaTiSiAl %	0.15	0.12	0.07	0.00	0.02	0.15	0.05
$NaFeSi_2$ % (acmite)	5.00	5.09	3.26	2.03	3.39	6.63	3.70
$CaAl_2Si$ % (kushiroite)	2.10	3.19	0.65	0.52	1.21	4.35	1.41
$CaMnSi_2$ % (johannsenite)	1.48	1.36	1.35	1.27	1.17	1.44	1.12
$Ca(FM)Si_2$ % (diopside)	79.33	80.45	83.70	84.53	85.28	75.47	84.19
$(FM)_2Si_2$ %	11.86	9.67	10.80	11.57	8.82	11.87	9.43

Table C 2. 4: Clinopyroxene EPMA data

Rock type	Glimmerite						
Sample	SC10-4-2 pyx 10	SC10-4-2 pyx 2	SC10-4-2 pyx 3	SC10-4-2 pyx 4	SC10-4-2 pyx 5	SC10-4-2 pyx 7	SC10-4-2 pyx 8
SiO_2	52.17	52.48	52.74	52.35	51.15	52.16	52.62
TiO_2	0.00	0.00	0.04	0.06	0.11	0.05	0.00
Al_2O_3	0.27	0.31	0.35	0.57	1.01	0.54	0.44
FeO	8.14	7.87	7.96	8.45	11.78	8.86	8.26
Fe_2O_3	2.08	1.86	2.00	2.35	2.85	2.43	1.96
MnO	0.50	0.45	0.42	0.47	0.53	0.52	0.50
MgO	12.45	12.86	12.47	12.03	9.47	11.68	12.44
CaO	21.18	21.68	21.63	21.25	20.69	21.08	21.33
Na_2O	0.79	0.70	0.78	0.92	1.13	0.95	0.75
K_2O	0.02	0.03	0.02	0.02	0.03	0.02	0.01
Cr_2O_3	0.00	0.05	0.04	0.02	0.00	0.00	0.00
NiO	0.00	0.00	0.00	0.00	0.00	0.00	0.00
Total	97.60	98.27	98.46	98.49	98.77	98.29	98.31
	Number of ions calculated on the basis of 6 O						
Al	0.01	0.01	0.02	0.03	0.05	0.02	0.02
Si	2.01	2.01	2.01	2.00	1.99	2.01	2.01
Ti	0.00	0.00	0.00	0.00	0.00	0.00	0.00
Na	0.06	0.05	0.06	0.07	0.09	0.07	0.06
Mg	0.72	0.73	0.71	0.69	0.55	0.67	0.71
Fe^{2+}	0.26	0.25	0.25	0.27	0.38	0.28	0.26
Fe^{3+}	0.06	0.05	0.06	0.07	0.08	0.07	0.06
Mn	0.02	0.01	0.01	0.02	0.02	0.02	0.02
Ni	0.00	0.00	0.00	0.00	0.00	0.00	0.00
Ca	0.87	0.89	0.88	0.87	0.86	0.87	0.87
K	0.00	0.00	0.00	0.00	0.00	0.00	0.00
Cr	0.00	0.00	0.00	0.00	0.00	0.00	0.00
Sum Cations	4.01	4.01	4.01	4.01	4.03	4.02	4.01
$KFeSi_2$ %	0.12	0.13	0.10	0.09	0.16	0.10	0.06
NaTiSiAl %	0.00	0.00	0.12	0.18	0.31	0.14	0.00
$NaFeSi_2$ % (acmite)	5.53	4.87	5.36	6.25	7.58	6.51	5.23
$CaAl_2Si$ % (kushiroite)	1.15	1.30	1.39	2.22	3.98	2.16	1.84
$CaMnSi_2$ % (johannsenite)	1.52	1.35	1.30	1.44	1.62	1.60	1.51
$Ca(FM)Si_2$ % (diopside)	79.31	80.67	81.54	78.12	74.30	77.70	78.70
$(FM)_2Si_2$ %	12.38	11.66	10.20	11.70	12.06	11.80	12.65

Table C 2. 5: Clinopyroxene EPMA data

Rock type	Glimmerite						
Sample	SC10-4-2 pyx 9	SC10-26-1_Py1	SC10-26-1_Py2	SC10-29-1-Py3	SC10-29-1-Py5	SC10-32-4_Py1	SC10-32-4_Py2
SiO_2	52.61	52.71	52.54	50.09	50.64	53.06	52.79
TiO_2	0.03	0.03	0.05	0.10	0.09	0.00	0.02
Al_2O_3	0.30	1.10	1.25	0.97	0.91	1.22	1.19
FeO	7.73	7.73	7.76	14.14	13.89	7.03	7.74
Fe_2O_3	2.21	3.54	3.70	6.53	6.21	3.62	3.78
MnO	0.39	0.38	0.45	0.62	0.59	0.39	0.42
MgO	12.41	11.12	11.05	5.66	5.70	11.79	11.43
CaO	21.48	21.46	21.43	18.49	18.63	21.08	20.81
Na_2O	0.85	1.37	1.43	2.56	2.43	1.39	1.45
K_2O	0.02	0.03	0.03	0.02	0.03	0.02	0.04
Cr_2O_3	0.03	0.03	0.04	0.00	0.00	0.08	0.01
NiO	0.02	0.00	0.00	0.00	0.00	0.01	0.02
Total	98.08	99.49	99.74	99.16	99.13	99.72	99.68
	Number of ions calculated on the basis of 6 O						
Al	0.01	0.05	0.06	0.05	0.04	0.05	0.05
Si	2.02	2.00	2.00	2.00	2.02	2.00	2.00
Ti	0.00	0.00	0.00	0.00	0.00	0.00	0.00
Na	0.06	0.10	0.11	0.20	0.19	0.10	0.11
Mg	0.71	0.63	0.63	0.34	0.34	0.66	0.65
Fe^{2+}	0.25	0.25	0.25	0.47	0.46	0.22	0.25
Fe^{3+}	0.06	0.10	0.11	0.20	0.19	0.10	0.11
Mn	0.01	0.01	0.01	0.02	0.02	0.01	0.01
Ni	0.00	0.00	0.00	0.00	0.00	0.00	0.00
Ca	0.88	0.87	0.87	0.79	0.80	0.85	0.85
K	0.00	0.00	0.00	0.00	0.00	0.00	0.00
Cr	0.00	0.00	0.00	0.00	0.00	0.00	0.00
Sum Cations	4.01	4.02	4.03	4.07	4.05	4.02	4.02
$KFeSi_2$ %	0.09	0.12	0.15	0.10	0.13	0.10	0.16
NaTiSiAl %	0.07	0.07	0.15	0.27	0.25	0.01	0.04
$NaFeSi_2$ % (acmite)	5.99	9.62	9.93	18.19	17.61	9.64	9.95
$CaAl_2Si$ % (kushiroite)	1.21	4.69	5.20	3.98	3.83	5.14	4.93
$CaMnSi_2$ % (johannsenite)	1.23	1.19	1.37	1.96	1.90	1.18	1.28
$Ca(FM)Si_2$ % (diopside)	81.84	78.26	76.61	67.85	70.01	74.49	73.12
$(FM)_2Si_2$ %	9.58	6.05	6.59	7.64	6.28	9.44	10.52

Table C 2. 6: Clinopyroxene EPMA data

Rock type	Glimmerite				Clinopyroxenite		
Sample	SC10-32-4_Py3	SC10-32-4_Py6	SC10-32-4_Py7	SC10-22-1 Pyx 1 C	SC10-2-2 Pyx 10 C	SC10-2-2 Pyx 2 C	SC10-2-2 Pyx 3 C
SiO_2	53.16	53.44	53.13	54.18	51.64	52.55	52.73
TiO_2	0.04	0.06	0.03	0.07	0.01	0.00	0.04
Al_2O_3	1.27	1.14	1.18	0.17	1.28	0.67	0.43
FeO	7.11	6.98	6.77	4.08	7.48	8.60	7.82
Fe_2O_3	3.78	3.34	3.62	1.09	1.70	1.64	1.52
MnO	0.37	0.36	0.38	0.24	0.27	0.38	0.38
MgO	11.64	11.74	11.80	15.56	12.18	11.87	12.13
CaO	21.04	21.24	21.29	22.72	22.25	22.44	22.32
Na_2O	1.46	1.30	1.40	0.43	0.64	0.62	0.58
K_2O	0.03	0.02	0.03	0.03	0.04	0.02	0.03
Cr_2O_3	0.01	0.00	0.00	0.00	0.00	0.02	0.02
NiO	0.00	0.02	0.00	0.01	0.00	0.00	0.01
Total	99.90	99.65	99.63	98.58	97.49	98.82	98.00
Number of ions calculated on the basis of 6 O							
Al	0.06	0.05	0.05	0.01	0.06	0.03	0.02
Si	2.01	2.01	2.01	2.02	1.99	2.00	2.02
Ti	0.00	0.00	0.00	0.00	0.00	0.00	0.00
Na	0.11	0.10	0.10	0.03	0.05	0.05	0.04
Mg	0.65	0.66	0.66	0.86	0.70	0.67	0.69
Fe^{2+}	0.22	0.22	0.21	0.13	0.24	0.27	0.25
Fe^{3+}	0.11	0.09	0.10	0.03	0.05	0.05	0.04
Mn	0.01	0.01	0.01	0.01	0.01	0.01	0.01
Ni	0.00	0.00	0.00	0.00	0.00	0.00	0.00
Ca	0.85	0.86	0.86	0.91	0.92	0.92	0.91
K	0.00	0.00	0.00	0.00	0.00	0.00	0.00
Cr	0.00	0.00	0.00	0.00	0.00	0.00	0.00
Sum Cations	4.02	4.01	4.02	3.99	4.01	4.01	3.99
$KFeSi_2$ %	0.13	0.10	0.14	0.12	0.18	0.11	0.15
NaTiSiAl %	0.10	0.16	0.08	0.18	0.03	0.01	0.12
$NaFeSi_2$ % (acmite)	10.05	9.03	9.71	2.83	4.48	4.44	4.14
$CaAl_2Si$ % (kushiroite)	5.24	4.74	4.93	0.55	5.46	2.88	1.80
$CaMnSi_2$ % (johannsenite)	1.13	1.12	1.15	0.73	0.85	1.18	1.21
$Ca(FM)Si_2$ % (diopside)	74.31	76.87	76.32	86.16	80.64	84.22	86.92
$(FM)_2Si_2$ %	9.04	7.98	7.67	9.42	8.36	7.17	5.65

Table C 2. 7: Clinopyroxene EPMA data

Rock type	Clinopyroxenite						
Sample	SC10-2-2 Pyx 4 C	SC10-2-2 Pyx 5 C	SC10-2-2 Pyx 6 C	SC10-2-2 Pyx 7 C	SC10-2-2 Pyx 8 C	SC10-2-2 Pyx 9 C	SC10-SC10-23_Py1
SiO_2	52.96	52.34	51.72	51.93	51.25	52.01	54.39
TiO_2	0.04	0.00	0.00	0.01	0.00	0.01	0.01
Al_2O_3	0.70	0.75	1.45	1.01	1.33	1.30	0.08
FeO	7.13	7.56	7.83	7.19	7.88	8.13	4.11
Fe_2O_3	1.36	1.35	2.08	1.57	1.60	1.68	1.19
MnO	0.32	0.30	0.36	0.32	0.32	0.28	0.32
MgO	12.95	12.81	12.22	12.75	12.04	12.16	15.53
CaO	22.79	22.57	21.97	22.17	22.29	22.52	23.56
Na_2O	0.53	0.50	0.79	0.60	0.61	0.64	0.44
K_2O	0.02	0.03	0.02	0.02	0.02	0.03	0.04
Cr_2O_3	0.00	0.00	0.00	0.00	0.00	0.00	0.00
NiO	0.00	0.00	0.04	0.00	0.01	0.00	0.00
Total	98.81	98.22	98.48	97.57	97.35	98.76	99.68
	Number of ions calculated on the basis of 6 O						
Al	0.03	0.03	0.07	0.05	0.06	0.06	0.00
Si	2.00	2.00	1.98	1.99	1.98	1.98	2.01
Ti	0.00	0.00	0.00	0.00	0.00	0.00	0.00
Na	0.04	0.04	0.06	0.04	0.05	0.05	0.03
Mg	0.73	0.73	0.70	0.73	0.69	0.69	0.86
Fe^{2+}	0.23	0.24	0.25	0.23	0.25	0.26	0.13
Fe^{3+}	0.04	0.04	0.06	0.05	0.05	0.05	0.03
Mn	0.01	0.01	0.01	0.01	0.01	0.01	0.01
Ni	0.00	0.00	0.00	0.00	0.00	0.00	0.00
Ca	0.92	0.92	0.90	0.91	0.92	0.92	0.93
K	0.00	0.00	0.00	0.00	0.00	0.00	0.00
Cr	0.00	0.00	0.00	0.00	0.00	0.00	0.00
Sum Cations	4.00	4.01	4.02	4.01	4.01	4.01	4.01
$KFeSi_2$ %	0.10	0.15	0.09	0.10	0.08	0.12	0.18
NaTiSiAl %	0.11	0.00	0.00	0.04	0.00	0.03	0.03
$NaFeSi_2$ % (acmite)	3.65	3.52	5.43	4.17	4.28	4.40	3.05
$CaAl_2Si$ % (kushiroite)	2.91	3.20	6.04	4.26	5.68	5.46	0.29
$CaMnSi_2$ % (johannsenite)	0.99	0.93	1.07	0.99	0.98	0.86	0.96
$Ca(FM)Si_2$ % (diopside)	85.21	83.59	75.94	80.66	79.92	79.94	89.40
$(FM)_2Si_2$ %	7.04	8.61	11.43	9.78	9.06	9.19	6.09

Table C 2. 8: Clinopyroxene EPMA data

Rock type	Clinopyroxenite						
Sample	SC10-23_Py2	SC10-23_Py3	SC10-23_Py4	SC10-23_Py6	SC10-25-1_Py1	SC10-25-1_Py10	SC10-25-1_Py2
SiO_2	54.45	54.45	54.19	54.26	55.07	54.28	54.59
TiO_2	0.03	0.07	0.06	0.09	0.02	0.03	0.05
Al_2O_3	0.10	0.10	0.09	0.11	0.09	0.11	0.12
FeO	4.08	4.05	4.08	4.16	3.83	4.10	4.24
Fe_2O_3	1.13	1.15	1.09	1.21	1.19	1.46	1.33
MnO	0.27	0.26	0.29	0.32	0.23	0.19	0.28
MgO	15.84	15.74	15.61	15.86	15.81	15.36	15.70
CaO	23.32	23.21	23.32	22.96	23.45	22.86	22.94
Na_2O	0.43	0.46	0.43	0.49	0.45	0.56	0.51
K_2O	0.04	0.02	0.02	0.03	0.03	0.03	0.03
Cr_2O_3	0.00	0.01	0.00	0.00	0.00	0.05	0.00
NiO	0.02	0.01	0.00	0.03	0.02	0.02	0.00
Total	99.72	99.51	99.19	99.53	100.22	99.07	99.80
	Number of ions calculated on the basis of 6 O						
Al	0.00	0.00	0.00	0.00	0.00	0.00	0.01
Si	2.01	2.01	2.01	2.01	2.02	2.02	2.01
Ti	0.00	0.00	0.00	0.00	0.00	0.00	0.00
Na	0.03	0.03	0.03	0.03	0.03	0.04	0.04
Mg	0.87	0.87	0.86	0.87	0.86	0.85	0.86
Fe^{2+}	0.13	0.12	0.13	0.13	0.12	0.13	0.13
Fe^{3+}	0.03	0.03	0.03	0.03	0.03	0.04	0.04
Mn	0.01	0.01	0.01	0.01	0.01	0.01	0.01
Ni	0.00	0.00	0.00	0.00	0.00	0.00	0.00
Ca	0.92	0.92	0.93	0.91	0.92	0.91	0.91
K	0.00	0.00	0.00	0.00	0.00	0.00	0.00
Cr	0.00	0.00	0.00	0.00	0.00	0.00	0.00
Sum Cations	4.00	4.00	4.00	4.01	4.00	4.00	4.00
$KFeSi_2$ %	0.17	0.08	0.09	0.14	0.15	0.12	0.15
NaTiSiAl %	0.09	0.19	0.16	0.25	0.06	0.09	0.14
$NaFeSi_2$ % (acmite)	2.84	3.01	2.87	3.07	3.07	3.84	3.39
$CaAl_2Si$ % (kushiroite)	0.32	0.22	0.20	0.22	0.34	0.38	0.36
$CaMnSi_2$ % (johannsenite)	0.81	0.79	0.89	0.96	0.71	0.59	0.83
$Ca(FM)Si_2$ % (diopside)	87.39	87.65	88.65	85.30	88.75	87.39	85.55
$(FM)_2Si_2$ %	8.38	8.07	7.15	10.05	6.93	7.58	9.59

Table C 2. 9: Clinopyroxene EPMA data

Rock type	Clinopyroxenite						
Sample	SC10-25-1_Py3	SC10-25-1_Py4	SC10-25-1_Py5	SC10-25-1_Py6	SC10-25-1_Py7	SC10-25-1_Py8	SC10-25-1_Py9
SiO_2	54.76	55.20	54.28	54.57	54.74	54.63	54.80
TiO_2	0.07	0.04	0.09	0.10	0.06	0.01	0.04
Al_2O_3	0.09	0.10	0.12	0.13	0.15	0.08	0.20
FeO	4.01	3.86	3.82	3.85	3.99	3.65	3.79
Fe_2O_3	1.44	1.82	1.46	1.51	1.43	1.52	1.60
MnO	0.24	0.21	0.24	0.22	0.22	0.27	0.17
MgO	15.62	15.55	15.74	15.78	15.59	15.86	15.60
CaO	22.94	22.44	22.91	22.58	22.64	22.93	22.73
Na_2O	0.56	0.71	0.58	0.60	0.57	0.57	0.61
K_2O	0.04	0.02	0.03	0.03	0.02	0.03	0.03
Cr_2O_3	0.00	0.02	0.07	0.00	0.01	0.00	0.01
NiO	0.02	0.00	0.01	0.00	0.00	0.00	0.01
Total	99.80	99.97	99.35	99.37	99.42	99.56	99.59
	Number of ions calculated on the basis of 6 O						
Al	0.00	0.00	0.01	0.01	0.01	0.00	0.01
Si	2.02	2.03	2.01	2.02	2.02	2.02	2.02
Ti	0.00	0.00	0.00	0.00	0.00	0.00	0.00
Na	0.04	0.05	0.04	0.04	0.04	0.04	0.04
Mg	0.86	0.85	0.87	0.87	0.86	0.87	0.86
Fe^{2+}	0.12	0.12	0.12	0.12	0.12	0.11	0.12
Fe^{3+}	0.04	0.05	0.04	0.04	0.04	0.04	0.04
Mn	0.01	0.01	0.01	0.01	0.01	0.01	0.01
Ni	0.00	0.00	0.00	0.00	0.00	0.00	0.00
Ca	0.91	0.88	0.91	0.89	0.90	0.91	0.90
K	0.00	0.00	0.00	0.00	0.00	0.00	0.00
Cr	0.00	0.00	0.00	0.00	0.00	0.00	0.00
Sum Cations	4.00	3.99	4.01	4.00	3.99	4.00	4.00
$KFeSi_2$ %	0.16	0.08	0.16	0.13	0.07	0.14	0.14
NaTiSiAl %	0.18	0.10	0.23	0.26	0.16	0.02	0.10
$NaFeSi_2$ % (acmite)	3.71	4.81	3.75	3.90	3.76	3.92	4.15
$CaAl_2Si$ % (kushiroite)	0.21	0.30	0.25	0.27	0.48	0.33	0.73
$CaMnSi_2$ % (johannsenite)	0.73	0.64	0.71	0.66	0.67	0.80	0.51
$Ca(FM)Si_2$ % (diopside)	86.70	84.71	86.42	84.81	85.44	86.12	85.72
$(FM)_2Si_2$ %	8.30	9.36	8.47	9.97	9.42	8.67	8.65

Table C 2. 10: Clinopyroxene EPMA data

Rock type	Clinopyroxenite					Magnetite-rich phoscorite	
Sample	SC10-6-1 Pyx 1 C	SC10-6-1 Pyx 2 C	SC10-6-1 Pyx 3 C	SC10-6-1 Pyx 4 C	SC10-6-1 Pyx 5 C	SC10-12-4 pyx 1	SC10-12-4 Pyx 11 R
SiO_2	53.89	54.35	54.15	54.23	51.22	51.12	53.18
TiO_2	0.08	0.08	0.01	0.03	0.03	0.03	0.05
Al_2O_3	0.14	0.35	0.10	0.22	1.31	0.78	0.14
FeO	3.38	4.11	3.62	3.36	10.45	11.71	5.90
Fe_2O_3	1.06	0.65	0.96	0.76	2.23	2.44	1.31
MnO	0.13	0.20	0.19	0.21	0.41	0.61	0.46
MgO	16.24	15.97	16.18	16.39	10.66	9.51	14.51
CaO	23.18	22.97	23.03	23.17	21.46	21.11	21.79
Na_2O	0.43	0.27	0.36	0.29	0.87	0.94	0.51
K_2O	0.02	0.03	0.01	0.02	0.02	0.03	0.03
Cr_2O_3	0.01	0.04	0.07	0.05	0.00	0.03	0.05
NiO	0.03	0.00	0.00	0.01	0.00	0.03	0.02
Total	98.60	99.03	98.69	98.75	98.66	98.33	97.95
Number of ions calculated on the basis of 6 O							
Al	0.01	0.02	0.00	0.01	0.06	0.04	0.01
Si	2.00	2.01	2.01	2.01	1.98	2.00	2.01
Ti	0.00	0.00	0.00	0.00	0.00	0.00	0.00
Na	0.03	0.02	0.03	0.02	0.07	0.07	0.04
Mg	0.90	0.88	0.90	0.90	0.61	0.55	0.82
Fe^{2+}	0.11	0.13	0.11	0.10	0.34	0.38	0.19
Fe^{3+}	0.03	0.02	0.03	0.02	0.06	0.07	0.04
Mn	0.00	0.01	0.01	0.01	0.01	0.02	0.01
Ni	0.00	0.00	0.00	0.00	0.00	0.00	0.00
Ca	0.92	0.91	0.92	0.92	0.89	0.88	0.88
K	0.00	0.00	0.00	0.00	0.00	0.00	0.00
Cr	0.00	0.00	0.00	0.00	0.00	0.00	0.00
Sum Cations	4.01	3.99	4.00	4.00	4.02	4.02	4.00
$KFeSi_2$ %	0.11	0.12	0.06	0.08	0.07	0.13	0.14
NaTiSiAl %	0.22	0.22	0.02	0.08	0.09	0.10	0.12
$NaFeSi_2$ % (acmite)	2.73	1.62	2.50	1.94	5.89	6.60	3.37
$CaAl_2Si$ % (kushiroite)	0.38	1.24	0.38	0.84	5.38	3.26	0.48
$CaMnSi_2$ % (johannsenite)	0.39	0.60	0.57	0.62	1.22	1.88	1.39
$Ca(FM)Si_2$ % (diopside)	87.54	85.04	86.74	86.44	74.96	77.92	81.17
$(FM)_2Si_2$ %	8.63	11.17	9.73	10.00	12.39	10.10	13.32

Table C 2. 11: Clinopyroxene EPMA data

Rock type	Magnetite-rich phoscorite						
Sample	SC10-12-4 Pyx 11 Rim	SC10-12-4 Pyx 12 C	SC10-12-4 Pyx 13 C	SC10-12-4 Pyx 14 C	SC10-12-4 Pyx 15 C	SC10-12-4 Pyx 16 C	SC10-12-4 Pyx 17 C
SiO_2	53.13	50.24	50.61	51.36	50.65	51.98	49.48
TiO_2	0.02	0.17	0.09	0.07	0.15	0.05	0.14
Al_2O_3	0.15	1.27	0.88	0.43	1.40	0.57	1.46
FeO	6.11	13.80	12.58	13.01	12.26	9.41	13.57
Fe_2O_3	1.21	3.26	2.51	2.24	3.13	2.20	3.24
MnO	0.49	0.54	0.62	0.67	0.62	0.47	0.55
MgO	14.26	7.60	8.77	8.85	8.39	11.14	7.82
CaO	22.16	20.12	20.69	21.09	20.28	21.54	19.94
Na_2O	0.46	1.31	0.99	0.88	1.26	0.85	1.29
K_2O	0.03	0.03	0.03	0.02	0.01	0.03	0.02
Cr_2O_3	0.04	0.00	0.00	0.00	0.04	0.01	0.00
NiO	0.05	0.02	0.00	0.00	0.00	0.00	0.00
Total	98.11	98.38	97.78	98.62	98.20	98.26	97.52
	Number of ions calculated on the basis of 6 O						
Al	0.01	0.06	0.04	0.02	0.06	0.03	0.07
Si	2.01	1.99	2.00	2.01	1.99	2.01	1.98
Ti	0.00	0.01	0.00	0.00	0.00	0.00	0.00
Na	0.03	0.10	0.08	0.07	0.10	0.06	0.10
Mg	0.80	0.45	0.52	0.52	0.49	0.64	0.47
Fe^{2+}	0.19	0.46	0.42	0.43	0.40	0.30	0.45
Fe^{3+}	0.03	0.10	0.07	0.07	0.09	0.06	0.10
Mn	0.02	0.02	0.02	0.02	0.02	0.02	0.02
Ni	0.00	0.00	0.00	0.00	0.00	0.00	0.00
Ca	0.90	0.85	0.87	0.88	0.85	0.89	0.85
K	0.00	0.00	0.00	0.00	0.00	0.00	0.00
Cr	0.00	0.00	0.00	0.00	0.00	0.00	0.00
Sum Cations	4.00	4.03	4.02	4.01	4.02	4.01	4.04
$KFeSi_2$ %	0.12	0.13	0.14	0.10	0.07	0.15	0.12
NaTiSiAl %	0.06	0.47	0.26	0.21	0.43	0.14	0.39
$NaFeSi_2$ % (acmite)	3.14	8.87	6.85	6.18	8.56	5.93	8.70
$CaAl_2Si$ % (kushiroite)	0.59	5.03	3.56	1.67	5.60	2.32	5.82
$CaMnSi_2$ % (johannsenite)	1.48	1.69	1.96	2.11	1.93	1.46	1.70
$Ca(FM)Si_2$ % (diopside)	83.15	72.29	76.45	80.47	72.09	81.07	69.84
$(FM)_2Si_2$ %	11.46	11.53	10.79	9.25	11.32	8.93	13.44

Table C 2. 12: Clinopyroxene EPMA data

Rock type	Magnetite-rich phoscorite						
Sample	SC10-12-4 Pyx 18 C	SC10-12-4 Pyx 19 C	SC10-12-4 pyx 2	SC10-12-4 Pyx 20 C	SC10-12-4 Pyx 21 C	SC10-12-4 Pyx 22 C	SC10-12-4 Pyx 23 C
SiO_2	50.70	51.94	51.49	50.31	51.99	51.64	50.59
TiO_2	0.03	0.10	0.04	0.10	0.07	0.02	0.12
Al_2O_3	0.84	0.53	1.16	1.09	0.56	0.61	1.29
FeO	12.99	10.82	9.44	13.04	10.64	10.95	12.19
Fe_2O_3	2.61	2.23	3.12	2.96	1.94	2.11	3.16
MnO	0.69	0.45	0.58	0.52	0.50	0.58	0.54
MgO	8.31	10.32	10.70	8.00	10.56	10.43	8.51
CaO	20.90	21.18	20.57	20.72	21.45	21.32	20.21
Na_2O	1.02	0.88	1.20	1.17	0.77	0.82	1.26
K_2O	0.01	0.03	0.03	0.02	0.01	0.01	0.02
Cr_2O_3	0.02	0.02	0.00	0.00	0.00	0.05	0.00
NiO	0.00	0.00	0.00	0.06	0.00	0.03	0.00
Total	98.13	98.52	98.33	97.99	98.51	98.57	97.92
	Number of ions calculated on the basis of 6 O						
Al	0.04	0.02	0.05	0.05	0.03	0.03	0.06
Si	2.00	2.01	1.99	1.99	2.01	2.00	1.99
Ti	0.00	0.00	0.00	0.00	0.00	0.00	0.00
Na	0.08	0.07	0.09	0.09	0.06	0.06	0.10
Mg	0.49	0.60	0.62	0.47	0.61	0.60	0.50
Fe^{2+}	0.43	0.35	0.31	0.43	0.34	0.35	0.40
Fe^{3+}	0.08	0.07	0.09	0.09	0.06	0.06	0.09
Mn	0.02	0.01	0.02	0.02	0.02	0.02	0.02
Ni	0.00	0.00	0.00	0.00	0.00	0.00	0.00
Ca	0.88	0.88	0.85	0.88	0.89	0.88	0.85
K	0.00	0.00	0.00	0.00	0.00	0.00	0.00
Cr	0.00	0.00	0.00	0.00	0.00	0.00	0.00
Sum Cations	4.02	4.01	4.03	4.03	4.01	4.02	4.02
$KFeSi_2$ %	0.07	0.16	0.16	0.10	0.05	0.05	0.11
NaTiSiAl %	0.09	0.27	0.11	0.28	0.20	0.05	0.33
$NaFeSi_2$ % (acmite)	7.27	6.03	8.20	8.20	5.32	5.72	8.63
$CaAl_2Si$ % (kushiroite)	3.63	2.03	4.75	4.52	2.21	2.57	5.27
$CaMnSi_2$ % (johannsenite)	2.18	1.42	1.76	1.65	1.57	1.79	1.69
$Ca(FM)Si_2$ % (diopside)	77.77	80.19	72.07	76.75	80.76	78.73	72.51
$(FM)_2Si_2$ %	9.00	9.90	12.94	8.49	9.89	11.10	11.47

Table C 2. 13: Clinopyroxene EPMA data

Rock type	Magnetite-rich phoscorite						
Sample	SC10-5-2 pyx 1	SC10-5-2 pyx 10	SC10-5-2 pyx 2	SC10-5-2 pyx 3	SC10-5-2 pyx 4	SC10-5-2 pyx 5	SC10-5-2 pyx 6
SiO_2	51.46	52.63	51.24	51.47	53.10	53.36	53.53
TiO_2	0.06	0.05	0.02	0.01	0.01	0.07	0.00
Al_2O_3	0.79	0.14	0.80	0.98	0.27	0.33	0.31
FeO	11.11	6.06	11.83	10.44	7.84	5.77	6.41
Fe_2O_3	1.86	0.34	1.89	2.05	0.82	0.69	0.76
MnO	0.39	0.50	0.46	0.39	0.40	0.41	0.33
MgO	10.08	14.50	9.83	10.40	12.66	14.35	14.04
CaO	22.21	24.06	21.94	21.93	23.28	23.46	23.39
Na_2O	0.73	0.12	0.72	0.78	0.30	0.28	0.28
K_2O	0.03	0.04	0.03	0.02	0.03	0.03	0.02
Cr_2O_3	0.01	0.00	0.05	0.00	0.00	0.04	0.04
NiO	0.04	0.02	0.00	0.00	0.02	0.02	0.03
Total	98.78	98.48	98.83	98.46	98.73	98.81	99.15
	Number of ions calculated on the basis of 6 O						
Al	0.04	0.01	0.04	0.04	0.01	0.01	0.01
Si	1.99	1.99	1.99	1.99	2.01	2.00	2.01
Ti	0.00	0.00	0.00	0.00	0.00	0.00	0.00
Na	0.05	0.01	0.05	0.06	0.02	0.02	0.02
Mg	0.58	0.82	0.57	0.60	0.72	0.80	0.78
Fe^{2+}	0.36	0.19	0.38	0.34	0.25	0.18	0.20
Fe^{3+}	0.05	0.01	0.06	0.06	0.02	0.02	0.02
Mn	0.01	0.02	0.02	0.01	0.01	0.01	0.01
Ni	0.00	0.00	0.00	0.00	0.00	0.00	0.00
Ca	0.92	0.97	0.91	0.91	0.95	0.94	0.94
K	0.00	0.00	0.00	0.00	0.00	0.00	0.00
Cr	0.00	0.00	0.00	0.00	0.00	0.00	0.00
Sum Cations	4.02	4.01	4.02	4.02	3.99	4.00	4.00
$KFeSi_2$ %	0.14	0.19	0.14	0.11	0.16	0.13	0.09
NaTiSiAl %	0.17	0.13	0.07	0.02	0.04	0.21	0.00
$NaFeSi_2$ % (acmite)	5.05	0.75	5.08	5.54	2.14	1.75	1.98
$CaAl_2Si$ % (kushiroite)	3.28	0.49	3.39	4.23	1.17	1.20	1.33
$CaMnSi_2$ % (johannsenite)	1.23	1.54	1.42	1.20	1.27	1.27	1.01
$Ca(FM)Si_2$ % (diopside)	83.67	91.60	81.27	80.76	90.95	89.06	88.75
$(FM)_2Si_2$ %	6.47	5.30	8.63	8.15	4.26	6.39	6.85

Table C 2. 14: Clinopyroxene EPMA data

Rock type	Magnetite-rich phoscorite			Carbonatite			
Sample	SC10-5-2 pyx 7	SC10-5-2 pyx 8	SC10-5-2 pyx 9	SC8-1_Py1	SC8-1_Py10	SC8-1_Py3	SC8-1_Py4
SiO_2	52.21	51.26	51.83	54.92	54.44	55.02	54.88
TiO_2	0.05	0.04	0.00	0.02	0.02	0.06	0.00
Al_2O_3	0.85	0.92	0.15	0.02	0.18	0.04	0.02
FeO	9.73	9.71	12.02	3.25	4.03	3.26	3.07
Fe_2O_3	1.77	1.55	0.85	1.90	3.22	1.84	1.58
MnO	0.43	0.35	0.55	0.20	0.12	0.22	0.17
MgO	11.38	11.27	10.01	16.05	14.63	16.25	16.26
CaO	22.08	22.09	22.87	22.53	21.93	22.56	23.29
Na_2O	0.69	0.60	0.32	0.73	1.24	0.73	0.59
K_2O	0.03	0.02	0.01	0.02	0.03	0.01	0.03
Cr_2O_3	0.00	0.03	0.00	0.01	0.05	0.04	0.00
NiO	0.06	0.02	0.05	0.00	0.00	0.00	0.04
Total	99.28	97.86	98.68	99.67	99.87	100.03	99.94
Number of ions calculated on the basis of 6 O							
Al	0.04	0.04	0.01	0.00	0.01	0.00	0.00
Si	1.99	1.99	2.01	2.02	2.02	2.02	2.01
Ti	0.00	0.00	0.00	0.00	0.00	0.00	0.00
Na	0.05	0.05	0.02	0.05	0.09	0.05	0.04
Mg	0.65	0.65	0.58	0.88	0.81	0.89	0.89
Fe^{2+}	0.31	0.31	0.39	0.10	0.12	0.10	0.09
Fe^{3+}	0.05	0.05	0.02	0.05	0.09	0.05	0.04
Mn	0.01	0.01	0.02	0.01	0.00	0.01	0.01
Ni	0.00	0.00	0.00	0.00	0.00	0.00	0.00
Ca	0.90	0.92	0.95	0.89	0.87	0.89	0.92
K	0.00	0.00	0.00	0.00	0.00	0.00	0.00
Cr	0.00	0.00	0.00	0.00	0.00	0.00	0.00
Sum Cations	4.01	4.01	4.00	4.00	4.02	4.01	4.01
$KFeSi_2$ %	0.14	0.08	0.06	0.09	0.12	0.07	0.12
NaTiSiAl %	0.13	0.11	0.00	0.06	0.05	0.16	0.00
$NaFeSi_2$ % (acmite)	4.66	4.16	2.37	4.98	8.55	4.79	4.09
$CaAl_2Si$ % (kushiroite)	3.46	3.82	0.69	0.04	0.73	0.00	0.08
$CaMnSi_2$ % (johannsenite)	1.31	1.09	1.78	0.61	0.35	0.66	0.52
$Ca(FM)Si_2$ % (diopside)	80.36	81.27	90.81	84.70	83.07	83.95	87.99
$(FM)_2Si_2$ %	9.95	9.46	4.28	9.53	7.13	10.38	7.20

Table C 2. 15: Clinopyroxene EPMA data

Rock type	Carbonatite						
Sample	SC8-1_Py5	SC8-1_Py6	SC8-1_Py7	SC8-1_Py8	SC8-1_Py9	SC8-4_Py1	SC8-4_Py10
SiO_2	54.76	54.60	54.61	54.44	54.57	54.43	54.35
TiO_2	0.03	0.00	0.00	0.04	0.05	0.05	0.00
Al_2O_3	0.18	0.25	0.21	0.23	0.18	0.25	0.48
FeO	4.34	4.13	4.22	4.37	4.14	4.08	3.93
Fe_2O_3	2.60	3.48	3.39	4.17	3.47	2.57	3.52
MnO	0.19	0.23	0.19	0.14	0.19	0.13	0.12
MgO	14.64	13.93	14.16	13.71	14.17	14.88	14.47
CaO	22.17	21.42	21.61	21.09	21.65	22.35	21.24
Na_2O	1.00	1.34	1.30	1.62	1.35	0.99	1.35
K_2O	0.02	0.02	0.03	0.02	0.03	0.03	0.03
Cr_2O_3	0.00	0.04	0.01	0.04	0.05	0.00	0.02
NiO	0.00	0.00	0.00	0.00	0.00	0.04	0.00
Total	99.94	99.45	99.73	99.87	99.87	99.79	99.52
	Number of ions calculated on the basis of 6 O						
Al	0.01	0.01	0.01	0.01	0.01	0.01	0.02
Si	2.03	2.03	2.03	2.03	2.03	2.02	2.02
Ti	0.00	0.00	0.00	0.00	0.00	0.00	0.00
Na	0.07	0.10	0.09	0.12	0.10	0.07	0.10
Mg	0.81	0.77	0.78	0.76	0.78	0.82	0.80
Fe^{2+}	0.13	0.13	0.13	0.14	0.13	0.13	0.12
Fe^{3+}	0.07	0.10	0.09	0.12	0.10	0.07	0.10
Mn	0.01	0.01	0.01	0.00	0.01	0.00	0.00
Ni	0.00	0.00	0.00	0.00	0.00	0.00	0.00
Ca	0.88	0.86	0.86	0.84	0.86	0.89	0.85
K	0.00	0.00	0.00	0.00	0.00	0.00	0.00
Cr	0.00	0.00	0.00	0.00	0.00	0.00	0.00
Sum Cations	4.01	4.01	4.01	4.02	4.02	4.01	4.02
$KFeSi_2$ %	0.11	0.10	0.12	0.11	0.12	0.16	0.13
NaTiSiAl %	0.08	0.00	0.00	0.11	0.15	0.12	0.01
$NaFeSi_2$ % (acmite)	6.93	9.48	9.12	11.27	9.35	6.77	9.28
$CaAl_2Si$ % (kushiroite)	0.67	1.10	0.88	0.85	0.60	0.94	2.00
$CaMnSi_2$ % (johannsenite)	0.58	0.71	0.58	0.43	0.59	0.39	0.35
$Ca(FM)Si_2$ % (diopside)	84.25	82.15	82.48	80.52	82.94	84.42	78.42
$(FM)_2Si_2$ %	7.38	6.46	6.82	6.71	6.24	7.21	9.80

Table C 2. 16: Clinopyroxene EPMA data

Rock type	Carbonatite						
Sample	SC8-4_Py2	SC8-4_Py3	SC8-4_Py4	SC8-4_Py5	SC8-4_Py6	SC8-4_Py7	SC8-4_Py9
SiO_2	54.67	54.77	54.34	54.53	54.30	53.68	54.61
TiO_2	0.02	0.10	0.08	0.03	0.06	0.11	0.03
Al_2O_3	0.20	0.30	0.30	0.29	0.27	0.90	0.36
FeO	3.74	3.78	4.10	3.94	3.82	3.81	3.15
Fe_2O_3	2.81	2.97	2.83	3.30	2.66	3.81	2.70
MnO	0.12	0.12	0.10	0.08	0.12	0.16	0.14
MgO	15.24	14.98	14.54	14.81	14.94	14.16	15.58
CaO	22.18	21.84	22.14	21.69	21.95	21.16	22.21
Na_2O	1.07	1.18	1.12	1.28	1.03	1.51	1.04
K_2O	0.04	0.01	0.02	0.02	0.03	0.02	0.03
Cr_2O_3	0.00	0.04	0.07	0.05	0.00	0.00	0.00
NiO	0.00	0.05	0.00	0.00	0.00	0.00	0.01
Total	100.10	100.15	99.64	100.03	99.18	99.32	99.85
	Number of ions calculated on the basis of 6 O						
Al	0.01	0.01	0.01	0.01	0.01	0.04	0.02
Si	2.02	2.02	2.02	2.02	2.02	2.01	2.01
Ti	0.00	0.00	0.00	0.00	0.00	0.00	0.00
Na	0.08	0.08	0.08	0.09	0.07	0.11	0.07
Mg	0.84	0.82	0.80	0.82	0.83	0.79	0.86
Fe^{2+}	0.12	0.12	0.13	0.12	0.12	0.12	0.10
Fe^{3+}	0.08	0.08	0.08	0.09	0.07	0.11	0.07
Mn	0.00	0.00	0.00	0.00	0.00	0.01	0.00
Ni	0.00	0.00	0.00	0.00	0.00	0.00	0.00
Ca	0.88	0.86	0.88	0.86	0.88	0.85	0.88
K	0.00	0.00	0.00	0.00	0.00	0.00	0.00
Cr	0.00	0.00	0.00	0.00	0.00	0.00	0.00
Sum Cations	4.02	4.01	4.01	4.02	4.01	4.03	4.02
$KFeSi_2$ %	0.17	0.05	0.09	0.10	0.15	0.09	0.12
NaTiSiAl %	0.06	0.26	0.23	0.09	0.16	0.30	0.08
$NaFeSi_2$ % (acmite)	7.29	7.87	7.61	8.68	7.02	10.00	7.02
$CaAl_2Si$ % (kushiroite)	0.79	1.00	1.06	1.12	0.98	3.45	1.40
$CaMnSi_2$ % (johannsenite)	0.37	0.35	0.31	0.25	0.37	0.49	0.43
$Ca(FM)Si_2$ % (diopside)	82.83	81.68	84.35	80.82	82.98	76.01	81.86
$(FM)_2Si_2$ %	8.49	8.79	6.35	8.93	8.35	9.66	9.09

Table C 2. 17: Clinopyroxene EPMA data

Rock type	Carbonatite					
Sample	SC8-4_Pyr1a	SC8-4_Pyr1	SC8-17_Pyr2	SC8-17_Pyr4	SC8-17_Pyr6	SC8-11_Pyr3
SiO_2	57.76	58.52	54.74	54.95	53.73	55.28
TiO_2	0.07	0.00	0.04	0.06	0.05	0.10
Al_2O_3	0.05	0.01	0.12	0.07	0.12	0.02
FeO	0.30	0.23	2.62	2.06	2.32	2.26
Fe_2O_3	2.64	2.07	1.48	1.07	1.25	0.89
MnO	0.04	0.03	0.09	0.08	0.06	0.11
MgO	22.81	22.80	16.38	16.93	16.29	17.01
CaO	11.88	12.43	23.34	23.59	23.50	23.81
Na_2O	0.84	0.67	0.57	0.42	0.49	0.37
K_2O	0.31	0.21	0.03	0.02	0.02	0.02
Cr_2O_3	0.02	0.09	0.00	0.03	0.03	0.00
NiO	0.00	0.00	0.01	0.00	0.02	0.00
Total	96.73	97.07	99.41	99.28	97.87	99.87
	Number of ions calculated on the basis of 6 O					
Al	0.00	0.00	0.01	0.00	0.01	0.00
Si	2.09	2.10	2.01	2.01	2.01	2.01
Ti	0.00	0.00	0.00	0.00	0.00	0.00
Na	0.06	0.05	0.04	0.03	0.04	0.03
Mg	1.23	1.22	0.90	0.93	0.91	0.92
Fe^{2+}	0.01	0.01	0.08	0.06	0.07	0.07
Fe^{3+}	0.07	0.06	0.04	0.03	0.04	0.02
Mn	0.00	0.00	0.00	0.00	0.00	0.00
Ni	0.00	0.00	0.00	0.00	0.00	0.00
Ca	0.46	0.48	0.92	0.93	0.94	0.93
K	0.01	0.01	0.00	0.00	0.00	0.00
Cr	0.00	0.00	0.00	0.00	0.00	0.00
Sum Cations	3.94	3.92	4.00	4.00	4.01	4.00
$KFeSi_2$ %	1.11	0.74	0.16	0.11	0.12	0.10
NaTiSiAl %	0.15	0.01	0.11	0.16	0.13	0.27
$NaFeSi_2$ % (acmite)	4.36	3.62	3.83	2.77	3.31	2.29
$CaAl_2Si$ % (kushiroite)	0.00	0.03	0.38	0.15	0.37	-0.19
$CaMnSi_2$ % (johannsenite)	0.10	0.06	0.27	0.24	0.20	0.33
$Ca(FM)Si_2$ % (diopside)	34.94	37.14	88.88	90.15	91.51	90.85
$(FM)_2Si_2$ %	59.35	58.40	6.37	6.42	4.37	6.36

Appendix C.3: Amphibole EPMA Data

Table C 3. 1: Amphibole EPMA data

Rock Type	Clinopyroxenite				Glimmerite			
Sample	SC10-25-1-Amph1	SC10-25-1-Amph2	SC10-25-1-Amph3	SC10-25-1-Amph4	SC10-11 -2 - Amph - 1	SC10-11 -2 - Amph - 2	SC10-11 -2 -Amph - 3	SC10-11-2-Amph–4
SiO_2	57.10	57.29	57.46	57.77	55.62	55.49	55.18	55.89
TiO_2	0.11	0.05	0.03	0.02	0.00	0.07	0.07	0.10
Al_2O_3	0.32	0.36	0.26	0.23	0.41	0.24	0.46	0.48
MnO	0.15	0.29	0.17	0.18	0.40	0.41	0.49	0.48
Mn_2O_3	0.00	0.00	0.00	0.00	0.00	0.00	0.00	0.00
FeO	5.38	2.43	4.35	4.12	9.62	9.80	10.60	10.05
Fe_2O_3	0.86	1.34	0.40	0.34	0.78	0.88	0.86	0.73
MgO	20.69	22.00	21.43	21.79	17.64	17.83	16.80	17.50
CaO	12.33	11.44	12.70	12.59	12.43	12.29	12.04	12.01
Na_2O	0.58	1.12	0.36	0.37	0.34	0.26	0.47	0.47
K_2O	0.22	0.42	0.11	0.16	0.09	0.06	0.11	0.09
H_2O+*	2.08	2.16	2.13	2.11	2.02	2.02	2.04	2.00
F	0.16	0.05	0.08	0.14	0.19	0.18	0.13	0.24
O=F,Cl (calc)	-0.07	-0.02	-0.03	-0.06	-0.08	-0.08	-0.05	-0.10
Total	99.91	98.94	99.43	99.75	99.45	99.45	99.19	99.93
	Number of ions calculated on the basis of 24 (O,OH,F)							
T (ideally 8 apfu)								
Si	7.95	7.96	7.98	7.99	7.93	7.92	7.93	7.94
Al ^{iv}	0.05	0.04	0.02	0.01	0.07	0.04	0.07	0.06
Ti ^{iv}	0.00					0.01		
$Fe^{3+\,iv}$						0.03		
T subtotal	8.00	8.00	8.00	8.00	8.00	8.00	8.00	8.00
C (ideally 5 apfu)								
Ti ^{vi}	0.01	0.01	0.00	0.00			0.01	0.01
Al ^{vi}		0.02	0.02	0.02	0.00		0.01	0.02
Mn^{3+}								
$Fe^{3+\,vi}$	0.09	0.14	0.04	0.04	0.08	0.07	0.09	0.08
$Mn^{2+\,C}$					0.01		0.02	
$Fe^{2+\,C}$	0.61	0.28	0.50	0.45	1.15	1.14	1.28	1.18
Mg	4.29	4.56	4.44	4.49	3.75	3.80	3.60	3.71
C subtotal	5.00	5.00	5.00	5.00	5.00	5.00	5.00	5.00
B (ideally 2 apfu)								
$Mn^{2+\,B}$	0.02	0.03	0.02	0.02	0.03	0.05	0.05	0.06
$Fe^{2+\,B}$	0.02	0.01	0.01	0.03	0.00	0.03	0.00	0.01
Ca	1.84	1.70	1.89	1.86	1.90	1.88	1.86	1.83
Na B	0.13	0.26	0.08	0.09	0.07	0.04	0.10	0.10
B subtotal	2.00	2.00	2.00	2.00	2.00	2.00	2.00	2.00
A (from 0 to 1 apfu)								
Na A	0.03	0.05	0.01	0.01	0.03	0.03	0.03	0.03
K	0.04	0.08	0.02	0.03	0.02	0.01	0.02	0.02
A subtotal	0.07	0.12	0.03	0.04	0.04	0.04	0.05	0.04
O (non-W)	22.00	22.00	22.00	22.00	22.00	22.00	22.00	22.00
W (ideally 2 apfu)								
OH	1.93	1.98	1.96	1.94	1.91	1.92	1.94	1.89
F Cal	0.07	0.02	0.04	0.06	0.09	0.08	0.06	0.11
W subtotal	2.00	2.00	2.00	2.00	2.00	2.00	2.00	2.00
Sum Cations	15.07	15.12	15.03	15.04	15.04	15.04	15.05	15.04

Table C 3. 2: Amphibole EPMA data

Rock Type	Glimmerite							
Sample	SC10-11 - 2-Amph-5	SC10-112-Amph-6	SC10-11-2-Amph-7	SC10-11-2-Amph-8	SC10-4-2-Amph-1	SC10-4-2-Amph-2	SC10-4-2-Amph-3	SC10-4-2-Amph-4
SiO_2	55.11	54.52	55.21	55.76	54.29	53.01	54.47	53.99
TiO_2	0.07	0.07	0.12	0.10	0.06	0.19	0.14	0.10
Al_2O_3	0.42	0.55	1.12	0.40	1.27	1.88	0.95	1.43
MnO	0.43	0.53	0.43	0.52	0.31	0.44	0.31	0.36
Mn_2O_3	0.00	0.00	0.00	0.00	0.00	0.00	0.00	0.00
FeO	8.83	9.57	8.74	10.50	8.82	10.80	9.36	10.19
Fe_2O_3	1.61	1.44	1.29	0.63	2.40	2.53	1.98	1.98
MgO	17.89	17.37	17.97	17.29	17.38	15.83	17.20	16.51
CaO	12.73	11.84	12.39	11.78	11.59	11.78	12.06	11.60
Na_2O	0.37	0.46	0.41	0.47	0.93	0.81	0.71	0.83
K_2O	0.11	0.09	0.11	0.12	0.36	0.50	0.25	0.40
H_2O+*	2.04	2.03	2.12	2.03	1.90	1.99	1.98	1.95
F	0.15	0.17	0.00	0.17	0.44	0.19	0.27	0.30
O=F,Cl (calc)	-0.06	-0.07	0.00	-0.07	-0.19	-0.08	-0.11	-0.13
Total	99.70	98.55	99.91	99.71	99.57	99.85	99.56	99.52
Number of ions calculated on the basis of 24 (O,OH,F)								
T (ideally 8 apfu)								
Si	7.86	7.87	7.83	7.95	7.77	7.66	7.80	7.77
Al ^{iv}	0.07	0.09	0.17	0.05	0.21	0.32	0.16	0.23
Ti ^{iv}	0.01	0.01			0.01	0.02	0.02	
$Fe^{3+\,iv}$	0.07	0.03			0.01	0.00	0.02	
T subtotal	8.00	8.00	8.00	8.00	8.00	8.00	8.00	8.00
C (ideally 5 apfu)								
Ti ^{vi}			0.01	0.01				0.01
Al ^{vi}			0.01	0.02				0.01
Mn^{3+}								
$Fe^{3+\,vi}$	0.11	0.13	0.14	0.07	0.25	0.27	0.19	0.22
$Mn^{2+\,C}$	0.04		0.00			0.01	0.01	
$Fe^{2+\,C}$	1.05	1.13	1.04	1.22	1.04	1.30	1.12	1.22
Mg	3.80	3.74	3.80	3.68	3.71	3.41	3.67	3.54
C subtotal	5.00	5.00	5.00	5.00	5.00	5.00	5.00	5.00
B (ideally 2 apfu)								
$Mn^{2+\,B}$	0.01	0.06	0.05	0.06	0.04	0.04	0.02	0.04
$Fe^{2+\,B}$	0.00	0.03	0.00	0.03	0.01	0.00	0.00	0.01
Ca	1.94	1.83	1.88	1.80	1.78	1.82	1.85	1.79
Na B	0.05	0.08	0.07	0.11	0.17	0.14	0.13	0.16
B subtotal	2.00	2.00	2.00	2.00	2.00	2.00	2.00	2.00
A (from 0 to 1 apfu)								
Na A	0.06	0.05	0.05	0.02	0.09	0.09	0.07	0.07
K	0.02	0.02	0.02	0.02	0.07	0.09	0.05	0.07
A subtotal	0.08	0.07	0.07	0.04	0.15	0.18	0.12	0.15
O (non-W)	22.00	22.00	22.00	22.00	22.00	22.00	22.00	22.00
W (ideally 2 apfu)								
OH	1.93	1.92	2.00	1.92	1.80	1.91	1.88	1.86
F Cal	0.07	0.08		0.08	0.20	0.09	0.12	0.14
W subtotal	2.00	2.00	2.00	2.00	2.00	2.00	2.00	2.00
Sum Cations	15.08	15.07	15.07	15.04	15.15	15.18	15.12	15.15

Table C 3. 3: Amphibole EPMA data

Rock Type	Glimmerite			Magnetite-rich phoscorite				
Sample	SC10-4 -2 - Amph-5	SC10-4 -2 - Amph-6	SC10-4 -2 - Amph-7	SC10-12 -2 - Amph-1	SC10-12 -2 - Amph-10	SC10-12 -2 - Amph-2	SC10-12 -2 - Amph-4	SC10-12 -2 - Amph-5
SiO_2	54.78	52.03	54.84	55.08	55.69	55.96	53.98	55.68
TiO_2	0.08	0.20	0.06	0.04	0.05	0.02	0.05	0.08
Al_2O_3	0.60	2.72	0.85	1.30	0.99	0.85	1.15	0.85
MnO	0.42	0.43	0.35	0.39	0.32	0.31	0.33	0.35
Mn_2O_3	0.00	0.00	0.00	0.00	0.00	0.00	0.00	0.00
FeO	11.59	10.07	9.93	7.13	6.93	7.27	6.54	5.80
Fe_2O_3	1.24	3.08	1.23	1.69	1.39	0.86	2.32	1.44
MgO	16.32	15.37	17.26	18.59	19.23	19.11	18.58	20.10
CaO	11.97	12.47	12.00	12.69	12.40	12.56	12.87	12.01
Na_2O	0.50	0.74	0.50	0.49	0.48	0.36	0.45	0.56
K_2O	0.24	0.26	0.23	0.17	0.17	0.14	0.17	0.34
H_2O+*	1.93	1.91	2.01	2.05	2.04	2.01	2.05	2.05
F	0.33	0.36	0.21	0.17	0.20	0.26	0.15	0.20
O=F,Cl (calc)	-0.14	-0.15	-0.09	-0.07	-0.08	-0.11	-0.06	-0.09
Total	99.85	99.48	99.39	99.70	99.82	99.60	98.58	99.35
Number of ions calculated on the basis of 24 (O,OH,F)								
T (ideally 8 apfu)								
Si	7.88	7.55	7.86	7.79	7.84	7.89	7.74	7.84
Al ^{iv}	0.10	0.45	0.14	0.21	0.16	0.11	0.19	0.14
Ti ^{iv}	0.01						0.01	0.01
$Fe^{3+\,iv}$	0.01						0.06	0.01
T subtotal	8.00	8.00	8.00	8.00	8.00	8.00	8.00	8.00
C (ideally 5 apfu)								
Ti ^{vi}		0.02	0.01	0.00	0.01	0.00		
Al ^{vi}		0.01	0.00	0.01	0.00	0.03		
Mn^{3+}								
$Fe^{3+\,vi}$	0.12	0.34	0.13	0.18	0.15	0.09	0.19	0.14
$Mn^{2+\,C}$		0.05		0.05		0.00	0.04	
$Fe^{2+\,C}$	1.38	1.22	1.17	0.84	0.81	0.86	0.78	0.64
Mg	3.50	3.32	3.69	3.92	4.04	4.02	3.97	4.22
C subtotal	5.00	4.97	5.00	5.00	5.00	5.00	4.98	5.00
B (ideally 2 apfu)								
$Mn^{2+\,B}$	0.05		0.04	0.00	0.04	0.03		0.04
$Fe^{2+\,B}$	0.01	0.00	0.02	0.00	0.01	0.00	0.00	0.05
Ca	1.84	1.94	1.84	1.92	1.87	1.90	1.98	1.81
Na B	0.09	0.06	0.09	0.08	0.08	0.07	0.02	0.10
B subtotal	2.00	2.00	2.00	2.00	2.00	2.00	2.00	2.00
A (from 0 to 1 apfu)								
Na A	0.04	0.15	0.04	0.06	0.05	0.03	0.10	0.05
K	0.04	0.05	0.04	0.03	0.03	0.03	0.03	0.06
A subtotal	0.09	0.19	0.09	0.09	0.08	0.06	0.13	0.11
O (non-W)	22.00	22.00	22.00	22.00	22.00	22.00	22.00	22.00
W (ideally 2 apfu)								
OH	1.85	1.84	1.91	1.93	1.91	1.89	1.93	1.91
F Cal	0.15	0.16	0.10	0.08	0.09	0.12	0.07	0.09
W subtotal	2.00	2.00	2.00	2.00	2.00	2.00	2.00	2.00
Sum Cations	15.09	15.16	15.09	15.09	15.08	15.05	15.11	15.11

Table C 3. 4: Amphibole EPMA data

Rock Type	Magnetite-rich phoscorite							
Sample	SC10-12 -2 - Amph-6	SC10-12 -2 - Amph-7	SC10-12 -2 - Amph-8	SC10-12 -2 - Amph-9	SC10-5 -2 - Amph-1	SC10-5 -2 - Amph-2	SC10-5 -2 - Amph-3	SC10-5 -2 - Amph-4
SiO_2	55.23	55.32	54.56	56.01	58.29	58.38	58.17	57.54
TiO_2	0.09	0.07	0.10	0.01	0.01	0.04	0.02	0.02
Al_2O_3	1.17	0.99	0.37	0.27	0.08	0.08	0.07	0.08
MnO	0.34	0.30	0.36	0.28	0.31	0.30	0.27	0.28
Mn_2O_3	0.00	0.00	0.00	0.00	0.00	0.00	0.00	0.00
FeO	6.09	7.51	7.72	8.13	3.27	3.10	3.43	3.13
Fe_2O_3	2.50	1.44	1.26	0.58	0.05	0.12	0.15	0.25
MgO	19.61	18.65	18.43	18.74	22.47	22.84	22.64	22.32
CaO	11.80	12.66	12.81	12.99	13.33	13.04	13.00	13.10
Na_2O	0.85	0.43	0.20	0.15	0.08	0.10	0.10	0.12
K_2O	0.41	0.16	0.08	0.06	0.05	0.06	0.10	0.09
H_2O+*	1.95	2.09	2.03	2.11	2.17	2.06	2.08	2.07
F	0.37	0.08	0.20	0.03	0.02	0.26	0.23	0.23
O=F,Cl (calc)	-0.16	-0.03	-0.08	-0.01	-0.01	-0.11	-0.09	-0.10
Total	100.26	99.67	98.03	99.35	100.13	100.27	100.15	99.14
	Number of ions calculated on the basis of 24 (O,OH,F)							
T (ideally 8 apfu)								
Si	7.75	7.83	7.87	7.94	8.00	7.99	7.98	7.98
Al^{iv}	0.19	0.17	0.06	0.05	0.01	0.01	0.01	0.01
Ti^{iv}	0.01	0.01	0.01	0.00			0.00	0.00
$Fe^{3+\,iv}$	0.04		0.06	0.01			0.00	0.01
T subtotal	8.00	8.00	8.00	8.00	8.00	8.00	8.00	8.00
C (ideally 5 apfu)								
Ti^{vi}					0.00	0.00		
Al^{vi}					0.01			
Mn^{3+}								
$Fe^{3+\,vi}$	0.22	0.15	0.08	0.05	0.01	0.01	0.01	0.02
$Mn^{2+\,C}$		0.02	0.03	0.03	0.02			0.00
$Fe^{2+\,C}$	0.68	0.89	0.93	0.96	0.38	0.32	0.36	0.36
Mg	4.10	3.93	3.96	3.96	4.60	4.66	4.63	4.61
C subtotal	5.00	5.00	5.00	5.00	5.00	5.00	5.00	5.00
B (ideally 2 apfu)								
$Mn^{2+\,B}$	0.04	0.01	0.01	0.01	0.02	0.04	0.03	0.03
$Fe^{2+\,B}$	0.04	0.00	0.00	0.00	0.00	0.03	0.04	0.00
Ca	1.78	1.92	1.98	1.97	1.96	1.91	1.91	1.95
Na B	0.14	0.07	0.01	0.02	0.02	0.02	0.02	0.03
B subtotal	2.00	2.00	2.00	2.00	2.00	2.00	2.00	2.00
A (from 0 to 1 apfu)								
Na A	0.09	0.05	0.05	0.02	0.00	0.00	0.01	0.01
K	0.07	0.03	0.02	0.01	0.01	0.01	0.02	0.02
A subtotal	0.16	0.08	0.06	0.03	0.01	0.02	0.02	0.03
O (non-W)	22.00	22.00	22.00	22.00	22.00	22.00	22.00	22.00
W (ideally 2 apfu)								
OH	1.84	1.97	1.91	1.99	1.99	1.89	1.90	1.90
F Cal	0.17	0.04	0.09	0.01	0.01	0.11	0.10	0.10
W subtotal	2.00	2.00	2.00	2.00	2.00	2.00	2.00	2.00
Sum Cations	15.16	15.08	15.06	15.03	15.01	15.02	15.02	15.03

Table C 3. 5: Amphibole EPMA data

Rock Type	Magnetite-rich phoscorite		Carbonatite					
Sample	SC10-5 -2 - Amph - 5	SC10-5 -2 - Amph - 6	SC8-1 -Amph1	SC8-1 -Amph2	SC8-1 -Amph3	SC8-1 -Amph4	SC8-1 -Amph5	SC8-1 -Amph6
SiO_2	58.40	58.03	56.09	56.91	56.84	56.68	56.23	57.41
TiO_2	0.00	0.01	0.16	0.06	0.07	0.14	0.01	0.03
Al_2O_3	0.12	0.14	0.51	0.38	0.42	0.64	0.34	0.12
MnO	0.29	0.32	0.17	0.10	0.15	0.17	0.12	0.22
Mn_2O_3	0.00	0.00	0.00	0.00	0.00	0.00	0.00	0.00
FeO	3.34	3.72	4.51	4.05	4.91	3.86	7.96	3.64
Fe_2O_3	0.01	0.03	4.39	3.61	3.11	4.19	4.50	3.62
MgO	23.01	22.71	18.91	19.92	19.81	19.71	17.19	20.04
CaO	12.66	12.39	8.99	9.62	9.37	9.11	7.47	9.61
Na_2O	0.07	0.11	3.05	2.64	2.41	2.97	3.39	2.69
K_2O	0.06	0.11	0.91	0.99	0.88	1.02	0.74	0.69
H_2O+*	2.10	2.09	2.08	2.08	2.04	2.11	2.03	2.08
F	0.19	0.19	0.13	0.14	0.22	0.06	0.18	0.17
O=F,Cl (calc)	-0.08	-0.08	-0.05	-0.06	-0.09	-0.03	-0.08	-0.07
Total	100.16	99.76	99.85	100.44	100.15	100.62	100.07	100.24
Number of ions calculated on the basis of 24 (O,OH,F)								
T (ideally 8 apfu)								
Si	7.99	7.99	7.89	7.92	7.94	7.88	7.97	7.97
Al ^{iv}	0.01	0.01	0.08	0.06	0.07	0.10	0.03	0.02
Ti ^{iv}			0.02	0.01		0.02		0.00
$Fe^{3+\,iv}$			0.01	0.01		0.00		0.00
T subtotal	8.00	8.00	8.00	8.00	8.00	8.00	8.00	8.00
C (ideally 5 apfu)								
Ti ^{vi}		0.00			0.01		0.00	
Al ^{vi}	0.01	0.01			0.00		0.03	
Mn^{3+}								
$Fe^{3+\,vi}$	0.00	0.00	0.45	0.36	0.33	0.44	0.48	0.37
$Mn^{2+\,C}$			0.02	0.01		0.02		0.03
$Fe^{2+\,C}$	0.29	0.32	0.53	0.47	0.54	0.45	0.86	0.42
Mg	4.70	4.66	3.96	4.13	4.12	4.08	3.63	4.15
C subtotal	5.00	5.00	4.97	4.98	5.00	4.99	5.00	4.97
B (ideally 2 apfu)								
$Mn^{2+\,B}$	0.03	0.04			0.02		0.01	
$Fe^{2+\,B}$	0.09	0.11	0.00	0.00	0.04	0.00	0.08	0.00
Ca	1.86	1.83	1.36	1.43	1.40	1.36	1.13	1.43
Na B	0.02	0.03	0.65	0.57	0.55	0.64	0.77	0.57
B subtotal	2.00	2.00	2.00	2.00	2.00	2.00	2.00	2.00
A (from 0 to 1 apfu)								
Na A	0.00	0.00	0.19	0.15	0.11	0.16	0.16	0.15
K	0.01	0.02	0.16	0.18	0.16	0.18	0.13	0.12
A subtotal	0.01	0.02	0.35	0.32	0.27	0.34	0.29	0.27
O (non-W)	22.00	22.00	22.00	22.00	22.00	22.00	22.00	22.00
W (ideally 2 apfu)								
OH	1.92	1.92	1.94	1.94	1.90	1.97	1.92	1.93
F Cal	0.08	0.08	0.06	0.06	0.10	0.03	0.08	0.07
W subtotal	2.00	2.00	2.00	2.00	2.00	2.00	2.00	2.00
Sum Cations	15.01	15.02	15.32	15.30	15.26	15.33	15.29	15.25

Table C 3. 6: Amphibole EPMA data

Rock Type	Carbonatite							
Sample	SC8-1 -Amph7	SC8-17 -Amph1	SC8-11 -Amph1	SC8-11 -Amph2	SC8-11 -Amph3	SC8-21 -Amph1	SC8-21 -Amph2	SC8-21 -Amph3
SiO_2	57.53	58.16	58.55	58.29	58.87	58.66	58.42	58.57
TiO_2	0.04	0.08	0.07	0.06	0.00	0.05	0.07	0.04
Al_2O_3	0.10	0.21	0.03	0.03	0.02	0.02	0.01	0.03
MnO	0.19	0.19	0.03	0.10	0.07	0.10	0.13	0.12
Mn_2O_3	0.00	0.00	0.00	0.00	0.00	0.00	0.00	0.00
FeO	2.89	5.18	1.34	1.68	1.77	2.92	3.18	3.33
Fe_2O_3	3.37	0.00	0.85	0.97	0.73	0.00	0.00	0.00
MgO	20.59	21.32	23.33	23.03	23.24	22.58	22.45	22.51
CaO	10.29	13.29	12.62	12.15	12.49	13.52	13.27	13.27
Na_2O	2.47	0.07	0.71	0.86	0.73	0.00	0.02	0.01
K_2O	0.64	0.06	0.21	0.32	0.25	0.03	0.04	0.04
H_2O+*	2.04	2.17	2.14	2.11	2.09	2.19	2.19	2.19
F	0.26	0.00	0.11	0.18	0.23	0.01	0.00	0.00
O=F,Cl (calc)	-0.11	0.00	-0.05	-0.08	-0.09	0.00	0.00	0.00
Total	100.30	100.72	99.93	99.70	100.38	100.08	99.78	100.11
Number of ions calculated on the basis of 24 (O,OH,F)								
T (ideally 8 apfu)								
Si	7.96	7.99	7.99	7.99	8.01	8.03	8.02	8.02
Al ^{iv}	0.02	0.01	0.00	0.01				
Ti ^{iv}	0.00		0.00					
$Fe^{3+\,iv}$	0.02							
T subtotal	8.00	8.00	8.00	8.00	8.01	8.03	8.02	8.02
C (ideally 5 apfu)								
Ti ^{vi}		0.01	0.01	0.01		0.01	0.01	0.00
Al ^{vi}		0.02			0.00	0.00	0.00	0.01
Mn^{3+}								
$Fe^{3+\,vi}$	0.33		0.09	0.10	0.07			
$Mn^{2+\,C}$	0.02	0.01	0.00		0.01	0.01	0.02	0.01
$Fe^{2+\,C}$	0.33	0.60	0.15	0.19	0.20	0.33	0.37	0.38
Mg	4.25	4.37	4.75	4.71	4.71	4.60	4.60	4.60
C subtotal	4.94	5.00	5.00	5.00	5.00	4.96	4.99	5.00
B (ideally 2 apfu)								
$Mn^{2+\,B}$		0.01		0.01				0.00
$Fe^{2+\,B}$	0.00	0.00	0.00	0.01	0.00	0.00	0.00	0.00
Ca	1.53	1.96	1.85	1.79	1.82	1.98	1.95	1.95
Na B	0.47	0.02	0.15	0.20	0.18	0.00	0.01	0.00
B subtotal	2.00	1.99	2.00	2.00	2.00	1.98	1.96	1.95
A (from 0 to 1 apfu)								
Na A	0.19	0.00	0.03	0.03	0.01	0.00	0.00	0.00
K	0.11	0.01	0.04	0.06	0.04	0.00	0.01	0.01
A subtotal	0.30	0.01	0.07	0.09	0.06	0.00	0.01	0.01
O (non-W)	22.00	22.00	22.00	22.00	22.00	22.00	22.00	22.00
W (ideally 2 apfu)								
OH	1.89	2.00	1.95	1.92	1.90	2.00	2.00	2.00
F Cal	0.11		0.05	0.08	0.10	0.00		
W subtotal	2.00	2.00	2.00	2.00	2.00	2.00	2.00	2.00
Sum Cations	15.24	15.00	15.07	15.09	15.07	14.97	14.97	14.98

Table C 3. 7: Amphibole EPMA data

Rock Type	Carbonatite				
Sample	SC8-21 -Amph4	SC8-21 -Amph5	SC8-21 -Amph6	SC8-21 -Amph7	SC8-21 -Amph8
SiO_2	58.76	58.42	58.37	59.02	57.68
TiO_2	0.00	0.02	0.04	0.00	0.04
Al_2O_3	0.02	0.04	0.04	0.03	0.50
MnO	0.12	0.16	0.14	0.19	0.08
Mn_2O_3	0.00	0.00	0.00	0.00	0.00
FeO	3.07	3.62	3.36	3.43	1.53
Fe_2O_3	0.00	0.00	0.00	0.00	1.78
MgO	22.71	22.27	22.23	22.96	22.83
CaO	12.96	13.17	13.18	12.59	11.07
Na_2O	0.02	0.02	0.02	0.02	1.37
K_2O	0.04	0.03	0.04	0.04	0.54
H_2O+*	2.19	2.17	2.18	2.19	2.12
F	0.01	0.03	0.02	0.00	0.15
O=F,Cl (calc)	-0.01	-0.01	-0.01	0.00	-0.06
Total	99.89	99.95	99.60	100.47	99.63
	Number of ions calculated on the basis of 24 (O,OH,F)				
T (ideally 8 apfu)					
Si	8.04	8.02	8.03	8.04	7.93
Al^{iv}					0.07
Ti^{iv}					
$Fe^{3+\,iv}$					
T subtotal	8.04	8.02	8.03	8.04	8.00
C (ideally 5 apfu)					
Ti^{vi}		0.00	0.01		0.00
Al^{vi}	0.00	0.01	0.01	0.00	0.01
Mn^{3+}					
$Fe^{3+\,vi}$					0.19
$Mn^{2+\,C}$	0.01	0.02	0.02		
$Fe^{2+\,C}$	0.35	0.42	0.39	0.33	0.12
Mg	4.63	4.56	4.56	4.66	4.68
C subtotal	5.00	5.00	4.97	5.00	5.00
B (ideally 2 apfu)					
$Mn^{2+\,B}$	0.00	0.00		0.02	0.01
$Fe^{2+\,B}$	0.00	0.00	0.00	0.06	0.06
Ca	1.90	1.94	1.94	1.84	1.63
Na B	0.01	0.01	0.01	0.00	0.30
B subtotal	1.91	1.95	1.95	1.92	2.00
A (from 0 to 1 apfu)					
Na A	0.00	0.00	0.00	0.00	0.07
K	0.01	0.01	0.01	0.01	0.10
A subtotal	0.01	0.01	0.01	0.01	0.16
O (non-W)	22.00	22.00	22.00	22.00	22.00
W (ideally 2 apfu)					
OH	2.00	1.99	1.99	2.00	1.94
F Cal	0.01	0.02	0.01		0.06
W subtotal	2.00	2.00	2.00	2.00	2.00
Sum Cations	14.96	14.98	14.97	14.97	15.16

Appendix C.4: Olivine EPMA Data

Table C 4. 1: Olivine EPMA data

Rock type	Carbonatite									
Sample	SC8-11_Olv1	SC8-11_Olv2	SC8-11_Olv2R	SC8-11_Olv3C	SC8-11_Olv4	SC8-11_Olv5	SC8-11_Olv6C	SC8-11_Olv6R	SC8-17_Olv3	SC8-17_Olv6C
SiO_2	39.13	39.52	39.68	38.91	39.66	39.53	39.37	39.48	39.49	39.16
TiO_2	0.00	0.00	0.01	0.04	0.00	0.00	0.02	0.00	0.03	0.01
Al_2O_3	0.00	0.00	0.02	0.00	0.00	0.02	0.04	0.00	0.00	0.00
Fe_2O_3			0.25	0.24		0.90		0.77		0.10
FeO	17.69	17.45	14.75	18.14	17.45	15.10	17.71	15.35	16.72	16.42
MnO	0.32	0.31	0.27	0.30	0.31	0.33	0.35	0.27	0.31	0.35
MgO	42.23	42.72	44.86	41.95	43.11	44.58	42.32	44.38	43.23	43.15
CaO	0.01	0.01	0.04	0.01	0.02	0.05	0.03	0.02	0.00	0.02
Na_2O	0.01	0.02	0.02	0.00	0.03	0.02	0.04	0.04	0.00	0.01
K_2O	0.02	0.04	0.02	0.02	0.03	0.04	0.03	0.03	0.04	0.03
Cr_2O_3	0.03	0.00	0.00	0.01	0.00	0.01	0.00	0.00	0.00	0.00
NiO	0.00	0.00	0.00	0.02	0.03	0.01	0.00	0.03	0.04	0.00
Total	99.45	100.07	99.90	99.64	100.63	100.58	99.90	100.37	99.86	99.24
	Number of ions calculated on the basis of 4 O									
Si	1.00	1.00	1.00	1.00	1.00	0.99	1.00	0.99	1.00	1.00
Ti	0.00	0.00	0.00	0.00	0.00	0.00	0.00	0.00	0.00	0.00
Al	0.00	0.00	0.00	0.00	0.00	0.00	0.00	0.00	0.00	0.00
Cr	0.00	0.00	0.00	0.00	0.00	0.00	0.00	0.00	0.00	0.00
Fe^{3+}	0.00	0.00	0.00	0.00	0.00	0.01	0.00	0.01	0.00	0.00
Fe^{2+}	0.38	0.37	0.31	0.39	0.37	0.32	0.38	0.32	0.35	0.35
Mn	0.01	0.01	0.01	0.01	0.01	0.01	0.01	0.01	0.01	0.01
Mg	1.61	1.62	1.68	1.60	1.62	1.67	1.61	1.66	1.64	1.64
Ca	0.00	0.00	0.00	0.00	0.00	0.00	0.00	0.00	0.00	0.00
Na	0.00	0.00	0.00	0.00	0.00	0.00	0.00	0.00	0.00	0.00
Ni	0.00	0.00	0.00	0.00	0.00	0.00	0.00	0.00	0.00	0.00
K	0.00	0.00	0.00	0.00	0.00	0.00	0.00	0.00	0.00	0.00
Sum Cations	3.00	3.00	3.00	3.00	3.00	2.99	3.00	2.99	3.00	3.00
Fo %	80.68	81.08	84.05	80.11	81.20	83.33	80.65	83.18	81.90	82.04
Fa %	18.96	18.58	15.50	19.43	18.44	15.84	18.94	16.14	17.77	17.51
Te %	0.34	0.33	0.28	0.32	0.33	0.35	0.38	0.29	0.33	0.38

Table C 4. 2: Olivine EPMA data

Rock type	Carbonatite									
Sample	SC8-17_Olv6R	SC8-24_Olv1	SC8-24_Olv2	SC8-24_Olv3	SC8-24_Olv4	SC8-24_Olv5	SC8-24_Olv6	SC8-24_Olv7	SC8-24_Olv8	SC8-24_olv6
SiO_2	39.37	39.69	40.02	39.71	39.74	39.78	39.73	39.59	39.41	39.43
TiO_2	0.00	0.02	0.00	0.00	0.00	0.00	0.00	0.06	0.00	0.00
Al_2O_3	0.00	0.00	0.00	0.02	0.02	0.01	0.01	0.02	0.01	0.00
Fe_2O_3		0.55								
FeO	16.47	14.97	14.58	15.60	15.06	15.50	15.37	15.77	16.21	16.60
MnO	0.31	0.32	0.27	0.31	0.25	0.33	0.31	0.30	0.28	0.33
MgO	43.29	44.79	44.90	43.80	44.32	44.40	44.49	43.83	43.59	43.43
CaO	0.03	0.04	0.05	0.02	0.02	0.06	0.02	0.04	0.02	0.01
Na_2O	0.02	0.04	0.00	0.01	0.05	0.00	0.01	0.04	0.01	0.00
K_2O	0.03	0.02	0.03	0.02	0.03	0.03	0.04	0.04	0.03	0.02
Cr_2O_3	0.00	0.00	0.07	0.00	0.00	0.02	0.04	0.02	0.01	0.17
NiO	0.03	0.00	0.01	0.00	0.00	0.02	0.04	0.03	0.00	0.00
Total	99.55	100.44	99.92	99.50	99.49	100.15	100.05	99.73	99.56	100.00
	Number of ions calculated on the basis of 4 O									
Si	1.00	0.99	1.00	1.01	1.00	1.00	1.00	1.00	1.00	1.00
Ti	0.00	0.00	0.00	0.00	0.00	0.00	0.00	0.00	0.00	0.00
Al	0.00	0.00	0.00	0.00	0.00	0.00	0.00	0.00	0.00	0.00
Cr	0.00	0.00	0.00	0.00	0.00	0.00	0.00	0.00	0.00	0.00
Fe^{3+}	0.00	0.01	0.00	0.00	0.00	0.00	0.00	0.00	0.00	0.00
Fe^{2+}	0.35	0.31	0.31	0.33	0.32	0.33	0.32	0.33	0.34	0.35
Mn	0.01	0.01	0.01	0.01	0.01	0.01	0.01	0.01	0.01	0.01
Mg	1.64	1.67	1.68	1.65	1.67	1.66	1.67	1.65	1.65	1.64
Ca	0.00	0.00	0.00	0.00	0.00	0.00	0.00	0.00	0.00	0.00
Na	0.00	0.00	0.00	0.00	0.00	0.00	0.00	0.00	0.00	0.00
Ni	0.00	0.00	0.00	0.00	0.00	0.00	0.00	0.00	0.00	0.00
K	0.00	0.00	0.00	0.00	0.00	0.00	0.00	0.00	0.00	0.00
Sum Cations	3.00	2.99	3.00	3.00	3.00	3.00	3.00	3.00	3.00	3.00
Fo %	82.10	83.66	84.29	83.04	83.74	83.26	83.47	82.90	82.47	82.03
Fa %	17.52	15.69	15.35	16.59	15.96	16.30	16.18	16.73	17.20	17.59
Te %	0.33	0.34	0.28	0.33	0.27	0.35	0.33	0.33	0.30	0.36

Appendix C.5: Serpentine EPMA Data

Table C 5. 1: Serpentine EPMA data

Rock type	Carbonatite									
Sample	SC-8-11_Serp1	SC-8-11_Serp2	SC-8-11_Serp3	SC-8-11_Serp4	SC-8-11_Serp5	SC-8-21_Serp1	SC-8-21_Serp2	SC-8-21_Serp4	SC-8-21_Serp5	SC-8-21_Serp6
SiO_2	44.38	44.87	44.07	45.74	42.85	43.97	43.31	43.67	43.68	43.90
TiO_2	0.08	0.05	0.01	0.00	0.00	0.12	0.12	0.12	0.00	0.03
Al_2O_3	0.03	0.00	0.03	0.02	0.00	0.41	0.56	0.40	0.37	0.75
Na_2O	0.00	0.00	0.00	0.02	0.07	0.03	0.08	0.05	0.02	0.00
MgO	42.09	41.41	41.56	41.89	42.55	35.05	35.36	35.26	37.04	37.49
FeO	1.99	1.60	2.04	1.68	2.47	8.46	8.41	8.16	7.87	6.33
MnO	0.00	0.01	0.03	0.05	0.10	0.30	0.29	0.34	0.26	0.12
CaO	0.01	0.12	0.08	0.05	0.92	0.01	0.11	0.07	0.06	0.40
K_2O	0.04	0.06	0.09	0.01	0.05	0.79	0.60	0.59	0.05	0.04
NiO	0.00	0.02	0.07	0.09	0.00	0.00	0.02	0.02	0.00	0.00
Cr_2O_3	0.04	0.05	0.00	0.00	0.07	0.00	0.11	0.08	0.00	0.11
H_2O*	11.36	11.81	12.03	10.46	10.91	10.86	11.02	11.23	10.65	10.84
Total	100.00	100.00	100.00	100.00	100.00	100.00	100.00	100.00	100.00	100.00
	Number of ions calculated on the basis of 9 (O, OH)									
Al	0.00	0.00	0.00	0.00	0.00	0.02	0.03	0.02	0.02	0.04
Si	2.09	2.10	2.06	2.16	2.04	2.14	2.10	2.11	2.12	2.11
Ti	0.00	0.00	0.00	0.00	0.00	0.00	0.00	0.00	0.00	0.00
Na	0.00	0.00	0.00	0.00	0.01	0.00	0.01	0.01	0.00	0.00
Mg	2.95	2.89	2.90	2.95	3.02	2.54	2.56	2.54	2.68	2.69
Fe	0.08	0.06	0.08	0.07	0.10	0.34	0.34	0.33	0.32	0.25
Ni	0.00	0.00	0.00	0.00	0.00	0.00	0.00	0.00	0.00	0.00
Mn	0.00	0.00	0.00	0.00	0.00	0.01	0.01	0.01	0.01	0.01
Ca	0.00	0.01	0.00	0.00	0.05	0.00	0.01	0.00	0.00	0.02
K	0.00	0.00	0.01	0.00	0.00	0.05	0.04	0.04	0.00	0.00
Cr	0.00	0.00	0.00	0.00	0.00	0.00	0.00	0.00	0.00	0.00
OH	3.57	3.68	3.76	3.30	3.47	3.52	3.57	3.62	3.44	3.48
Sum	8.69	8.74	8.82	8.49	8.70	8.63	8.68	8.70	8.60	8.60

Appendix C.6: Magnetite EPMA Data

Table C 6. 1: Magnetite EPMA data

Rock type	Glimmerite												
Sample	SC10-4 - 2 - mag -1	SC10-4 - 2-mag-2	SC10-4 - 2 - mag - 4	SC10-4 - 2 - mag - 5	SC10-4 - 2 - mag - 6	SC10-4 - 2 - mag - 7	SC10-4 - 2 - mag - 8	SC10-4 - 2 - mag - 9	SC10-4 - 2 - mag - 10	SC10-4 - 2 - mag - 12	SC10-11-2 - mag - 1	SC10-11-2 - mag - 2	SC10-11-2 - mag - 3
SiO_2	0.09	0.03	0.04	0.06	0.06	0.04	0.03	0.05	0.07	0.09	0.07	0.03	0.03
TiO_2	0.04	0.18	0.03	0.03	0.05	0.09	0.03	0.14	0.04	0.36	0.01	0.01	0.06
Al_2O_3	0.13	0.08	0.12	0.07	0.13	0.10	0.03	0.02	0.10	0.06	0.06	0.15	0.11
Fe_2O_3	68.08	66.87	67.89	67.95	67.71	67.71	68.61	67.75	68.31	66.72	67.74	68.53	67.85
FeO	30.95	30.44	30.76	30.80	30.76	30.78	30.99	30.82	30.97	30.81	30.70	31.04	30.72
MnO	0.04	0.04	0.04	0.02	0.01	0.02	0.03	0.07	0.04	0.09	0.02	0.01	0.04
MgO	0.03	0.03	0.00	0.00	0.00	0.00	0.00	0.00	0.02	0.01	0.00	0.01	0.02
CaO	0.00	0.00	0.00	0.00	0.00	0.00	0.00	0.00	0.00	0.00	0.00	0.00	0.00
NiO	0.04	0.02	0.01	0.00	0.02	0.00	0.01	0.03	0.04	0.00	0.00	0.04	0.01
Cr_2O_3	0.01	0.00	0.04	0.00	0.00	0.00	0.02	0.02	0.05	0.00	0.04	0.04	0.02
V_2O_3	0.01	0.00	0.05	0.00	0.00	0.00	0.00	0.00	0.00	0.07	0.07	0.03	0.04
Total	99.42	97.69	98.97	98.93	98.74	98.74	99.74	98.91	99.65	98.22	98.70	99.89	98.89
Number of ions calculated on the basis of 32 O													
Si	0.00	0.00	0.00	0.00	0.00	0.00	0.00	0.00	0.00	0.00	0.00	0.00	0.00
Ti	0.00	0.01	0.00	0.00	0.00	0.00	0.00	0.00	0.00	0.01	0.00	0.00	0.00
Al	0.01	0.00	0.01	0.00	0.01	0.00	0.00	0.00	0.00	0.00	0.00	0.01	0.00
Cr	0.00	0.00	0.00	0.00	0.00	0.00	0.00	0.00	0.00	0.00	0.00	0.00	0.00
Fe^{3+}	1.98	1.98	1.99	1.99	1.99	1.99	1.99	1.99	1.99	1.97	1.99	1.99	1.99
Fe^{2+}	1.00	1.00	1.00	1.00	1.00	1.00	1.00	1.00	1.00	1.01	1.00	1.00	1.00
Mn	0.00	0.00	0.00	0.00	0.00	0.00	0.00	0.00	0.00	0.00	0.00	0.00	0.00
Mg	0.00	0.00	0.00	0.00	0.00	0.00	0.00	0.00	0.00	0.00	0.00	0.00	0.00
Ni	0.00	0.00	0.00	0.00	0.00	0.00	0.00	0.00	0.00	0.00	0.00	0.00	0.00
Ca	0.00	0.00	0.00	0.00	0.00	0.00	0.00	0.00	0.00	0.00	0.00	0.00	0.00
V	0.00	0.00	0.00	0.00	0.00	0.00	0.00	0.00	0.00	0.00	0.00	0.00	0.00
Sum	3.00	3.00	3.00	3.00	3.00	3.00	3.00	3.00	3.00	3.00	3.00	3.00	3.00

Table C 6. 2: Magnetite EPMA data

Rock type	Glimmerite												
Sample	SC10-11-2-mag-4	SC10-11-2-mag-5	SC10-11-2-mag-6	SC10-11-2-mag-7	SC10-11-2 – mag-8	SC10-11-2 - mag - 9	SC10-11-2 - mag - 10	SC10-11-2 - mag - 11	SC10-11-2 - mag - 12	SC10-22 - 1 - mag - 1	SC10-22 - 1 - mag - 2	SC10-22 - 1 - mag - 3	SC10-22 - 1 - mag - 4
SiO_2	0.09	0.05	0.07	0.05	0.04	0.06	0.04	0.02	0.04	0.08	0.07	0.07	0.06
TiO_2	0.23	0.01	0.05	0.14	0.05	0.03	0.05	0.14	0.08	0.05	0.04	0.02	0.08
Al_2O_3	0.04	0.02	0.03	0.20	0.13	0.24	0.09	0.17	0.18	0.05	0.08	0.01	0.03
Fe_2O_3	67.49	67.63	68.00	67.42	67.75	67.23	67.96	67.61	67.80	68.35	68.11	67.85	67.85
FeO	31.00	30.52	30.85	30.78	30.74	30.49	30.82	30.77	30.76	30.99	30.90	30.69	30.83
MnO	0.06	0.05	0.04	0.04	0.01	0.00	0.01	0.08	0.05	0.07	0.04	0.03	0.01
MgO	0.00	0.02	0.00	0.01	0.02	0.07	0.00	0.00	0.03	0.01	0.02	0.02	0.02
CaO	0.00	0.03	0.02	0.00	0.00	0.00	0.03	0.00	0.02	0.02	0.01	0.00	0.00
NiO	0.00	0.00	0.00	0.00	0.00	0.00	0.00	0.00	0.00	0.00	0.00	0.00	0.00
Cr_2O_3	0.08	0.05	0.09	0.02	0.05	0.03	0.01	0.02	0.00	0.02	0.06	0.03	0.06
V_2O_3	0.09	0.02	0.05	0.02	0.00	0.04	0.00	0.03	0.04	0.00	0.00	0.08	0.00
Total	99.08	98.38	99.19	98.69	98.78	98.19	99.00	98.85	98.98	99.65	99.32	98.81	98.95
Number of ions calculated on the basis of 32 O													
Si	0.00	0.00	0.00	0.00	0.00	0.00	0.00	0.00	0.00	0.00	0.00	0.00	0.00
Ti	0.01	0.00	0.00	0.00	0.00	0.00	0.00	0.00	0.00	0.00	0.00	0.00	0.00
Al	0.00	0.00	0.00	0.01	0.01	0.01	0.00	0.01	0.01	0.00	0.00	0.00	0.00
Cr	0.00	0.00	0.00	0.00	0.00	0.00	0.00	0.00	0.00	0.00	0.00	0.00	0.00
Fe^{3+}	1.97	1.99	1.99	1.98	1.99	1.98	1.99	1.98	1.98	1.99	1.99	1.99	1.99
Fe^{2+}	1.01	1.00	1.00	1.00	1.00	1.00	1.00	1.00	1.00	1.00	1.00	1.00	1.00
Mn	0.00	0.00	0.00	0.00	0.00	0.00	0.00	0.00	0.00	0.00	0.00	0.00	0.00
Mg	0.00	0.00	0.00	0.00	0.00	0.00	0.00	0.00	0.00	0.00	0.00	0.00	0.00
Ni	0.00	0.00	0.00	0.00	0.00	0.00	0.00	0.00	0.00	0.00	0.00	0.00	0.00
Ca	0.00	0.00	0.00	0.00	0.00	0.00	0.00	0.00	0.00	0.00	0.00	0.00	0.00
V	0.00	0.00	0.00	0.00	0.00	0.00	0.00	0.00	0.00	0.00	0.00	0.00	0.00
Sum	3.00	3.00	3.00	3.00	3.00	3.00	3.00	3.00	3.00	3.00	3.00	3.00	3.00

Table C 6. 3: Magnetite EPMA data

Rock type	Glimmerite												
Sample	SC10-22-1-mag-5	SC10-22 -1-mag- 6	SC10-22-1-mag-7	SC10-22 - 1 - mag - 8	SC10-22 - 1 - mag - 9	SC10-22 - 1 - mag - 10	SC10-22 - 1 - mag - 11	SC10-22 - 1 - mag - 12	SC10-22 - 1 - mag - 13	SC10-22 - 1 - mag - 14	SC10-22 - 1 - mag - 15	SC10-22 - 1 - mag - 16	SC10-22 - 1-mag - 17
SiO_2	0.06	0.10	0.03	0.05	0.10	0.10	0.01	0.08	0.04	0.05	0.05	0.02	0.03
TiO_2	0.04	0.02	0.16	0.19	0.04	0.78	0.02	0.08	0.68	0.04	0.05	0.09	0.04
Al_2O_3	0.05	0.03	0.06	0.03	0.06	0.09	0.12	0.06	0.03	0.10	0.04	0.05	0.01
Fe_2O_3	68.22	68.39	67.99	68.29	67.73	65.47	67.90	67.50	66.71	67.83	68.00	68.24	67.73
FeO	30.90	31.03	30.93	31.16	30.77	30.79	30.60	30.69	31.06	30.77	30.80	30.85	30.57
MnO	0.03	0.01	0.01	0.02	0.02	0.30	0.06	0.04	0.27	0.01	0.03	0.00	0.02
MgO	0.03	0.03	0.02	0.03	0.02	0.05	0.02	0.01	0.01	0.01	0.01	0.07	0.02
CaO	0.00	0.00	0.04	0.03	0.02	0.05	0.00	0.01	0.00	0.00	0.02	0.00	0.01
NiO	0.02	0.00	0.00	0.00	0.07	0.00	0.03	0.02	0.00	0.01	0.00	0.01	0.06
Cr_2O_3	0.03	0.03	0.00	0.04	0.04	0.01	0.02	0.00	0.00	0.06	0.03	0.04	0.01
V_2O_3	0.00	0.00	0.04	0.00	0.06	0.01	0.04	0.03	0.01	0.02	0.00	0.00	0.00
Total	99.37	99.65	99.28	99.83	98.93	97.66	98.80	98.50	98.80	98.89	99.02	99.37	98.47
	Number of ions calculated on the basis of 32 O												
Si	0.00	0.00	0.00	0.00	0.00	0.00	0.00	0.00	0.00	0.00	0.00	0.00	0.00
Ti	0.00	0.00	0.00	0.01	0.00	0.02	0.00	0.00	0.02	0.00	0.00	0.00	0.00
Al	0.00	0.00	0.00	0.00	0.00	0.00	0.01	0.00	0.00	0.00	0.00	0.00	0.00
Cr	0.00	0.00	0.00	0.00	0.00	0.00	0.00	0.00	0.00	0.00	0.00	0.00	0.00
Fe^{3+}	1.99	1.99	1.98	1.98	1.98	1.94	1.99	1.99	1.96	1.99	1.99	1.99	1.99
Fe^{2+}	1.00	1.00	1.00	1.00	1.00	1.01	1.00	1.00	1.01	1.00	1.00	1.00	1.00
Mn	0.00	0.00	0.00	0.00	0.00	0.01	0.00	0.00	0.01	0.00	0.00	0.00	0.00
Mg	0.00	0.00	0.00	0.00	0.00	0.00	0.00	0.00	0.00	0.00	0.00	0.00	0.00
Ni	0.00	0.00	0.00	0.00	0.00	0.00	0.00	0.00	0.00	0.00	0.00	0.00	0.00
Ca	0.00	0.00	0.00	0.00	0.00	0.00	0.00	0.00	0.00	0.00	0.00	0.00	0.00
V	0.00	0.00	0.00	0.00	0.00	0.00	0.00	0.00	0.00	0.00	0.00	0.00	0.00
Sum	3.00	3.00	3.00	3.00	3.00	3.00	3.00	3.00	3.00	3.00	3.00	3.00	3.00

Table C 6. 4: Magnetite EPMA data

Rock type	Clinopyroxenite												
Sample	SC10-6 - 1-mag-1	SC10-6-1-mag-2C	SC10-6 - 1 - mag-3	SC10-6 - 1 - mag - 4	SC10-6 - 1 - mag - 5	SC10-6 - 1 - mag - 6	SC10-6 - 1 - mag - 7	SC10-6 - 1 - mag - 8	SC10-6 - 1 - mag - 9	SC10-6 - 1 - mag - 10	SC10-6 - 1 - mag - 11	SC10-6 - 1 - mag - 12	SC10-6 - 1 - mag - 13 D
SiO_2	0.04	0.08	0.04	0.05	0.06	0.04	0.04	0.11	0.04	0.02	0.07	0.08	0.05
TiO_2	0.37	0.05	0.01	1.26	0.05	0.05	0.06	0.08	0.09	0.05	0.04	0.06	0.06
Al_2O_3	0.08	0.06	0.07	0.07	0.10	0.04	0.05	0.14	0.03	0.04	0.03	0.10	0.04
Fe_2O_3	67.20	67.92	67.60	66.99	67.81	67.88	68.32	67.83	67.61	67.78	67.66	67.99	67.95
FeO	30.79	30.84	30.39	31.81	30.62	30.67	30.89	30.73	30.53	30.55	30.62	30.82	30.82
MnO	0.23	0.05	0.12	0.58	0.05	0.08	0.04	0.09	0.07	0.03	0.05	0.08	0.03
MgO	0.03	0.00	0.04	0.10	0.08	0.00	0.03	0.12	0.04	0.04	0.02	0.03	0.01
CaO	0.00	0.00	0.00	0.00	0.01	0.00	0.02	0.01	0.00	0.00	0.01	0.00	0.00
NiO	0.00	0.00	0.00	0.02	0.00	0.00	0.00	0.00	0.00	0.01	0.00	0.00	0.00
Cr_2O_3	0.00	0.02	0.00	0.04	0.02	0.02	0.00	0.02	0.00	0.01	0.04	0.00	0.06
V_2O_3	0.00	0.00	0.00	0.07	0.00	0.00	0.00	0.00	0.00	0.00	0.00	0.00	0.00
Total	98.74	99.03	98.27	100.98	98.79	98.78	99.45	99.11	98.39	98.53	98.52	99.15	99.04
	Number of ions calculated on the basis of 32 O												
Si	0.00	0.00	0.00	0.00	0.00	0.00	0.00	0.00	0.00	0.00	0.00	0.00	0.00
Ti	0.01	0.00	0.00	0.04	0.00	0.00	0.00	0.00	0.00	0.00	0.00	0.00	0.00
Al	0.00	0.00	0.00	0.00	0.00	0.00	0.00	0.01	0.00	0.00	0.00	0.00	0.00
Cr	0.00	0.00	0.00	0.00	0.00	0.00	0.00	0.00	0.00	0.00	0.00	0.00	0.00
Fe^{3+}	1.97	1.99	1.99	1.92	1.99	1.99	1.99	1.98	1.99	1.99	1.99	1.99	1.99
Fe^{2+}	1.00	1.00	1.00	1.01	1.00	1.00	1.00	1.00	1.00	1.00	1.00	1.00	1.00
Mn	0.01	0.00	0.00	0.02	0.00	0.00	0.00	0.00	0.00	0.00	0.00	0.00	0.00
Mg	0.00	0.00	0.00	0.01	0.00	0.00	0.00	0.01	0.00	0.00	0.00	0.00	0.00
Ni	0.00	0.00	0.00	0.00	0.00	0.00	0.00	0.00	0.00	0.00	0.00	0.00	0.00
Ca	0.00	0.00	0.00	0.00	0.00	0.00	0.00	0.00	0.00	0.00	0.00	0.00	0.00
V	0.00	0.00	0.00	0.00	0.00	0.00	0.00	0.00	0.00	0.00	0.00	0.00	0.00
Sum	3.00	3.00	3.00	3.00	3.00	3.00	3.00	3.00	3.00	3.00	3.00	3.00	3.00

Table C 6. 5: Magnetite EPMA data

Rock type	Clinopyroxenite		Magnetite-rich phoscorite										
Sample	SC10-6 - 1-mag-14	SC10-6-1- mag-15	SC10-12 -4-mag-1	SC10-12 - 4 - mag - 2	SC10-12 - 4 - mag - 3	SC10-12 - 4 - mag - 4	SC10-12 - 4 - mag - 5	SC10-12 - 4 - mag - 6	SC10-12 - 4 - mag - 7	SC10-12 - 4 - mag - 8 L	SC10-12 - 4-mag-10	SC10-5 - 2-mag-1	SC10-5 - 2 -mag-2
SiO_2	0.08	0.05	0.06	0.03	0.09	0.08	0.05	0.06	0.04	0.07	0.07	0.06	0.02
TiO_2	0.04	0.02	0.10	0.04	0.04	0.05	0.24	0.04	0.04	0.42	0.10	0.25	0.05
Al_2O_3	0.07	0.03	0.08	0.07	0.02	0.00	0.03	0.01	0.02	0.00	0.05	0.31	0.10
Fe_2O_3	68.45	68.18	68.11	68.17	67.27	68.37	67.84	69.39	67.64	67.53	67.69	67.76	68.53
FeO	30.96	30.66	30.99	30.85	30.55	31.04	31.02	31.44	30.63	31.20	30.78	31.09	30.85
MnO	0.07	0.07	0.04	0.03	0.02	0.00	0.04	0.00	0.00	0.07	0.04	0.14	0.09
MgO	0.05	0.07	0.00	0.00	0.00	0.00	0.02	0.01	0.00	0.01	0.01	0.04	0.05
CaO	0.00	0.00	0.00	0.00	0.01	0.00	0.02	0.00	0.15	0.01	0.01	0.00	0.00
NiO	0.00	0.04	0.08	0.00	0.01	0.00	0.03	0.00	0.00	0.00	0.00	0.04	0.00
Cr_2O_3	0.04	0.00	0.03	0.02	0.02	0.02	0.02	0.03	0.07	0.00	0.02	0.00	0.02
V_2O_3	0.00	0.00	0.00	0.00	0.00	0.06	0.00	0.00	0.00	0.03	0.03	0.03	0.00
Total	99.75	99.13	99.49	99.20	98.02	99.63	99.30	100.99	98.59	99.34	98.80	99.71	99.70
			Number of ions calculated on the basis of 32 O										
Si	0.00	0.00	0.00	0.00	0.00	0.00	0.00	0.00	0.00	0.00	0.00	0.00	0.00
Ti	0.00	0.00	0.00	0.00	0.00	0.00	0.01	0.00	0.00	0.01	0.00	0.01	0.00
Al	0.00	0.00	0.00	0.00	0.00	0.00	0.00	0.00	0.00	0.00	0.00	0.01	0.00
Cr	0.00	0.00	0.00	0.00	0.00	0.00	0.00	0.00	0.00	0.00	0.00	0.00	0.00
Fe^{3+}	1.99	1.99	1.98	1.99	1.99	1.99	1.98	1.99	1.99	1.97	1.98	1.97	1.99
Fe^{2+}	1.00	1.00	1.00	1.00	1.00	1.00	1.01	1.00	1.00	1.01	1.00	1.00	1.00
Mn	0.00	0.00	0.00	0.00	0.00	0.00	0.00	0.00	0.00	0.00	0.00	0.00	0.00
Mg	0.00	0.00	0.00	0.00	0.00	0.00	0.00	0.00	0.00	0.00	0.00	0.00	0.00
Ni	0.00	0.00	0.00	0.00	0.00	0.00	0.00	0.00	0.00	0.00	0.00	0.00	0.00
Ca	0.00	0.00	0.00	0.00	0.00	0.00	0.00	0.00	0.01	0.00	0.00	0.00	0.00
V	0.00	0.00	0.00	0.00	0.00	0.00	0.00	0.00	0.00	0.00	0.00	0.00	0.00
Sum	3.00	3.00	3.00	3.00	3.00	3.00	3.00	3.00	3.00	3.00	3.00	3.00	3.00

Table C 6. 6: Magnetite EPMA data

Rock type	Magnetite-rich phoscorite												
Sample	SC10-5-2-mag-3	SC10-5 - 2 - mag - 4	SC10-5 - 2 - mag - 5	SC10-5 - 2 - mag - 6	SC10-5 - 2 - mag - 7	SC10-5 - 2 - mag - 8	SC10-5 - 2 - mag - 9	SC10-5 - 2 - mag - 10	SC10-5 - 2 - mag - 11	SC10-5 - 2 - mag - 12	SC10-12-2 - mag - 2	SC10-12-2 - mag - 3	SC10-12-2 - mag - 4
SiO_2	0.07	0.04	0.08	0.10	0.11	0.07	0.03	0.07	0.06	0.06	0.01	0.02	0.08
TiO_2	0.09	0.07	0.00	0.03	0.06	0.07	0.21	0.04	0.03	0.03	0.01	0.04	0.03
Al_2O_3	0.01	0.14	0.05	0.09	0.05	0.14	0.16	0.05	0.16	0.10	0.06	0.05	0.05
Fe_2O_3	68.63	68.64	68.35	67.88	67.75	68.16	67.34	68.46	68.19	68.75	67.71	68.53	68.05
FeO	31.05	31.09	30.90	30.80	30.81	30.93	30.78	30.90	30.79	31.05	30.45	30.89	30.88
MnO	0.05	0.09	0.08	0.09	0.06	0.04	0.06	0.06	0.14	0.08	0.02	0.04	0.00
MgO	0.06	0.01	0.01	0.00	0.00	0.06	0.02	0.07	0.05	0.03	0.04	0.04	0.01
CaO	0.01	0.00	0.01	0.00	0.00	0.00	0.01	0.00	0.00	0.00	0.00	0.00	0.00
NiO	0.00	0.00	0.00	0.00	0.00	0.00	0.00	0.00	0.00	0.01	0.01	0.00	0.00
Cr_2O_3	0.00	0.00	0.04	0.02	0.00	0.07	0.00	0.00	0.04	0.00	0.00	0.01	0.02
V_2O_3	0.00	0.00	0.00	0.00	0.00	0.00	0.00	0.00	0.00	0.00	0.00	0.00	0.00
Total	99.97	100.08	99.52	98.99	98.84	99.53	98.60	99.64	99.45	100.11	98.32	99.62	99.12
	Number of ions calculated on the basis of 32 O												
Si	0.00	0.00	0.00	0.00	0.00	0.00	0.00	0.00	0.00	0.00	0.00	0.00	0.00
Ti	0.00	0.00	0.00	0.00	0.00	0.00	0.01	0.00	0.00	0.00	0.00	0.00	0.00
Al	0.00	0.01	0.00	0.00	0.00	0.01	0.01	0.00	0.01	0.00	0.00	0.00	0.00
Cr	0.00	0.00	0.00	0.00	0.00	0.00	0.00	0.00	0.00	0.00	0.00	0.00	0.00
Fe^{3+}	1.99	1.99	1.99	1.99	1.99	1.98	1.98	1.99	1.98	1.99	2.00	1.99	1.99
Fe^{2+}	1.00	1.00	1.00	1.00	1.00	1.00	1.00	1.00	1.00	1.00	1.00	1.00	1.00
Mn	0.00	0.00	0.00	0.00	0.00	0.00	0.00	0.00	0.00	0.00	0.00	0.00	0.00
Mg	0.00	0.00	0.00	0.00	0.00	0.00	0.00	0.00	0.00	0.00	0.00	0.00	0.00
Ni	0.00	0.00	0.00	0.00	0.00	0.00	0.00	0.00	0.00	0.00	0.00	0.00	0.00
Ca	0.00	0.00	0.00	0.00	0.00	0.00	0.00	0.00	0.00	0.00	0.00	0.00	0.00
V	0.00	0.00	0.00	0.00	0.00	0.00	0.00	0.00	0.00	0.00	0.00	0.00	0.00
Sum	3.00	3.00	3.00	3.00	3.00	3.00	3.00	3.00	3.00	3.00	3.00	3.00	3.00

Table C 6. 7: Magnetite EPMA data

Rock type	Magnetite-rich phoscorite										
Sample	SC10-12-2 - mag - 5	SC10-12-2 - mag - 8	SC10-12-2 - mag - 9	SC10-12-2 - mag - 10	SC10-12-2 - mag - 11	SC10-12-2 - mag - 12	SC10-12-2 - mag - 13	SC10-12-2 - mag - 14	SC10-12-2 - mag - 15	SC10-12-2 - mag - 16	SC10-12-2 - mag - 17
SiO_2	0.03	0.03	0.05	0.01	0.04	0.04	0.02	0.01	0.05	0.02	0.06
TiO_2	0.08	0.02	0.00	0.01	0.06	0.03	0.05	0.07	0.05	0.06	0.09
Al_2O_3	0.12	0.01	0.02	0.05	0.10	0.06	0.04	0.10	0.04	0.10	0.04
Fe_2O_3	67.52	67.09	68.20	68.00	68.26	67.53	68.00	67.72	68.44	68.02	67.71
FeO	30.65	30.29	30.79	30.66	30.96	30.52	30.63	30.63	30.99	30.77	30.77
MnO	0.00	0.02	0.02	0.02	0.00	0.01	0.11	0.03	0.04	0.02	0.00
MgO	0.01	0.00	0.02	0.01	0.01	0.03	0.01	0.02	0.00	0.02	0.01
CaO	0.00	0.01	0.02	0.00	0.00	0.01	0.00	0.00	0.00	0.00	0.00
NiO	0.00	0.00	0.04	0.00	0.00	0.00	0.04	0.00	0.00	0.00	0.00
Cr_2O_3	0.00	0.00	0.06	0.01	0.02	0.00	0.03	0.01	0.04	0.01	0.02
V_2O_3	0.00	0.00	0.00	0.02	0.04	0.02	0.00	0.00	0.00	0.00	0.01
Total	98.41	97.47	99.22	98.79	99.46	98.26	98.91	98.59	99.64	99.02	98.70
	Number of ions calculated on the basis of 32 O										
Si	0.00	0.00	0.00	0.00	0.00	0.00	0.00	0.00	0.00	0.00	0.00
Ti	0.00	0.00	0.00	0.00	0.00	0.00	0.00	0.00	0.00	0.00	0.00
Al	0.01	0.00	0.00	0.00	0.00	0.00	0.00	0.00	0.00	0.00	0.00
Cr	0.00	0.00	0.00	0.00	0.00	0.00	0.00	0.00	0.00	0.00	0.00
Fe^{3+}	1.99	2.00	1.99	2.00	1.99	1.99	1.99	1.99	1.99	1.99	1.99
Fe^{2+}	1.00	1.00	1.00	1.00	1.00	1.00	1.00	1.00	1.00	1.00	1.00
Mn	0.00	0.00	0.00	0.00	0.00	0.00	0.00	0.00	0.00	0.00	0.00
Mg	0.00	0.00	0.00	0.00	0.00	0.00	0.00	0.00	0.00	0.00	0.00
Ni	0.00	0.00	0.00	0.00	0.00	0.00	0.00	0.00	0.00	0.00	0.00
Ca	0.00	0.00	0.00	0.00	0.00	0.00	0.00	0.00	0.00	0.00	0.00
V	0.00	0.00	0.00	0.00	0.00	0.00	0.00	0.00	0.00	0.00	0.00
Sum	3.00	3.00	3.00	3.00	3.00	3.00	3.00	3.00	3.00	3.00	3.00

Appendix C.7: Apatite EPMA Data

Table C 7. 1: Apatite EPMA data

Rock type	Glimmerite											
Sample	SC10-32.4_Apatite1	SC10-32.4_Apatite2L	SC10-32.4_Apatite2D	SC10-32.4_Apatite3	SC10-32.4_Apatite4	SC10-32.4_Apatite5D	SC10-32.4_Apatite5L	SC10-32.4_Apatite6L	SC10-32.4_Apatite6M	SC10-32.4_Apatite6D	SC10-32.4_Apatite7	SC10-32.4_Apatite8
SiO_2	0.36	0.86	0.17	0.73	0.76	0.36	1.16	1.34	0.76	0.17	0.87	1.14
FeO	0.05	0.03	0.01	0.08	0.07	0.20	0.07	0.12	0.16	0.18	0.07	0.13
MnO	0.08	0.06	0.01	0.03	0.04	0.04	0.02	0.05	0.04	0.01	0.03	0.02
MgO	0.00	0.00	0.00	0.00	0.00	0.01	0.02	0.00	0.02	0.00	0.02	0.03
CaO	51.83	50.77	52.12	51.10	50.57	51.41	49.12	50.21	50.79	51.69	50.70	50.20
P_2O_5	41.45	38.87	42.13	40.03	40.65	41.13	38.94	38.60	39.80	40.28	39.97	39.40
Ce_2O_3	0.41	1.37	0.27	0.77	0.86	0.28	1.18	1.30	0.72	0.41	1.07	1.15
SrO	1.67	1.73	1.78	1.80	1.76	1.79	1.72	1.70	1.74	1.77	1.71	1.76
F	2.08	2.07	1.98	2.23	1.91	2.05	2.02	1.91	2.02	2.21	2.32	1.70
Cl	0.38	0.43	0.28	0.40	0.35	0.33	0.34	0.45	0.43	0.20	0.35	0.48
Subtotal	98.31	96.19	98.74	97.17	96.98	97.60	94.59	95.66	96.48	96.92	97.12	96.01
O = F, Cl	0.96	0.97	0.90	1.03	0.88	0.94	0.93	0.90	0.95	0.97	1.06	0.82
Total	97.35	95.21	97.85	96.14	96.09	96.66	93.66	94.76	95.54	95.95	96.06	95.19
Number of ions calculated on the basis of 26 (O,OH,Cl,F)												
P	6.13	5.95	6.19	6.02	6.10	6.13	6.01	5.92	6.03	6.07	6.01	6.01
Si	0.06	0.16	0.03	0.13	0.14	0.06	0.21	0.24	0.14	0.03	0.15	0.20
Mg	0.00	0.00	0.00	0.00	0.00	0.00	0.00	0.00	0.01	0.00	0.00	0.01
Ca	9.70	9.83	9.69	9.73	9.61	9.69	9.60	9.75	9.73	9.86	9.65	9.69
Ce	0.03	0.09	0.02	0.05	0.06	0.02	0.08	0.09	0.05	0.03	0.07	0.08
Fe	0.01	0.00	0.00	0.01	0.01	0.03	0.01	0.02	0.02	0.03	0.01	0.02
Mn	0.01	0.01	0.00	0.00	0.01	0.01	0.00	0.01	0.01	0.00	0.00	0.00
F	1.15	1.19	1.09	1.25	1.07	1.14	1.17	1.09	1.14	1.24	1.30	0.97
Cl	0.11	0.13	0.08	0.12	0.11	0.10	0.10	0.14	0.13	0.06	0.11	0.15
Sr	0.17	0.18	0.18	0.19	0.18	0.18	0.18	0.18	0.18	0.18	0.18	0.18
Sum	17.53	17.72	17.45	17.69	17.45	17.54	17.55	17.62	17.61	17.68	17.67	17.49

Table C 7. 2: Apatite EPMA data

Rock type	Glimmerite	Magnetite-rich phoscorite									
Sample	SC10-32.4_Apatite9	SC10-12.1_Apatite1	SC10-12.1_Apatite2	SC10-12.1_Apatite3	SC10-12.1_Apatite4	SC10-12.1_Apatite5	SC10-12.1_Apatite6	SC10-12.1_Apatite7	SC10-12.1_Apatite8	SC10-12.1_Apatite9	SC10-12.1_Apatite10
SiO_2	0.51	0.26	0.21	0.17	0.13	0.13	0.06	0.13	0.18	0.11	0.15
FeO	0.07	0.01	0.02	0.02	0.09	0.06	0.05	0.00	0.02	0.05	0.00
MnO	0.06	0.13	0.08	0.05	0.17	0.02	0.01	0.04	0.05	0.06	0.06
MgO	0.01	0.02	0.01	0.04	0.05	0.06	0.01	0.01	0.00	0.03	0.01
CaO	50.70	51.11	51.66	51.47	51.40	51.61	52.10	51.07	51.36	50.74	51.91
P_2O_5	39.96	41.12	40.01	41.22	41.60	41.19	40.94	40.58	40.62	41.25	40.96
Ce_2O_3	0.75	0.57	0.47	0.47	0.63	0.35	0.48	0.56	0.60	0.65	0.43
SrO	1.69	2.50	2.60	2.29	2.57	2.31	2.47	2.39	2.29	2.91	2.45
F	2.15	2.56	2.20	2.54	2.69	2.63	2.57	2.30	2.67	2.50	2.75
Cl	0.47	0.44	0.50	0.31	0.50	0.31	0.33	0.33	0.33	0.37	0.30
Subtotal	96.37	98.70	97.75	98.56	99.83	98.66	99.02	97.41	98.11	98.66	99.01
O = F, Cl	1.01	1.18	1.04	1.14	1.24	1.18	1.16	1.04	1.20	1.14	1.22
Total	95.35	97.52	96.72	97.43	98.59	97.48	97.86	96.36	96.91	97.53	97.78
Number of ions calculated on the basis of 26 (O,OH,Cl,F)											
P	6.06	6.09	6.02	6.10	6.10	6.09	6.06	6.10	6.06	6.12	6.05
Si	0.09	0.05	0.04	0.03	0.02	0.02	0.01	0.02	0.03	0.02	0.03
Mg	0.00	0.00	0.00	0.01	0.01	0.01	0.00	0.00	0.00	0.01	0.00
Ca	9.73	9.58	9.84	9.64	9.53	9.66	9.76	9.71	9.70	9.53	9.71
Ce	0.05	0.04	0.03	0.03	0.04	0.02	0.03	0.04	0.04	0.04	0.03
Fe	0.01	0.00	0.00	0.00	0.01	0.01	0.01	0.00	0.00	0.01	0.00
Mn	0.01	0.02	0.01	0.01	0.02	0.00	0.00	0.01	0.01	0.01	0.01
F	1.22	1.41	1.23	1.40	1.47	1.45	1.42	1.29	1.49	1.39	1.52
Cl	0.14	0.13	0.15	0.09	0.15	0.09	0.10	0.10	0.10	0.11	0.09
Sr	0.17	0.25	0.27	0.23	0.26	0.23	0.25	0.25	0.23	0.30	0.25
Sum	17.65	17.83	17.87	17.78	17.88	17.83	17.89	17.75	17.89	17.82	17.93

Table C 7. 3: Apatite EPMA data

Rock type	Clinopyroxenite											
Sample	SC10-2.2_Apatite1	SC10-2.2_Apatite2	SC10-2.2_Apatite3	SC10-2.2_Apatite4	SC10-2.2_Apatite5	SC10-2.2_Apatite6	SC10-2.2_Apatite7	SC10-2.2_Apatite8	SC10-2.2_Apatite9	SC10-2.2_Apatite10	SC10-24.2_Apatite1	SC10-24.2_Apatite2
SiO_2	1.13	0.40	0.86	1.43	0.92	0.25	1.17	1.24	1.25	0.84	0.24	0.32
FeO	0.02	0.00	0.08	0.08	0.06	0.04	0.10	0.12	0.08	0.10	0.00	0.00
MnO	0.00	0.06	0.04	0.01	0.00	0.00	0.00	0.03	0.04	0.06	0.08	0.02
MgO	0.00	0.03	0.00	0.00	0.00	0.00	0.00	0.03	0.00	0.01	0.06	0.05
CaO	51.74	53.29	52.55	51.44	51.86	52.85	51.55	52.01	52.10	51.82	51.85	51.79
P_2O_5	38.93	41.13	39.50	38.90	38.81	41.30	39.46	39.79	40.01	40.92	40.99	40.89
Ce_2O_3	0.25	0.00	0.41	0.38	0.21	0.15	0.31	0.47	0.36	0.28	0.63	0.95
SrO	0.60	0.73	0.60	0.57	0.70	1.00	0.76	0.55	0.66	0.75	1.49	1.32
F	2.72	3.07	2.86	3.12	3.57	2.89	2.64	3.13	2.74	3.49	1.81	1.73
Cl	0.05	0.05	0.04	0.02	0.13	0.02	0.11	0.04	0.05	0.07	0.52	0.60
Subtotal	95.43	98.75	96.94	95.94	96.25	98.51	96.09	97.41	97.28	98.33	97.67	97.67
O = F, Cl	1.15	1.30	1.21	1.32	1.53	1.22	1.14	1.33	1.16	1.48	0.88	0.86
Total	94.27	97.44	95.72	94.62	94.71	97.29	94.95	96.08	96.12	96.84	96.79	96.81
Number of ions calculated on the basis of 26 (O,OH,Cl,F)												
P	5.91	6.02	5.92	5.87	5.86	6.07	5.95	5.91	5.95	6.00	6.12	6.11
Si	0.20	0.07	0.15	0.25	0.16	0.04	0.21	0.22	0.22	0.14	0.04	0.06
Mg	0.00	0.01	0.00	0.00	0.00	0.00	0.00	0.01	0.00	0.00	0.02	0.01
Ca	9.95	9.87	9.97	9.82	9.90	9.83	9.83	9.78	9.80	9.62	9.80	9.80
Ce	0.02	0.00	0.03	0.02	0.01	0.01	0.02	0.03	0.02	0.02	0.04	0.06
Fe	0.00	0.00	0.01	0.01	0.01	0.01	0.01	0.02	0.01	0.01	0.00	0.00
Mn	0.00	0.01	0.01	0.00	0.00	0.00	0.00	0.00	0.01	0.01	0.01	0.00
F	1.54	1.68	1.60	1.76	2.01	1.59	1.49	1.74	1.52	1.91	1.01	0.96
Cl	0.02	0.01	0.01	0.01	0.04	0.01	0.03	0.01	0.01	0.02	0.16	0.18
Sr	0.06	0.07	0.06	0.06	0.07	0.10	0.08	0.06	0.07	0.08	0.15	0.13
Sum	17.76	17.82	17.82	17.87	18.14	17.75	17.70	17.83	17.68	17.89	17.49	17.45

Table C 7. 4: Apatite EPMA data

Rock type	Clinopyroxenite	Carbonatite										
Sample	SC10-24.2_Apatite3	SC10-24.2_Apatite4	SC10-24.2_Apatite5	SC10-24.2_Apatite6	SC10-24.2_Apatite7	SC10-24.2_Apatite8	SC10-24.2_Apatite9	SC10-24.2_Apatite10D	SC10-24.2_Apatite10L	SC-8-11_Apatite1	SC-8-11_Apatite2	SC-8-11_Apatite3
SiO_2	0.23	0.33	0.23	0.33	0.29	0.24	0.28	0.35	0.63	0.15	0.14	0.11
FeO	0.03	0.02	0.00	0.07	0.08	0.07	0.01	0.01	0.04	0.04	0.04	0.06
MnO	0.04	0.03	0.12	0.05	0.00	0.04	0.06	0.06	0.15	0.02	0.03	0.04
MgO	0.05	0.04	0.03	0.04	0.10	0.04	0.00	0.02	0.05	0.04	0.01	0.03
CaO	51.64	51.60	51.95	51.46	51.62	51.89	51.55	51.58	50.88	52.98	53.16	53.70
P_2O_5	40.68	40.72	40.99	41.41	40.62	41.24	40.56	39.50	39.10	42.40	42.25	41.65
Ce_2O_3	0.63	0.56	0.65	0.95	0.53	0.79	0.60	0.72	0.99	0.46	0.47	0.34
SrO	1.43	1.38	1.41	1.39	1.52	1.53	1.39	1.47	1.48	0.77	0.82	0.80
F	2.00	2.21	2.14	2.01	1.86	1.97	2.10	2.05	1.79	1.89	1.73	1.71
Cl	0.43	0.50	0.45	0.49	0.47	0.48	0.51	0.44	0.49	0.24	0.38	0.27
Subtotal	97.16	97.40	97.97	98.18	97.09	98.29	97.06	96.20	95.58	99.00	99.02	98.70
O = F, Cl	0.94	1.05	1.00	0.96	0.89	0.93	1.00	0.96	0.86	0.85	0.81	0.78
Total	96.22	96.35	96.96	97.22	96.20	97.35	96.06	95.24	94.72	98.15	98.20	97.92
Number of ions calculated on the basis of 26 (O,OH,Cl,F)												
P	6.10	6.09	6.10	6.14	6.10	6.12	6.09	6.02	6.00	6.19	6.18	6.13
Si	0.04	0.06	0.04	0.06	0.05	0.04	0.05	0.06	0.11	0.03	0.02	0.02
Mg	0.01	0.01	0.01	0.01	0.03	0.01	0.00	0.00	0.01	0.01	0.00	0.01
Ca	9.80	9.76	9.78	9.65	9.81	9.74	9.80	9.94	9.89	9.79	9.84	10.00
Ce	0.04	0.04	0.04	0.06	0.03	0.05	0.04	0.05	0.07	0.03	0.03	0.02
Fe	0.00	0.00	0.00	0.01	0.01	0.01	0.00	0.00	0.01	0.01	0.01	0.01
Mn	0.01	0.00	0.02	0.01	0.00	0.01	0.01	0.01	0.02	0.00	0.00	0.01
F	1.12	1.24	1.19	1.11	1.05	1.09	1.18	1.17	1.02	1.03	0.94	0.94
Cl	0.13	0.15	0.14	0.14	0.14	0.14	0.15	0.13	0.15	0.07	0.11	0.08
Sr	0.15	0.14	0.14	0.14	0.16	0.16	0.14	0.15	0.16	0.08	0.08	0.08
Sum	17.56	17.63	17.60	17.47	17.53	17.53	17.60	17.69	17.59	17.30	17.30	17.37

Table C 7. 5: Apatite EPMA data

Rock type	Carbonatite											
Sample	SC-8-11_Apatite4	SC-8-11_Apatite5	SC-8-11_Apatite6	SC-8-11_Apatite7	SC-8-11_Apatite8	SC-8-11_Apatite9	SC-8-11_Apatite10	SC-8-21_Apatite1	SC-8-21_Apatite2	SC-8-21_Apatite3	SC-8-21_Apatite4	SC-8-21_Apatite5
SiO_2	0.16	0.14	0.15	0.09	0.17	0.10	0.08	0.12	0.08	0.14	0.19	0.14
FeO	0.03	0.01	0.05	0.00	0.00	0.02	0.03	0.00	0.07	0.01	0.00	0.04
MnO	0.00	0.00	0.00	0.04	0.07	0.00	0.01	0.03	0.02	0.00	0.00	0.00
MgO	0.04	0.01	0.06	0.03	0.03	0.06	0.04	0.06	0.05	0.06	0.04	0.02
CaO	52.73	53.13	52.70	53.08	53.34	53.35	52.98	53.38	52.87	53.46	52.60	52.96
P_2O_5	42.02	41.32	41.14	42.32	41.44	41.82	42.01	41.71	41.62	41.67	41.95	41.66
Ce_2O_3	0.63	0.48	0.40	0.46	0.66	0.41	0.62	0.66	0.42	0.51	0.46	0.47
SrO	0.80	0.76	0.82	0.76	0.87	0.76	0.82	0.75	0.71	0.74	0.67	0.69
F	1.90	1.77	1.57	1.73	1.52	1.58	1.90	1.50	1.48	1.44	1.49	1.31
Cl	0.33	0.29	0.42	0.40	0.37	0.46	0.46	0.37	0.31	0.33	0.32	0.36
Subtotal	98.66	97.90	97.30	98.90	98.46	98.56	98.95	98.58	97.64	98.34	97.72	97.65
O = F, Cl	0.88	0.81	0.76	0.82	0.72	0.77	0.90	0.72	0.69	0.68	0.70	0.63
Total	97.78	97.09	96.55	98.08	97.74	97.80	98.05	97.86	96.94	97.66	97.02	97.02
Number of ions calculated on the basis of 26 (O,OH,Cl,F)												
P	6.17	6.13	6.14	6.19	6.13	6.16	6.16	6.15	6.18	6.15	6.20	6.18
Si	0.03	0.03	0.03	0.02	0.03	0.02	0.01	0.02	0.01	0.02	0.03	0.03
Mg	0.01	0.00	0.02	0.01	0.01	0.02	0.01	0.01	0.01	0.01	0.01	0.01
Ca	9.80	9.97	9.95	9.83	9.98	9.94	9.83	9.96	9.93	9.99	9.84	9.95
Ce	0.04	0.03	0.03	0.03	0.04	0.03	0.04	0.04	0.03	0.03	0.03	0.03
Fe	0.00	0.00	0.01	0.00	0.00	0.00	0.00	0.00	0.01	0.00	0.00	0.01
Mn	0.00	0.00	0.00	0.01	0.01	0.00	0.00	0.00	0.00	0.00	0.00	0.00
F	1.04	0.98	0.88	0.95	0.84	0.87	1.04	0.83	0.82	0.79	0.82	0.73
Cl	0.10	0.09	0.12	0.12	0.11	0.13	0.14	0.11	0.09	0.10	0.10	0.11
Sr	0.08	0.08	0.08	0.08	0.09	0.08	0.08	0.08	0.07	0.07	0.07	0.07
Sum	17.35	17.38	17.34	17.29	17.32	17.31	17.40	17.28	17.23	17.25	17.17	17.17

Table C 7. 6: Apatite EPMA data

Rock type	Carbonatite											
Sample	SC-8-21_Apatite6	SC-8-21_Apatite7	SC-8-21_Apatite8	SC-8-21_Apatite9	SC-8-21_Apatite10	SC-8-1_Apatite1	SC-8-1_Apatite2	SC-8-1_Apatite3	SC-8-1_Apatite4	SC-8-1_Apatite5	SC-8-1_Apatite6	SC-8-1_Apatite7
SiO_2	0.14	0.13	0.10	0.11	0.20	0.08	0.59	0.35	0.25	0.11	0.12	0.13
FeO	0.00	0.09	0.03	0.00	0.04	0.07	0.00	0.08	0.05	0.02	0.15	0.12
MnO	0.03	0.01	0.02	0.00	0.00	0.02	0.00	0.01	0.05	0.01	0.00	0.06
MgO	0.03	0.07	0.02	0.05	0.06	0.03	0.04	0.04	0.05	0.07	0.00	0.03
CaO	52.90	53.20	53.57	53.10	52.97	52.96	50.81	51.79	52.07	52.44	52.43	52.02
P_2O_5	42.62	42.29	41.92	41.31	41.89	41.92	40.09	39.72	40.26	41.11	42.06	40.94
Ce_2O_3	0.45	0.50	0.29	0.44	0.52	0.66	1.07	0.82	0.66	0.82	0.68	0.59
SrO	0.61	0.66	0.63	0.73	0.71	1.09	1.13	1.11	1.14	1.17	1.09	1.13
F	1.30	1.50	1.81	1.61	1.68	1.51	1.28	1.41	1.29	0.99	1.84	1.48
Cl	0.36	0.33	0.37	0.34	0.38	0.31	0.36	0.42	0.29	0.30	0.30	0.28
Subtotal	98.43	98.79	98.74	97.69	98.45	98.63	95.36	95.75	96.11	97.01	98.66	96.78
O = F, Cl	0.63	0.71	0.84	0.76	0.79	0.71	0.62	0.69	0.61	0.48	0.84	0.69
Total	97.80	98.08	97.89	96.93	97.66	97.92	94.74	95.06	95.50	96.53	97.82	96.09
Number of ions calculated on the basis of 26 (O,OH,Cl,F)												
P	6.25	6.19	6.15	6.14	6.16	6.18	6.12	6.07	6.11	6.18	6.18	6.16
Si	0.02	0.02	0.02	0.02	0.04	0.01	0.11	0.06	0.05	0.02	0.02	0.02
Mg	0.01	0.02	0.00	0.01	0.02	0.01	0.01	0.01	0.01	0.02	0.00	0.01
Ca	9.81	9.86	9.94	9.99	9.86	9.88	9.82	10.01	10.01	9.97	9.76	9.90
Ce	0.03	0.03	0.02	0.03	0.03	0.04	0.07	0.05	0.04	0.05	0.04	0.04
Fe	0.00	0.01	0.00	0.00	0.01	0.01	0.00	0.01	0.01	0.00	0.02	0.02
Mn	0.00	0.00	0.00	0.00	0.00	0.00	0.00	0.00	0.01	0.00	0.00	0.01
F	0.71	0.82	0.99	0.89	0.92	0.83	0.73	0.80	0.73	0.55	1.01	0.83
Cl	0.11	0.10	0.11	0.10	0.11	0.09	0.11	0.13	0.09	0.09	0.09	0.08
Sr	0.06	0.07	0.06	0.07	0.07	0.11	0.12	0.12	0.12	0.12	0.11	0.12
Sum	17.06	17.20	17.36	17.33	17.29	17.27	17.21	17.39	17.29	17.13	17.34	17.30

Table C 7. 7: Apatite EPMA data

Rock type	Carbonatite												
Sample	SC-8-1_Apatite8	SC-8-1_Apatite9	SC-8-1_Apatite10	SC-8-4_Apatite1	SC-8-4_Apatite2	SC-8-4_Apatite3	SC-8-4_Apatite4	SC-8-4_Apatite5	SC-8-4_Apatite6	SC-8-4_Apatite7	SC-8-4_Apatite8	SC-8-4_Apatite9	SC-8-4_Apatite10
SiO_2	0.16	0.08	0.15	0.00	0.21	0.20	0.19	0.14	0.18	0.16	0.11	0.12	0.23
FeO	0.05	0.08	0.08	0.09	0.11	0.02	0.01	0.07	0.00	0.02	0.00	0.00	0.03
MnO	0.01	0.00	0.01	0.00	0.11	0.02	0.00	0.00	0.00	0.00	0.00	0.00	0.01
MgO	0.03	0.01	0.00	0.02	0.05	0.06	0.05	0.06	0.06	0.02	0.02	0.00	0.00
CaO	52.23	52.08	52.52	42.64	51.05	51.40	51.83	52.47	52.08	51.90	51.73	52.05	51.99
P_2O_5	41.35	41.70	40.96	39.39	40.11	41.25	39.92	41.16	41.51	41.88	41.75	41.72	41.52
Ce_2O_3	0.41	0.47	0.77	0.67	0.86	1.02	0.77	0.61	0.68	0.75	0.67	0.93	0.96
SrO	1.11	1.13	1.12	0.67	0.79	0.79	0.78	0.83	0.83	0.82	0.85	0.80	0.89
F	1.53	1.57	1.70	1.79	1.86	1.74	1.94	1.55	1.74	2.07	2.26	1.85	2.36
Cl	0.31	0.27	0.27	0.39	0.35	0.39	0.27	0.40	0.35	0.20	0.40	0.38	0.16
Subtotal	97.19	97.40	97.57	85.67	95.48	96.88	95.76	97.30	97.43	97.83	97.79	97.85	98.14
O = F, Cl	0.71	0.72	0.78	0.84	0.86	0.82	0.88	0.74	0.81	0.92	1.04	0.86	1.03
Total	96.47	96.68	96.79	84.82	94.62	96.06	94.88	96.56	96.62	96.91	96.75	96.98	97.11
Number of ions calculated on the basis of 26 (O,OH,Cl,F)													
P	6.17	6.21	6.12	6.52	6.11	6.18	6.07	6.15	6.17	6.19	6.18	6.18	6.13
Si	0.03	0.01	0.03	0.00	0.04	0.03	0.03	0.02	0.03	0.03	0.02	0.02	0.04
Mg	0.01	0.00	0.00	0.01	0.01	0.02	0.01	0.02	0.02	0.01	0.00	0.00	0.00
Ca	9.87	9.81	9.93	8.93	9.85	9.74	9.98	9.92	9.80	9.71	9.68	9.76	9.72
Ce	0.03	0.03	0.05	0.05	0.06	0.07	0.05	0.04	0.04	0.05	0.04	0.06	0.06
Fe	0.01	0.01	0.01	0.01	0.02	0.00	0.00	0.01	0.00	0.00	0.00	0.00	0.00
Mn	0.00	0.00	0.00	0.00	0.02	0.00	0.00	0.00	0.00	0.00	0.00	0.00	0.00
F	0.85	0.87	0.95	1.11	1.06	0.97	1.10	0.86	0.96	1.14	1.25	1.02	1.30
Cl	0.09	0.08	0.08	0.13	0.11	0.12	0.08	0.12	0.10	0.06	0.12	0.11	0.05
Sr	0.11	0.12	0.11	0.08	0.08	0.08	0.08	0.09	0.08	0.08	0.09	0.08	0.09
Sum	17.28	17.25	17.40	16.90	17.43	17.29	17.50	17.31	17.31	17.35	17.47	17.32	17.49

Appendix D: Whole-rock XRF and Trace Element LA-ICPMS

Appendix D.1: Whole-rock XRF and Trace Element LA-ICPMS Data of all Schiel Complex Rocks Analysed

Table D 1: Whole-rock XRF and trace element ICPMS data for all samples analysed

Sample	SC10-1.2	SC10-2.2	SC10-18.3	SC10-21.2	SC10-24.1	SC10-30.4	SC10-4.3.1	SC10-4.3.2	SC10-5.2	SC10-7.1	SC10-12.3	SC10-14.4	SC10-15.3
Rock type	**Glimmerite**						**Clinopyroxenite**		**Mt-rich Phoscorite**				
SiO_2	41.73	44.35	39.08	40.64	36.40	26.94	44.39	44.30	23.74	25.95	22.99	30.14	18.50
TiO_2	0.30	0.17	0.29	0.53	0.70	0.52	0.27	0.27	0.80	0.76	1.01	1.21	1.23
Al_2O_3	9.36	7.08	8.25	7.32	8.54	6.75	3.48	3.47	1.37	5.97	1.48	3.07	0.75
Fe_2O_3	13.99	13.86	13.42	12.80	12.74	17.93	24.65	24.94	40.50	41.05	37.90	39.11	47.85
MnO	0.18	0.25	0.21	0.24	0.10	0.16	0.35	0.36	0.29	0.19	0.26	0.30	0.24
MgO	16.81	13.86	13.44	12.46	20.11	12.88	7.37	7.35	7.04	12.88	7.61	10.20	6.18
CaO	7.39	13.07	13.22	14.19	7.27	16.72	16.59	17.25	17.99	5.07	18.24	9.22	16.89
K_2O	6.84	4.40	5.24	4.71	7.41	5.33	0.98	0.96	0.50	4.82	0.98	2.47	0.49
Na_2O	0.12	0.35	0.30	0.39	0.07	0.14	1.07	1.03	0.26	0.05	0.21	0.24	0.13
P_2O_5	1.09	0.70	3.76	2.55	3.98	10.94	0.17	0.17	7.01	2.13	8.68	0.33	7.87
Cr_2O_3	bdl	bdl	bdl	bdl	bdl	bdl	bdl	bdl	bdl	bdl	bdl	bdl	bdl
L.O.I.	1.19	0.97	2.45	4.87	1.75	0.79	0.46	-0.15	-0.34	0.20	-0.34	4.22	-1.11
Sum	99.00	99.06	99.66	100.70	99.07	99.10	99.78	99.95	99.16	99.07	99.02	100.51	99.02
Sc	24.03	49.75	23.96	42.83	12.52	10.80	19.00	18.86	14.80	12.34	8.38	21.65	12.34
V	17.35	18.36	39.42	49.95	45.95	92.30	53.45	54.55	217.25	238.25	210.80	257.55	295.95
Cr	29.40	25.65	18.70	19.60	23.80	15.00	19.45	17.10	16.55	17.75	24.50	22.75	19.00
Co	50.55	44.00	51.90	48.95	56.25	46.75	37.08	37.35	43.80	59.80	50.05	62.25	45.25
Ni	13.32	11.00	11.02	14.88	24.30	17.75	8.89	12.89	17.32	15.46	21.50	23.90	24.20
Cu	12.51	7.88	8.24	6.61	8.48	9.13	7.03	7.46	6.36	8.84	9.15	6.47	5.82
Zn	254.10	251.95	305.30	273.70	179.85	265.05	216.25	220.40	295.95	276.40	239.25	304.95	311.70
Rb	604.50	381.25	376.65	262.65	415.50	275.80	27.44	27.84	36.10	341.80	67.25	167.95	32.68
Sr	301.85	778.00	1092.50	1725.00	974.50	3106.00	1341.00	1339.50	1648.00	713.50	3160.50	443.00	2544.00
Y	162.85	127.60	90.55	70.70	41.40	91.85	96.35	94.50	135.85	42.90	127.60	27.38	96.20
Zr	581.50	755.00	71.85	340.30	19.45	40.95	522.00	526.00	262.60	213.15	48.75	577.50	99.90
Nb	144.15	123.25	41.22	41.26	24.15	23.57	18.04	18.02	8.51	25.62	21.77	23.57	7.59
Mo	0.53	0.54	0.47	0.46	0.26	0.41	0.92	1.02	1.76	1.25	1.56	1.45	2.31
Cs	23.96	16.09	15.21	10.38	12.16	9.20	0.91	0.97	2.07	15.40	3.05	7.00	1.73
Ba	2245.50	1979.50	2199.00	2736.00	1785.50	3293.00	1138.50	1155.50	120.10	1199.50	266.35	1050.00	70.95
La	68.90	408.25	211.30	301.25	180.65	439.40	613.50	604.00	231.70	226.25	513.50	77.70	345.05
Ce	274.80	1040.50	547.40	679.00	435.00	1000.00	1184.50	1156.50	532.50	481.00	1165.50	149.55	831.00
Pr	46.95	131.70	76.55	84.20	54.80	125.55	129.45	129.00	67.55	56.55	143.80	18.12	106.80
Nd	266.60	543.50	348.70	343.20	220.40	504.50	477.30	478.00	298.70	220.90	594.50	73.00	455.65
Sm	78.90	104.85	73.90	62.90	40.60	94.85	83.80	81.90	71.50	39.75	111.30	14.60	86.75
Eu	12.45	17.26	15.93	12.81	8.68	20.08	15.04	14.91	17.78	7.86	24.18	3.24	17.45
Gd	68.80	68.40	53.15	42.55	27.36	63.40	51.95	51.65	60.95	26.43	75.70	11.54	60.15
Tb	7.81	7.22	5.42	4.23	2.69	6.06	5.45	5.44	6.67	2.61	7.61	1.36	5.93
Dy	38.75	33.21	23.33	18.53	11.22	25.39	25.11	25.00	31.66	11.05	33.51	6.67	25.67
Ho	5.91	4.68	3.31	2.63	1.55	3.49	3.63	3.65	4.82	1.62	4.71	1.01	3.56
Er	13.41	10.51	7.10	5.57	3.31	7.04	8.57	8.38	11.01	3.52	10.44	2.35	7.79
Tm	1.49	1.22	0.74	0.61	0.35	0.72	1.06	1.08	1.26	0.39	1.20	0.31	0.85
Yb	8.01	6.91	3.96	3.38	1.78	3.61	6.87	6.70	6.87	2.08	6.37	1.98	4.53
Lu	0.96	0.91	0.50	0.45	0.20	0.46	1.04	1.07	0.88	0.27	0.80	0.33	0.60
Hf	11.50	15.35	2.94	9.59	0.92	1.25	14.18	14.22	7.60	6.39	1.86	16.05	3.30
Ta	7.51	5.75	2.53	3.61	2.19	1.89	1.25	1.27	0.81	3.13	1.92	2.56	1.34
Pb	188.65	84.20	19.47	26.50	9.69	22.52	69.00	70.55	17.71	26.23	23.73	13.76	16.03
Th	1528.50	521.00	98.80	129.10	45.30	89.35	331.75	323.70	47.10	103.00	106.35	60.00	89.95
U	514.00	273.35	17.33	19.41	6.11	11.10	72.30	75.80	17.36	25.93	20.29	12.21	22.75
$^1Eu/Eu_N$*	0.50	0.58	0.74	0.71	0.75	0.74	0.65	0.65	0.80	0.70	0.76	0.74	0.70

Table D 2: Whole-rock XRF and trace element ICPMS data for all samples analysed (cont.)

Sample	SC09-05	SC09-09	SC8-2	SC8-5	SC8-8	SC8-11	SC8-13	SC8-14	SC8-15	SC8-16	SC8-19	SC8-23
Rock type	Olv-bearing glimmerite		Carbonatite									
SiO_2	37.42	36.94	3.27	0.91	4.42	2.84	31.54	3.85	5.62	2.81	2.16	3.07
TiO_2	0.52	0.43	0.34	0.03	0.20	0.17	0.22	0.11	0.42	0.28	0.27	0.26
Al_2O_3	6.77	8.58	0.05	0.10	0.17	0.39	7.70	0.57	0.19	0.12	0.03	0.23
Fe_2O_3	11.68	10.87	7.75	1.01	6.31	3.89	4.02	2.60	13.53	8.81	7.84	7.28
MnO	0.19	0.15	0.11	0.13	0.11	0.12	0.11	0.10	0.12	0.11	0.10	0.09
MgO	14.92	19.92	4.78	2.56	5.61	3.56	3.15	4.43	6.01	3.63	3.62	3.59
CaO	14.66	8.39	46.24	52.90	45.83	48.82	26.83	48.32	41.26	46.88	47.21	47.19
K_2O	5.29	7.26	0.05	0.07	0.15	0.30	5.73	0.50	0.16	0.09	0.02	0.14
Na_2O	0.33	0.13	0.04	0.04	0.05	0.05	0.57	0.03	0.03	0.05	0.04	0.06
P_2O_5	4.33	4.94	2.02	0.56	4.78	2.63	3.39	4.68	5.49	4.92	3.95	7.49
Cr_2O_3	bdl	bdl	bdl	bdl	bdl	bdl	bdl	bdl	bdl	bdl	bdl	bdl
L.O.I.	2.95	1.70	34.61	40.94	31.85	36.31	15.90	33.94	26.99	32.24	33.92	29.71
Sum Of Conc.	99.06	99.31	99.26	99.25	99.48	99.08	99.16	99.13	99.82	99.94	99.16	99.11
Sc	23.34	15.365	8.72	5.01	8.06	7.26	12.90	7.00	10.88	8.90	8.49	8.58
V	52.1	29.565	56.20	1.73	38.95	27.15	34.45	14.37	102.15	75.85	66.70	66.25
Cr	16.65	21.75	13.20	13.55	9.78	10.15	24.05	11.28	13.45	11.70	10.33	10.53
Co	45.95	51.45	15.95	1.91	15.08	9.08	9.99	8.36	27.74	15.88	13.82	14.60
Ni	16.015	28.1	11.87	2.89	10.46	9.17	14.26	9.72	13.16	8.28	10.22	20.25
Cu	8.59	7.28	7.83	6.72	8.21	6.81	9.53	7.17	5.85	6.71	7.02	5.73
Zn	246.05	232.45	62.55	16.25	51.10	39.75	65.05	36.35	81.55	52.75	51.35	49.75
Rb	303.2	374.6	1.93	2.29	5.42	11.40	104.80	21.60	6.22	3.34	0.62	5.64
Sr	2297.5	1542	4565.00	4865.00	4500.00	6515.00	4986.00	5650.00	4885.00	4745.00	4745.00	4753.50
Y	84.5	71.65	88.05	91.35	93.35	109.60	83.40	106.15	88.10	93.60	92.80	107.60
Zr	488.05	288.25	196.70	4.26	206.85	258.90	220.60	424.00	745.50	39.76	1487.00	29.26
Nb	26.04	24.685	2.15	0.68	1.48	1.96	3.98	1.94	4.39	2.49	3.35	2.33
Mo	0.3755	0.48	0.33	0.25	0.26	0.24	0.42	0.24	0.32	0.25	0.23	0.26
Cs	10.635	11.93	0.19	0.18	0.25	0.44	1.25	0.68	0.43	0.14	0.06	0.45
Ba	3144.5	2638	2008.50	1429.50	1477.50	1990.50	8930.00	1435.50	905.00	1030.50	1133.50	1109.50
La	389	358	303.50	301.50	321.90	403.50	370.25	374.50	316.90	302.95	297.40	357.75
Ce	866	807	639.00	601.50	696.00	822.50	778.00	799.50	717.00	678.50	661.00	813.00
Pr	105.25	98	78.25	71.35	84.95	97.95	93.10	99.10	89.75	85.35	81.50	100.85
Nd	421.5	393.2	321.50	297.00	353.40	397.00	371.85	408.00	380.05	356.65	342.50	427.00
Sm	78.95	71.5	62.10	56.55	68.30	74.65	69.00	78.65	71.40	69.30	66.40	83.10
Eu	16.845	14.875	13.78	12.67	15.42	16.95	15.62	17.39	15.89	15.06	15.07	18.20
Gd	53.7	47.55	47.25	41.15	51.01	55.85	47.85	58.60	51.85	51.20	49.00	61.85
Tb	5.23	4.47	4.76	4.45	5.11	5.57	4.68	5.79	5.05	5.05	4.90	5.97
Dy	22.94	19.265	21.05	19.82	22.78	25.15	20.78	25.70	21.97	22.68	22.06	26.80
Ho	3.18	2.67	3.09	3.11	3.29	3.72	2.93	3.72	3.08	3.31	3.21	3.90
Er	6.82	5.53	6.76	6.82	7.02	8.29	6.43	8.05	6.71	7.18	6.96	8.09
Tm	0.685	0.565	0.74	0.72	0.77	0.92	0.71	0.86	0.72	0.74	0.77	0.84
Yb	3.87	2.945	3.87	4.18	3.99	4.95	3.83	4.53	3.71	4.16	4.04	4.70
Lu	0.5115	0.38	0.56	0.56	0.58	0.66	0.56	0.61	0.48	0.56	0.56	0.62
Hf	12.705	6.3	4.31	0.14	4.44	5.60	5.22	8.44	14.62	1.44	29.42	1.08
Ta	2.258	2.3145	0.30	0.08	0.26	0.23	0.34	0.28	0.85	0.34	0.79	0.27
Pb	25.195	22.51	21.47	27.30	19.51	25.50	23.30	19.46	17.57	17.91	14.53	15.23
Th	116.6	120.45	11.29	7.66	16.10	16.28	27.43	17.41	21.05	14.09	10.70	19.46
U	10.335	10.215	1.20	0.55	2.06	1.69	4.28	2.93	3.91	1.63	2.48	3.58
[1]Eu/Eu_N*	0.75	0.73	0.75	0.76	0.76	0.77	0.79	0.75	0.76	0.74	0.77	0.74

[1]$Eu/Eu_N^* = Eu_N/(0.5x(Sm_N+Gd_N))$

Appendix D.2: Analytical and Instrument Conditions for the Trace Element ICPMS Analyses

Analytical Conditions:

Laser:

- Resonetics 193nm Excimer laser
- Energy: 6 J/cm^2
- Frequency: 10 Hz
- Spot: 2 spots of 228µm per sample
- Ablation gas: He @ 0.35L/min
- Ablation time: 15 sec background, 35 sec ablation

ICP-MS:

- Agilent 7700
- Carrier gas: 0,9L/min Ar + 0.007L/min Nitrogen
- 1:10 sample: Flux ratio

Reference standard values:

- BHVO glass - Jochum, K. P., Nohl, U., Herwig, K., Lammel, E., Stoll, B. and Hofmann, A. W. (2005), GeoReM: A New Geochemical Database for Reference Materials and Isotopic Standards. Geostandards and Geoanalytical Research, 29: 333–338. doi: 10.1111/j.1751-908X.2005.tb00904.x
- BHVO powder - Jochum, K. P., Weis, U., Schwager, B., Stoll, B., Wilson, S. A., Haug, G. H., Andreae, M. O. and Enzweiler, J. (2016), Reference Values Following ISO Guidelines for Frequently Requested Rock Reference Materials. Geostandards and Geoanalytical Research. doi: 10.1111/j.1751-908X.2015.00392.x

Appendix D.3: ICPMS Instrument Conditions:

Table D 3. 1: ICPMS Instrument Conditions

Analysis sequence	**Fusion Traces**
ICP-MS Instrument connected to laser	Agilent 7700
ICP-MS Software	Mass Hunter v 4.01
ICP-MS Settings	
RF Power (W)	1400
Carrier gas (L/min)	0,8
Sample depth (mm)	5
He Cell gas flow (ml/min)	n/a
H2 Cell gas flow (ml/min)	n/a
O2 Cell gas flow (ml/min)	n/a
Detector type	Photo multiplier
Laser Ablation Instrument	193nm Resolution M50 SE Excimer
Controlling Software	Geostar v 8.93
Laser Settings	
Frequency (Hz)	10
Fluence (J/cm2)	6
Spot size (µm)	228
Ablation gas (He) flow (ml/min)	350
Additional gas (N2) flow (ml/min)	7
Background acquisition time (sec)	15
Ablation time (sec)	35
Washout time (sec)	20
Calibration stds	NIST 610
Quality Control stds	BCR, BHVO
Calibration method	Standard - Sample bracketing every 15 - 20 samples
Data processing software	Iolite v 3.34

Appendix D.4: ICPMS Reference Values:

Table D 4. 1: BHVO glass reference values

Values in ppm	Instrument DL	Fusion Method DL	Certified BHVO glass	BHVO - 1	BHVO - 2	BHVO - 3	BHVO - 4	BHVO - 5	BHVO - 6	BHVO - 7	BHVO - 8	**Average Analysed**	**% Deviation**
Sc	0,08	0,58	33,00	31,38	32,67	32,23	31,89	31,60	31,68	30,65	31,23	**31,67**	**4,04**
V	0,02	0,17	308,00	304,10	307,20	309,90	310,60	309,70	309,50	307,50	306,10	**308,08**	**0,02**
Cr	0,59	6,86	293,00	266,30	269,30	274,30	271,10	275,70	274,00	269,00	268,20	**270,99**	**7,51**
Co	0,01	0,14	44,00	41,76	42,62	41,38	41,73	42,04	41,27	40,19	41,24	**41,53**	**5,62**
Ni	0,53	6,15	116,00	116,10	118,90	116,70	118,30	117,90	117,70	116,30	118,00	**117,49**	**1,28**
Cu	0,04	0,35	127,00	126,10	122,30	120,50	121,20	120,60	123,90	120,30	119,60	**121,81**	**4,08**
Zn	0,07	1,83	102,00	104,30	106,90	107,60	106,40	107,50	109,40	112,20	111,60	**108,24**	**6,12**
Rb	0,03	0,34	9,20	8,68	9,26	8,92	8,83	8,80	9,04	8,85	8,75	**8,89**	**3,36**
Sr	0,00	0,04	396,00	371,30	379,70	379,30	378,80	377,80	381,80	378,60	382,00	**378,66**	**4,38**
Y	0,00	0,01	26,00	21,99	23,19	22,95	23,39	22,97	23,04	23,04	22,95	**22,94**	**11,77**
Zr	0,00	0,04	170,00	147,60	153,40	153,50	152,80	152,20	154,60	152,80	154,10	**152,63**	**10,22**
Nb	0,00	0,03	18,30	16,14	16,15	16,15	16,11	15,85	16,07	15,93	15,91	**16,04**	**12,36**
Mo	0,01	0,07	3,80	3,72	3,85	3,98	3,87	3,99	3,89	3,99	3,97	**3,91**	**2,82**
Cs	0,02	0,14	0,10	0,09	0,09	0,09	0,09	0,09	0,10	0,10	0,09	**0,09**	**10,86**
Ba	0,01	0,30	131,00	123,90	124,50	125,40	126,30	123,00	127,70	125,50	125,70	**125,25**	**4,39**
La	0,00	0,02	15,20	14,09	13,97	14,25	14,20	14,07	14,22	13,94	13,84	**14,07**	**7,42**
Ce	0,00	0,91	37,60	34,24	35,02	34,66	34,75	34,24	34,64	33,95	33,89	**34,42**	**8,45**
Pr	0,00	0,01	5,35	4,77	4,83	4,95	4,90	4,78	4,88	4,79	4,74	**4,83**	**9,70**
Nd	0,00	0,07	24,50	21,98	22,30	23,01	22,99	22,84	22,81	23,04	23,03	**22,75**	**7,14**
Sm	0,01	0,07	6,10	5,52	5,68	5,89	5,73	5,69	5,88	5,83	5,72	**5,74**	**5,86**
Eu	0,00	0,02	2,07	1,86	1,88	1,87	1,91	1,88	1,89	1,86	1,92	**1,88**	**9,02**
Gd	0,00	0,05	6,16	5,64	5,77	5,93	5,99	5,98	5,94	5,92	6,15	**5,92**	**3,98**
Tb	0,00	0,03	0,92	0,81	0,82	0,81	0,84	0,84	0,84	0,80	0,81	**0,82**	**10,72**
Dy	0,00	0,03	5,28	4,77	4,96	5,00	4,89	4,93	5,01	4,92	4,92	**4,92**	**6,73**
Ho	0,00	0,01	0,98	0,87	0,89	0,91	0,91	0,89	0,92	0,87	0,87	**0,89**	**8,58**
Er	0,05	0,02	2,56	2,30	2,37	2,41	2,35	2,39	2,41	2,32	2,35	**2,36**	**7,76**
Tm	0,00	0,07	0,34	0,30	0,30	0,30	0,29	0,30	0,30	0,29	0,30	**0,30**	**11,99**
Yb	0,00	0,03	2,01	1,79	1,81	1,80	1,90	1,84	1,81	1,91	1,84	**1,84**	**8,63**
Lu	0,00	0,01	0,28	0,25	0,25	0,26	0,25	0,25	0,26	0,25	0,25	**0,25**	**10,38**
Hf	0,00	0,02	4,32	3,98	4,13	4,07	4,28	4,15	4,28	4,18	4,11	**4,15**	**4,09**
Ta	0,00	0,02	1,15	0,96	0,98	0,99	1,00	0,98	1,00	0,98	0,96	**0,98**	**14,87**
Pb	0,02	0,05	1,70	1,61	1,73	1,72	1,75	1,77	1,80	1,80	1,72	**1,74**	**2,15**
Th	0,00	0,01	1,22	1,11	1,14	1,12	1,14	1,14	1,14	1,10	1,12	**1,13**	**7,30**
U	0,00	0,03	0,40	0,38	0,41	0,40	0,40	0,40	0,41	0,38	0,38	**0,39**	**2,05**

Table D 4. 2: BCR glass reference values

Values in ppm	Instrument DL	Fusion Method DL	Certified BCR glass	BCR - 1	BCR - 2	BCR - 3	BCR - 4	BCR - 5	BCR - 6	BCR - 7	BCR - 8	**Average Analysed**	**% Deviation**
Sc	0,08	0,58	33,00	33,91	36,25	33,99	33,84	33,24	31,83	32,65	31,25	**33,37**	**1,12**
V	0,02	0,17	425,00	420,50	420,70	415,90	417,50	413,80	415,20	417,30	407,00	**415,99**	**2,12**
Cr	0,59	6,86	17,00	14,91	14,93	14,32	15,25	14,57	14,30	15,55	14,95	**14,85**	**12,66**
Co	0,01	0,14	38,00	35,48	36,42	35,53	34,91	35,60	34,38	34,64	37,00	**35,50**	**6,59**
Ni	0,53	6,15	13,00	11,85	12,35	11,97	11,71	12,08	11,96	12,45	11,91	**12,04**	**7,42**
Cu	0,04	0,35	21,00	17,69	17,45	16,62	17,13	16,52	16,72	16,83	17,99	**17,12**	**18,48**
Zn	0,07	1,83	125,00	150,10	144,30	141,10	147,80	150,60	149,90	148,10	143,70	**146,95**	**17,56**
Rb	0,03	0,34	47,00	46,28	47,49	46,10	45,90	45,45	45,62	45,79	46,60	**46,15**	**1,80**
Sr	0,00	0,04	342,00	334,60	336,60	330,60	334,40	334,30	327,70	329,80	315,70	**330,46**	**3,37**
Y	0,00	0,01	35,00	32,85	33,09	32,18	32,49	31,98	32,04	32,08	29,06	**31,97**	**8,65**
Zr	0,00	0,04	184,00	173,90	173,10	171,00	170,40	168,70	171,40	170,60	153,90	**169,13**	**8,08**
Nb	0,00	0,03	12,50	11,16	11,30	11,17	11,13	11,08	11,04	11,09	11,01	**11,12**	**11,02**
Mo	0,01	0,07	270,00	249,90	247,50	248,10	247,20	246,30	248,10	248,50	245,50	**247,64**	**8,28**
Cs	0,02	0,14	1,16	1,07	1,10	1,06	1,08	1,07	1,06	1,05	1,15	**1,08**	**7,08**
Ba	0,01	0,30	683,00	677,00	670,00	661,20	664,00	664,00	670,00	666,80	656,00	**666,13**	**2,47**
La	0,00	0,02	24,70	24,20	24,38	23,84	23,63	23,41	23,45	23,42	22,88	**23,65**	**4,25**
Ce	0,00	0,91	53,30	50,68	51,18	50,34	50,50	49,49	49,13	49,18	49,70	**50,03**	**6,14**
Pr	0,00	0,01	6,70	6,41	6,47	6,43	6,31	6,28	6,25	6,31	6,21	**6,33**	**5,47**
Nd	0,00	0,07	28,90	27,05	27,58	27,40	27,47	26,79	27,80	28,00	25,40	**27,19**	**5,93**
Sm	0,01	0,07	6,59	6,36	6,37	6,34	6,34	6,07	6,43	6,31	5,81	**6,25**	**5,10**
Eu	0,00	0,02	1,97	1,85	1,91	1,83	1,86	1,86	1,80	1,79	1,76	**1,83**	**7,03**
Gd	0,00	0,05	6,71	6,66	6,60	6,46	6,49	6,41	6,59	6,70	5,85	**6,47**	**3,58**
Tb	0,00	0,03	1,02	0,96	0,99	0,93	0,96	0,93	0,94	0,93	0,89	**0,94**	**7,62**
Dy	0,00	0,03	6,44	6,11	6,26	6,15	6,18	6,05	6,03	6,15	5,41	**6,04**	**6,17**
Ho	0,00	0,01	1,27	1,22	1,27	1,21	1,21	1,19	1,20	1,19	1,08	**1,20**	**5,78**
Er	0,05	0,02	3,70	3,54	3,59	3,49	3,48	3,47	3,44	3,50	3,12	**3,45**	**6,65**
Tm	0,00	0,07	0,51	0,49	0,50	0,47	0,48	0,47	0,47	0,47	0,42	**0,47**	**7,50**
Yb	0,00	0,03	3,39	3,28	3,31	3,13	3,18	3,11	3,22	3,18	2,88	**3,16**	**6,77**
Lu	0,00	0,01	0,50	0,49	0,47	0,47	0,47	0,46	0,48	0,46	0,42	**0,46**	**7,68**
Hf	0,00	0,02	4,84	4,78	4,84	4,68	4,74	4,64	4,70	4,77	4,13	**4,66**	**3,73**
Ta	0,00	0,02	0,78	0,68	0,70	0,68	0,68	0,67	0,67	0,68	0,62	**0,67**	**13,77**
Pb	0,02	0,05	11,00	10,41	10,29	9,93	10,43	10,53	10,10	10,03	9,89	**10,20**	**7,26**
Th	0,00	0,01	5,90	5,72	5,76	5,61	5,64	5,58	5,41	5,49	5,07	**5,54**	**6,19**
U	0,00	0,03	1,69	1,66	1,70	1,63	1,63	1,63	1,59	1,64	1,63	**1,64**	**3,09**

Table D 4. 3: BHVO powder reference values

Values in ppm	Instrument DL	Fusion Method DL	Certified BHVO powder (fusion)	BHVOf - 1	BHVOf - 2	BHVOf - 3	BHVOf - 4	BHVOf - 5	BHVOf - 6	**Average Analysed**	**% Deviation**
Sc	0,08	0,58	31,42	33,05	32,00	31,70	31,70	31,30	31,40	**31,86**	**1,40**
V	0,02	0,17	313,80	289,90	292,50	289,10	298,10	292,00	296,10	**292,95**	**6,64**
Cr	0,59	6,86	287,60	266,90	278,00	272,90	283,00	278,40	278,20	**276,23**	**3,95**
Co	0,01	0,14	44,90	38,50	39,29	39,20	40,40	40,00	39,80	**39,53**	**11,96**
Ni	0,53	6,15	120,00	136,70	136,90	126,20	137,20	139,20	142,20	**136,40**	**13,67**
Cu	0,04	0,35	137,20	130,90	131,50	127,00	132,80	135,40	136,30	**132,32**	**3,56**
Zn	0,07	1,83	105,10	128,00	106,40	114,90	115,60	110,50	119,20	**115,77**	**10,15**
Rb	0,03	0,34	9,52	9,06	8,40	7,94	8,82	8,44	8,59	**8,54**	**10,28**
Sr	0,00	0,04	399,20	367,10	368,10	365,00	373,00	366,60	373,50	**368,88**	**7,59**
Y	0,00	0,01	26,23	23,02	23,70	23,12	23,61	23,40	23,69	**23,42**	**10,70**
Zr	0,00	0,04	174,60	151,60	152,90	152,50	153,60	154,60	156,50	**153,62**	**12,02**
Nb	0,00	0,03	18,53	15,78	15,70	15,77	16,11	15,79	15,92	**15,85**	**14,49**
Mo	0,01	0,07	1,06	1,46	1,40	1,74	1,37	1,60	1,62	**1,53**	**44,36**
Cs	0,02	0,14	0,10	0,26	0,25	0,30	0,28	0,26	0,25	**0,27**	**157,59**
Ba	0,01	0,30	134,40	126,80	120,40	123,20	125,50	120,40	122,40	**123,12**	**8,40**
La	0,00	0,02	15,44	14,27	14,15	14,12	14,32	14,28	14,36	**14,25**	**7,71**
Ce	0,00	0,91	38,08	34,11	34,76	34,21	34,94	35,33	35,48	**34,81**	**8,60**
Pr	0,00	0,01	5,42	4,67	4,78	4,69	4,91	4,88	4,76	**4,78**	**11,76**
Nd	0,00	0,07	24,78	21,80	23,01	22,61	22,90	22,05	22,80	**22,53**	**9,09**
Sm	0,01	0,07	6,17	5,31	5,75	5,70	5,78	6,03	5,37	**5,66**	**8,25**
Eu	0,00	0,02	2,05	1,98	1,94	1,86	2,01	1,78	1,81	**1,90**	**7,61**
Gd	0,00	0,05	6,29	6,08	6,21	5,64	6,20	5,66	6,29	**6,01**	**4,32**
Tb	0,00	0,03	0,95	0,86	0,83	0,83	0,86	0,82	0,86	**0,84**	**10,77**
Dy	0,00	0,03	5,27	4,70	4,94	4,83	5,09	5,03	5,11	**4,95**	**6,11**
Ho	0,00	0,01	0,98	0,86	0,96	0,89	1,00	0,95	0,89	**0,92**	**6,22**
Er	0,05	0,02	2,50	2,34	2,43	2,38	2,23	2,29	2,44	**2,35**	**5,97**
Tm	0,00	0,07	0,33	0,30	0,30	0,30	0,33	0,33	0,33	**0,31**	**4,53**
Yb	0,00	0,03	1,99	1,76	1,68	1,85	1,86	1,86	1,78	**1,80**	**9,50**
Lu	0,00	0,01	0,28	0,35	0,30	0,26	0,27	0,24	0,27	**0,28**	**1,38**
Hf	0,00	0,02	4,44	4,23	4,35	4,11	4,12	4,07	4,27	**4,19**	**5,59**
Ta	0,00	0,02	1,17	1,00	0,97	0,98	1,03	0,96	1,01	**0,99**	**15,47**
Pb	0,02	0,05	2,04	2,72	2,75	2,90	2,72	2,67	3,12	**2,81**	**38,11**
Th	0,00	0,01	1,23	1,20	1,17	1,08	1,18	1,15	1,19	**1,16**	**5,18**
U	0,00	0,03	0,42	0,41	0,41	0,38	0,37	0,39	0,38	**0,39**	**6,90**

Table D 4. 4: BCR powder reference values

Values in ppm	Instrument DL	Fusion Method DL	Certified BCR powder (fusion)	BCRf - 1	BCRf - 2	BCRf - 3	BCRf - 4	BCRf - 5	BCRf - 6	**Average Analysed**	**% Deviation**
Sc	0,08	0,58	33,53	34,10	33,15	34,53	32,80	33,44	33,30	**33,55**	**0,07**
V	0,02	0,17	417,60	383,90	389,60	390,90	383,00	393,30	386,20	**387,82**	**7,13**
Cr	0,59	6,86	15,85	22,60	20,00	22,20	19,40	22,10	20,70	**21,17**	**33,54**
Co	0,01	0,14	37,33	34,60	35,36	34,70	34,90	34,60	34,30	**34,74**	**6,93**
Ni	0,53	6,15	12,57	20,60	19,90	21,30	19,60	19,40	17,60	**19,73**	**56,99**
Cu	0,04	0,35	19,66	33,70	35,70	35,10	34,10	35,70	35,30	**34,93**	**77,69**
Zn	0,07	1,83	129,50	131,20	136,40	144,90	128,80	140,90	132,10	**135,72**	**4,80**
Rb	0,03	0,34	46,02	42,20	42,90	42,60	42,70	42,60	41,60	**42,43**	**7,79**
Sr	0,00	0,04	337,40	314,30	315,50	315,10	317,70	322,40	317,60	**317,10**	**6,02**
Y	0,00	0,01	36,07	31,98	32,16	32,02	31,40	32,35	32,18	**32,02**	**11,24**
Zr	0,00	0,04	186,50	162,90	167,50	168,60	164,90	169,30	168,30	**166,92**	**10,50**
Nb	0,00	0,03	12,44	10,59	10,69	10,68	10,76	10,63	10,48	**10,64**	**14,48**
Mo	0,01	0,07	250,60	234,30	234,00	235,90	234,20	239,20	234,00	**235,27**	**6,12**
Cs	0,02	0,14	1,16	0,93	1,04	0,95	1,03	1,09	1,01	**1,01**	**13,07**
Ba	0,01	0,30	683,90	622,60	631,00	631,00	642,00	647,00	639,00	**635,43**	**7,09**
La	0,00	0,02	25,08	22,34	22,76	23,15	22,80	23,79	23,00	**22,97**	**8,40**
Ce	0,00	0,91	53,12	47,30	48,07	48,44	48,28	49,30	48,71	**48,35**	**8,98**
Pr	0,00	0,01	6,83	6,12	6,28	6,15	5,97	6,30	6,33	**6,19**	**9,31**
Nd	0,00	0,07	28,26	26,40	25,92	26,24	26,10	26,80	25,70	**26,19**	**7,31**
Sm	0,01	0,07	6,55	6,10	5,91	6,48	6,27	6,40	6,06	**6,20**	**5,25**
Eu	0,00	0,02	1,99	1,69	1,74	1,76	1,76	1,81	1,98	**1,79**	**10,04**
Gd	0,00	0,05	6,81	6,05	6,14	6,21	6,42	6,49	6,09	**6,23**	**8,48**
Tb	0,00	0,03	1,08	0,89	0,98	0,97	0,90	1,01	0,93	**0,95**	**12,01**
Dy	0,00	0,03	6,42	5,79	6,03	5,81	5,88	6,24	6,04	**5,97**	**7,15**
Ho	0,00	0,01	1,31	1,13	1,20	1,20	1,12	1,26	1,20	**1,19**	**9,65**
Er	0,05	0,02	3,67	3,34	3,45	3,28	3,51	3,38	3,44	**3,40**	**7,36**
Tm	0,00	0,07	0,53	0,49	0,48	0,49	0,48	0,51	0,50	**0,49**	**8,54**
Yb	0,00	0,03	3,39	3,04	3,11	3,15	3,16	3,13	3,17	**3,13**	**7,82**
Lu	0,00	0,01	0,50	0,44	0,47	0,51	0,42	0,50	0,46	**0,46**	**8,03**
Hf	0,00	0,02	4,97	4,37	4,67	4,60	4,68	4,96	5,00	**4,71**	**5,20**
Ta	0,00	0,02	0,79	0,62	0,70	0,63	0,62	0,67	0,67	**0,65**	**16,75**
Pb	0,02	0,05	10,59	8,50	9,07	9,18	8,88	9,10	9,23	**8,99**	**15,08**
Th	0,00	0,01	5,83	5,18	5,39	5,57	5,41	5,78	5,47	**5,47**	**6,20**
U	0,00	0,03	1,68	1,63	1,52	1,65	1,66	1,60	1,60	**1,61**	**4,34**

Appendix D.5: XRF Reference Values

Table D 5. 1: XRF basalt reference values

Sample name			Meas. date/time	Al2O3 (%)	CaO (%)	Cr2O3 (%)	Fe2O3 (%)	K2O (%)	MgO (%)	MnO (%)	Na2O (%)	P2O5 (%)	SiO2 (%)	TiO2 (%)	Sum Of Conc. (%)
Basalt Reference values				**10,05**	**14,03**		**12,84**	**1,40**	**13,15**	**0,20**	**3,18**	**1,06**	**38,38**	**2,59**	**96,88**
BE-N	**STD**	Majors Interm32	2016-01-15 16:01	10,05	14,06	0,01	12,88	1,41	13,23	0,20	3,16	1,08	38,25	2,69	97,02
BEN	**std**	MajorBasic32+Zn	2016-02-02 22:16	10,06	14,02	0,05	12,82	1,41	13,18	0,20	3,11	1,09	37,95	2,64	96,53
BE-N	**STD**	Majors Interm32	2016-02-12 19:49	9,96	14,06	0,01	12,85	1,40	13,23	0,20	3,15	1,07	38,14	2,69	96,76
BE-N	**STD**	MajorBasic32+Zn	2016-02-12 19:56	10,09	14,02	0,05	12,80	1,41	13,20	0,20	3,16	1,09	37,92	2,63	96,57
BE-N	**std**	MajorBasic32+Zn	2016-03-08 16:42	10,10	14,05	0,05	12,85	1,42	13,28	0,19	3,11	1,09	38,18	2,66	96,98
BE-N	**STD**	Majors Interm32	2016-03-09 16:42	9,87	14,06	0,05	12,90	1,41	13,01	0,20	3,05	1,10	37,83	2,67	96,15
BE-N	**std**	MajorBasic32+Zn	2016-03-18 23:56	10,05	14,03	0,05	12,84	1,42	13,26	0,19	3,11	1,09	37,99	2,65	96,68
BE-N	**STD**	MajorBasic32+Zn	2016-03-23 14:08	10,08	14,04	0,05	12,87	1,40	13,23	0,20	3,12	1,10	38,10	2,67	96,86
BE-N	**STD**	MajorBasic32+Zn	2016-04-15 06:31	10,10	14,02	0,05	12,85	1,42	13,13	0,19	3,11	1,09	37,99	2,65	96,60
BE-N	**STD**	MajorBasic32+Zn	2016-04-19 08:41	10,04	14,03	0,05	12,80	1,40	13,12	0,20	3,13	1,10	38,08	2,67	96,62
BE-N	**STD**	MajorBasic32+Zn	2016-04-20 00:50	10,10	14,03	0,05	12,88	1,42	13,12	0,20	3,13	1,10	37,94	2,64	96,61
BE-N	**STD**	MajorBasic32+Zn	2016-05-05 01:05	10,01	14,06	0,05	12,84	1,42	13,08	0,20	3,18	1,09	38,19	2,65	96,77
BE-N	**STD**	MajorBasic32+Zn	2016-05-05 21:37	10,09	14,03	0,05	12,83	1,42	13,14	0,21	3,18	1,09	37,97	2,64	96,65
BE-N	**std**	MajorBasic32+Zn	2016-05-17 13:43	10,04	14,04	0,05	12,79	1,41	13,07	0,20	3,17	1,08	37,98	2,66	96,49
BEN	**STD**	MajorBasic32+Zn	2016-05-20 10:34	10,04	14,01	0,05	12,87	1,42	13,13	0,19	3,16	1,08	37,89	2,64	96,48
BE-N	**STD**	MajorBasic32+Zn	2016-06-07 00:54	10,06	14,06	0,05	12,82	1,42	13,13	0,20	3,18	1,08	38,11	2,65	96,76
BE-N	**STD**	MajorBasic32+Zn	2016-06-07 23:52	10,05	14,03	0,05	12,82	1,41	13,11	0,20	3,19	1,09	38,16	2,65	96,76
BE-N	**std**	MajorBasic32+Zn	2016-06-20 15:58	10,14	14,03	0,05	12,88	1,41	13,07	0,20	3,07	1,08	38,19	2,66	96,78
BE-N	**STD**	MajorBasic32+Zn	2016-07-11 14:36	10,04	13,94	0,05	12,83	1,42	13,18	0,19	2,42	1,10	38,64	2,65	96,46
BE-N	**STD**	MajorBasic32+Zn	2016-07-22 20:59	10,08	14,04	0,05	12,79	1,41	13,14	0,20	3,17	1,10	38,30	2,66	96,94
BE-N	**std**	MajorBasic32+Zn	2016-08-02 23:54	10,04	14,02	0,05	12,79	1,41	13,13	0,20	3,12	1,09	37,99	2,66	96,50
BE-N	**std**	MajorBasic32+Zn	2016-08-24 21:10	10,01	14,05	0,05	12,80	1,41	13,12	0,19	3,12	1,10	37,94	2,64	96,43
BE-N	**std**	MajorBasic32+Zn	2016-09-02 12:51	10,03	14,00	0,05	12,79	1,41	13,20	0,20	3,21	1,09	37,81	2,65	96,44
BE-N	**STD**	MajorBasic32+Zn	2016-09-07 17:19	10,06	14,12	0,04	12,89	1,42	13,18	0,20	3,16	1,09	38,17	2,66	96,99
BE-N	**STD**	MajorBasic32+Zn	2016-10-07 23:04	10,08	14,13	0,05	12,84	1,37	13,12	0,20	3,14	1,07	38,26	2,64	96,90
BE-N	**STD**	MajorBasic32+Zn	2016-10-19 18:55	10,01	14,11	0,05	12,84	1,37	13,06	0,20	3,15	1,07	37,92	2,64	96,42
BE-N	**STD**	MajorBasic32+Zn	2016-10-20 23:07	10,09	14,10	0,05	12,78	1,37	13,15	0,20	3,10	1,07	37,97	2,62	96,50
BE-N	**STD**	MajorBasic32+Zn	2016-11-08 22:32	9,99	14,11	0,05	12,84	1,41	13,13	0,19	3,11	1,10	38,11	2,64	96,68
BE-N	**STD**	MajorBasic32+Zn	2016-11-28 20:16	10,04	14,14	0,05	12,82	1,41	13,08	0,20	3,19	1,09	37,90	2,65	96,57
BE-N	**STD**	MajorBasic32+Zn	2016-12-10 00:23	10,05	14,09	0,05	12,83	1,41	13,08	0,00	3,12	1,08	37,92	2,65	96,28
BE-N	**STD**	MajorBasic32+Zn	2017-03-08 14:47	10,08	14,04	0,05	12,78	1,42	13,19	0,20	3,16	1,08	38,28	2,63	96,91
BE-N	**STD**	Majors Interm32	2017-03-17 13:03	9,90	14,01	0,05	12,86	1,41	12,93	0,20	3,01	1,10	37,90	2,64	96,01
BE-N	**STD**	Majors Interm32	2017-04-04 17:20	9,88	14,01	0,05	12,87	1,40	12,87	0,20	2,97	1,10	37,85	2,66	95,86

BE-N	**std**	MajorBasic32+Zn	2017-05-02 11:42	10,01	14,06	0,05	12,84	1,41	13,03	0,19	3,16	1,09	38,28	2,64	96,76
BE-N	**STD**	Majors Interm32	2017-05-16 13:03	9,81	13,99	0,05	12,88	1,41	12,90	0,20	3,01	1,10	37,77	2,65	95,77
BE-N	**STD**	MajorBasic32+Zn	2017-05-17 15:30	10,01	14,05	0,05	12,83	1,41	13,09	0,20	3,11	1,08	38,44	2,65	96,92
be-n	**std**	Majors Interm32	2017-06-05 16:40	9,88	14,04	0,06	12,86	1,41	12,91	0,20	3,00	1,11	37,65	2,65	95,77
BE-N	**std**	MajorBasic32+Zn	2017-06-27 00:00	9,96	14,05	0,05	12,83	1,40	13,05	0,20	3,11	1,07	38,43	2,65	96,80
be-n	**std**	Majors Interm32	2017-06-27 00:08	9,96	14,05	0,05	12,87	1,40	12,95	0,20	3,01	1,11	37,76	2,67	96,03
BE-N	**std**	MajorBasic32+Zn	2017-07-14 12:17	9,99	14,01	0,05	12,81	1,41	13,04	0,20	3,16	1,10	38,43	2,65	96,85
BE-N	**STD**	MajorBasic32+Zn	2017-07-20 16:40	9,98	14,02	0,05	12,82	1,43	13,07	0,20	3,11	1,10	38,51	2,64	96,93
BE-N	**STD**	MajorBasic32+Zn	2017-07-24 23:10	10,02	14,04	0,05	12,83	1,42	13,10	0,20	3,10	1,09	38,36	2,65	96,86
BE-N	**STD**	MajorBasic32+Zn	2017-08-18 14:51	9,99	14,01	0,05	12,81	1,41	13,11	0,20	3,11	1,09	38,35	2,63	96,76
BE-N	**STD**	MajorBasic32+Zn	2017-08-21 23:30	9,97	14,03	0,04	12,78	1,41	13,06	0,19	3,15	1,08	38,40	2,64	96,75
BE-N	**STD**	MajorBasic32+Zn	2017-08-23 16:04	9,99	14,04	0,05	12,85	1,41	13,07	0,20	3,10	1,09	38,49	2,66	96,95
BE-N	**std**	MajorBasic32+Zn	2017-09-11 20:40	9,97	14,01	0,04	12,82	1,41	13,08	0,20	3,12	1,09	38,26	2,63	96,63
BE-N	**std**	MajorBasic32+Zn	2017-09-19 14:49	10,03	14,03	0,05	12,88	1,41	13,09	0,20	3,12	1,11	38,42	2,66	97,00
BE-N	**STD**	MajorBasic32+Zn	2017-10-12 10:08	10,03	14,02	0,05	12,88	1,41	13,03	0,20	3,08	1,09	38,57	2,66	97,02
BE-N	**STD**	MajorBasic32+Zn	2017-10-25 16:55	9,98	14,03	0,05	12,91	1,41	13,03	0,20	3,14	1,10	38,47	2,65	96,97
BE-N	**STD**	MajorBasic32+Zn	2017-11-09 14:34	10,09	14,08	0,05	12,87	1,40	13,03	0,20	3,19	1,11	38,53	2,64	97,19
BE-N	**STD**	MajorBasic32+Zn	2017-11-14 00:00	10,03	14,05	0,04	12,87	1,42	13,05	0,20	3,10	1,11	38,47	2,65	96,99
BE-N	**STD**	MajorBasic32+Zn	2017-11-15 22:58	10,02	14,02	0,05	12,84	1,41	13,06	0,20	3,08	1,08	38,53	2,65	96,94
BE-N	**STD**	MajorBasic32+Zn	2017-11-20 17:25	9,93	14,02	0,05	12,87	1,41	13,13	0,20	3,07	1,10	38,56	2,64	96,98
BE-N	**STD**	MajorBasic32+Zn	2018-01-25 19:10	9,86	14,48	0,05	12,85	1,37	12,88	0,19	3,12	1,08	38,04	2,62	96,54
BE-N	**std**	MajorBasic32+Zn	2018-02-12 18:11	10,27	14,15	0,05	12,89	1,42	13,25	0,20	3,22	1,08	38,41	2,68	97,62
BE-N	**std**	MajorBasic32+Zn	2018-02-15 07:49	10,13	14,09	0,05	12,82	1,41	13,21	0,19	3,23	1,08	38,08	2,66	96,95
BE-N	**STD**	MajorBasic32+Zn	2018-02-15 22:18	10,19	14,00	0,05	12,83	1,41	13,19	0,20	3,20	1,08	38,10	2,66	96,91
BE-N	**STD**	MajorBasic32+Zn	2018-02-17 00:00	10,08	14,03	0,05	12,78	1,41	13,14	0,20	3,15	1,07	38,01	2,65	96,57
BE-N	**STD**	MajorBasic32+Zn	2018-02-20 23:00	10,06	13,96	0,05	12,76	1,40	13,03	0,19	3,08	1,07	37,75	2,65	96,00
BE-N	**STD**	MajorBasic32+Zn	2018-02-21 21:20	10,11	13,95	0,05	12,75	1,40	13,15	0,19	2,47	1,08	38,13	2,63	95,91
BE-N	**std**	MajorBasic32+Zn	2018-02-26 14:50	10,08	14,00	0,05	12,79	1,41	13,17	0,20	2,48	1,08	38,13	2,65	96,04
BE-N	**std**	MajorBasic32+Zn	2018-03-12 21:02	10,12	13,98	0,05	12,82	1,40	13,17	0,20	3,10	1,08	38,09	2,66	96,67
BE-N	**std**	MajorBasic32+Zn	2018-03-23 11:35	10,10	14,05	0,05	12,84	1,40	13,16	0,20	3,18	1,09	38,21	2,68	96,96
BE-N	**STD**	MajorBasic32+Zn	2018-03-26 20:49	10,06	13,97	0,05	12,80	1,41	13,10	0,19	3,17	1,07	38,08	2,65	96,55
BE-N	**STD**	MajorBasic32+Zn	2018-04-04 21:44	9,99	13,91	0,05	12,77	1,40	13,02	0,20	3,13	1,07	37,88	2,65	96,07
BE-N	**STD**	MajorBasic32+Zn	2018-04-22 18:22	9,99	14,07	0,05	12,77	1,40	13,04	0,19	3,15	1,06	37,47	2,65	95,84
BE-N	**std**	MajorBasic32+Zn	2018-05-11 13:04	10,10	13,97	0,05	12,82	1,41	13,18	0,20	3,19	1,08	38,69	2,65	97,34
BE-N	**STD**	MajorBasic32+Zn	2018-05-16 18:11	10,08	14,08	0,05	12,90	1,42	13,20	0,20	3,15	1,10	38,80	2,65	97,63
BE-N	**STD**	MajorBasic32+Zn	2018-05-17 16:19	10,04	14,08	0,05	12,91	1,40	13,17	0,20	3,18	1,09	38,62	2,65	97,39
BE-N	**std**	MajorBasic32+Zn	2018-05-25 11:23	10,12	14,08	0,05	12,85	1,41	13,13	0,20	3,18	1,09	38,49	2,65	97,25
Average				10,03	14,04	0,04	12,85	1,41	13,20	0,20	3,12	1,09	38,05	2,66	96,72
Relative standard deviation (%)				0,17	0,10		0,09	0,75	0,40	1,25	1,81	2,27	0,88	2,85	0,17

Table D 5. 2: XRF basalt (depleted) reference values

Sample name			Meas. date/time	Al2O3	CaO	Cr2O3	Fe2O3	K2O	MgO	MnO	Na2O	P2O5	SiO2	TiO2	Sum Of Conc.
				(%)	(%)	(%)	(%)	(%)	(%)	(%)	(%)	(%)	(%)	(%)	(%)
JB-1				**14,53**	**9,29**	**0,07**	**8,97**	**1,43**	**7,73**	**0,16**	**2,79**	**0,26**	**52,17**	**1,34**	**98,74**
Basalt (depleted) Reference values															
JB-1	**STD**	Majors Interm32	2016-01-15 15:52	14,62	9,27	0,01	8,87	1,44	7,84	0,16	2,79	0,26	52,61	1,33	99,20
JB-1	**STD**	Majors Interm32	2016-02-12 19:15	14,58	9,30	0,01	8,86	1,44	7,80	0,16	2,80	0,27	52,45	1,32	98,99
JB-1	**STD**	MajorBasic32+Zn	2016-02-12 19:23	14,66	9,26	0,06	8,84	1,44	7,71	0,17	2,83	0,26	52,43	1,31	98,97
JB-1	**std**	MajorBasic32+Zn	2016-03-08 17:06	14,72	9,29	0,06	8,84	1,45	7,82	0,16	2,79	0,26	52,82	1,31	99,52
JB-1	**STD**	Majors Interm32	2016-03-09 16:34	14,48	9,30	0,07	8,89	1,43	7,69	0,16	2,75	0,27	52,20	1,32	98,56
JB-1	**std**	MajorBasic32+Zn	2016-03-19 00:20	14,82	9,29	0,06	8,85	1,44	7,82	0,16	2,77	0,26	52,76	1,32	99,55
JB-1	**STD**	MajorBasic32+Zn	2016-03-23 14:39	14,66	9,29	0,06	8,86	1,44	7,82	0,16	2,77	0,26	53,02	1,31	99,65
JB-1	**STD**	MajorBasic32+Zn	2016-04-15 06:41	14,70	9,29	0,06	8,87	1,45	7,73	0,17	2,84	0,26	52,71	1,31	99,39
JB-1	**STD**	MajorBasic32+Zn	2016-04-19 08:50	14,64	9,26	0,06	8,85	1,44	7,72	0,16	2,81	0,27	52,94	1,31	99,46
JB-1	**STD**	MajorBasic32+Zn	2016-04-20 00:59	14,71	9,25	0,06	8,84	1,43	7,73	0,16	2,79	0,26	52,80	1,31	99,34
JB-1	**STD**	MajorBasic32+Zn	2016-05-05 01:14	14,74	9,28	0,06	8,87	1,46	7,72	0,17	2,81	0,27	52,85	1,31	99,54
JB-1	**STD**	MajorBasic32+Zn	2016-05-05 21:46	14,68	9,24	0,07	8,86	1,44	7,74	0,16	2,82	0,26	52,71	1,32	99,30
JB-1	**std**	MajorBasic32+Zn	2016-05-17 13:53	14,67	9,31	0,06	8,84	1,44	7,76	0,16	2,83	0,27	52,76	1,31	99,41
JB-1	**STD**	MajorBasic32+Zn	2016-05-20 10:51	14,69	9,28	0,06	8,86	1,43	7,69	0,16	2,80	0,27	52,80	1,32	99,36
JB-1	**STD**	MajorBasic32+Zn	2016-06-07 01:03	14,71	9,30	0,07	8,85	1,44	7,74	0,16	2,81	0,27	52,74	1,31	99,40
JB-1	**STD**	MajorBasic32+Zn	2016-06-08 00:01	14,64	9,30	0,06	8,86	1,44	7,69	0,16	2,78	0,27	52,75	1,32	99,27
JB-1	**std**	MajorBasic32+Zn	2016-06-20 16:07	14,80	9,25	0,06	8,84	1,45	7,69	0,16	2,80	0,27	53,03	1,31	99,66
JB-1	**std**	MajorBasic32+Zn	2016-07-11 14:53	14,65	9,15	0,06	8,80	1,45	7,67	0,16	2,15	0,26	52,46	1,31	98,12
JB-1	**STD**	MajorBasic32+Zn	2016-07-22 21:15	14,61	9,30	0,06	8,86	1,45	7,73	0,16	2,88	0,27	53,00	1,31	99,63
JB-1	**std**	MajorBasic32+Zn	2016-08-03 00:03	14,73	9,28	0,06	8,85	1,45	7,73	0,16	2,81	0,26	53,01	1,32	99,66
JB-1	**std**	MajorBasic32+Zn	2016-08-24 21:19	14,72	9,27	0,06	8,85	1,46	7,79	0,16	2,81	0,27	52,95	1,30	99,64
JB-1	**std**	MajorBasic32+Zn	2016-09-02 13:08	14,67	9,29	0,06	8,84	1,44	7,74	0,16	2,84	0,27	52,84	1,31	99,46
JB-1	**STD**	MajorBasic32+Zn	2016-09-07 17:28	14,64	9,35	0,06	8,87	1,45	7,78	0,16	2,83	0,27	52,91	1,31	99,63
JB-1	**STD**	MajorBasic32+Zn	2016-10-07 23:13	14,72	9,33	0,06	8,90	1,40	7,72	0,16	2,80	0,26	53,10	1,29	99,74
JB-1	**STD**	MajorBasic32+Zn	2016-10-19 18:13	14,74	9,36	0,06	8,86	1,41	7,72	0,17	2,78	0,26	52,79	1,29	99,44
JB-1	**STD**	MajorBasic32+Zn	2016-10-20 23:16	14,71	9,34	0,06	8,87	1,40	7,74	0,16	2,86	0,27	52,95	1,28	99,64
JB-1	**STD**	MajorBasic32+Zn	2016-11-08 22:41	14,63	9,32	0,06	8,86	1,44	7,71	0,16	2,81	0,27	52,76	1,31	99,33
JB-1	**STD**	MajorBasic32+Zn	2016-11-28 20:25	14,64	9,33	0,07	8,85	1,43	7,73	0,16	2,81	0,26	52,96	1,32	99,56
JB-1	**STD**	MajorBasic32+Zn	2016-12-10 00:32	14,70	9,27	0,07	8,83	1,44	7,74	0,00	2,81	0,27	52,62	1,31	99,06
JB-1	**STD**	MajorBasic32+Zn	2017-03-08 15:12	14,80	9,29	0,06	8,84	1,45	7,82	0,16	2,85	0,28	52,94	1,31	99,80
JB-1	**STD**	Majors Interm32	2017-03-17 13:19	14,55	9,28	0,07	8,88	1,42	7,66	0,16	2,71	0,27	52,54	1,31	98,85
JB-1	**STD**	Majors Interm32	2017-04-04 17:12	14,47	9,28	0,07	8,89	1,43	7,65	0,16	2,69	0,27	52,49	1,32	98,72
JB-1	**std**	MajorBasic32+Zn	2017-05-02 11:59	14,67	9,26	0,07	8,86	1,45	7,74	0,16	2,79	0,26	52,76	1,31	99,33
JB-1	**STD**	Majors Interm32	2017-05-16 12:55	14,44	9,27	0,07	8,88	1,43	7,68	0,16	2,70	0,27	52,53	1,31	98,74
JB-1	**STD**	MajorBasic32+Zn	2017-05-17 15:39	14,60	9,29	0,06	8,81	1,45	7,73	0,16	2,79	0,27	52,73	1,31	99,20
jb-1	**std**	Majors Interm32	2017-06-05 16:31	14,56	9,28	0,07	8,87	1,43	7,68	0,16	2,71	0,27	52,42	1,32	98,77

JB-1	**std**	MajorBasic32+Zn	2017-06-27 00:16	14,76	9,27	0,06	8,85	1,44	7,73	0,17	2,79	0,27	52,81	1,32	99,47
jb-1	**std**	Majors Interm32	2017-06-27 00:24	14,60	9,27	0,07	8,89	1,44	7,69	0,16	2,72	0,27	52,46	1,32	98,89
JB-1	**std**	MajorBasic32+Zn	2017-07-14 12:26	14,64	9,29	0,06	8,81	1,44	7,75	0,16	2,76	0,28	52,83	1,32	99,34
JB-1	**STD**	MajorBasic32+Zn	2017-07-20 16:31	14,61	9,32	0,06	8,83	1,45	7,73	0,16	2,76	0,27	52,63	1,32	99,14
JB-1	**STD**	MajorBasic32+Zn	2017-07-24 23:20	14,73	9,25	0,06	8,83	1,45	7,71	0,17	2,77	0,26	52,59	1,32	99,14
JB-1	**STD**	MajorBasic32+Zn	2017-08-18 15:00	14,58	9,29	0,06	8,85	1,44	7,68	0,16	2,80	0,26	52,68	1,31	99,11
JB-1	**STD**	MajorBasic32+Zn	2017-08-21 23:39	14,61	9,25	0,06	8,80	1,44	7,72	0,16	2,82	0,27	52,60	1,31	99,04
JB-1	**STD**	Majors Interm32	2017-08-22 16:13	14,44	9,28	0,06	8,87	1,44	7,69	0,16	2,74	0,28	52,48	1,31	98,75
JB-1	**STD**	MajorBasic32+Zn	2017-08-23 16:13	14,72	9,28	0,07	8,87	1,43	7,75	0,16	2,77	0,27	52,89	1,31	99,52
JB-1	**std**	MajorBasic32+Zn	2017-09-11 20:49	14,65	9,31	0,06	8,86	1,44	7,80	0,16	2,83	0,27	52,92	1,31	99,61
JB-1	**std**	MajorBasic32+Zn	2017-09-19 14:58	14,69	9,27	0,06	8,88	1,44	7,74	0,16	2,82	0,27	52,85	1,32	99,50
JB-1	**STD**	MajorBasic32+Zn	2017-10-12 10:17	14,76	9,33	0,06	8,88	1,45	7,80	0,16	2,84	0,28	52,64	1,31	99,51
JB-1	**STD**	MajorBasic32+Zn	2017-10-25 17:04	14,72	9,32	0,06	8,91	1,45	7,78	0,16	2,78	0,27	52,85	1,32	99,62
JB-1	**STD**	MajorBasic32+Zn	2017-11-09 14:43	14,62	9,28	0,06	8,90	1,45	7,79	0,16	2,82	0,26	52,73	1,31	99,38
JB-1	**STD**	MajorBasic32+Zn	2017-11-14 00:09	14,64	9,26	0,06	8,87	1,44	7,72	0,16	2,82	0,27	52,82	1,30	99,36
JB-1	**STD**	MajorBasic32+Zn	2017-11-15 23:14	14,66	9,30	0,06	8,90	1,44	7,78	0,17	2,79	0,27	52,87	1,31	99,55
JB-1	**STD**	MajorBasic32+Zn	2017-11-20 17:34	14,65	9,31	0,06	8,88	1,45	7,77	0,17	2,83	0,27	52,95	1,32	99,66
JB-1	**STD**	MajorBasic32+Zn	2018-01-25 19:19	14,55	9,54	0,06	8,87	1,39	7,69	0,16	2,88	0,26	52,40	1,28	99,08
JB-1	**std**	MajorBasic32+Zn	2018-02-12 18:35	15,02	9,35	0,06	8,87	1,46	7,81	0,16	2,90	0,28	53,01	1,31	100,23
JB-1	**std**	MajorBasic32+Zn	2018-02-15 08:14	14,92	9,33	0,06	8,85	1,45	7,90	0,17	2,89	0,27	52,87	1,32	100,03
JB-1	**STD**	MajorBasic32+Zn	2018-02-15 22:27	14,88	9,24	0,06	8,81	1,45	7,79	0,16	2,85	0,27	52,74	1,31	99,56
JB-1	**STD**	MajorBasic32+Zn	2018-02-17 00:09	14,87	9,27	0,06	8,83	1,44	7,85	0,16	2,83	0,27	52,30	1,31	99,19
JB-1	**STD**	MajorBasic32+Zn	2018-02-20 23:10	14,73	9,19	0,06	8,83	1,43	7,81	0,17	2,89	0,27	52,28	1,31	98,97
JB-1	**STD**	MajorBasic32+Zn	2018-02-21 21:29	14,79	9,24	0,06	8,77	1,44	7,79	0,16	2,24	0,27	52,46	1,31	98,53
JB-1	**std**	MajorBasic32+Zn	2018-02-26 14:59	14,87	9,27	0,06	8,82	1,43	7,78	0,17	2,29	0,26	52,59	1,32	98,86
JB-1	**std**	MajorBasic32+Zn	2018-03-12 21:12	14,78	9,24	0,06	8,84	1,43	7,83	0,16	2,87	0,26	52,59	1,32	99,38
JB-1	**std**	MajorBasic32+Zn	2018-03-23 11:44	14,81	9,26	0,06	8,85	1,44	7,85	0,16	2,86	0,26	52,47	1,32	99,34
JB-1	**STD**	MajorBasic32+Zn	2018-03-26 20:58	14,67	9,23	0,06	8,82	1,43	7,80	0,16	2,88	0,27	52,40	1,31	99,03
JB-1	**STD**	MajorBasic32+Zn	2018-04-04 21:53	14,58	9,18	0,06	8,83	1,43	7,75	0,16	2,82	0,26	52,06	1,30	98,43
JB-1	**STD**	MajorBasic32+Zn	2018-04-22 18:31	14,78	9,31	0,07	8,84	1,43	7,74	0,17	2,85	0,27	51,90	1,31	98,67
JB-1	**std**	MajorBasic32+Zn	2018-05-11 13:13	14,97	9,28	0,06	8,88	1,43	7,86	0,17	2,82	0,27	53,14	1,32	100,20
JB-1	**STD**	MajorBasic32+Zn	2018-05-16 18:20	14,97	9,33	0,06	8,90	1,44	7,83	0,17	2,82	0,27	52,52	1,32	99,63
JB-1	**STD**	MajorBasic32+Zn	2018-05-17 16:28	14,83	9,33	0,06	8,92	1,43	7,87	0,16	2,87	0,28	52,33	1,31	99,39
JB-1	**std**	MajorBasic32+Zn	2018-05-25 12:12	14,78	9,29	0,06	8,87	1,44	7,83	0,16	2,83	0,27	52,90	1,31	99,74
Average				14,60	9,29	0,01	8,87	1,44	7,82	0,16	2,80	0,27	52,53	1,33	99,10
Relative standard deviation (%)				0,48	0,05	85,29	1,17	0,70	1,16	0,00	0,18	1,92	0,69	1,12	0,36

Table D 5. 3: XRF BHVO basalt reference values

Sample name		Meas. date/time	Al2O3 (%)	CaO (%)	Cr2O3 (%)	Fe2O3 (%)	K2O (%)	MgO (%)	MnO (%)	Na2O (%)	P2O5 (%)	SiO2 (%)	TiO2 (%)	L.O.I. (%)	Sum Of Conc. (%)
BHVO-1 Basalt Reference values			**13,71**	**11,39**	**0,04**	**12,36**	**0,54**	**7,22**	**0,17**	**2,31**	**0,27**	**49,82**	**2,73**	**0,52**	**101,08**
BHVO-1	MajorBasic32+Zn	2015-08-27 15:31	13,64	11,29	0,03	12,31	0,52	7,13	0,17	2,23	0,27	49,38	2,72	0,52	100,21
BHVO-1 std	MajorBasic32+Zn	2016-02-02 22:41	13,75	11,40	0,04	12,28	0,52	7,20	0,17	2,22	0,27	49,94	2,73	0,52	101,04
MONITOR BHVO-1	MajorBasic32+Zn	2016-03-22 13:14	13,79	11,40	0,04	12,29	0,52	7,24	0,17	2,24	0,28	49,89	2,74	0,52	101,12
MONITOR BHVO-1	Majors Acid32	2016-03-22 13:39	13,49	11,57	0,02	12,36	0,52	7,19	0,17	2,18	0,27	50,36	2,92	0,52	101,57
BHVO-1 MONITOR	Majors Acid32	2016-04-12 23:57	13,48	11,49	0,02	12,34	0,52	7,17	0,17	2,14	0,27	50,11	2,91	0,52	101,14
BHVO-1 MONITOR	MajorBasic32+Zn	2016-04-15 06:22	13,75	11,40	0,04	12,26	0,52	7,16	0,17	2,25	0,27	50,00	2,74	0,52	101,08
BHVO-1 MONITOR	Majors Acid32	2016-04-15 06:14	13,55	11,47	0,02	12,36	0,53	7,18	0,17	2,15	0,28	50,14	2,90	0,52	101,27
MONITOR BHVO-1	MajorBasic32+Zn	2016-04-19 09:08	13,74	11,42	0,04	12,27	0,53	7,19	0,16	2,20	0,27	49,86	2,74	0,52	100,94
MONITOR BHVO-1	MajorBasic32+Zn	2016-04-20 01:17	13,72	11,41	0,04	12,30	0,52	7,12	0,17	2,21	0,28	49,95	2,74	0,52	100,98
MONITOR BHVO-1	Majors Acid32	2016-05-05 00:41	13,48	11,52	0,02	12,35	0,53	7,16	0,17	2,14	0,28	50,46	2,89	0,52	101,52
MONITOR BHVO-1	MajorBasic32+Zn	2016-05-05 00:49	13,71	11,40	0,04	12,27	0,53	7,19	0,17	2,22	0,28	49,91	2,73	0,52	100,97
MONITOR bhvo-1	MajorBasic32+Zn	2016-05-17 14:13	13,71	11,39	0,04	12,26	0,52	7,20	0,16	2,28	0,28	50,03	2,73	0,52	101,12
MONITOR BHVO-1	MajorBasic32+Zn	2016-05-20 11:23	13,73	11,45	0,03	12,33	0,52	7,21	0,17	2,23	0,28	50,12	2,74	0,52	101,33
MONITOR BHVO-1	Majors Acid32	2016-06-07 01:37	13,44	11,51	0,02	12,35	0,52	7,21	0,17	2,15	0,28	50,25	2,91	0,52	101,33
MONITOR BHVO-1	MajorBasic32+Zn	2016-06-07 01:21	13,72	11,44	0,04	12,29	0,52	7,15	0,17	2,29	0,27	50,02	2,75	0,52	101,18
MONITOR BHVO-1	MajorBasic32+Zn	2016-06-08 00:19	13,74	11,42	0,04	12,27	0,52	7,18	0,17	2,21	0,28	50,17	2,73	0,52	101,25
MONITOR bhvo-1	MajorBasic32+Zn	2016-06-20 16:25	13,78	11,40	0,04	12,32	0,52	7,17	0,17	2,24	0,28	50,29	2,72	0,52	101,45
MONITOR BHVO-1	MajorBasic32+Zn	2016-07-11 15:52	13,68	11,30	0,04	12,27	0,52	7,15	0,17	1,73	0,27	50,12	2,73	0,52	100,50
MONITOR BHVO-1	MajorBasic32+Zn	2016-07-22 21:48	13,71	11,40	0,04	12,25	0,53	7,24	0,17	2,24	0,27	49,84	2,73	0,52	100,94
MONITOR bhvo-1	MajorBasic32+Zn	2016-08-03 00:21	13,81	11,37	0,04	12,27	0,52	7,16	0,17	2,22	0,29	50,09	2,73	0,52	101,19
MONITOR bhvo-1	Majors Acid32	2016-08-24 21:45	13,55	11,51	0,02	12,33	0,53	7,17	0,17	2,13	0,28	50,18	2,90	0,52	101,29
MONITOR bhvo-1	MajorBasic32+Zn	2016-08-24 21:37	13,82	11,39	0,04	12,27	0,52	7,19	0,16	2,25	0,28	49,99	2,73	0,52	101,16
MONITOR bhvo-1	Majors Acid32	2016-08-31 03:32	13,46	11,49	0,02	12,36	0,52	7,20	0,17	2,15	0,28	50,26	2,91	0,52	101,34
MONITOR BHVO-1	MajorBasic32+Zn	2016-09-02 13:41	13,76	11,42	0,04	12,30	0,52	7,17	0,17	2,23	0,27	50,15	2,75	0,52	101,30
MONITOR BHVO-1	Majors Acid32	2016-09-01 04:26	13,54	11,50	0,02	12,36	0,53	7,20	0,18	2,15	0,28	50,45	2,91	0,52	101,64
MONITOR BHVO-1	Majors Acid32	2016-09-02 13:56	13,55	11,49	0,02	12,37	0,53	7,20	0,18	2,19	0,28	50,44	2,90	0,52	101,67
MONITOR BHVO-1	MajorBasic32+Zn	2016-09-07 17:10	13,67	11,50	0,04	12,30	0,52	7,17	0,17	2,23	0,28	50,18	2,74	0,52	101,32
MONITOR BHVO-1	Majors Acid32	2016-09-07 17:03	13,48	11,48	0,02	12,35	0,52	7,17	0,17	2,15	0,29	50,39	2,89	0,52	101,43
MONITOR BHVO-1	MajorBasic32+Zn	2016-10-07 23:31	13,61	11,47	0,03	12,29	0,51	7,18	0,17	2,20	0,28	50,17	2,75	0,52	101,18
MONITOR BHVO-1	MajorBasic32+Zn	2016-10-19 18:46	13,77	11,46	0,04	12,26	0,51	7,17	0,17	2,27	0,27	49,90	2,72	0,52	101,06
MONITOR BHVO-1	MajorBasic32+Zn	2016-10-20 23:34	13,69	11,44	0,03	12,30	0,51	7,11	0,17	2,24	0,27	50,10	2,73	0,52	101,11
MONITOR BHV01	MajorBasic32+Zn	2016-11-08 23:04	13,70	11,52	0,04	12,27	0,52	7,20	0,17	2,24	0,28	50,15	2,76	0,52	101,37
MONITOR bhvo-1	Majors Acid32	2016-11-02 21:07	13,41	11,50	0,02	12,35	0,52	7,16	0,17	2,05	0,28	50,18	2,90	0,52	101,06
MONITOR BHVO-1	MajorBasic32+Zn	2016-11-28 20:07	13,73	11,48	0,04	12,31	0,53	7,17	0,18	2,23	0,28	50,00	2,74	0,52	101,21
MONITOR BHVO-1	Majors Acid32	2016-11-28 19:59	13,44	11,55	0,02	12,36	0,52	7,19	0,17	2,16	0,28	50,48	2,89	0,52	101,58
MONITOR BHVO-1	MajorBasic32+Zn	2016-12-10 01:01	13,74	11,52	0,04	12,29	0,51	7,22	0,00	2,25	0,28	50,05	2,75	0,52	101,17
BHVO-1 STD	MajorBasic32+Zn	2017-03-08 15:45	13,73	11,41	0,04	12,28	0,52	7,22	0,17	2,29	0,28	50,18	2,73	0,52	101,37
BHVO-1 std	MajorBasic32+Zn	2017-05-02 10:44	13,69	11,42	0,04	12,28	0,53	7,19	0,17	2,26	0,28	50,14	2,74	0,52	101,26
MONITOR bhvo-1	MajorBasic32+Zn	2017-05-02 10:53	13,75	11,43	0,04	12,28	0,53	7,20	0,17	2,22	0,28	49,93	2,72	0,52	101,07
MONITOR bhvo-1	Majors Acid32	2017-05-02 11:01	13,48	11,51	0,02	12,35	0,53	7,18	0,17	2,17	0,28	50,42	2,91	0,52	101,54
BHVO-1 MONITOR	MajorBasic32+Zn	2017-05-17 15:48	13,82	11,39	0,04	12,24	0,52	7,14	0,17	2,23	0,28	50,01	2,74	0,52	101,10
MONITOR bhvo-1	Majors Acid32	2017-06-26 23:43	13,56	11,50	0,02	11,09	0,53	7,18	0,17	2,18	0,28	50,36	2,90	0,52	100,29

MONITOR bhvo-1	MajorBasic32+Zn	2017-06-26 23:50	13,79	11,43	0,04	12,26	0,53	7,18	0,17	2,27	0,27	50,16	2,73	0,52	101,35
BHVO-1 STD	Majors Acid32	2017-07-03 13:53	13,57	11,49	0,02	11,09	0,52	7,14	0,17	2,13	0,29	50,29	2,91	0,52	100,14
BHVO-1 std	MajorBasic32+Zn	2017-07-14 12:35	13,65	11,43	0,03	12,23	0,52	7,19	0,17	2,21	0,28	50,02	2,73	0,52	100,98
MONITOR BHVO-1	MajorBasic32+Zn	2017-07-20 16:58	13,66	11,42	0,04	12,29	0,53	7,17	0,17	2,23	0,28	49,85	2,73	0,52	100,89
MONITOR BHVO-1	Majors Acid32	2017-07-24 23:47	13,54	11,58	0,02	12,35	0,52	7,22	0,17	2,15	0,29	50,48	2,90	0,52	101,74
MONITOR BHVO-1	MajorBasic32+Zn	2017-07-24 23:38	13,71	11,40	0,03	12,26	0,52	7,17	0,17	2,22	0,28	50,05	2,74	0,52	101,07
MONITOR BHVO-1	MajorBasic32+Zn	2017-08-18 15:18	13,76	11,41	0,04	12,26	0,53	7,16	0,17	2,25	0,28	50,04	2,73	0,52	101,15
MONITOR BHVO-1	Majors Acid32	2017-08-18 15:26	13,58	11,50	0,02	11,06	0,53	7,20	0,17	2,15	0,28	50,41	2,89	0,52	100,31
BHVO-1 STD	Majors Acid32	2017-08-21 23:14	13,44	11,50	0,02	11,08	0,52	7,15	0,17	2,16	0,28	50,41	2,88	0,52	100,13
BHVO-1 STD	MajorBasic32+Zn	2017-08-21 23:21	13,80	11,40	0,04	12,28	0,52	7,17	0,17	2,25	0,28	49,81	2,73	0,52	100,97
MONITOR BHVO-1	Majors Interm32	2017-08-22 16:56	13,58	11,37	0,04	12,31	0,52	7,12	0,17	2,13	0,28	49,76	2,75	0,52	100,55
MONITOR bhvo-1	MajorBasic32+Zn	2017-09-11 21:07	13,72	11,42	0,04	12,30	0,52	7,19	0,17	2,19	0,29	50,16	2,73	0,52	101,25
BHVO-1 monitor	Majors Acid32	2017-09-14 20:39	13,48	11,49	0,02	11,09	0,53	7,20	0,17	2,17	0,28	50,35	2,89	0,52	100,19
MONITOR bhvo-1	MajorBasic32+Zn	2017-09-19 15:16	13,69	11,40	0,03	12,31	0,52	7,13	0,17	2,24	0,27	49,95	2,74	0,52	100,97
BHVO-1 std	Majors Acid32	2017-10-02 18:33	13,56	11,51	0,02	11,07	0,53	7,21	0,17	2,16	0,29	50,59	2,91	0,52	100,54
MONITOR BHVO-1	Majors Acid32	2017-10-04 17:57	13,45	11,51	0,02	11,09	0,52	7,19	0,17	2,21	0,28	50,25	2,92	0,52	100,13
MONITOR BHVO-1	MajorBasic32+Zn	2017-10-12 10:35	13,72	11,43	0,03	12,33	0,52	7,13	0,17	2,24	0,28	49,76	2,75	0,52	100,88
MONITOR bhvo-1	Majors Acid32	2017-10-12 18:40	13,53	11,53	0,02	11,07	0,53	7,20	0,17	2,18	0,28	50,35	2,91	0,52	100,29
MONITOR BHVO-1	MajorBasic32+Zn	2017-10-25 16:45	13,67	11,41	0,03	12,34	0,53	7,17	0,17	2,22	0,28	50,05	2,75	0,52	101,14
MONITOR BHVO-1	Majors Acid32	2017-10-25 16:38	13,45	11,50	0,02	11,09	0,52	7,17	0,17	2,18	0,29	50,33	2,90	0,52	100,14
MONITOR BHVO-1	Majors Acid32	2017-11-09 15:09	13,52	11,47	0,02	11,05	0,53	7,18	0,17	2,18	0,29	50,31	2,91	0,52	100,15
MONITOR BHVO-1	MajorBasic32+Zn	2017-11-09 15:01	13,70	11,43	0,04	12,33	0,53	7,21	0,17	2,23	0,28	50,10	2,74	0,52	101,28
BHVO-1 STD	MajorBasic32+Zn	2017-11-13 23:51	13,71	11,37	0,04	12,31	0,52	7,20	0,17	2,21	0,29	50,24	2,74	0,52	101,32
MONITOR BHVO-1	Majors Acid32	2017-11-13 23:44	13,52	11,48	0,02	11,09	0,52	7,16	0,17	2,17	0,29	50,11	2,89	0,52	99,94
MONITOR BHVO-1	MajorBasic32+Zn	2017-11-15 23:47	13,70	11,40	0,04	12,32	0,52	7,15	0,17	2,23	0,28	50,16	2,72	0,52	101,21
MONITOR BHVO-1	MajorBasic32+Zn	2017-11-20 17:52	13,66	11,48	0,04	12,29	0,52	7,19	0,17	2,22	0,28	50,09	2,75	0,52	101,21
MONITOR BHVO-1	Majors Acid32	2017-12-11 13:45	13,54	11,48	0,02	11,08	0,53	7,18	0,17	2,19	0,29	50,18	2,91	0,52	100,09
BHVO-1 STD	MajorBasic32+Zn	2018-01-25 19:37	13,48	11,71	0,03	12,25	0,51	7,13	0,17	2,25	0,28	49,56	2,70	0,52	100,59
MONITOR bhvo-1	MajorBasic32+Zn	2018-02-12 19:27	14,02	11,49	0,04	12,30	0,52	7,29	0,17	2,30	0,28	50,12	2,77	0,52	101,82
MONITOR bhvo-1	MajorBasic32+Zn	2018-02-15 09:05	13,90	11,45	0,04	12,29	0,52	7,28	0,17	2,35	0,27	49,87	2,74	0,52	101,40
MONITOR BHVO-1	MajorBasic32+Zn	2018-02-15 22:45	13,97	11,43	0,04	12,26	0,52	7,20	0,17	2,29	0,28	50,07	2,75	0,52	101,50
MONITOR BHVO-1	MajorBasic32+Zn	2018-02-17 00:27	13,87	11,38	0,04	12,26	0,52	7,25	0,17	2,27	0,28	49,71	2,74	0,52	101,01
MONITOR BHVO-1	MajorBasic32+Zn	2018-02-20 23:28	13,79	11,34	0,04	12,28	0,53	7,17	0,17	2,26	0,28	49,55	2,75	0,52	100,68
MONITOR BHVO-1	MajorBasic32+Zn	2018-02-21 21:38	13,86	11,36	0,04	12,27	0,52	7,21	0,17	1,80	0,28	49,47	2,75	0,52	100,25
MONITOR bhvo-1	MajorBasic32+Zn	2018-02-26 15:17	13,98	11,34	0,04	12,23	0,52	7,22	0,17	1,79	0,28	49,41	2,77	0,52	100,27
MONITOR bhvo-1	MajorBasic32+Zn	2018-03-12 21:21	13,76	11,35	0,04	12,28	0,52	7,24	0,17	2,26	0,28	49,52	2,76	0,52	100,70
BHVO-1 std	MajorBasic32+Zn	2018-03-23 12:02	13,84	11,42	0,04	12,28	0,52	7,24	0,17	2,29	0,27	49,62	2,75	0,52	100,96
MONITOR BHVO-1	MajorBasic32+Zn	2018-03-26 21:07	13,77	11,34	0,04	12,31	0,52	7,24	0,17	2,28	0,28	49,40	2,75	0,52	100,62
MONITOR BHVO-1	MajorBasic32+Zn	2018-04-04 22:02	13,77	11,29	0,04	12,23	0,52	7,21	0,17	2,25	0,28	49,07	2,74	0,52	100,09
BHVO-1 STD	MajorBasic32+Zn	2018-04-22 18:40	13,69	11,43	0,04	12,21	0,52	7,20	0,17	2,26	0,28	49,31	2,75	0,52	100,38
MONITOR bhvo-1	MajorBasic32+Zn	2018-05-11 13:31	13,96	11,38	0,04	12,35	0,52	7,25	0,17	2,27	0,29	50,41	2,74	0,52	101,90
MONITOR BHVO-1	MajorBasic32+Zn	2018-05-16 18:29	13,92	11,46	0,04	12,33	0,52	7,28	0,17	2,33	0,28	50,29	2,74	0,52	101,88
MONITOR BHVO-1	MajorBasic32+Zn	2018-05-17 16:37	13,77	11,42	0,03	12,36	0,52	7,25	0,17	2,28	0,29	50,61	2,75	0,52	101,97
MONITOR bhvo-1	MajorBasic32+Zn	2018-05-25 13:19	13,81	11,44	0,04	12,36	0,52	7,26	0,16	2,31	0,28	50,36	2,74	0,52	101,80
Average			13,63	11,43		12,32	0,52	7,19	0,17	2,20	0,27	49,94	2,80	0,52	101,02
Relative standard deviation (%)			0,58	0,35		0,36	3,70	0,47	0,00	4,68	0,74	0,23	2,71		0,06

Table D 5. 4: XRF granodiorite reference values

Sample name		Meas. date/time	Al2O3	CaO	Cr2O3	Fe2O3	K2O	MgO	MnO	Na2O	P2O5	SiO2	TiO2	Sum Of Conc.
			(%)	(%)	(%)	(%)	(%)	(%)	(%)	(%)	(%)	(%)	(%)	(%)
JG-1 Granodiorite Reference values			**14,20**	**2,18**	**0,01**	**2,14**	**3,97**	**0,74**	**0,06**	**3,39**	**0,10**	**72,30**	**0,26**	**99,35**
JG-1 STD	Majors Interm32	2014-12-10 14:42	14,14	2,17	0,01	2,12	4,01	0,73	0,07	3,35	0,10	72,95	0,25	99,90
STANDARD JG-1	Majors Acid32	2015-09-01 12:44	14,34	2,19	0,01	2,12	4,02	0,78	0,07	3,60	0,10	72,13	0,27	99,63
JG-1 std	Majors Acid32	2015-10-01 11:33	14,44	2,20	0,01	2,14	4,03	0,77	0,07	3,63	0,10	72,80	0,26	100,45
JG-1 std	Majors Acid32	2015-10-06 12:43	14,37	2,20	0,01	2,13	4,02	0,78	0,07	3,56	0,09	72,72	0,26	100,21
JG-1 STD	Majors Acid32	2015-10-29 11:44	14,45	2,21	0,01	2,12	4,02	0,77	0,06	3,68	0,10	72,48	0,26	100,16
JG-1 STD	Majors Acid32	2016-01-15 11:26	14,36	2,21	0,01	2,13	4,03	0,77	0,07	3,67	0,10	72,57	0,27	100,19
JG-1 std	Majors Acid32	2016-02-04 20:44	14,37	2,21	0,01	2,13	4,02	0,79	0,07	3,66	0,10	72,18	0,26	99,80
JG-1 STD	Majors Acid32	2016-02-11 17:46	14,34	2,21	0,01	2,13	4,03	0,78	0,06	3,61	0,10	72,19	0,27	99,73
JG-1 std	Majors Acid32	2016-03-08 16:08	14,13	2,21	0,01	2,13	4,02	0,75	0,07	3,43	0,09	72,03	0,26	99,13
J-G std	Majors Acid32	2016-03-14 22:57	14,12	2,21	0,01	2,13	3,98	0,75	0,07	3,42	0,10	71,98	0,26	99,03
JG-1 STD	Majors Acid32	2016-03-18 23:22	14,03	2,20	0,01	2,13	4,00	0,77	0,06	3,46	0,10	71,95	0,26	98,97
JG-1 STD	Majors Acid32	2016-04-12 23:22	14,11	2,21	0,01	2,13	4,00	0,76	0,07	3,42	0,10	72,13	0,26	99,20
JG-1 STD	Majors Acid32	2016-04-15 05:39	14,00	2,21	0,01	2,13	3,99	0,75	0,07	3,44	0,10	72,02	0,26	98,98
JG-1 std	Majors Acid32	2016-05-05 00:07	14,06	2,21	0,01	2,13	4,01	0,76	0,07	3,43	0,10	72,05	0,26	99,09
JG-1 STD	Majors Acid32	2016-06-07 00:20	14,00	2,20	0,01	2,13	4,01	0,77	0,07	3,44	0,10	71,81	0,26	98,80
JG-1 STD	Majors Acid32	2016-07-26 23:39	13,99	2,20	0,01	2,13	4,00	0,78	0,06	3,39	0,10	71,98	0,26	98,90
JG-1 std	Majors Acid32	2016-08-23 00:29	14,04	2,19	0,01	2,13	3,99	0,76	0,07	3,36	0,10	71,80	0,26	98,71
JG-1 std	Majors Acid32	2016-08-24 20:35	13,98	2,20	0,01	2,13	4,01	0,74	0,07	3,41	0,10	71,66	0,26	98,57
JG-1 std	Majors Acid32	2016-08-25 17:09	13,95	2,20	0,01	2,13	4,02	0,76	0,07	3,38	0,10	71,97	0,26	98,85
JG-1 std	Majors Acid32	2016-08-31 02:22	14,01	2,20	0,01	2,13	4,00	0,74	0,06	3,42	0,10	71,88	0,26	98,81
JG-1 STD	Majors Acid32	2016-09-01 03:51	14,01	2,19	0,01	2,12	3,98	0,75	0,07	3,43	0,10	71,72	0,26	98,64
JG-1 STD	Majors Acid32	2016-09-07 16:28	14,01	2,20	0,01	2,13	3,99	0,75	0,07	3,39	0,10	71,96	0,26	98,87
JG-1 STD	Majors Acid32	2016-10-17 22:31	13,94	2,17	0,01	2,12	4,00	0,73	0,07	3,24	0,09	71,76	0,26	98,39
JG-1 STD	Majors Acid32	2016-09-30 05:23	13,83	2,17	0,01	2,12	3,98	0,74	0,07	3,25	0,10	71,65	0,25	98,17
JG-1 std	Majors Acid32	2016-11-02 20:31	13,79	2,18	0,01	2,13	3,98	0,73	0,07	3,20	0,10	71,63	0,26	98,08
JG-1 STD	Majors Acid32	2016-11-28 19:25	13,85	2,19	0,01	2,13	3,98	0,74	0,07	3,29	0,10	71,69	0,26	98,31
JG-1 STD	Majors Acid32	2017-03-20 17:33	13,82	2,19	0,01	2,12	3,97	0,73	0,06	3,18	0,10	71,02	0,25	97,45
JG-1 std	Majors Acid32	2017-05-02 09:45	13,84	2,19	0,01	2,12	3,98	0,73	0,06	3,23	0,10	70,85	0,26	97,37
JG-1 STD	Majors Acid32	2017-07-03 13:17	13,76	2,19	0,01	2,00	3,98	0,74	0,06	3,17	0,10	71,01	0,26	97,28
JG-1 STD	Majors Acid32	2017-07-24 23:55	13,70	2,20	0,01	2,12	3,95	0,74	0,07	3,19	0,10	71,00	0,25	97,33
JG-1 STD	Majors Acid32	2017-08-18 16:38	13,76	2,18	0,01	1,99	3,98	0,71	0,07	3,24	0,10	72,05	0,25	98,34
JG-1 STD	Majors Acid32	2017-08-21 22:39	13,76	2,18	0,01	2,00	3,97	0,73	0,07	3,21	0,10	72,12	0,26	98,41
JG-1 std	Majors Acid32	2017-09-14 20:05	13,69	2,19	0,01	2,00	3,96	0,74	0,06	3,22	0,10	72,01	0,26	98,24
JG-1 std	Majors Acid32	2017-10-02 17:59	13,83	2,19	0,01	1,99	3,97	0,74	0,07	3,20	0,10	72,37	0,26	98,73
JG-1 STD	Majors Acid32	2017-10-04 17:23	13,67	2,20	0,01	2,00	3,96	0,74	0,06	3,21	0,11	72,04	0,26	98,26

JG-1	**std**	Majors Acid32	2017-10-12 18:06	13,73	2,19	0,01	2,00	4,00	0,73	0,07	3,23	0,10	72,11	0,26	98,43
JG-1	**STD**	Majors Acid32	2017-10-25 16:04	13,76	2,19	0,01	2,00	3,99	0,73	0,07	3,23	0,10	72,22	0,26	98,56
JG-1	**STD**	Majors Acid32	2017-11-09 13:59	13,72	2,19	0,01	2,00	3,98	0,74	0,07	3,21	0,10	72,09	0,26	98,37
JG	**STD**	Majors Acid32	2017-11-13 23:09	13,63	2,18	0,01	2,00	3,98	0,72	0,07	3,18	0,10	72,12	0,26	98,25
JG-1	**STD**	Majors Acid32	2017-12-11 13:10	13,72	2,19	0,01	1,99	3,99	0,74	0,07	3,23	0,11	71,97	0,26	98,28
JG-1	**STD**	MajorBasic32+Zn	2018-02-20 22:24	14,38	2,13	0,01	2,08	4,00	0,65	0,06	3,40	0,08	71,85	0,26	98,90
JG-1	**std**	MajorBasic32+Zn	2018-02-21 20:43	14,39	2,17	0,01	2,17	4,02	0,65	0,06	2,63	0,08	72,01	0,26	98,45
JG-1	**std**	MajorBasic32+Zn	2018-02-26 14:22	14,38	2,13	0,00	2,06	4,03	0,64	0,07	2,66	0,09	72,13	0,26	98,45
JG-1	**std**	MajorBasic32+Zn	2018-03-12 20:35	14,45	2,13	0,00	2,07	4,02	0,65	0,07	3,31	0,08	72,25	0,26	99,29
JG-1	**std**	MajorBasic32+Zn	2018-03-23 10:58	14,53	2,16	0,01	2,07	4,06	0,63	0,07	3,46	0,09	72,58	0,26	99,92
JG-1	**STD**	MajorBasic32+Zn	2018-03-26 20:22	14,38	2,12	0,01	2,08	4,02	0,64	0,07	3,41	0,09	71,99	0,26	99,07
JG-1	**STD**	MajorBasic32+Zn	2018-04-04 21:17	14,25	2,12	0,01	2,06	3,99	0,65	0,06	3,39	0,09	71,70	0,26	98,58
JG-1	**STD**	MajorBasic32+Zn	2018-04-22 17:55	14,42	2,15	0,01	2,07	4,02	0,64	0,06	3,33	0,09	71,65	0,25	98,69
JG-1	**std**	MajorBasic32+Zn	2018-05-11 11:44	14,52	2,15	0,00	2,07	3,98	0,67	0,06	3,40	0,09	73,49	0,26	100,69
JG-1	**STD**	MajorBasic32+Zn	2018-05-16 17:44	14,54	2,18	0,01	2,08	3,98	0,65	0,06	3,41	0,09	72,86	0,26	100,12
JG-1	**STD**	MajorBasic32+Zn	2018-05-17 15:51	14,42	2,16	0,00	2,07	3,95	0,64	0,06	3,38	0,09	73,36	0,26	100,39
JG-1	**STD**	MajorBasic32+Zn	2018-05-25 14:39	14,43	2,15	0,00	2,07	3,96	0,66	0,06	3,35	0,09	73,28	0,27	100,32
Average				14,10	2,20	0,01	2,13	4,00	0,76	0,07	3,44	0,10	72,07	0,26	99,14
Relative standard deviation (%)				0,69	0,81	6,38	0,56	0,87	2,39	8,06	1,61	1,90	0,33	0,15	0,21

Table D 5. 5: XRF quality control for 2010-2011

Sample name		Meas. date/time	Al2O3	CaO	Cr2O3	Fe2O3	K2O	MgO	MnO	Na2O	P2O5	SiO2	TiO2	L.O.I.	Sum Of Conc.
			(%)	(%)	(%)	(%)	(%)	(%)	(%)	(%)	(%)	(%)	(%)	**(%)**	(%)
Quality control for 2010-2011															
Average HUSG		**1900-01-13 17:55**	**13,75**	**1,52**	**0,00**	**3,78**	**4,66**	**1,04**	**0,06**	**2,57**	**0,21**	**69,77**	**0,54**	**0,73**	**98,65**
STDEV		**1900-01-00 04:51**	**0,20**	**0,04**	**0,00**	**0,14**	**0,06**	**0,04**	**0,01**	**0,18**	**0,01**	**0,54**	**0,02**	**0,05**	**0,71**
MIN		**1900-01-13 00:57**	**13,04**	**1,48**	**0,00**	**3,64**	**4,55**	**0,94**	**0,05**	**2,30**	**0,20**	**68,42**	**0,52**	**0,53**	**97,23**
MAX		**1900-01-14 07:06**	**14,30**	**1,63**	**0,01**	**4,56**	**4,80**	**1,22**	**0,08**	**3,30**	**0,23**	**70,96**	**0,60**	**0,80**	**100,40**
HUSG STD	Majors Acid32	2016-01-15 11:44	13,87	1,58	0,00	3,75	4,68	1,11	0,06	2,74	0,22	70,73	0,56	0,90	100,20
HUSG STD	Majors Interm32	2016-01-15 11:52	13,87	1,56	0,01	3,75	4,65	1,11	0,06	2,69	0,23	70,81	0,56	0,90	100,20
HUSG-1 std	Majors Acid32	2016-02-01 14:31	13,84	1,57	0,00	3,74	4,67	1,11	0,05	2,73	0,22	70,51	0,56	0,90	99,90
HUSG-1 std	Majors Acid32	2016-02-04 21:12	13,84	1,56	0,01	3,73	4,65	1,11	0,06	2,71	0,22	70,37	0,56	0,90	99,72
HUSG-1 STD	Majors Interm32	2016-02-12 15:49	13,76	1,57	0,01	3,74	4,65	1,11	0,06	2,71	0,21	70,36	0,54	0,90	99,62
HUSG-1 std	Majors Acid32	2016-03-08 16:25	13,69	1,58	0,01	3,75	4,68	1,11	0,06	2,64	0,22	70,63	0,56	0,90	99,83
HUS-G std	Majors Acid32	2016-03-14 23:14	13,68	1,57	0,01	3,74	4,64	1,10	0,05	2,63	0,22	70,58	0,57	0,90	99,69
HUSG-1 STD	Majors Acid32	2016-03-18 23:39	13,59	1,58	0,01	3,74	4,65	1,11	0,06	2,61	0,23	70,61	0,57	0,90	99,66
HUSG-1 STD	Majors Acid32	2016-04-12 23:40	13,67	1,57	0,01	3,74	4,62	1,10	0,06	2,63	0,23	70,34	0,56	0,90	99,43
HUSG-1 STD	Majors Acid32	2016-04-15 05:56	13,69	1,57	0,01	3,75	4,65	1,10	0,06	2,63	0,23	70,39	0,56	0,90	99,54
HUSG-1 std	Majors Acid32	2016-05-05 00:24	13,69	1,57	0,01	3,76	4,65	1,10	0,06	2,61	0,22	70,41	0,57	0,90	99,55
HUSG-1 STD	Majors Acid32	2016-06-07 00:45	13,75	1,57	0,00	3,75	4,65	1,08	0,06	2,62	0,22	70,41	0,57	0,90	99,58
HUS-G std	MajorBasic32+Zn	2016-06-20 15:49	13,90	1,56	0,00	3,72	4,66	1,00	0,05	2,69	0,22	71,37	0,54	0,90	100,61
HUS-G STD	MajorBasic32+Zn	2016-07-11 14:11	13,87	1,54	0,00	3,71	4,65	1,02	0,05	2,03	0,22	70,36	0,55	0,90	98,90
HUSG-1 STD	Majors Acid32	2016-07-27 00:04	13,63	1,57	0,00	3,73	4,66	1,10	0,06	2,66	0,23	70,59	0,57	0,90	99,70
HUS-G std	Majors Acid32	2016-08-22 23:53	13,67	1,55	0,00	3,73	4,64	1,09	0,06	2,60	0,22	70,60	0,58	0,90	99,64
HUSG-1 std	Majors Acid32	2016-08-24 21:01	13,66	1,57	0,00	3,74	4,67	1,09	0,06	2,61	0,22	70,43	0,57	0,90	99,52
HUSG-1 std	Majors Acid32	2016-08-25 17:34	13,65	1,57	0,00	3,74	4,67	1,10	0,06	2,61	0,22	70,48	0,56	0,90	99,56
HUSG-1 std	Majors Acid32	2016-08-31 02:48	13,61	1,57	0,00	3,74	4,63	1,10	0,06	2,62	0,23	70,41	0,56	0,90	99,43
HUSG-1 STD	Majors Acid32	2016-09-01 04:17	13,67	1,56	0,00	3,74	4,63	1,10	0,06	2,64	0,22	70,52	0,56	0,90	99,60
HUSG-1 STD	Majors Acid32	2016-09-02 14:28	13,69	1,56	0,00	3,74	4,64	1,10	0,06	2,62	0,22	70,52	0,56	0,90	99,61
HUSG-1 STD	Majors Acid32	2016-09-07 16:54	13,66	1,57	0,00	3,74	4,64	1,11	0,06	2,60	0,22	70,39	0,56	0,90	99,45
HUS-G STD	Majors Acid32	2016-10-17 21:33	13,62	1,55	0,00	3,74	4,66	1,08	0,06	2,50	0,22	70,40	0,56	0,90	99,29
HUSG-1 STD	Majors Acid32	2016-09-30 05:48	13,53	1,54	0,00	3,73	4,66	1,10	0,06	2,54	0,22	70,55	0,56	0,90	99,39
HUSG-1 std	Majors Acid32	2016-11-02 20:58	13,53	1,55	0,00	3,73	4,63	1,08	0,06	2,47	0,22	70,52	0,56	0,90	99,25
HUSG-1 STD	Majors Acid32	2016-11-28 19:51	13,63	1,58	0,00	3,75	4,64	1,11	0,05	2,60	0,23	70,63	0,56	0,90	99,68
HUSG-1 std	Majors Acid32	2017-03-17 08:38	13,72	1,57	0,00	3,73	4,63	1,08	0,06	2,59	0,22	70,39	0,57	0,90	99,46
HUSG-1 STD	Majors Interm32	2017-03-17 12:46	13,75	1,56	0,01	3,74	4,61	1,08	0,05	2,59	0,22	70,55	0,54	0,90	99,60
HUSG-1 STD	Majors Acid32	2017-03-20 17:59	13,70	1,57	0,00	3,75	4,64	1,10	0,06	2,63	0,22	70,53	0,57	0,90	99,67
HUSG-1 STD	Majors Interm32	2017-04-04 18:04	13,71	1,55	0,01	3,74	4,61	1,08	0,06	2,60	0,22	70,42	0,54	0,90	99,44
HUSG-1 std	Majors Acid32	2017-05-02 10:20	13,66	1,56	0,00	3,74	4,66	1,10	0,05	2,61	0,22	70,63	0,57	0,90	99,70
HUSG-1 STD	Majors Interm32	2017-05-16 13:47	13,59	1,55	0,01	3,75	4,62	1,08	0,06	2,58	0,21	70,62	0,53	0,90	99,50
HUSG-1 STD	Majors Acid32	2017-05-19 21:12	13,55	1,55	0,00	3,42	4,62	1,09	0,06	2,56	0,22	70,28	0,59	0,90	98,84
husg-1 std	Majors Interm32	2017-06-05 17:26	13,73	1,54	0,01	3,70	4,62	1,07	0,05	2,61	0,22	70,48	0,57	0,90	99,50
HUSG-1 std	Majors Acid32	2017-06-26 23:27	13,68	1,55	0,01	3,41	4,62	1,09	0,06	2,61	0,22	70,27	0,60	0,90	99,02
husg-1 std	Majors Interm32	2017-06-26 23:34	13,63	1,55	0,01	3,70	4,60	1,08	0,06	2,61	0,22	70,38	0,57	0,90	99,31
HUSG-1 STD	Majors Acid32	2017-07-03 13:44	13,63	1,58	0,01	3,44	4,62	1,09	0,06	2,60	0,23	70,33	0,56	0,90	99,05
HUSG-1 STD	Majors Acid32	2017-07-21 11:03	13,62	1,57	0,01	3,73	4,61	1,08	0,06	2,60	0,23	70,37	0,56	0,90	99,34

HUSG-1 STD	Majors Acid32	2017-07-25 00:22	13,57	1,58	0,01	3,74	4,63	1,09	0,06	2,62	0,23	70,44	0,56	0,90	99,43
HUSG-1 STD	Majors Acid32	2017-08-18 17:04	13,65	1,56	0,01	3,44	4,63	1,09	0,06	2,65	0,23	70,53	0,56	0,90	99,31
HUSG-1 STD	Majors Acid32	2017-08-21 23:05	13,59	1,56	0,00	3,41	4,64	1,09	0,05	2,62	0,22	70,41	0,59	0,90	99,08
HUSG-1 STD	Majors Interm32	2017-08-22 16:48	13,71	1,55	0,01	3,70	4,63	1,08	0,06	2,62	0,21	70,52	0,56	0,90	99,55
HUSG-1 std	Majors Acid32	2017-09-14 20:30	13,66	1,56	0,00	3,41	4,64	1,10	0,06	2,56	0,22	70,29	0,59	0,90	98,99
HUSG-1 std	Majors Acid32	2017-10-02 18:25	13,75	1,56	0,00	3,40	4,63	1,09	0,06	2,62	0,22	70,47	0,59	0,90	99,29
HUSG-1 STD	Majors Acid32	2017-10-04 17:48	13,55	1,57	0,00	3,41	4,62	1,11	0,06	2,61	0,23	70,46	0,59	0,90	99,11
HUSG-1 std	Majors Acid32	2017-10-12 18:32	13,64	1,57	0,00	3,42	4,63	1,10	0,06	2,59	0,22	70,58	0,59	0,90	99,30
HUSG-1 STD	Majors Acid32	2017-10-25 16:29	13,60	1,57	0,00	3,41	4,65	1,09	0,06	2,61	0,22	70,38	0,58	0,90	99,07
HUSG-1 STD	Majors Acid32	2017-11-09 14:25	13,63	1,56	0,00	3,41	4,64	1,08	0,06	2,60	0,22	70,41	0,59	0,90	99,10
HUSG-1 STD	Majors Acid32	2017-11-13 23:35	13,65	1,57	0,00	3,41	4,64	1,09	0,06	2,62	0,22	70,26	0,58	0,90	99,00
HUSG-1 STD	Majors Acid32	2017-12-11 13:36	13,61	1,55	0,00	3,41	4,61	1,10	0,05	2,61	0,22	70,21	0,60	0,90	98,87
HUSG-1 STD	MajorBasic32+Zn	2018-02-15 22:09	14,02	1,53	0,00	3,66	4,70	1,02	0,05	2,74	0,21	70,24	0,57	0,90	99,64
HUSG-1 STD	MajorBasic32+Zn	2018-02-16 23:51	14,08	1,54	0,00	3,65	4,66	1,04	0,06	2,72	0,22	69,62	0,57	0,90	99,06
HUSG-1 STD	MajorBasic32+Zn	2018-02-20 22:51	14,04	1,52	0,00	3,66	4,65	1,01	0,05	2,73	0,21	69,42	0,57	0,90	98,76
HUSG-1 STD	MajorBasic32+Zn	2018-02-21 21:11	13,95	1,52	0,00	3,66	4,66	1,01	0,06	2,12	0,21	69,33	0,57	0,90	97,99
HUSG-1 std	MajorBasic32+Zn	2018-02-26 14:41	14,07	1,53	0,00	3,64	4,67	1,01	0,05	2,16	0,22	69,63	0,57	0,90	98,45
HUSG-1 std	MajorBasic32+Zn	2018-03-12 20:53	14,04	1,53	0,00	3,65	4,69	1,05	0,06	2,75	0,21	69,93	0,56	0,90	99,37
HUSG-1 std	MajorBasic32+Zn	2018-03-23 11:26	14,12	1,54	0,00	3,68	4,71	1,04	0,06	2,74	0,21	70,23	0,56	0,90	99,79
HUSG-1 STD	MajorBasic32+Zn	2018-03-26 20:40	13,92	1,53	0,00	3,65	4,68	1,02	0,06	2,73	0,21	69,76	0,57	0,90	99,03
HUSG-1 STD	MajorBasic32+Zn	2018-04-04 21:35	13,80	1,52	0,00	3,64	4,65	1,02	0,05	2,74	0,22	69,44	0,55	0,90	98,53
HUSG-1 STD	MajorBasic32+Zn	2018-04-22 18:13	13,88	1,54	0,00	3,66	4,65	1,02	0,06	2,70	0,21	68,91	0,56	0,90	98,09
HUSG-1 std	MajorBasic32+Zn	2018-05-11 12:55	14,05	1,55	0,00	3,68	4,62	1,02	0,06	2,74	0,21	70,72	0,56	0,90	100,11
HUSG-1 STD	MajorBasic32+Zn	2018-05-16 18:02	14,00	1,56	0,00	3,68	4,60	1,01	0,05	2,72	0,22	70,09	0,56	0,90	99,39
HUSG-1 STD	MajorBasic32+Zn	2018-05-17 16:10	14,10	1,54	0,00	3,69	4,62	1,01	0,05	2,71	0,22	70,74	0,56	0,90	100,14
HUSG-1 STD	MajorBasic32+Zn	2018-05-25 10:49	14,00	1,55	0,00	3,67	4,60	1,03	0,05	2,70	0,21	70,58	0,56	0,90	99,85
Average			13,79	1,57	0,01	3,74	4,66	1,11	0,06	2,69	0,22	70,57	0,56	0,90	99,88
Relative standard deviation (%)			0,34	3,20	45,08	0,89	0,10	6,17	11,31	4,82	3,53	1,15	2,98	23,28	1,25

Table D 5. 6: XRF granite reference values

Sample name		Meas. date/time	Al2O3 (%)	CaO (%)	Cr2O3 (%)	Fe2O3 (%)	K2O (%)	MgO (%)	MnO (%)	Na2O (%)	P2O5 (%)	SiO2 (%)	TiO2 (%)	L.O.I. (%)	Sum Of Conc. (%)
WITS-G															
Granite Reference values			**11,53**	**1,51**		**3,58**	**4,46**	**0,10**	**0,05**	**2,97**	**0,04**	**74,53**	**0,29**	**0,08**	**99,14**
WITS-G			**11,73**	**1,44**		**3,43**	**4,29**	**0,21**	**0,03**	**2,39**	**0,05**	**74,26**	**0,29**	**0,07**	**98,19**
WITS-G (AUG)			**12,01**	**1,46**		**3,51**	**4,26**	**0,05**	**0,02**	**2,39**	**0,06**	**74,56**	**0,30**	**0,07**	**98,69**
WITS-G (OCT)			**11,52**	**1,47**		**3,47**	**4,33**	**0,00**	**0,05**	**2,37**	**0,03**	**73,57**	**0,28**	**0,07**	**97,14**
WITS-G (DEC)			**11,45**	**1,47**		**3,50**	**4,39**	**0,06**	**0,05**	**2,45**	**0,04**	**75,45**	**0,28**	**0,07**	**99,22**
Average reference value			**11,65**	**1,47**		**3,50**	**4,34**	**0,08**	**0,04**	**2,51**	**0,04**	**74,47**	**0,29**	**0,07**	**98,48**
WITS-G STD	Majors Acid32	2016-01-14 16:57	11,77	1,50	0,00	3,46	4,43	0,09	0,05	2,68	0,04	75,13	0,31	0,07	**99,53**
WITS-G STD	Majors Interm32	2016-01-15 12:09	11,79	1,48	0,00	3,46	4,42	0,08	0,05	2,62	0,03	75,57	0,30	0,07	**99,87**
WITS-G std	Majors Acid32	2016-02-01 14:22	11,81	1,49	0,00	3,46	4,43	0,09	0,05	2,67	0,04	75,03	0,31	0,07	**99,45**
WITS-G std	Majors Acid32	2016-02-04 21:02	11,80	1,49	0,00	3,46	4,43	0,08	0,05	2,64	0,04	74,89	0,31	0,07	**99,26**
WITS-G STD	Majors Interm32	2016-02-11 15:32	11,69	1,47	0,01	3,45	4,41	0,08	0,05	2,61	0,03	75,04	0,30	0,07	**99,21**
WITS-G STD	Majors Acid32	2016-02-11 15:40	11,73	1,49	0,00	3,45	4,43	0,08	0,05	2,68	0,04	74,92	0,31	0,07	**99,25**
WITS-G std	Majors Acid32	2016-03-08 16:34	11,63	1,49	0,00	3,46	4,42	0,09	0,05	2,56	0,04	74,90	0,30	0,07	**99,01**
WITS-G STD	Majors Interm32	2016-03-09 16:59	11,62	1,47	0,00	3,47	4,40	0,08	0,05	2,56	0,03	75,32	0,29	0,07	**99,36**
WITS-G std	Majors Acid32	2016-03-14 23:22	11,62	1,49	0,00	3,47	4,42	0,10	0,05	2,54	0,04	75,13	0,30	0,07	**99,23**
WITS-G STD	Majors Acid32	2016-03-18 23:47	11,55	1,48	0,00	3,45	4,41	0,09	0,05	2,55	0,03	75,03	0,30	0,07	**99,01**
WITS-G STD	Majors Acid32	2016-04-12 23:48	11,59	1,49	0,00	3,46	4,41	0,09	0,05	2,54	0,04	74,99	0,30	0,07	**99,03**
WITS-G STD	Majors Acid32	2016-04-15 06:05	11,64	1,48	0,00	3,47	4,41	0,10	0,05	2,62	0,04	75,02	0,30	0,07	**99,20**
WITS-G std	Majors Acid32	2016-05-05 00:33	11,64	1,49	0,00	3,47	4,42	0,09	0,05	2,59	0,04	75,11	0,30	0,07	**99,27**
WITS-G STD	Majors Acid32	2016-06-07 00:37	11,65	1,49	0,00	3,46	4,41	0,10	0,05	2,56	0,04	74,92	0,31	0,07	**99,06**
WITS-G STD	Majors Acid32	2016-07-26 23:56	11,61	1,48	0,00	3,45	4,42	0,09	0,05	2,59	0,04	75,06	0,31	0,07	**99,17**
WITS-G std	Majors Acid32	2016-08-23 00:07	11,70	1,48	0,00	3,46	4,40	0,10	0,05	2,56	0,04	75,21	0,30	0,07	**99,37**
WITS-G std	Majors Acid32	2016-08-24 20:53	11,65	1,48	0,00	3,47	4,43	0,10	0,05	2,58	0,04	74,83	0,30	0,07	**99,00**
WITS-G std	Majors Acid32	2016-08-25 17:26	11,63	1,49	0,00	3,47	4,44	0,09	0,05	2,60	0,04	75,14	0,31	0,07	**99,33**
WITS-G std	Majors Acid32	2016-08-31 02:40	11,71	1,49	0,00	3,47	4,42	0,10	0,05	2,58	0,04	75,30	0,30	0,07	**99,53**
WITS-G STD	Majors Acid32	2016-09-01 04:09	11,62	1,47	0,00	3,46	4,43	0,09	0,05	2,58	0,04	75,27	0,30	0,07	**99,38**
WITS-G STD	Majors Acid32	2016-09-02 14:12	11,70	1,48	0,00	3,47	4,42	0,10	0,05	2,59	0,04	75,19	0,30	0,07	**99,41**
WITS-G STD	Majors Acid32	2016-09-07 16:45	11,57	1,49	0,00	3,47	4,44	0,09	0,05	2,60	0,04	75,21	0,30	0,07	**99,33**
WITS-G STD	Majors Acid32	2016-10-17 22:15	11,50	1,48	0,00	3,47	4,43	0,10	0,05	2,47	0,04	75,19	0,30	0,07	**99,10**
WITS-G STD	Majors Acid32	2016-09-30 05:40	11,53	1,47	0,00	3,45	4,41	0,10	0,05	2,44	0,04	74,92	0,30	0,07	**98,78**
WITS-G std	Majors Acid32	2016-11-02 20:49	11,48	1,47	0,00	3,47	4,40	0,10	0,05	2,49	0,04	75,09	0,29	0,07	**98,95**
WITS-G STD	Majors Acid32	2016-11-28 19:42	11,61	1,49	0,00	3,46	4,41	0,10	0,05	2,57	0,04	74,94	0,31	0,07	**99,05**
WITS-G std	Majors Acid32	2017-03-17 12:23	11,67	1,48	0,00	3,38	4,41	0,09	0,05	2,55	0,04	74,93	0,27	0,07	**98,94**
WITS-G STD	Majors Interm32	2017-03-17 12:30	11,64	1,48	0,00	3,37	4,38	0,07	0,05	2,55	0,03	75,01	0,27	0,07	**98,92**
WITS-G STD	Majors Acid32	2017-03-20 17:50	11,61	1,49	0,00	3,38	4,43	0,09	0,05	2,55	0,04	74,91	0,27	0,07	**98,89**
WITS-G STD	Majors Interm32	2017-04-04 17:55	11,67	1,47	0,00	3,37	4,40	0,08	0,05	2,55	0,03	75,42	0,27	0,07	**99,38**
WITS-G std	Majors Acid32	2017-05-02 10:03	11,64	1,49	0,00	3,38	4,44	0,10	0,05	2,53	0,04	75,23	0,27	0,07	**99,24**
WITS-G STD	Majors Interm32	2017-05-16 13:39	11,69	1,47	0,00	3,37	4,41	0,07	0,05	2,58	0,03	75,27	0,26	0,07	**99,27**
WITS-G STD	Majors Acid32	2017-05-19 20:58	11,62	1,48	0,00	3,11	4,41	0,10	0,05	2,58	0,04	74,91	0,27	0,07	**98,64**
wits-g std	Majors Interm32	2017-06-05 17:17	11,65	1,48	0,00	3,36	4,40	0,09	0,05	2,56	0,03	75,30	0,27	0,07	**99,26**

WITS-G std	Majors Acid32	2017-06-26 23:11	11,63	1,49	0,00	3,13	4,43	0,09	0,05	2,57	0,04	74,79	0,27	0,07	**98,56**
wits-g std	Majors Interm32	2017-06-26 23:19	11,67	1,47	0,00	3,38	4,40	0,08	0,05	2,58	0,03	75,27	0,27	0,07	**99,27**
WITS-G STD	Majors Acid32	2017-07-03 13:35	11,62	1,48	0,00	3,12	4,43	0,09	0,05	2,56	0,04	75,11	0,27	0,07	**98,84**
WITS-G STD	Majors Acid32	2017-07-21 10:55	11,54	1,49	0,00	3,38	4,40	0,08	0,05	2,59	0,04	74,92	0,27	0,07	**98,83**
WITS-G STD	Majors Acid32	2017-07-25 00:13	11,61	1,50	0,00	3,38	4,41	0,09	0,05	2,58	0,04	74,86	0,27	0,07	**98,86**
WITS-G STD	Majors Acid32	2017-08-18 16:55	11,64	1,48	0,00	3,11	4,43	0,10	0,05	2,59	0,04	75,12	0,27	0,07	**98,90**
WITS-G STD	Majors Acid32	2017-08-21 22:56	11,53	1,49	0,00	3,12	4,43	0,09	0,05	2,56	0,04	75,07	0,27	0,07	**98,72**
WITS-G std	Majors Acid32	2017-09-14 20:22	11,61	1,49	0,00	3,11	4,43	0,09	0,05	2,59	0,04	75,19	0,27	0,07	**98,94**
WITS-G std	Majors Acid32	2017-10-02 18:16	11,73	1,49	0,00	3,11	4,43	0,09	0,05	2,59	0,04	75,33	0,27	0,07	**99,20**
WITS-G STD	Majors Acid32	2017-10-04 17:40	11,54	1,48	0,00	3,12	4,41	0,09	0,05	2,58	0,04	75,04	0,27	0,07	**98,69**
WITS-G std	Majors Acid32	2017-10-12 18:23	11,61	1,50	0,00	3,11	4,41	0,09	0,05	2,60	0,04	75,06	0,28	0,07	**98,82**
WITS-G STD	Majors Acid32	2017-10-25 16:21	11,67	1,49	0,00	3,11	4,43	0,10	0,05	2,62	0,04	75,12	0,27	0,07	**98,97**
WITS-G STD	Majors Acid32	2017-11-09 14:17	11,56	1,49	0,00	3,11	4,41	0,11	0,05	2,58	0,04	75,17	0,28	0,07	**98,87**
WITS-G STD	Majors Acid32	2017-11-13 23:27	11,63	1,49	0,00	3,12	4,44	0,11	0,05	2,61	0,04	75,32	0,28	0,07	**99,16**
WITS-G STD	Majors Acid32	2017-12-11 13:28	11,58	1,50	0,00	3,12	4,44	0,11	0,05	2,60	0,04	75,34	0,27	0,07	**99,12**
WITS-G std	MajorBasic32+Zn	2018-02-15 06:58	12,20	1,48	-0,01	3,35	4,52	0,03	0,05	2,71	0,03	75,24	0,27	0,07	**99,94**
WITS-G STD	MajorBasic32+Zn	2018-02-15 21:59	12,09	1,48	0,00	3,36	4,50	0,01	0,05	2,73	0,03	75,07	0,27	0,07	**99,66**
WITS-G STD	MajorBasic32+Zn	2018-02-16 23:42	12,03	1,48	-0,01	3,34	4,49	0,02	0,05	2,77	0,03	74,77	0,27	0,07	**99,31**
WITS-G STD	MajorBasic32+Zn	2018-02-20 22:42	11,94	1,46	-0,01	3,33	4,45	0,01	0,05	2,71	0,03	74,63	0,27	0,07	**98,94**
WITS-G STD	MajorBasic32+Zn	2018-02-21 21:01	12,05	1,46	0,00	3,34	4,47	0,01	0,05	2,16	0,03	74,70	0,27	0,07	**98,61**
WITS-G std	MajorBasic32+Zn	2018-02-26 14:32	12,00	1,46	-0,01	3,33	4,48	0,02	0,05	2,14	0,04	74,97	0,27	0,07	**98,82**
WITS-G std	MajorBasic32+Zn	2018-03-12 20:44	11,95	1,47	0,00	3,35	4,47	0,01	0,05	2,70	0,03	75,06	0,27	0,07	**99,43**
WITS-G std	MajorBasic32+Zn	2018-03-23 11:17	12,04	1,48	0,00	3,37	4,52	0,01	0,05	2,76	0,03	75,20	0,27	0,07	**99,80**
WITS-G STD	MajorBasic32+Zn	2018-03-26 20:31	12,00	1,47	-0,01	3,33	4,48	0,02	0,05	2,78	0,03	74,67	0,27	0,07	**99,16**
WITS-G STD	MajorBasic32+Zn	2018-04-04 21:26	11,97	1,46	-0,01	3,33	4,44	0,01	0,05	2,67	0,04	74,43	0,27	0,07	**98,73**
WITS-G STD	MajorBasic32+Zn	2018-04-22 18:04	12,00	1,49	0,00	3,32	4,46	0,03	0,05	2,75	0,03	74,24	0,26	0,07	**98,70**
WITS-G std	MajorBasic32+Zn	2018-05-11 12:10	12,17	1,48	-0,01	3,36	4,41	0,02	0,04	2,75	0,03	75,80	0,27	0,07	**100,39**
WITS-G STD	MajorBasic32+Zn	2018-05-16 17:53	12,10	1,51	-0,01	3,37	4,42	0,02	0,05	2,71	0,03	75,37	0,27	0,07	**99,91**
WITS-G STD	MajorBasic32+Zn	2018-05-17 16:00	12,00	1,48	-0,01	3,37	4,41	0,02	0,05	2,77	0,04	75,17	0,27	0,07	**99,64**
WITS-G std	MajorBasic32+Zn	2018-05-25 15:21	11,89	1,49	0,00	3,35	4,43	0,03	0,05	2,73	0,04	75,03	0,27	0,07	**99,38**
Average			11,69	1,49	0,00	3,46	4,42	0,08	0,05	2,64	0,04	75,13	0,31	0,07	99,46
Relative standard deviation (%)			1,36	1,59		3,41	0,81	16,00	0,00	10,98	10,00	0,81	5,52	12,50	0,33

Appendix E.1: Conditions Recorded for Geochronological Analyses

Table E 1: Conditions recorded during SIMS geochronological analyses

Sample #	Power b	Power a	Power sa	$Pb/U_{std,}P$	U ppm	Conc.	Conc.	Th/U	± (%)
	Quad. a	Quad. c	±std err (%)	Pb/U_{std}	std.	slope	int.	factor	
SC08@1	1.800	-1.164	1.6370	0.17916,P6	81.2	4.3104	0	0.12796	6.36
SC08@60	1.800	-1.164	1.6370	0.17916,P6	81.2	4.3104	0	0.12796	6.36
SC08@61	1.800	-1.164	1.6370	0.17916,P6	81.2	4.3104	0	0.12796	6.36
SC08@62	1.800	-1.164	1.6370	0.17916,P6	81.2	4.3104	0	0.12796	6.36
SC10@6	1.800	-1.164	1.6370	0.17916,P6	81.2	4.3104	0	0.12796	6.36
SC10@8	1.800	-1.164	1.6370	0.17916,P6	81.2	4.3104	0	0.12796	6.36
SC10@10	1.800	-1.164	1.6370	0.17916,P6	81.2	4.3104	0	0.12796	6.36
SC10@11	1.800	-1.164	1.6370	0.17916,P6	81.2	4.3104	0	0.12796	6.36
SC10@12	1.800	-1.164	1.6370	0.17916,P6	81.2	4.3104	0	0.12796	6.36
SC10@15	1.800	-1.164	1.6370	0.17916,P6	81.2	4.3104	0	0.12796	6.36
SC10@16	1.800	-1.164	1.6370	0.17916,P6	81.2	4.3104	0	0.12796	6.36
SC10@18	1.800	-1.164	1.6370	0.17916,P6	81.2	4.3104	0	0.12796	6.36
SC10@19	1.800	-1.164	1.6370	0.17916,P6	81.2	4.3104	0	0.12796	6.36
SC10@21	1.800	-1.164	1.6370	0.17916,P6	81.2	4.3104	0	0.12796	6.36
SC10@23	1.800	-1.164	1.6370	0.17916,P6	81.2	4.3104	0	0.12796	6.36
SC10@24	1.800	-1.164	1.6370	0.17916,P6	81.2	4.3104	0	0.12796	6.36
SC10@27	1.800	-1.164	1.6370	0.17916,P6	81.2	4.3104	0	0.12796	6.36
SC10@28	1.800	-1.164	1.6370	0.17916,P6	81.2	4.3104	0	0.12796	6.36
SC10@29	1.800	-1.164	1.6370	0.17916,P6	81.2	4.3104	0	0.12796	6.36
SC10@32	1.800	-1.164	1.6370	0.17916,P6	81.2	4.3104	0	0.12796	6.36
SC10@33	1.800	-1.164	1.6370	0.17916,P6	81.2	4.3104	0	0.12796	6.36
SC10@36	1.800	-1.164	1.6370	0.17916,P6	81.2	4.3104	0	0.12796	6.36
SC10@37	1.800	-1.164	1.6370	0.17916,P6	81.2	4.3104	0	0.12796	6.36
SC10@61	1.800	-1.164	1.6370	0.17916,P6	81.2	4.3104	0	0.12796	6.36

Appendix E.2: Geochronology Results

Table E 2. 1: Results of SIMS geochronology analyses

		Conventional concordia columns (Pbc corr.)									*TW concordia columns (Pbc corr.)*				*TW concordia columns (Pbc uncorr.)*			
Sample/	Group	^{207}Pb	±s	^{206}Pb	±s	r	^{208}Pb	±s	Disc. %	Disc. %	^{238}U	±s	^{207}Pb	±s	^{238}U	±s	^{207}Pb	±s
spot #		^{235}U	%	^{238}U	%		^{232}Th	%	conv.	2s lim.	^{206}Pb	%	^{206}Pb	%	^{206}Pb	%	^{206}Pb	%
SC08@1	no CL	5.36795	2.23	0.3111	2.19	0.98097	0.08	7.35	-16.0	-11.8	3.214	2.19	0.12513	0.43	3.211	2.19	0.12581	0.43
SC08@60	no CL	2.38897	1.94	0.1685	1.83	0.94318	0.10	7.84	-43.2	-39.4	5.934	1.83	0.10282	0.64	5.858	1.83	0.11222	0.45
SC08@61	no CL	2.58225	1.78	0.1670	1.66	0.93430	0.06	7.46	-49.3	-45.8	5.989	1.66	0.11217	0.64	5.907	1.67	0.12214	0.46
SC08@62	no CL	5.86358	2.07	0.3336	2.02	0.97696	0.10	9.76	-11.6	-7.5	2.998	2.02	0.12748	0.44	2.994	2.02	0.12847	0.41
SC10@6	light	2.46508	3.32	0.1577	1.82	0.54714	0.13	13.57	-52.7	-39.3	6.341	1.82	0.11337	2.78	6.176	1.83	0.13220	1.32
SC10@8	rim	3.46436	2.04	0.2201	2.02	0.99070	0.07	7.15	-34.5	-31.5	4.543	2.02	0.11415	0.28	4.534	2.02	0.11562	0.27
SC10@10	core	4.77823	2.01	0.2852	1.98	0.98637	0.09	9.95	-20.6	-17.1	3.506	1.98	0.12149	0.33	3.470	1.99	0.12869	0.19
SC10@11	rim	1.74876	2.80	0.1245	1.93	0.68872	0.11	7.20	-57.6	-46.9	8.035	1.93	0.10190	2.03	7.557	1.97	0.14551	0.96
SC10@12	light	5.51773	1.70	0.3231	1.67	0.98473	0.14	7.08	-11.8	-8.6	3.095	1.67	0.12386	0.30	3.075	1.67	0.12838	0.22
SC10@15	light	3.26584	1.71	0.2056	1.65	0.96823	0.07	6.79	-39.4	-36.6	4.864	1.65	0.11520	0.43	4.789	1.66	0.12623	0.28
SC10@16	rim	1.39178	2.07	0.1020	2.05	0.98777	0.03	7.00	-63.9	-61.6	9.804	2.05	0.09897	0.32	9.678	2.06	0.10844	0.24
SC10@18	rim	~~8.14138~~	~~6.39~~	~~0.4946~~	~~3.67~~	~~0.57404~~	5.04	8.83	40.3	11.6	2.022	3.67	0.11938	5.23	1.728	4.19	0.22334	1.71
SC10@19	rim	~~1.43836~~	~~24.54~~	~~0.1075~~	~~11.42~~	~~0.46546~~	0.07	42.07	-61.0		9.303	11.42	0.09705	21.72	8.926	11.93	0.12698	10.75
SC10@21	rim	1.97529	1.83	0.1175	1.64	0.89613	0.55	7.15	-67.4	-63.3	8.513	1.64	0.12196	0.81	8.041	1.64	0.16158	0.45
SC10@23	light	2.91805	1.72	0.1871	1.69	0.98047	0.11	7.68	-43.7	-41.2	5.343	1.69	0.11309	0.34	5.285	1.69	0.12092	0.23
SC10@24	rim	2.35801	2.61	0.1613	2.12	0.81240	0.21	7.37	-47.7	-39.8	6.200	2.12	0.10602	1.52	5.851	2.18	0.14700	0.77
SC10@27	rim	3.88435	1.69	0.2326	1.64	0.97293	0.11	7.18	-35.1	-32.3	4.300	1.64	0.12114	0.39	4.268	1.64	0.12649	0.32
SC10@28	light	2.21868	2.04	0.1439	2.04	0.99756	0.05	6.90	-56.1	-54.2	6.949	2.04	0.11182	0.14	6.940	2.04	0.11281	0.13
SC10@29	light	1.27060	1.76	0.1007	1.73	0.98528	0.05	6.89	-60.3	-58.0	9.926	1.73	0.09147	0.30	9.870	1.73	0.09566	0.26
SC10@32	rim	0.72361	2.30	0.0603	2.10	0.91104	0.01	10.59	-74.4	-68.2	16.585	2.10	0.08704	0.95	16.177	2.12	0.10542	0.47
SC10@33	core	1.37091	1.92	0.1099	1.64	0.85375	0.04	9.92	-55.9	-50.1	9.097	1.64	0.09045	1.00	9.046	1.64	0.09464	0.74
SC10@36	core	2.21357	4.42	0.1465	1.96	0.44249	0.13	12.43	-54.3	-34.9	6.827	1.96	0.10961	3.97	6.474	2.01	0.14718	2.05
SC10@37	rim	2.07735	1.67	0.1412	1.65	0.99118	0.15	6.83	-54.6	-52.7	7.083	1.65	0.10671	0.22	7.032	1.65	0.11190	0.17
SC10@61	no CL	~~no data~~	~~no data~~	~~0.2502~~	~~3.76~~	~~no data~~	no data	no data	no data	-52.7	3.996	3.76	no data	no data	3.440	3.58	0.12653	0.42

Table E 2. 2: Results of SIMS geochronology analyses (cont.)

Sample/ spot #	$^{207}Pb/^{206}Pb$	±s	$^{207}Pb/^{235}U$	±s	$^{206}Pb/^{238}U$	±s	$^{208}Pb/^{232}Th$	±s	207-corr age (Ma)	±s
SC08@1	2030.6	7.6	1879.8	19.3	1746.3	33.6	1514.3	106.9	>1200	
SC08@60	1675.7	11.8	1239.3	14.0	1003.9	17.0	1953.7	145.6	965.4	18.5
SC08@61	1834.8	11.5	1295.6	13.1	995.4	15.4	1239.1	89.4	945.0	17.5
SC08@62	2063.6	7.8	1955.9	18.1	1855.7	32.7	1928.2	178.6	>1200	
SC10@6	1854.2	49.4	1261.9	24.3	943.9	16.0	2419.1	307.0	892.7	18.9
SC10@8	1866.6	5.0	1519.1	16.2	1282.4	23.5	1366.2	94.2	>1200	
SC10@10	1978.2	5.9	1781.1	17.0	1617.7	28.4	1695.1	161.2	>1200	
SC10@11	1659.1	37.1	1026.7	18.2	756.2	13.8	2063.2	140.8	720.5	17.6
SC10@12	2012.6	5.2	1903.4	14.7	1804.8	26.3	2660.8	175.6	>1200	
SC10@15	1883.0	7.7	1473.0	13.4	1205.4	18.2	1411.0	92.3	1151.4	21.0
SC10@16	1604.7	6.0	885.5	12.3	626.1	12.2	619.9	42.7	595.9	13.0
SC10@18	~~1946.9~~	~~90.7~~	~~2246.9~~	~~59.5~~	~~2590.7~~	~~78.7~~	~~36354.7~~	~~1436.4~~	~~>1200~~	
SC10@19	~~1568.2~~	~~359.9~~	~~905.0~~	~~158.8~~	~~658.1~~	~~71.9~~	~~1376.0~~	~~552.0~~	~~628.7~~	74.3
SC10@21	1985.1	14.4	1107.1	12.4	715.9	11.1	8862.6	506.8	662.9	16.3
SC10@23	1849.6	6.1	1386.6	13.1	1105.9	17.1	2185.4	158.5	1054.1	19.3
SC10@24	1732.1	27.7	1230.0	18.8	964.0	19.0	3875.5	258.3	921.5	23.5
SC10@27	1973.0	6.9	1610.4	13.7	1347.9	20.0	2162.8	146.8	>1200	
SC10@28	1829.3	2.6	1187.0	14.4	866.7	16.6	1016.1	68.3	818.6	17.5
SC10@29	1456.4	5.7	832.7	10.0	618.8	10.2	1068.4	71.6	594.6	10.7
SC10@32	1361.3	18.2	552.8	9.9	377.4	7.7	179.1	18.9	361.8	8.2
SC10@33	1435.0	18.9	876.6	11.3	672.3	10.5	704.8	68.6	648.2	11.0
SC10@36	1792.9	70.6	1185.3	31.4	881.2	16.1	2518.1	292.2	835.3	20.7
SC10@37	1744.0	4.0	1141.4	11.5	851.4	13.2	2899.5	183.6	809.1	14.5
SC10@61	~~no data~~	~~no data~~	~~no data~~	~~no data~~	~~1439.7~~	~~48.7~~	~~no data~~	~~no data~~	~~>1200~~	

Table E 2. 3: Results of SIMS geochronology analyses (cont.)

Sample/ spot #	[U] ppm	[Th] ppm	[Pb] ppm	Th/U calc	Th/U Meas.	Isotope	$^{206}Pb/^{204}Pb$ common	$^{207}Pb/^{204}Pb$ common	$^{208}Pb/^{204}Pb$ common	$^{206}Pb/^{204}Pb$ measured	f_{206}%
SC08@1	188	184	80	0.721	0.979	204	18.703	15.629	38.631	19525	0.10
SC08@60	1966	789	445	0.471	0.401	204	18.703	15.629	38.631	1459	1.28
SC08@61	1638	1167	378	0.474	0.713	204	18.703	15.629	38.631	1357	1.38
SC08@62	60	71	30	1.104	1.185	204	18.703	15.629	38.631	13365	0.14
SC10@6	1618	316	324	0.258	0.195	204	18.703	15.629	38.631	718	2.61
SC10@8	1362	711	384	0.378	0.522	204	18.703	15.629	38.631	9189	0.20
SC10@10	950	1081	399	0.968	1.137	204	18.703	15.629	38.631	1856	1.01
SC10@11	2365	1326	467	0.704	0.561	204	18.703	15.629	38.631	315	5.94
SC10@12	868	162	338	0.251	0.187	204	18.703	15.629	38.631	2945	0.64
SC10@15	1152	1203	351	0.773	1.044	204	18.703	15.629	38.631	1222	1.53
SC10@16	2493	3362	384	0.508	1.348	204	18.703	15.629	38.631	1454	1.29
SC10@18	1516	158	1638	5.210	0.104	204	18.703	15.629	38.631	129	14.52
SC10@19	3331	1869	524	0.490	0.561	204	18.703	15.629	38.631	462	4.05
SC10@21	3575	385	683	0.574	0.108	204	18.703	15.629	38.631	337	5.55
SC10@23	2173	400	498	0.219	0.184	204	18.703	15.629	38.631	1724	1.08
SC10@24	2452	573	559	0.552	0.234	204	18.703	15.629	38.631	333	5.62
SC10@27	1048	209	297	0.220	0.200	204	18.703	15.629	38.631	2499	0.75
SC10@28	2451	182	402	0.040	0.074	204	18.703	15.629	38.631	13791	0.14
SC10@29	3011	292	347	0.071	0.097	204	18.703	15.629	38.631	3325	0.56
SC10@32	4167	3856	307	0.118	0.925	204	18.703	15.629	38.631	761	2.46
SC10@33	2375	699	310	0.142	0.294	204	18.703	15.629	38.631	3323	0.56
SC10@36	3367	2378	863	1.010	0.706	204	18.703	15.629	38.631	361	5.17
SC10@37	1988	150	334	0.129	0.075	204	18.703	15.629	38.631	2627	0.71
SC10@61	1073	287	no data	no data	0.267	204	18.703	15.629	38.631	134	13.93

Appendix F.1: Ultramafic Rock Chemistry Comparison between Various Phoscorite-bearing Complexes

Table F 1. 1: Ultramafic rock major element comparison between various phoscorite-bearing complexes.

	Schiel Alkaline Province, RSA						Phalaborwa Complex, RSA (Fourie & De jager, 1896)	Kovdor Complex, Russia (Zaitsev et al., 2015)			Kovdor Complex, Russia (Krasnova, 2004)						Sokli Complex, Finland (Lee et al., 2004)			Seblyavr Massif, Russia (Balaganskaya et al., 2007)			
Sample	Mt-rich Phoscorite		Glimmerite		Clinopyroxenite		Ph	Ph1	Ph2	Ph3	Fo-rich Ph		Ap-rich Ph		Mt-rich Ph		P1	P2	P3	Prx	Ph I	Ph II	Ph III
	1	2	1	2	1	2	1				1	2	1	2	1	2							
SiO_2	23.74	25.95	36.94	39.08	44.30	44.39	13.97	32.38	10.28	12.69	34.12	24.32	5.99	6.05	7.02	6.50	16.57	4.52	14.96	30.00	22.43	16.40	5.60
TiO_2	0.80	0.76	0.43	0.29	0.27	0.27	3.76	0.09	-0.47	0.27	<0.01	<0.01	0.30	0.15	0.52	0.57	0.98	0.89	2.27	10.91	3.52	1.66	0.73
Al_2O_3	1.37	5.97	8.58	8.25	3.47	3.48	0.75	0.22	1.33	3.16	0.35	0.44	0.87	0.06	2.99	2.18	1.00	0.17	1.72	3.93	3.75	1.32	0.19
Fe_2O_3	40.50	41.05	10.87	13.42	24.94	24.65	25.08	9.30	47.51	45,97	2,53	4.07	9.39	5.84	40.46	37.91	24.45	50.89	42.47	11.12	14.73	18.63	31.82
FeO							16.13				6.01	5.76	5.01	2.69	7.32	11.89				10.13	8.24	7.40	12.00
MnO	0.29	0.19	0.15	0.21	0.36	0.35	0.43	0.27	0.35	0.37	0.32	0.22	0.13	0.11	0.33	0.35	0.70	0.68	0.54	0.22	0.35	0.54	0.48
MgO	7.04	12.88	19.92	13.44	7.35	7.37	8.13	41.84	16.75	18.08	44.20	31.28	8.33	10.30	13.95	13.51	20.81	5.15	13.93	11.31	10.18	16.15	8.86
CaO	17.99	5.07	8.39	13.22	17.25	16.59	16.79	9.68	14.20	10.44	5.71	18.56	40.22	42.10	14.88	15.70	15.62	18.38	9.59	17.30	19.73	16.38	18.60
Na_2O	0.26	0.05	0.13	0.30	1.03	1.07	0.10	0.08	0.10	0.12	0.25	0.20	0.50	0.39	0.09	0.21	0.14	0.05	0.28	0.63	1.14	0.21	0.36
K_2O	0.50	4.82	7.26	5.24	0.96	0.98	0.37	0.12	0.06	1.28	<0.01	0.25	0.25	0.25	0.78	0.10	0.83	0.11	2.10	1.05	2.30	1.36	0.54
P_2O_5	7.01	2.13	4.94	3.76	0.17	0.17	10.59	7.04	10.45	0.09	6.10	15.00	27.91	29.07	6.37	8.47	2.60	4.99	4.11	0.52	5.16	8.63	6.10
F							-				0.06	0.08	0.27	0.06	0.16	-				0.09	0.36	0.54	0.36
CO_2							0.30	1.00	<0.01	9.08	0.23	2.22			3.78	1.26				0.84	6.92	6.30	13.80
S							-				-	-	-	-	-	-				0.03		0.33	0.50
H_2O^-							-				-	-	0.04	0.14	-	<0.01				0.18	0.34	0.40	0.36
H_2O^+							2.66				<0.01	0.07	0.41	0.12	0.47	-							
LOI	-0.34	0.20	1.70	2.45	-0.15	0.46	-										15.66	8.86	6.04	1.3		2.96	
O=F,S											0.02	0.03	0.11	0.02	0.07	-				-0.05	-0.15	-0.39	-0.4
Total	99.16	99.07	99.31	99.66	99.95	99.78	99.06	102.01	101.51	101.56	99.78	100.54	99.74	99.53	99.05	98.65	100.02	98.27	99.33	99.52	99.00	99.21	99.90

Table F 1. 2: Ultramafic rock trace element comparison between various phoscorite-bearing complexes.

	Schiel Alkaline Complex, RSA						Phalaborwa Complex, RSA (Hornig-Kjarsgaard, 1998)	Kovdor Complex, Russia (Zaitsev et al., 2015)			Sokli Complex, Finland (Hornig-Kjarsgaard, 1998)	Seblyavr Complex, Russia (Balaganskaya et al., 2007)	
Sample	Phoscorite		Glimmerite		Clinopyroxenite		Phos	Ph1	Ph2	Ph3	SO2	Ph I	Ph II
La	231.70	226.25	358	211.30	604.00	613.50	204	37.20	32.10	31.20	219	214	309
Ce	532.50	481	807	547.40	1156.50	1184.50	529	72.50	70.50	56.30	506	510	727
Pr	67.55	56.55	98	76.55	129.00	129.45	75	8.72	9.17	6.20	56	63	94
Nd	298.70	220.90	393.20	348.70	478.00	477.30	299	30.40	33.30	20.50	247	245	387
Sm	71.50	39.75	71.50	73.90	81.90	83.80	63.20	4.76	5.45	2.96	37.20	41	61
Eu	17.78	7.86	14.88	15.93	14.91	15.04	14.40	1.27	1.43	0.87	10.12	12.20	17.50
Gd	60.95	26.43	47.55	53.15	51.65	51.95	38.80	3.91	4.50	2.55	30.30	33	54
Tb	6.67	2.61	4.47	5.42	5.44	5.45	4.56	0.43	0.51	0.27	4.09		
Dy	31.66	11.05	19.27	23.33	25.00	25.11	17.60	1.79	2.19	1.17	11.70	17.70	25
Y	135.85	42.90	71.65	90.55	94.50	96.35		7.02	7.63	4.78			
Ho	4.82	1.62	2.67	3.31	3.65	3.63	2.59	0.28	0.35	0.19	1.44	2.70	3.20
Er	11.01	3.52	5.53	7.10	8.38	8.57	5.05	0.64	0.77	0.47	2.47	5.50	6.80
Tm	1.26	0.39	0.57	0.74	1.08	1.06		0.07	0.08	0.05			
Yb	6.87	2.08	2.95	3.96	6.70	6.87	1.83	0.38	0.48	0.48	1.66	2.90	3.50
Lu	0.88	0.27	0.38	0.50	1.07	1.04	0	0.05	0.06	0.05	0.16	0.36	0.42

Appendix F.2: Carbonatite Rock Chemistry Comparison between Various Phoscorite-bearing Complexes

Table F 2. 1: Carbonatite rock major element comparison between various phoscorite-bearing complexes.

	Schiel Alkaline Complex							Kovdor Complex, Russia (Verhulst et al., 2000)			Sokli Complex, Finland (Lee et al., 2004)			Seblyavr Complex, Russia (Balaganskaya et al., 2007)		
Sample	SC8-2	SC8-5	SC8-8	SC8-15	SC8-16	SC8-20	SC8-23	C I	C II	C III	C1	C2a	C3	C I	C II	C III
SiO_2	3.27	0.91	4.42	5.62	2.81	2.16	3.07	1.96	0.95	1.09	4.99	2.07	2.51	3.33	0.93	3.27
TiO_2	0.34	0.03	0.20	0.42	0.28	0.27	0.26	0.03	0.11	u.d.l	0.26	0.2	0.21	0.18	0.04	0.09
Al_2O_3	0.05	0.10	0.17	0.19	0.12	0.03	0.23	0.14	0.19	0.31	0.32	0.15	0.25	0	0.25	0.36
Fe_2O_3	7.75	1.01	6.31	13.53	8.81	7.84	7.28	1.38	3.99	0.92	7.44	10.95	5.33	2.41	1.6	2.77
FeO								1.08	N.a	-				1.24	1	0.87
MnO	0.11	0.13	0.11	0.12	0.11	0.10	0.09	0.08	0.07	0.18	0.25	0.29	0.3	0.18	0.15	0.12
MgO	4.78	2.56	5.61	6.01	3.63	3.62	3.59	3.01	1.87	20.62	6.82	4.12	4.57	3.14	1.87	2.6
CaO	46.24	52.90	45.83	41.26	46.88	47.21	47.19	51.57	49.7	30.96	42.23	43.61	45.66	48.06	51.67	48.37
Na_2O	0.04	0.04	0.05	0.03	0.05	0.04	0.06	0.02	0.02	0.04	0.07	0.05	0.13	0.22	0.05	0.08
K_2O	0.05	0.07	0.15	0.16	0.09	0.02	0.14	0.08	0.18	0.19	0.2	0.06	0.32	0.31	0.19	0.48
P_2O_5	2.02	0.56	4.78	5.49	4.92	3.95	7.49	0.89	1.9	1.08	4.13	2.75	3.24	2.27	1.06	1.93
F														0.19	n.a	0.16
CO_2										45.13				37.08	40.96	37.82
Cl														0.01	n.a	0.02
S														0.44	n.a	2.04
H_2O^-														0.22	n.a	0.21
LOI	34.61	40.94	31.85	26.99	32.24	33.92	29.71	40.12	37.49		31.39	33.04	34.6	0	n.a	0
O=F,S														-0.3	n.a	-0.4
Total	99.26	99.25	99.48	99.82	99.94	99.16	99.11	100.36	96.47	100.52	98.71	98.02	98.05	98.98	99.77	99.42

Table F 2. 2: Carbonatite rock trace element comparison between various phoscorite-bearing complexes.

	Schiel Alkaline Complex, RSA							Phalaborwa Complex, RSA (Hornig-Kjarsgaard, 1998)		Kovdor Complex, Russia (Verhulst et al., 2000)			Sokli Complex, Finland (Hornig-Kjarsgaard, 1998)	Seblyavr Complex, Russia (Balaganskaya et al., 2007)	
Sample	SC8-2	SC8-5	SC8-8	SC8-15	SC8-16	SC8-19	SC8-23	BMS	SCS	C I	C II	C III	SO1	C I Seb	C II Seb
La	303.50	301.50	321.90	316.90	302.95	297.40	357.75	213	296	102	190	26.80	124	232	122
Ce	639	601.50	696	717	678.50	661	813	397	609	190	467	56	262	491	251
Pr	78.25	71.35	84.95	89.75	85.35	81.50	100.85	58	82	21.6	39.7	6.42	35	56	30.20
Nd	321.50	297	353.40	380.05	356.65	342.50	427	249	382	76	140	22.90	144	206	113
Sm	62.10	56.55	68.30	71.40	69.30	66.40	83.10	47	66.80	10.7	18.5	3.05	20.10	31.00	17.40
Eu	13.78	12.67	15.42	15.89	15.06	15.07	18.20	11.80	10.10	3	4.97	0.82	6.48	9.30	5.05
Gd	47.25	41.15	51.01	51.85	51.20	49	61.85	28.60	33	7.92	12.6	2.11	16.80	26.00	13.60
Tb	4.76	4.45	5.11	5.05	5.05	4.90	5.97	3.08	2.93						1.88
Dy	21.05	19.82	22.78	21.97	22.68	22.06	26.80	12.90	11.00	4.89	6.94	1.01	7.59	13.90	8.76
Y	88.05	91.35	93.35	88.10	93.60	92.80	107.60			22.6	29	3.90			
Ho	3.09	3.11	3.29	3.08	3.31	3.21	3.90	2.13	1.48	0.87	1.15	0.16	1.15	2.20	1.54
Er	6.76	6.82	7.02	6.71	7.18	6.96	8.09	4.31	2.77	1.8	2.04	0.26	2.34	4.70	3.20
Tm	0.74	0.72	0.77	0.72	0.74	0.77	0.84								
Yb	3.87	4.18	3.99	3.71	4.16	4.04	4.70	1.57	1.39	1.33	1.34	0.17	1.35	2.80	2.30
Lu	0.56	0.56	0.58	0.48	0.56	0.56	0.62	0.15	0.11	0.2	0.2	<0.02	0.13	0.35	0.33

Appendix F.3: Mica Chemistry Comparison between Various Rocks Present in Phoscorite-bearing Complexes

Table F 3. 1: Mica Chemistry comparison between various ultramafic rocks present in phoscorite-bearing complexes.

	Schiel Alkaline Complex, RSA				Phalaborwa Complex, RSA (Hillier et al., 2013)		Phalaborwa Complex, RSA (Giebel et al., 2018)					Kovdor Complex, Russia (Krasnova, 2004)			Sokli complex, Finland (Lee et al., 2004)			Seblyavr Massif, Russia (Balaganskaya et al., 2007)	
Rock type	Clinopyroxenite	Mt-rich Ph	Mt-rich Ph	Glimmerite			Pyroxenite	Fenite	Phoscorite	Phoscorite	Phoscorite							Pyroxenite	Phoscorite
Mica type	Mg-rich Biotite	Phlogopite	Mg-rich biotite	Phlogopite	Phlogopite	Hydrobiotite	Biotite	Biotite	phlogopite	Al-rich Phlg	Tfl-phl	Phl	Phl	Tphl	P1	P2	P3		
SiO_2	36.57	40.77	38.80	41.16	41.73	42.01	39.97	41.31	42.92	42.49	42.62	37.80	38.75	41.40	40.78	41.88	39.88	38.77	40.93
TiO_2	2.97	1.23	1.83	0.80	1.19	0.96	0.90	0.21	0.26	0.03	0.04	0.26	0.14	0.31	0.27	0.21	0.06	1.76	0.79
Al_2O_3	13.33	11.68	11.76	12.20	8.98	9.65	11.73	11.81	10.25	12.74	7.15	16.49	15.43	b.d	14.39	10.74	0.06	15.78	13.38
Fe_2O_3		0.58		0.70	9.85	7.70			1.89		5.85	2.09	2.06	19.14					
FeO	21.68	10.32	16.30	5.67			18.10	13.85	4.25	2.38	4.11	1.26	1.21		2.59	5.04	18.64	7.11	6.95
MgO	10.36	20.58	15.47	24.36	23.94	26.46	16.00	19.70	25.93	27.18	25.56	25.38	27.51	25.25	26.23	26.37	23.57	23.15	24.52
MnO	0.29	0.18	0.18	0.10	0.07	0.00	0.19	0.18	0.02		0.04	0.04	0.07	0.02	0.02	0.13	0.09	0.07	0.14
CaO	0.02	0.00	0.013	0.01	0.00	0.12	0.05	0.01	0.01	0.02	0.05	0.68	0.53						
Na_2O	0.18	0.04	0.066	0.10	0.31	0.34	0.06	0.09	0.14	0.05	0.03	0.87	0.26	0.78	2.06	0.62	0.33	1.59	1.91
K_2O	9.89	10.66	10.40	10.75	9.64	4.61	10.32	10.43	10.60	10.85	10.85	9.75	9.60	10.13	7.10	9.63	9.77	9.28	8.83
Cr_2O_3															0.05	0.05			
NiO															0.01		0.06		
BaO							0.32	0.26	0.06	1.00	0.06				1.39	0.08	0.05		
H_2O^-												0.26	0.21						
H_2O^+	3.70	3.74	3.67	3.62			3.69	3.45	3.30	3.10	3.47	5.04	4.10						
Cl							0.22	0.05	0.02	0.01	0.02								
F	0.33	0.78	0.59	1.20			0.56	1.21	1.92	2.50	1.45	0.18	0.18		0.17	0.79	1.10		
O=F,Cl	0.14	0.33	0.25	0.50			0.29	0.52	0.82	1.06	0.62	0.07	0.07		0.07	0.33	0.46		
Total	99.18	100.22	98.83	100.14	95.77	91.88	101.82	102.04	100.75	101.29	100.68	100.03	99.98	97.03	95.05	95.20	93.15	97.50	97.46

Table F 3. 2: Mica chemistry comparison between various carbonatite rocks present in phoscorite-bearing complexes.

	Schiel Alkaline Complex, RSA					Phalaborwa Complex, RSA (Giebel et al., 2019)					Kovdor Complex, Russia (Verhulst et al., 2000)			Sokli Complex, Finland (Lee et al., 2004)		
Sample	SC8-1	SC8-1	SC8-4	SC8-21	SC8-24	BCB	BCB	BCB (tphl)	TCB (tphl)	TCB	C I	C II	C III	C1	C2b	C3
SiO_2	39.68	39.95	40.94	40.86	41.92	42.97	39.48	42.84	43.27	42.98	41.44	42.31	41.46	39.66	42.92	42.26
TiO_2	0.35	0.27	1.03	0.43	0.92	0.35	0.18	0.06	0.02	0.03	0.41	0.14	-	0.42	0.09	0.11
Al_2O_3	12.14	12.15	11.29	10.99	12.52	10.63	18.13	8.46	8.94	11.04	12.02	9.43	7.39	15.22	10.99	9.16
Fe_2O_3	0.33		2.91	2.92	1.14	1.44	0.65	4.88	1.93	1.48						
FeO	13.64	14.05	5.32	6.14	2.91	4.73	1.5	2.7	4.68	2.17	4.51	5.07	8.12	4.49	3.06	5.69
MgO	19.41	19.25	24.45	24.25	26.86	25.46	25.77	26.88	26.77	27.45	26.01	25.67	26.73	24.92	27.49	27.04
MnO	0.08	0.09	0.07	0.03	0.05	0.01	0.03		0.04		-	0.08	-	0.22	0.07	0.05
CaO	0.01	0.03	0.09	0.00	0.01	0.04	0.01	0.05			-	-	-			
Na_2O	0.04	0.11	0.15	0.05	1.08	0.05	0.03	0.05	0.03	0.02	0.66	0.22	1.3	2.07	1.01	0.23
K_2O	10.73	10.62	10.16	10.50	8.91	10.82	11.13	10.6	10.75	10.82	10.08	11.33	9.06	6.98	9.2	10.39
Cr_2O_3											0.08	-	-	-	0.16	
NiO											n.a	n.a	n.a	-		
BaO						0.38	0.88	0.79	0.36	0.98	n.a	n.a	n.a	1.1	0.23	0.17
H2O*	4.02	4.02	3.95	4.02	4.13	3.61	3.93	3.56	3.39	2.83	4.23	4.2	3.9			
Cl						0.03		0.02	0.02	0.01			-			
F	0.07	0.10	0.42	0.20	0.33	1.26	0.87	1.41	1.77	3.05			0.39	0.37	0.89	0.99
O=F,Cl	0.03	0.04	0.18	0.09	0.14	0.54	0.36	0.59	0.75	1.29		-	-0.16	0.16	0.37	0.42
Total	100.48	100.58	100.58	100.31	100.63	97.63	98.3	98.15	97.83	98.73	99.44	98.45	98.19	95.29	95.74	95.72

Appendix F.4: Magnetite Chemistry Variation between Various Ultramafic Rocks Present in Phoscorite-bearing Complexes

Table F 4. 1: Magnetite chemistry variation between various ultramafic rocks present in phoscorite-bearing assemblages.

	Schiel Alkaline Complex, RSA			Phalaborwa Complex, RSA Adapted from Sharygin et al. (2010)			Kovdor Complex, Russia (Krasnova et al., 2004)			Sokli complex, Finland (Lee et al., 2004)	
Rock type	Clinopyroxenite	Glimmerite	Phoscorite	Phoscorite			Forsterite-apatite	Mt-forsterite	Mt-cc-forsterite	Phoscorite	
Sample	SC10-4-2	SC10-6-1	SC10-12-4	1	2	3	1	2	3	P1	P3
SiO_2	0.03	0.04	0.07	0.00	0.00	0.00	0.69	1.00	0.10	0.16	0.18
TiO_2	0.03	0.06	0.42	0.95	1.11	1.73	0.36	2.90	4.65	2.81	1.33
Al_2O_3	0.03	0.05	0.00	0.10	0.13	0.17	0.59	0.60	0.27		
Cr_2O_3	0.02	0.00	0.00	0.00	0.00	0.00	0.01	b.d	b.d	0.07	0.04
Fe_2O_3	68.61	68.32	67.53	68.03	67.68	66.18	64.70	66.00	62.32	63.09	65.71
V2O3	0.00	0.00	0.02				0.08	0.05	0.12	0.28	0.28
FeO	30.99	30.89	31.20	29.12	29.26	30.74	29.82	27.54	28.74	32.4	31.82
MnO	0.03	0.04	0.07	0.16	0.19	0.09	0.44	0.57	0.57	0.25	0.42
MgO	0.00	0.03	0.01	1.74	1.73	1.22	2.41	2.01	4.05	1.13	0.6
NiO										0.08	0.04
Total	99.73	99.43	99.30	100.11	100.10	100.13	99.85	100.79	100.40	100.2	100.49

Appendix F.5: Clinopyroxene Chemistry Variation seen between Various Ultramafic Rocks Present in Phoscorite-bearing Complexes

Table F 5.1: Clinopyroxene variation seen between various ultramafic rocks present in phoscorite-bearing assemblages.

	Schiel Alkaline Complex, RSA					Phalaborwa Complex (Erikson, 1989)	Kovdor Complex, Russia (Krasnova et al., 2004)	Seblyavr Massif, Russia (Balaganskaya et al., 2007)	
Sample	SC10-2-2	SC10-6-1	SC10-11-2	SC10-22-1	SC10-5-2				
Rock Type	Glimmerite		Clinopyroxenite		Phos	Massive pyroxenite	Phoscorite	Pyroxenite	Phoscorite
SiO_2	52.01	54.35	53.08	54.18	52.21	54.1	58.22	52.09	53.52
TiO_2	0.01	0.08	0.03	0.07	0.05	0	0.10	0.99	0.36
Al_2O_3	1.30	0.35	0.42	0.17	0.85	0.26	0.28	1.46	0.49
Cr_2O_3	0.00	0.04	0.03	0.00	0.00		0.00		
Fe_2O_3	1.68	0.00	0.00	0.00	1.77		0.00	1.16	0.94
FeO	8.13	4.70	9.78	5.06	9.73	4.02	2.92	2.71	2.68
MnO	0.28	0.20	0.43	0.24	0.43	0	0.08	0.10	0.18
MgO	12.16	15.97	12.31	15.56	11.38	16.2	23.02	15.85	16.43
CaO	22.52	22.97	22.23	22.72	22.08	24.8	5.62	24.89	24.89
Na_2O	0.64	0.27	0.56	0.43	0.69	0.28	7.70	0.45	0.35
K_2O	0.03	0.03	0.01	0.03	0.03				
Total	98.70	98.94	98.88	98.43	99.28	99.66	98.11	99.70	100.01

Appendix F.6: Amphibole Chemistry Variation in Carbonatite Rocks Present in Phoscorite-bearing Complexes

Table F 6. 1: Amphibole chemistry variation seen in carbonatite rocks present in phoscorite-bearing assemblages.

	Schiel Alkaline Complex, RSA			Seblyavr Complex, Russia (Balaganskaya et al., 2007)
Rock type	Carbonatite (Ferri-winchite)	Carbonatite (Actinolite)	Carbonatite (Tremolite)	Carbonatite
Sample	SC8-1	SC8-1	SC8-21	C1
SiO_2	56.23	57.53	58.66	56.96
TiO_2	0.01	0.04	0.05	0.33
Al_2O_3	0.34	0.10	0.02	0.38
Fe_2O_3	4.50	3.37	0.00	
FeO	7.96	2.89	2.92	5.01
MnO	0.12	0.19	0.10	0.19
MgO	17.19	20.59	22.58	21.62
CaO	7.47	10.29	13.52	6.15
Na_2O	3.39	2.47	0.00	6.71
K_2O	0.74	0.64	0.03	0.73
H_2O	2.03	2.04	2.19	
F	0.18	0.26	0.01	
O=F, Cl	-0.08	-0.11	0.00	
Total	100.07	100.30	100.08	98.08

Appendix F.7: Apatite Chemistry Variation seen in Various Rocks Present in Phoscorite-bearing Complexes

Table F 7. 1: Apatite chemistry variation seen in various ultramafic rocks in phoscorite-bearing complexes.

	Schiel Alkaline Complex, RSA				Phalaborwa Complex, RSA (Giebel et al., 2019)		Kovdor Complex, Russia (Teiber et al., 2015)	Sokli Complex, Finland (Lee et al., 2004)	
Rock type	Glimmerite		Phos	Cpx	Phoscorite		Phoscorite	Phoscorite	
Sample	SC10-2-2	SC10-24-2	SC10-12-1	SC10-32-4	1	7	Kovd-10 (mean comp.)	P1	P3
P_2O_5	41.30	41.41	41.60	42.13	42.18	39.45	42.19	40.61	42.61
SiO_2	0.25	0.33	0.13	0.17	0.11	1.45	0.01	0.82	0.07
Na_2O					0.08	0.11	0.12	0.18	0.10
MgO	0.00	0.04	0.05	0.00				0.06	0.03
MnO	0.00	0.05	0.17	0.01	0.03		0.01	0.05	
FeO	0.04	0.07	0.09	0.01	0.04	0.10	0.01	0.07	
CaO	52.85	51.46	51.40	52.12	54.75	51.55	55.08	54.30	54.04
SrO	1.00	1.39	2.57	1.78	0.51	0.82	0.61	0.30	0.52
Y_2O_3								0.02	0.05
La_2O_3						0.74	0.04	0.28	0.08
Ce_2O_3	0.15	0.95	0.63	0.27	0.27	0.27	0.15	0.52	0.25
Pr_2O_3					0.08	0.30			
Nd_2O_3					0.16	0.99		0.37	0.18
SO_3						0.02	0.03		
F	2.89	2.01	2.69	1.98	2.53	2.72	1.51	2.07	3.09
Cl	0.02	0.49	0.50	0.28	0.07	0.02	0.05	0.01	0.01
H2O					0.57	0.44			
O=F,Cl	1.22	0.96	1.24	0.90	1.06	1.14	0.64	0.87	1.30
Total	97.29	97.22	98.59	97.85	99.75	99.01	100.16	98.78	99.72

Table F 7. 2: Apatite chemistry variation seen in various carbonatite rocks in phoscorite-bearing complexes.

	Schiel Alkaline Complex, RSA			Phalaborwa Complex, RSA (Giebel et al., 2019)				Kovdor Complex, Russia (Teiber et al., 2015)			Sokli Complex, Finland (Lee et al., 2004)			
Rock type	Carbonatite			BCB	BCB high-REE	TCB	TCB high-REE	Carbonatite			Carbonatite			
Sample	SC08-1	SC08-4	SC08-21					7/321	KDR-14	4/241	C2aC	C3PL	C4D	C5D
P_2O_5	42.06	41.88	41.89	41.63	40.62	39.45	41.42	42.11	42.23	42.41	42.38	42.61	42,75	40.72
SiO_2	0.12	0.16	0.20	0.08	0.05	1.45	0.1	0.09	0.02	0.01	0.17	0.07	0.17	0.57
Na_2O				0.12	0.76	0.11	0.47	0.17	0.19	0.15	0.24	0.1	0.18	0.56
MgO	0.00	0.02	0.06								0.06	0.03	-	0.07
MnO	0.00	0.00	0.00	0.05		0.02		0.01	0.02	0.01	-	-	-	-
FeO	0.15	0.02	0.04		0.05			0.01	0.02	0.02	0.01	0.04	0.04	0.05
CaO	52.43	51.90	52.97	54.88	49.35	51.55	52.24	55.04	54.9	55.17	54.05	54.04	53.45	50.68
SrO	1.09	0.82	0.71	0.67	2.63	0.82	1.41	0.34	0.23	0.23	0.3	0.52	0.86	2.27
Y_2O_3												0.05		
La_2O_3				0.11	0.91	0.74	0.56	0.03	0.01	0.03	0.09	0.08	0.18	0.58
Ce_2O_3	0.68	0.75	0.52	0.27	2.15	1.88	1.34	0.13	0.07	0.11	0.23	0.25	0.51	1.46
Pr_2O_3				0.2	0.24	0.3	0.16							
Nd_2O_3				0.18	0.82	0.99	0.57				0.31	0.18	0.02	0.64
SO_3				0.03	0.03	0.02	0.02	0.003	0.003					
F	1.84	2.07	1.68	2.56	2.35	2.72	2.69	1.67	0.86	1.47	2.09	3.06	3.16	3.57
Cl	0.30	0.20	0.38	0.05	0.02	0.02	0.02	0.01	0.02	0.01		0.01		
H2O				0.55	0.59	0.44	0.49							
O=F,Cl	0.84	0.92	0.79	1.07	0.99	1.14	1.13	0.7	0.37	0.62	0.88	1.3	1.33	1.5
Total	97.82	96.91	97.66	99.76	99	99.01	99.87	99.91	99.59	100.09	99.04	99.72	99.98	99.68

Appendix F.8: Olivine Chemistry Variation seen in Various Carbonatite Rocks in Phoscorite-bearing Complexes

Table F 8. 1: Olivine chemistry variation in carbonatite rocks present in phoscorite-bearing complexes.

	Schiel Alkaline Complex, RSA		Phalaborwa Complex, RSA (Erikson, 1989)	Kovdor Complex, Russia (Verhulst et al., 2000)	Sokli Complex, Finland (Lee et al., 2004)	
Sample	SC08-11	SC08-24	P42K	C1	C1	C2a
SiO_2	39.52	39.43	40.40	42.34	40.60	41.61
TiO_2	-	-				0.05
Al_2O_3	-	-			0.01	
FeO	17.45	16.06	12.00	6.19	8.72	4.74
MnO	0.31	0.33		0.47	1.26	0.91
MgO	42.72	43.43	47.70	51.58	48.49	52.62
CaO	0.01	0.01	0.03	0.10	0.42	0.06
Na_2O	0.02	-				
NiO	-	-	0.03	n.a		0.06
K_2O	0.04	0.02				
Cr_2O_3	0.003	0.17				0.02
Total	100.07	99.99	100.16	100.72	99.49	100.07